UNIVERSITY OF CALIFORNIA, SAN DIEGO

Leveraging Post-Translational Phosphopantetheinylation as a Versatile Biochemical Tool

A dissertation submitted in partial satisfaction of the requirements for the degree Doctor of Philosophy

in

Chemistry

by

Nicolas M. Kosa

Committee in charge:

Professor Michael D. Burkart, Chair
Professor Timothy Baker
Professor Michael Gilson
Professor Patricia Jennings
Professor Charles Perrin

2013

The Dissertation of Nicolas M. Kosa is approved, and it is acceptable in quality and form for publication on microfilm and electronically:

_____

_____

_____

_____

_____

Chair

University of California, San Diego

2013

DEDICATION

In recognition of my family's ever-constant support, encouragement, and value of education, I dedicate this dissertation to all the family members that have been there for me throughout my years.

EPIGRAPH

"Man's unique reward, however, is that while animals survive by adjusting themselves to their background, man survives by adjusting his background to himself."

Ayn Rand

TABLE OF CONTENTS

LIST OF ABBREVIATIONS

Phosphopantetheine	PPant
Carrier protein	CP
Acyl carrier protein	ACP
Peptidyl carrier protein	PCP
Coenzyme A	CoA
Modified coenzyme A	mCoA
Phosphoadenosinephosphate	PAP
Adenosine triphosphate	ATP
Phosphopantetheinyl transferase	PPTase
Human phosphopantetheinyl transferase	hPPTase
Acyl carrier protein hydrolase	AcpH
Pseudomonas aeruginosa AcpH	PaAcpH
Pseudomonas fluorescens AcpH	PfAcpH
Cyanothece PCC 7822 AcpH	CyAcpH
Shewanella oneidensis AcpH	SoAcpH
Fluorescein isothiocyanate	FITC
Fluorescence polarization	FP
Forster resonance energy transfer	FRET
Fatty acid synthase	FAS
Polyketide synthase	PKS
Non ribosomal peptide synthase	NRPS

LIST OF FIGURES

Figures: Leveraging post-translational phosphopantetheinylation as a versatile biochemical tool

Figures: Fluorescent techniques for discovery and characterization of phosphopantetheinyl transferase inhibitors

LIST OF TABLES

ACKNOWLEDGEMENTS

I would like to acknowledge Professor Michael D. Burkart for his support as my advisor and chair of my committee. Through his guidance and encouragement I have grown substantially as a scientist and been exposed to a breadth of fascinating research experiences.

My wife, Erica Kosa, has been a wonderful source of support and encouragement in coping with the trials of moving to pursue my PhD and the many years of toiling through the ups and downs of my graduate studies. She played an integral part in facilitating the extension of my scientific skillset and reaching the conclusion of my degree.

I additionally want to acknowledge the past and current members of the Burkart Laboratory. Their knowledge and guidance have served me immeasurably, as everyone has contributed to my overall research progress. I especially thank Lorillee Tallorin, for being an amazing friend, and making my last few years in graduate school much more memorable.

The chapter entitled “Fluorescent techniques for discovery and characterization of phosphopantetheinyl transferase inhibitors,” in full, is a reprint of the material as accepted by the Journal of Antibiotics. Kosa, Nicolas M.; Foley, Timothy L.; Burkart, Michael D. 2013. The dissertation author was the primary investigator and author of this paper.

The chapter entitled “Reversible labeling of native and fusion-protein motifs,” in full, is a reprint of the material as it appears in Nature Methods Vol. 9, 981-984, 2012. Kosa, Nicolas M.; Haushalter, Robert W.; Smith, Andrew R.; Burkart, Michael D. The dissertation author was the primary investigator and author of this paper.

The chapter entitled “Chemoenzymatic exchange of phosphopantetheine on protein and peptide,” in full, is currently being prepared for submission for publication of the material. Kosa, Nicolas M.; Pham, Kevin M.; Burkart, Michael D. The dissertation author was the primary investigator and author of this material.

VITA

2006	Bachelor of Science in Biochemistry, University of Texas, Austin
2007-2008	Chemist at Pharmaform LLC, Austin, TX
2009-2010	Teaching Assistant, Department of Chemistry and Biochemistry University of California, San Diego
2010	Master of Science in Chemistry, University of California, San Diego
2010-2013	Research Assistant, University of California, San Diego
2013	Doctor of Philosophy in Chemistry, University of California, San Diego

PUBLICATIONS

"Reversible labeling of native and fusion-protein motifs"

"Fluorescent techniques for discovery and characterization of phosphopantetheinyl transferase inhibitors"

FIELDS OF STUDY

Major Field: Chemistry (Biochemistry)

ABSTRACT OF THE DISSERTATION

Leveraging Post-Translational Phosphopantetheinylation as a Versatile Biochemical Tool

by

Nicolas M. Kosa

Doctor of Philosophy in Chemistry

University of California, San Diego, 2013

Professor Michael D. Burkart, Chair

Phosphopantetheine (PPant) transfer from coenzyme A (CoA) to carrier protein (CP) is a necessary post-translational modification required for much natural product biosynthesis. Since this enzymatic modification is essential to many pathogens, high-throughput detection of phosphopantetheinyl transferase (PPTase) activity in a fluorescence polarization format enables methodology to identify new antimicrobial compounds. The ability of the PPTase to utilize fluorescent analogs of phosphopantetheine and the CoA from which it is derived is critical to activity detection. However, the utility of appending phosphopantetheine labels extends past the application of fluorophores to a CP. Many other types of labels can be appended to a phosphopantetheine and attached to CP and short peptide substrates, such as affinity groups, substrate mimics, and crosslinking agents, all enabling various novel biochemical applications. Until recently, the facile removal of natural and synthetic PPant from CP was not possible. However, with the characterization of a stable acyl carrier protein hydrolase (AcpH) phosphodiesterase from the bacteria *Pseudomonas aeruginosa*, reversible labeling of the acyl carrier protein (ACP) was enabled, allowing new bioconjugation methods to label and regenerate both native and fusion CP. Further work with new AcpH homologs from the bacteria *Pseudomonas fluorescens* and cyanobacteria *Cyanothece* sp. PCC 7822 reveal enzymes with superior kinetic parameters and CP substrate promiscuity extending to small peptide activity.

Leveraging post-translational phosphopantetheinylation as a versatile biochemical tool

The post-translational modification (PTM) of naturally produced proteins provides a myriad of options for cellular functionalization and control that are not offered by the unmodified protein. Many examples of PTMs include phosphopantetheinylation,[1] phosphorylation,[2] acylation/alkylation,[3, 4] glycosylation,[5] and many others (**Figure 1**).[6] These PTMs may be leveraged *in vitro* in support of useful bioconjugation applications. The focus of our research lies in the elucidation of phosphopantetheine addition to and removal from various natural and synthetic substrates as a means to develop new drugs, diagnostics, and biochemical techniques.

Carrier proteins (CP) serve as a tethering point for the stepwise addition of substrates used in the creation of a range of products including fatty acids, antibacterials, anticancer drugs, and virulence factors (**Figure 2**).[1] Phosphopantetheinyl transfer occurs naturally via the phosphopantetheinyl transferase (PPTase) appending 4'-phosphopantetheine (PPant) from coenzyme A (CoA), thereby activating the functional CP unit of natural product biosynthetic pathways (**Figure 3a**).[1] However, the biochemical transfer of phosphopantetheine to the CP substrate is not limited to CoA. Modified versions of CoA including natural moeities like acyl/ malonyl starters may be appended to the PPant, as well as synthetic functional groups.[7] Research pioneered in the Burkart laboratory pursues the study of this biosynthetic machinery by implementing a plethora of synthetic PPant analogs integrating fluorophores (**Figure 3b**), substrate mimics, affinity groups, and crosslinking agents.[8-13]

Our lab began looking at PPTases as drug targets due to the essential nature of CP activation in certain diseases. In particular, Sfp-type PPTases, named after Sfp PPTase from the surfactin biosynthesis pathway in *Bacillus subtilis*, are implicated in primarily activating the natural product pathways specific to virulence in target organisms.[14-17] By utilizing fluorescent modified CoA (mCoA) substrates and a recent novel minimal CP peptide, the first

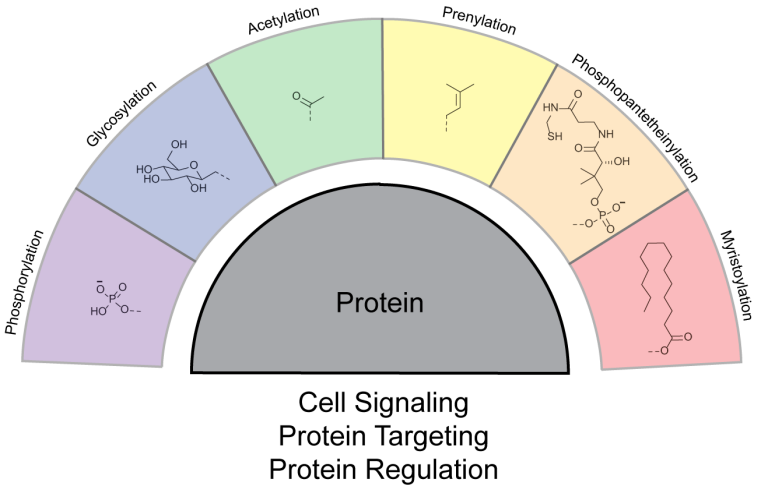

Figure 1. *Post-translational protein modifications*. A large variety of chemical appendages may be conjugated to proteins post-translationally both *in vivo* and *in vitro*.

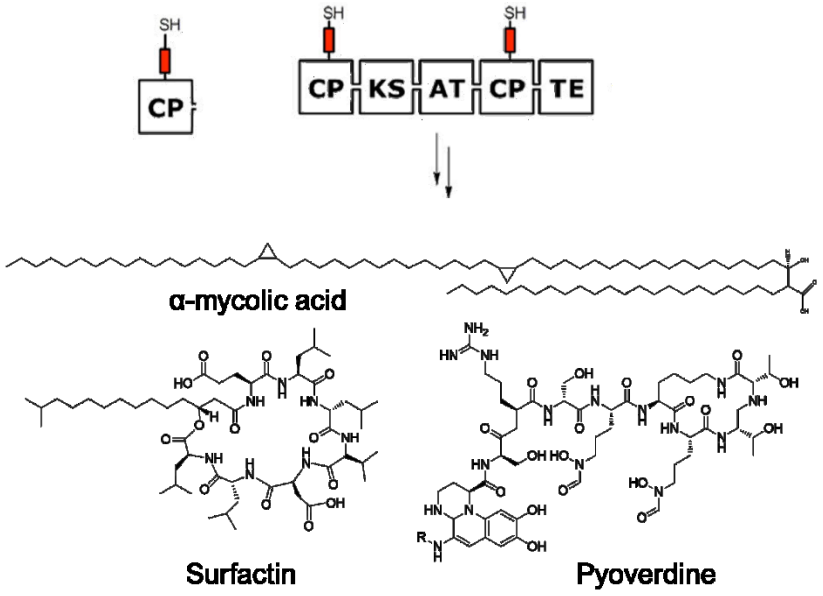

Figure 2. *Carrier protein role in natural product biosynthesis*. The carrier protein (CP) subunit servers as a tethering point for growing natural products through its free thiol added with the pantetheine moiety. CP act in conjunction with other modifying domains such as ketosynthase (KS), acyltransferase (AT) and thioesterase (TE) to elicit product formation. Many biologically relevant molecules are produced through the action of CP, such as antibiotics (surfactin) and virulence factors (mycolic acid and pyoverdine).

high-throughput screening (HTS) assay targeting the Sfp-type PPTase arose utilizing Förster resonance energy transfer (FRET) detection techniques (**Figure 4**).[10, 18, 19] However, this assay was not easily transferred to PPTases specifically derived from virulent organisms or from humans due to incompatibility with the minimal CP peptide.[20] Our transition to a fluorescence polarization format maintains high-throughput capability and functions with any PPTase demonstrating activity with mCoA, while allowing use of a variety of different intact CP substrates more comparable to natural targets (**Figure 5**). Fluorescence polarization detection of PPTase activity serves as a springboard for the detection and optimization of compounds necessary for discovering the next generation of antibiotics, as well as a facile detection method for evaluating target specificity and interference with the equivalent human PPTase enzyme.[20] More recently, this assay has been implemented alongside structural analysis of the Mycobacterium tuberculosis PPTase in our lab, which demonstrates an important role in organism virulence in *ex vivo* and *in vivo* studies.[15]

Phosphopantetheine labeling also possesses myriad uses outside of immediate drug development. CP labeling with PPant, conjugated to a tag of choice by a PPTase, represents one of the most flexible covalent protein labeling methods, as illustrated by its application in tagging minimal-ACP peptides,[21, 22] bio-gel formation[23] and ACP-dependent protein immobilization.[24] The labeling of ACP and ACP fusion proteins with PPant analogs is also successfully leveraged for visualization,[9, 25] isolation,[9] functional[11] and structural[12] studies of CP–dependent biosynthetic enzymes. While an enzyme had been previously identified in *E. coli* that is capable of PPant hydrolysis from acyl carrier protein (ACP), study of this ACP hydrolase (AcpH) proved difficult due to instability and poor expression.[26, 27] More recently, a homolog of this enzyme was discovered in *P. aeruginosa* that proved more amenable to study.[28] Our study of this *P. aeruginosa* AcpH yielded the discovery that AcpH could efficiently and completely remove a variety of PPant labels from ACP, including fluorescent probes and hydrocarbon acyl chains.[29]

This new technique proved suitable for reversibly labeling free ACP or another protein fused to ACP, such as luciferase, green fluorescent protein, or maltose binding protein.[29]

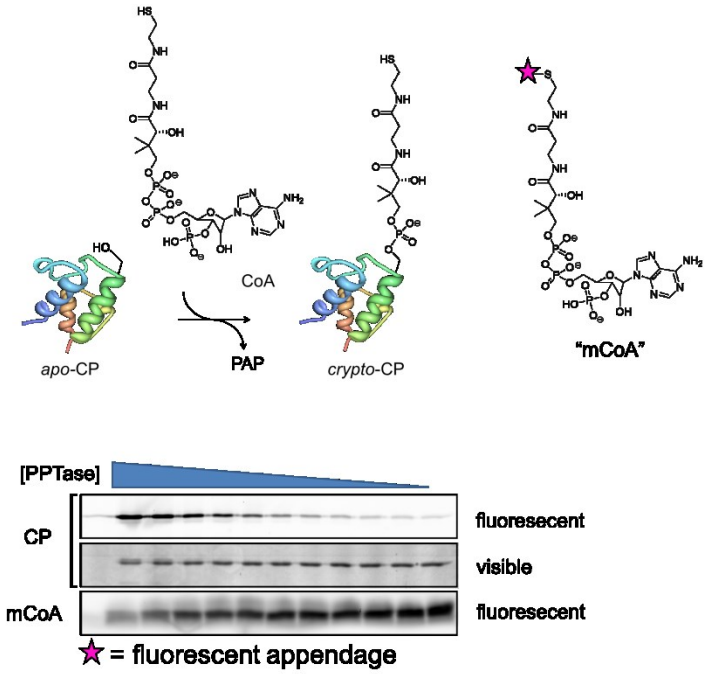

Figure 3. *The PPTase reaction accommodates coenzyme A modification*. Phosphopantetheine is transferred to a conserved serine on an apo-carrier protein (CP) through the action of a PPTase, generating the holo-carrier protein and phosphoadenosine phosphate (PAP). PPTases may also accommodate analogs of CoA (mCoA) possessing modified pantetheine.

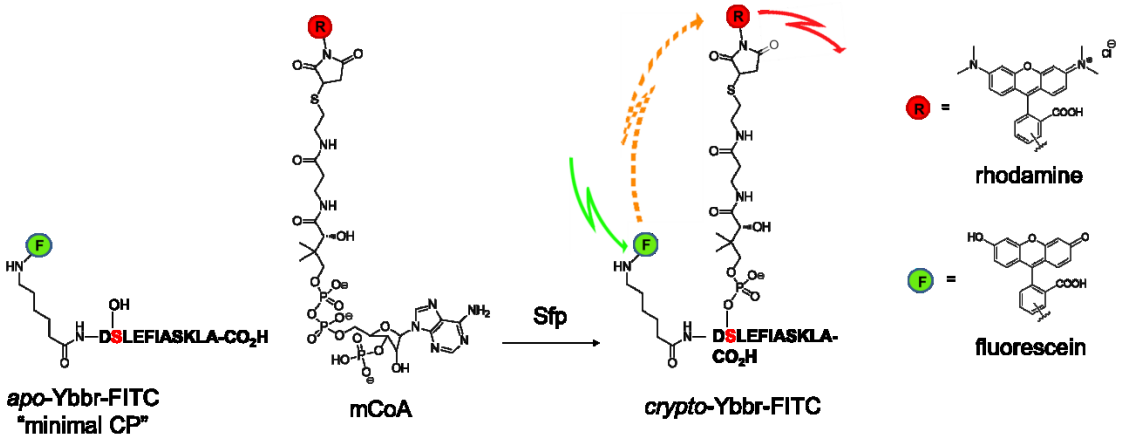

Figure 4. *Sfp PPTase high-throughput assay utilizing small peptide*. The first high throughput assay for a PPTase utilized Sfp from *B. subtilis* and the 11-amino acid Ybbr substrate. The flexibility of the peptide labeling reaction allowed for fluorescent modification of both the Ybbr and CoA substrate to allow FRET detection methods.

After establishing a basis for AcpH compatibility with various PPant labels (**Figure 6**), we realized the need for characterizing the CP component of the reaction in more detail. We observed that while the Sfp PPTase was able to label practically any CP, the AcpH did not demonstrate the same substrate flexibility with regard to the CP. Particularly, we noticed that AcpH demonstrated preference for ACPs from bacterial type II fatty acid synthesis (FAS). Thus, we set out to characterize CPs not only from FAS pathways, but also polyketide synthesis (PKS) and non-ribosomal peptide synthesis pathways (NRPS) in order to test the limits of this enzyme. Additionally, we realized that there was significant sequence variation displayed in AcpH homologs annotated in other bacteria, as demonstrated by the differences of *E. coli* versus *P. aeruginosa* AcpH. While expanding our CP substrate analysis, we also identified additional annotated AcpH homologs in *Pseudomonas fluorescens*, *Shewanella oneidensis*, and *Cyanothece* PCC 7822. Our analyses of these new AcpH targets with various carrier proteins confirmed a preference for FAS ACP, but also highlighted a capability for activity with PKS ACP and even NRPS peptidyl CP (PCP) to a lesser extent. While the hypothetical AcpH homolog from *S. oneidensis* was inactive, two of the newly studied AcpH homologs from *P. fluorescens* and *Cyanothece* PCC 7822 demonstrated not only dramatically improved kinetic rates with ACP versus the originally characterized *P. aeruginosa* variant, but also the capacity for activity with minimal CP peptide Ybbr.

The discovery of AcpH function with the Ybbr substrate is substantial, as the reversible labeling of small peptides is central to ongoing research to pioneer novel bioconjugation methods (**Figure 7**). Several varieties of peptides can be modified with a variety of unnatural labels via sortase,[30] farnesyl transferase,[31] transglutaminase,[32] or phosphopantetheinyl transferase.[21, 22] However, each of these labeling methods faces corresponding specific drawbacks. Sortase conjugation is reversible, but is equilibrium driven and thus has large substrate requirements for creating homogenous product. Farnesyl transferase possesses reasonable kinetics and unnatural label accomodations, but is not truly reversible and allows only C-terminal labeling of peptides.

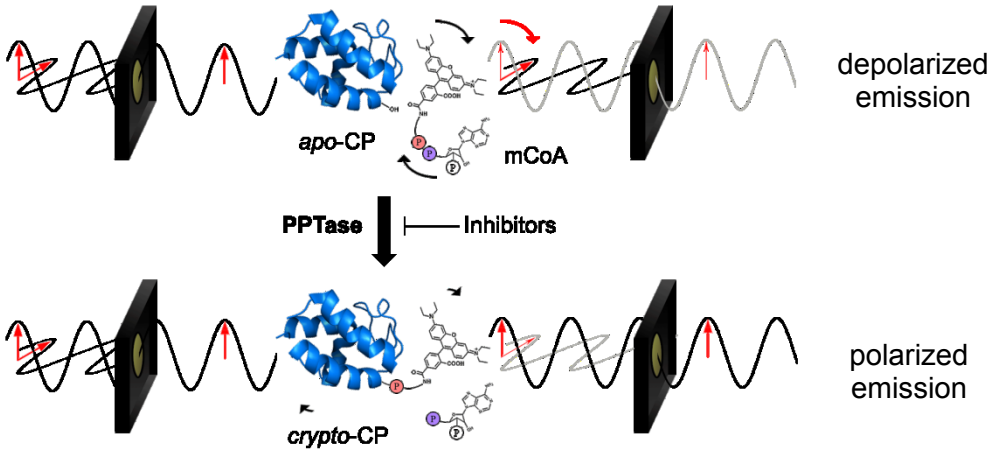

Figure 5. *A flexible fluorescence polarization PPTase assay*. Plane polarized light is used to excite a mixture of *apo*-carrier protein (CP) and fluorescently-tagged coenzyme A (mCoA). PPTase-dependent transfer of the fluorophore to a larger CP results in slowed fluorophore rotation and increases emission of plane-polarized light. Fluorescence polarization improves upon existing high-throughput PPTase assay methods by allowing substitutions with different PPTase and CP.

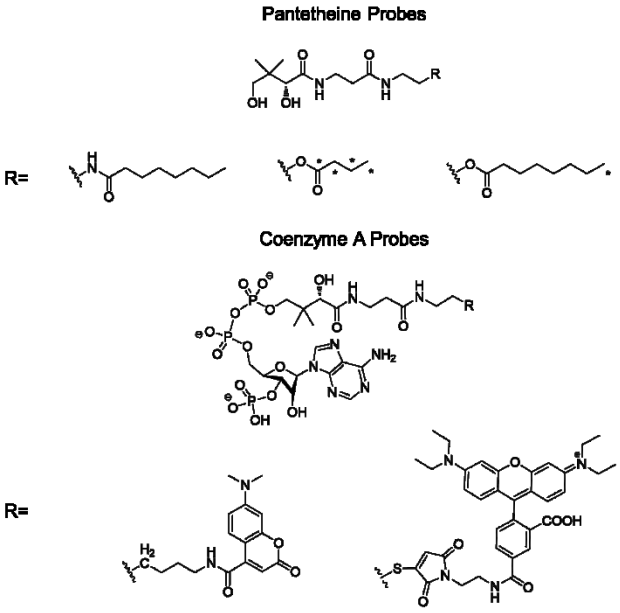

Figure 6. *Various phosphopantetheine analogs removed by AcpH*. Acyl carrier protein hydrolase is able to remove a variety of different tested phosphopantetheines from acyl carrier protein.

Transglutaminase is widely implemented in the food industry to solidify edible proteins, but only allows the crosslinking of peptides and is not easily or specifically reversed. Phosphopantetheinylation of the 11-amino acid Ybbr has proven to be quite flexible in terms of Ybbr placement practically anywhere in a fusion protein, as well as on solid surfaces. Additionally, chemical synthesis of pantetheine analogs allows a shortcut to facile generation of unnatural labels of interest for appending to the peptide.

Until now, the primary drawback of Ybbr PPant labeling was the lack of a specific enzymatic removal. Considering that existing peptide reversible labeling systems possess significant limitations,[31] our identification of AcpH activity with the Ybbr peptide enables the transfer of our reversible, site-specific labeling method to an even wider variety of applications. However, before this reversible peptide-labeling can become a truly entrenched method, it must first be optimized. Considering the Ybbr peptide sequence was originally discovered specifically for PPant addition using the enzyme Sfp from *B. subtilis*, it is likely that the PPant removal reaction could itself be optimized for AcpH. In order to accomplish this, the project continues with the assistance of computational learning methods to interpret the known active versus inactive CP sequences, and build a library of hundreds to thousands of possible minimal peptides to test both PPTase labeling and label removal by AcpH. This series of peptides also serves to inform the programming methods used to predict peptide substrates, thereby “training” the prediction methods. The current results generated in search of an improved scaffold for reversible PPant labeling are encouraging, and promise a bright future for bioconjugation technology.

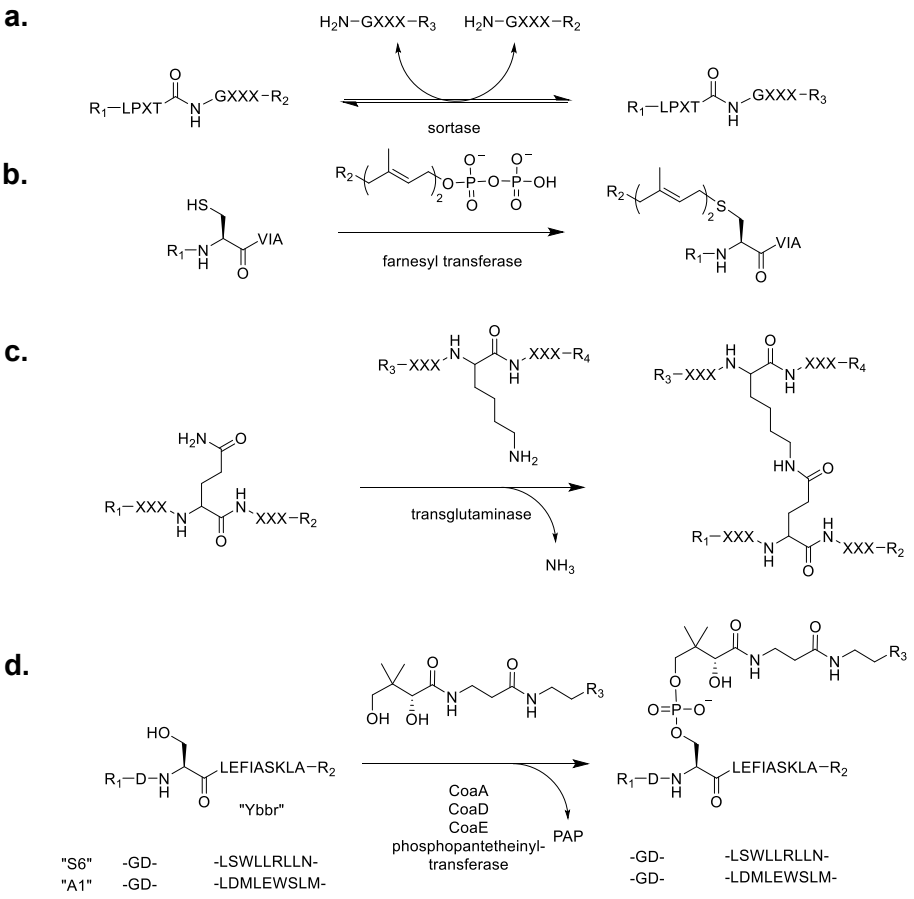

Figure 7. *Current methods for peptide labeling*. Various peptide labeling techniques include the equilibrium-driven sortase (**a**), the unidirectional farnesyl transferase (**b**), the unidirectional transglutaminase (**c**), and the newly site-specific and reversible phosphopantetheinyl transfer (**d**).

References

1. Mercer, A. C. & Burkart, M. D. The ubiquitous carrier protein--a window to metabolite biosynthesis. *Nat. Prod. Rep.* 24, 750-773 (2007).

2. Hunter, T. Protein Kinases and Phosphatases: The yin and yang of protein phosphorylation and signaling. *Cell* 80, 225-236 (1995).

3. Towler, D.A., Gordon, J. I., Adams, S. P., and Glaser, L. The biology and enzymology of eukaryotic protein acylation. *Ann. Rev. Biochem*. 57, 69-99 (1988).

4. Kara, U.A., Stenzel, D. J., Ingram, L. T., Bushell, G. R., Lopez, J. A. and Kidson C. Inhibitory monoclonal antibody against a (myristylated) small-molecular-weight antigen from Plasmodium falciparum associated with the parasitophorous vacuole membrane. *Infect. Immun.* 56, 903-909 (1988).

5. Spiro, R.G. Protein glycosylation: nature, distribution, enzymatic formation, and disease implications of glycopeptide bonds. *Glycobiology* 12, 43R-56R (2002).

6. Mann, M. and Jensen, O. N. Proteomic analysis of post-translational modifications. *Nat. Biotechnol.* 21, 255-261 (2003).

7. Quadri, L.E., Weinreb, P. H., Lei, M., Nakano, M. M., Zuber, P., and Walsh, C. T. Characterization of Sfp, a Bacillus subtilis phosphopantetheinyl transferase for peptidyl carrier protein domains in peptide synthetases. *Biochemistry* 37, 1585-1595 (1998).

8. Worthington, A.S. and Burkart, M.D. One-pot chemo-enzymatic synthesis of reporter-modified proteins. *Org. Biomol. Chem.* 4, 44-46 (2006).

9. La Clair, J.J., Foley, T.L., Schegg, T.R., Regan, C.M. and Burkart, M.D. Manipulation of carrier proteins in antibiotic biosynthesis. *Chem. Biol.* 11, 195-201 (2004).

10. Foley, T.L. and Burkart, M.D. A homogeneous resonance energy transfer assay for phosphopantetheinyl transferase. *Anal. Biochem.* 394, 39-47 (2009).

11. Ishikawa, F., Haushalter, R.W. and Burkart, M.D. Dehydratase-specific probes for fatty acid and polyketide synthases. *J. Am. Chem. Soc.* 134, 769-772 (2012).

12. Haushalter, R.W. et al. Binding and "pKa" modulation of a polycyclic substrate analogue in a type II polyketide acyl carrier protein. *ACS Chem. Biol.* 6, 413-418 (2011).

13. Shute, T. S., Matsushita, M., Dickerson, T. J., La Clair, J. J., Janda, K. D., and Bukart, M. D. A site-specific bifunctional protein labeling system for affinity and fluorescent analysis. *Bioconj. Chem.* 16, 1352-1355 (2005).

14. Chalut, C., Botella, L., de Sousa-D'Auria, C., Houssin, C. & Guilhot, C. The nonredundant roles of two 4'-phosphopantetheinyl transferases in vital processes of Mycobacteria. *Proc. Natl. Acad. Sci. U.S.A.* 103, 8511-8516 (2006).

15. Leblanc, C. et al. 4'-Phosphopantetheinyl transferase PptT, a new drug target required for Mycobacterium tuberculosis growth and persistence in vivo. *PLoS Pathog.* 8, e1003097 (2012).

16. Barekzi, N., Joshi, S., Irwin, S., Ontl, T., and Schweizer, H. P. Genetic characterization of pcpS, encoding the multifunctional phosphopantetheinyl transferase of Pseudomonas aeruginosa. *Microbiology* 150, 795-803 (2004).

17. Porter, J. L. *et al*. The cell wall-associated mycolactone polyketide synthases are necessary but not sufficient for mycolactone biosynthesis. *PLoS One* 8, e70520 (2013).

18. Foley, T.L. *et al*. Preparation of FRET reporters to support chemical probe development. *Org. Biomol. Chem.* 8, 4601-4606 (2010).

19. Yasgar, A. *et al*. A strategy to discover inhibitors of Bacillus subtilis surfactin-type phosphopantetheinyl transferase. *Mol. Biosyst.* 6, 365-375 (2010).

20. Kosa, N.M., Foley, T. L. and Burkart, M. D. Fluorescent techniques for discovery and characterization of phosphopantetheinyl transferase inhibitors. *J. Antibiot.* Accepted (2013).

21. Yin, J., Lin, A.J., Golan, D.E. and Walsh, C.T. Site-specific protein labeling by Sfp phosphopantetheinyl transferase. *Nat. Protoc.* 1, 280-285 (2006).

22. Yin, J. et al. Genetically encoded short peptide tag for versatile protein labeling by Sfp phosphopantetheinyl transferase. *Proc. Natl. Acad. Sci. U.S.A.* 102, 15815-15820 (2005).

23. Mosiewicz, K. A., Johnsson, K. and Lutolf, M. P. Phosphopantetheinyl transferase-catalyzed formation of bioactive hydrogels for tissue engineering. *J. Am. Chem. Soc.* 132, 5972-5974 (2010).

24. Wong, L.S., Thirlway, J., and Micklefield, J. Direct site-selective covalent protein immobilization catalyzed by a phosphopantetheinyl transferase. *J. Am. Chem. Soc.* 130, 12456-12464 (2008).

25. Foley, T.L., Young, B.S. and Burkart, M.D. Phosphopantetheinyl transferase inhibition and secondary metabolism. *FEBS J.* 276, 7134-7145 (2009).

26. Thomas, J., Rigden, D. J., and Cronan, J. E. Acyl carrier protein phosphodiesterase (AcpH) of Escherichia coli is a non-canonical member of the HD phosphatase/phosphodiesterase family. *Biochemistry* 46, 129-136 (2007).

27. Thomas, J. and Cronan, J.E. The enigmatic acyl carrier protein phosphodiesterase of Escherichia coli: genetic and enzymological characterization. *J. Biol. Chem.* 280, 34675-34683 (2005).

28. Murugan, E., Kong, R., Sun, H., Rao, F. and Liang, Z.X. Expression, purification and characterization of the acyl carrier protein phosphodiesterase from Pseudomonas Aeruginosa. *Prot. Expr. Purif.* 71, 132-138 (2010).

29. Kosa, N.M., Haushalter, R.W., Smith, A.R. and Burkart, M.D. Reversible labeling of native and fusion-protein motifs. *Nat. Methods* 9, 981-984 (2012).

30. Williamson, D.J., Fascione, M.A., Webb, M.E. and Turnbull, W.B. Efficient N-terminal labeling of proteins by use of sortase. *Angew. Chem. Int. Ed. Engl.* 51, 9377-9380 (2012).

31. Rashidian, M., Song, J.M., Pricer, R.E. and Distefano, M.D. Chemoenzymatic reversible immobilization and labeling of proteins without prior purification. *J. Am. Chem. Soc.* 134, 8455-8467 (2012).

32. Lee, J. H., *et al*. Glutamine (Q)-peptide screening for transglutaminase reaction using mRNA display. *Biotechnol. Bioeng.* 110, 353-362 (2012).

Fluorescent techniques for discovery and characterization of phosphopantetheinyl transferase inhibitors

Phosphopantetheinyl transferase (E.C. 2.7.8.-) activates biosynthetic pathways that synthesize both primary and secondary metabolites in bacteria. Inhibitors of these enzymes have the potential to serve as antibiotic compounds that function through a unique mode of action and possess clinical utility. Here we report a direct and continuous assay for this enzyme class based upon monitoring polarization of a fluorescent phosphopantetheine analog as it is transferred from a low molecular weight coenzyme A substrate to higher molecular weight protein acceptor. We demonstrate the utility of this method for the biochemical characterization of phosphopantetheinyl transferase Sfp, a canonical representative from this class. We also establish the portability of this technique to other homologs by adapting the assay to function with the human phosphopantetheinyl transferase, a target for which a microplate detection method does not currently exist. Comparison of these targets provides a basis to predict therapeutic index of inhibitor candidates and offers a valuable characterization of enzyme activity.

Introduction

Antibiotic resistance is a persistent threat to modern medicine that contributes to increasing mortality statistics in both developed and underdeveloped countries. The top threats currently challenging worldwide healthcare efforts include multidrug resistant (MDR) and extensively drug-resistant (XDR) *Mycobacterium tuberculosis*[1] and methicillin resistant *Staphlyococcus aureus* (MRSA).[2, 3] In addition to these noxious agents, *Vibrio cholera*,[4] *Pseudomonas aeruginosa*,[5] *Staphylococcus pneumonia*,[6] and bacteria responsible for meningococcal meningitis[7] have recently shown an increased capacity to resist current drug regimens. While industry has found some success though augmentation of known pharmacophores to circumvent resistance mechanisms, the development of new chemical entities that act on novel drug targets opens new avenues to antimicrobial development and extends the efficacy of existing therapeutics.

Among bacterial and fungal targets that are currently unaddressed in the clinic, Sfp-type phosphopantetheinyl transferases (Sfp-PPTases) have received much attention recently for their involvement in the virulence of many pathogenic bacteria[8-11] and fungi.[12, 13] Representative virulence factors from these organisms include mycolic acid and mycobactin in *M. tuberculosis*,[14, 15] pyoverdine in *P. aeruginosa*,[16] mycolactone in *M. ulcerans*,[17] vibriobactin in *V. cholera*,[18] and yersiniabactin in *Y. pestis*.[19] In addition to the manufacture of these compounds, Sfp-PPTases possess the additional capability to activate primary metabolism if the AcpS-PPTase gene becomes lost or inactivated, an event illustrated by genetic knockout *Streptomyces coelicolor* and *Bacillus subtilis* case studies[20, 21] and observed naturally in *Pseudomonas spp*.[10, 22]

To test hypotheses concerning the association of Sfp-PPTases with bacterial virulence, we have begun a campaign to identify inhibitors of Sfp from *B. subtilis*, the canonical representative and namesake of this enzyme class. During this work, we have found it necessary to assess compound cross-reactivity with the human PPTase (hPPTase),[23] where inhibitory action could induce mitochondrial damage and present a liability of mechanism-based toxicity. Herein, we detail the challenges encountered when adapting our established screening assay[24] for use with the human PPTase. To address this issue, we have developed a novel fluorescent polarization assay that monitors the complete process of the PPTase reaction. This new technique directly detects the incorporation of a fluorescent phosphopantetheinyl appendage onto a whole-protein product. We demonstrate the ability of this assay to biochemically characterize Sfp-PPTase, adapt the detection format to function with the human enzyme, and demonstrate that this methodology can reliably report the inhibitory activity of test compounds toward this critical anti-target in order to predict therapeutic index of inhibitor candidates.

Materials & Methods

General

Glassware and stir bars used in synthetic techniques were oven dried. General purpose solvents were ACS grade unless otherwise noted. Solvents used for HPLC were HPLC-grade

only. Tandem HPLC/ESI-MS analysis was performed on a Waters HPLC (Waters Corporation, Milford, MA) using an XBridge C18 2.5 µm 3.0 x 50 mm (Waters Corporation, Milford, MA) column, running on a gradient method using acetonitrile and water with 0.1% formic acid. A MicroMass ZMD (Waters Corporation, Milford, MA) electron spray injection mass spectrometer was in line with the HPLC. All protein concentrations were determined using UV absorbance. Rhodamine-CoA concentration was quantified through serial dilution and comparison of fluorescence (485 nm / 595 nm excitation / emission) to a 100 µM rhodamine-CoA standard stock using a HTS 7000 plus Bioassay Reader (Perkin Elmer, Waltham, MA). Rhodamine-CoA was prepared as previously described[25] and subjected to LC/MS analysis for product confirmation (**Supplementary Figure 1**).

Recombinant protein expression

Sfp in pET29b (Novagen, La Jolla, CA),[26] VibB in pET24b (Novagen, La Jolla, CA),[27] ActACP in pET24b,[28] and the 90 amino acid ACP (hACP) from human fatty acid synthase (EC 2.3.1.85) synthesized in a pJexpress401vector (DNA2.0, Menlo Park, CA) were transformed, expressed and purified using BL-21(DE3) *E. coli* cultured with rotary shaking at 37°C in lysogeny broth containing kanamycin (50 µg/mL). Native Sfp was prepared as previously described.[29] When the optical density (OD) reached 0.6, expression was induced by the addition of Isopropyl-β-D-1-thiogalactoside (IPTG) to a concentration of 1 mM, for a period of 4 hours at 37°C for Sfp, ActACP, hACP-containing cells and overnight at 16°C for VibB. hPPTase was cultured at 37°C in LB with 25 µg/mL chloramphenicol in TOP10 *E. coli* (Life Technologies, Grand Island, NY). Upon reaching OD of 0.6, 1 mM IPTG was added to induce hPPTase protein expression overnight at 16°C with shaking. Recombinant cell cultures were centrifuged at 2000 rpm for 30 minutes, with cell pellets frozen at -20°C until use.

Protein purification

Cells thawed on ice were re-suspended in lysis buffer [50 mM TrisCl pH 8.0, 500 mM NaCl, 1 mM DTT, 5 µg/mL DNase I & 5 µg/mL RNAse A, 0.1 mg/mL lysozyme and lysed with

either French pressure (Thermo Electron Corp/Thermo Scientific, Waltham, MA) or Model#110 F microfluidizer (Microfluidics Corporation, Newton, MA). Cell debris was cleared by centrifugation for 45 minutes at 10,000 g at 4°C. Soluble protein extracts were decanted and subjected to IMAC using Ni-NTA resin. Fractions containing the purified target proteins were dialyzed against 50 mM TrisCl pH 8.0, 500 mM NaCl, 1 mM DTT, the dialysate concentrated using Amicon-Ultra centrifugal filters (Millipore, Billerica, MA) appropriate for the target protein's molecular weight. Samples were flash frozen and stored at -80°C until use. Protein samples were evaluated for purity by SDS-PAGE (**Supplementary Figure 2**) and concentrations were determined using UV spectroscopy at 280 nm with calculated extinction coefficients[30]: Sfp = 28880 $M^{-1}cm^{-1}$, hPPTase = 56950 $M^{-1}cm^{-1}$, VibB = 48930 $M^{-1}cm^{-1}$, hACP = 1490 $M^{-1}cm^{-1}$, ActACP = 2980 $M^{-1}cm^{-1}$.

FRET-based PPTase assay

PPTase labeling activity of FITC-YbbR was determined using previously reported procedures.[24] The final buffer composition includes 50 mM HEPES pH 7.6, 10 mM $MgCl_2$, 1 mg/mL BSA, 0.01% Tween-20, and 10% DMSO. Briefly, 10 µL of 25 µM FITC-Ybbr & 25 µM rhodamine-CoA was added to 5 µL DMSO in a 96-well Costar cat no. 3694 black 96-well plate (Corning, Lowell, MA), and the reaction initiated by the addition of 35 µL enzyme solution (buffer blank, 37 nM Sfp, 143 nM hPPTase). Raw fluorescence units were acquired at 492 nm excitation and 535 nm emission using a HTS 7000 plus Bioassay Reader (Perkin Elmer, Waltham, MA).

Crypto- VibB, hACP, & ActACP preparation

A crypto-VibB standard was prepared via reaction of 50 µM (30 nmol) *apo*-VibB with 220 µM (110 nmol) rhodamine-CoA in 0.5 mL in 50 mM HEPES pH 7.5, 10 mM $MgCl_2$ and 20% glycerol with 200 nM native Sfp at 37ºC for 24 hours. *Crypto*-VibB was re-purified using Ni-NTA chromatography, desalted with PD-10 column (GE Healthcare BioSciences, Pittsburgh, PA) into desalt buffer [50 mM TrisCl pH 7.5, 250 mM NaCl, 10% glycerol], and spin-concentrated with a 0.5 mL 3 kDa MWCO Amicon-Ultra filters.

Crypto-hACP standard was prepared via 16 hour reaction at 37°C of 130 μM (33 nmol) *apo*-hACP with 270 μM (66 nmol) rhodamine-CoA in 0.25 mL in 50 mM HEPES pH 7.5, 10, $MgCl_2$, with 1 mM DTT and 200 nM native Sfp. *Crypto*- hACP was repurified using Ni-NTA chromatography, desalted into desalt buffer with 0.1 mM additional DTT, and spin-concentrated with a 0.5 mL 3 kDa MWCO Amicon-Ultra filter.

Crypto-ActACP was prepared via 16 hour reaction at 37°C of 150 μM (60 nmol) *apo*-hACP with 300 μM (120 nmol) rhodamine-CoA in 0.4 mL in 50 mM HEPES pH 7.5, 10, $MgCl_2$, and 200 nM native Sfp. *Crypto*-ActACP was repurified using Ni-NTA chromatography, desalted into desalt buffer, and spin-concentrated with a 0.5 mL 3 kDa MWCO Amicon-Ultra filter.

SDS-PAGE confirmed rhodamine-labeling of carrier proteins (**Supplementary Figure 3a**). Quantification of the concentrated crypto- carrier proteins was performed through serial dilution and comparison of fluorescence (485 nm excitation & 595 nm emission) to a 100 μM rhodamine-CoA standard stock on a HTS 7000 plus Bioassay Reader (Perkin Elmer, Waltham, MA).

Linear dilution of crypto- carrier proteins analyzed by fluorescence polarization

Crypto- VibB and ActACP were prepared in 50 mM TrisCl pH 8 at 10 μM with and without 1 mg/mL BSA for 100% labeled sample. *Apo*- VibB and ActACP at 10 μM with and without 1 mg/mL BSA were prepared with 10 μM free rhodamine-CoA as the 0% labeled sample. An 11-point linear dilution was prepared by combining the *crypto*- and *apo*- carrier protein mixtures in a 50 μL volume in Costar cat. no 3694 black 96-well plates (Corning, Lowell, MA) to give 0.5 μM increments of crypto from 0-10 μM.

Removal of coenzyme A from Sfp enzyme preparation

One aliquot of Sfp preparation was treated with calf intestinal phosphatase (CIP) (Worthington Biochemicals, Lakewood, NJ) to remove pre-bound CoA for comparison to untreated PPTase dissociation constants. CIP (100 U at 3800 U/mL) was added to Sfp (10 mg) in

5 mL 50 mM TrisCl pH 8, 250 mM NaCl, 10% glycerol, 10 mM $MgCl_2$, along with a sufficient quantity of nickel resin (1.5 mL bed volume) for binding. Incubation of the mixture proceeded with gentle rocking at room temperature. Nickel resin was washed with 50 mM MES pH 6.2, 500 mM NaCl, 10% glycerol, 1 mM $CaCl_2$ and then eluted with 300 mM imidazole in the same MES buffer as the wash. The resultant *apo*-Sfp was buffer exchanged with a centrifugal filter prior to use by concentrating the protein to 0.5 mL with a 10 kDa MWCO spin filter (EMD Millipore, Billerica, MA), and adding previous MES buffer without imidazole to 5 mL, mixing, and concentrating to 0.5 mL again. This cycle was repeated 3 times to reduce imidazole to a trivial concentration. Incubation of CIP-treated and untreated Sfp with *apo*-ACP from *E. coli* demonstrates effective re-purification (**Supplementary Figure 4a**) and removal of coenzyme A from Sfp preparation (**Supplementary Figure 4b**).

Determination of PPTase dissociation constant, K_D

The dissociation constant that the PPTase enzymes exhibit for Rhodamine-CoA was performed similarly to existing methods.[31] Briefly, a 1:2 serial dilution of PPTase in 50 mM HEPES pH 7.6, 0.01% Tween-20, 10 mM $MgCl_2$ was conducted across 11-points with a blank lacking PPTase. This enzyme serial dilution was pipetted in triplicate volumes of 25 µL into three rows of a 96-well plate containing 25 µL of 50 nM Rhodamine-CoA in the same buffer to give a range of 100 – 0.10 µM top final [hPPTase] and 86 – 0.08 µM top final [Sfp]. After mixing, plates were incubated for 20 minutes at room temperature, centrifuged 2 minutes at 2000 rpm, and measured using described fluorescence polarization parameters.

Data analysis

Dissociation constant (K_D) calculations for PPTases were performed by converting polarization values into anisotropy, and using JMP 10 (SAS Institute Inc., Cary, NC) software to obtain nonlinear fits with equations **1** and **2** used previously.[31]

$$A_{OBS} = \frac{QF_{SB}A_B+(1-F_{SB})A_F}{1-(1-Q)F_{SB}} \qquad (1)$$

$$F_{SB} = \frac{K_D + L_{ST} + R_T - \sqrt{(K_D + L_{ST} + R_T)^2 - 4L_{ST}R_T}}{2L_{ST}} \quad (2)$$

Raw data points and nonlinear regression were then plotted in GraphPad Prism 5.00 (GraphPad Software, La Jolla, CA). For IC_{50} determination, raw data were normalized by setting 0% activity to sample wells lacking PPTase, and 100% activity to sample wells that received control vehicle. Resulting percent activities were fitted to the 4-parameter Hill equation in GraphPad Prism. Dose-response curves that exhibited prominent activation or no response were labeled as inactive for the purposes of discussion.

Fluorescence-polarization-based phosphopantetheinylation assay

Activity assays were performed in Costar cat. no 3694 black 96-well plates (Corning, Lowell, MA) in a buffer containing 50 mM Sodium-HEPES, 10 mM $MgCl_2$, 1 mg/mL BSA, 10% DMSO, 0.01% Tween-20. PPTase in the assay is used at concentrations of 100 nM while measuring inhibitor response, and 5 nM for kinetic evaluation at various pH conditions. Substrates rhodamine-CoA and carrier protein (VibB or hACP) are present for all analysis at concentrations of 5 μM and 10 μM, respectively. Microwell reaction final volumes are 50 μL, evaluated at 45 minute time points for Sfp and hPPTase.

Evaluation of PPTase dilution labeling with fluorescence polarization

Sfp and human PPTase were diluted to 1.43 μM in 1.43X reaction buffer (72 mM Sodium-HEPES, 14.3 mM $MgCl_2$, 1.43 mg/mL BSA, 0.0143% Tween-20), and subjected to an 11-point 1:2 serial dilution into 1.43X reaction buffer. PPTase serial dilution (1430-1.4 nM, 35 μL) was then added to 5 μL DMSO blank and incubated at room temperature for 10-15 minutes. Reactions were initiated with the addition of 10 μL substrate mix (25 μM rhodamine-CoA & 50 μM VibB or hACP), centrifuged 2 minutes at 2000 rpm, and analyzed in kinetic mode for 70 minutes with previously mentioned fluorescence polarization setup (**Supplementary Figures 5 & 6**).

Detergent and DMSO evaluation with fluorescent polarization

Sfp and human PPTase were diluted to 143 nM in 1.43X reaction buffer (72 mM Sodium-HEPES, 14.3 mM $MgCl_2$, 1.43 mg/mL BSA) with 0.0143% Tween-20, Triton X-100, NP-40, or no detergent. PPTase (143 nM, 35 µL) was then added to 5 uL DMSO or milliQ water and incubated at room temperature for 10-15 minutes. Reactions were initiated with the addition of 10 µL substrate mix (25 µM rhodamine-CoA & 50 µM VibB or hACP), centrifuged 2 minutes at 2000 rpm, and analyzed in kinetic mode for 70 minutes with previously mentioned fluorescence polarization setup (**Supplementary Figure 7 & 8**).

PPTase pH-dependence with fluorescence polarization

Kinetic analysis of Sfp and hPPTase activity at various pH conditions was carried out similarly to the regular fluorescence polarization reaction conditions, but with lower final PPTase concentrations of 5 nM and various buffers. Buffers were prepared as 10X solutions at 500 mM with 100 mM $MgCl_2$, adjusted to pH with HCl or NaOH, and diluted with milliQ water. Sodium acetate (anhydrous) served as the pH 4.5 and 5.0 buffers. MES (free acid) served as the pH 5.5, 6.0, and 6.5 buffers. HEPES (sodium salt) served as the pH 7.0 and 7.5 buffers. Tris (base) served as the pH 8.0, 8.5, and 9.0 buffers. The 10X buffers were otherwise prepared and implemented as fluorescence polarization assay conditions describe. Samples were evaluated with 10% DMSO and the same substrate concentrations as the described fluorescence polarization assay conditions. Data analysis utilized the *crypto*-VibB (**Supplementary Figure 3b**) and hACP standards (**Supplementary Figure 3c**) prepared at 5, 2.5, 1.25, and 0 µM *crypto*-carrier protein concentrations to calculate activity from raw polarization over a 70 minute period. Linear fits from *crypto*- standards allowed calculation of activity from the earliest time-points to provide non-negative activities, typically ranging from 5-10% substrate consumption.

Statistical analysis

Statistical values including Z' value were calculated for the fluorescence polarization assay using triplicate samples (n=3) to gauge its suitability for high-throughput screening applications, in which the standard deviation (σ) and the signal (µ) in milli-polarization or mP units

for both bound (covalently attached rhodamine-VibB product) and unbound (mixture of unreacted rhodamine-CoA and *apo*-VibB carrier protein).

$$Z' = 1 - \frac{(3\,\sigma_{\max} + 3\sigma_{\min})}{|\mu_{\max} - \mu_{min}|} \qquad (3)$$

SDS-PAGE vs. fluorescence polarization signal comparison

Crypto-VibB standard linear dilutions were prepared at 50 µL volumes in Costar 3694 96-well plate in 50 mM TrisCl and 100 mM EDTA pH 7.0 in 0.5 µM increments from 0 µM to 5 µM, and supplemented with free rhodamine-CoA to a total *crypto*-VibB + rhodamine-CoA concentration of 5 µM to represent product completion in 10% increments. Fluorescence polarization was evaluated in the GenioS Pro plate reader (Tecan Systems Inc, San Jose, CA) at 535 nm polarized excitation and 580 nm polarized emission filters with a gain of 40 and g-factor of 0.76. These samples were then removed from the microtiter plate, diluted 1:10 in 50 mM TrisCl and 100 mM EDTA, an equal volume of 2X SDS-PAGE loading dye added, and heated to 70°C for 5 minutes. 10 µL of each sample loaded onto each lane of a 12% SDS-PAGE gel. The resulting gels were fixed 30 minutes in 40% methanol & 10% acetic acid, washed in warm milliQ water, and visualized on a Typhoon TRIO Variable Mode Imager (GE Healthcare BioSciences, Pittsburgh, PA) at 50-µm resolution with 532 nm green laser excitation and 580BP30 nm emission filter and a photomultiplier tube setting of 500. Gel image data was collected as a .gel file format and *crypto*-VibB protein bands were quantified using ImageJ software (NIH, Bethesda, MD), utilizing integrated pixel density, background subtraction from fluorescent protein bands and fixed scan regions. Signal data collected allowed comparison of FP data to gel data over increasing percent carrier protein labeling, as well as calculating a ratio of integrated pixel density to polarization units. Gel staining was also performed for validation of the fluorescent gel data.

Synthesis of 2'-deoxyadenosine-3,5-bisphosphate (2'-deoxy-PAP)

2'-deoxyadenosine-3,5-bisphosphate was prepared according to existing methodology.[32] Briefly, 2'-deoxyadenosine (270 mg, 1 mmol, Spectrum, Gardena, CA) and proton sponge (1 g, 5

mmol, Sigma, St. Louis, MO) were dried overnight over phosphorus pentoxide and subsequently transferred to a 100 mL round bottom flask with stir bar. Trimethyl phosphate (20 mL, 170 mmol) was added, and sealed with a septum under argon, stirring 5 minutes. The reaction was initiated with addition of phosphorus oxychloride (380 µL, 4 mmol, EMD Millipore, Billerica, MA) and was stirred on ice for 2 hours. The reaction was quenched by addition of triethyl ammonium bicarbonate (20 mL, 125 mmol, pH 7.5) and 30 mL milliQ water. Purification was performed with DEAE A-25 Sephadex (Amersham, Piscataway, NJ) rinsed with ethanol and swollen overnight in milliQ water. Resin was poured into a 30 x 2.5 cm column and equilibrated to the starting mobile phase at room temperature. Reaction mixture was loaded onto the gravity-fed column and separated using a gradient maker producing a gradient of approximately 0.01-0.5 M ammonium bicarbonate pH ~ 7.5. Fractions containing doubly-phosphorylated compound were discerned via normal phase TLC by lack of migration from baseline with 1:2:1 water:butanol:acetic acid mobile phase. Fractions containing the desired compound were combined, frozen, and lyophilized. Incomplete removal of solvent was followed by further concentration under centrifugation with vacuum. Final product was analyzed by ESI-MS (positive mode HR-ESI-FT-MS) to confirm desired molecular weight (**Supplementary Figure 9**).

Fluorescence polarization inhibitor screen

All inhibitors were serially diluted in DMSO and transferred in triplicate to a 96-well plate prior to enzyme addition. Inhibitors of Sfp from previous LOPAC screen[33] were serially diluted and utilized at final top concentrations of 100 µM except SCH-202676 which was used at final top concentration of 50 µM. 2'-deoxy-PAP and PAP were implemented at a top final concentration of 500 µM for both Sfp and hPPTase. Unmodified coenzyme A was used at a top final concentration of 500 µM and 100 µM for Sfp and hPPTase, respectively. Inhibitor in 5 µL DMSO was added to each well, followed by 35 µL of 143 nM Sfp in PPTase reaction buffer (72 mM HEPES pH 7.6, 1.43 mg/mL BSA, 0.0143 % Tween-20), mixed by pipetting. Plates were incubated 10 minutes at room temperature, followed by addition of 10 µL substrate mix (50 µM VibB, 25 µM rhodamine-CoA diluted into 10 mM Tris pH 8.0). Plates were centrifuged 2 minutes at 2000 rpm, and

acquisition began in kinetic mode for 1 hour on GenioS Pro plate reader (Tecan Systems Inc, San Jose, CA). 45 minute time points (post-addition) were used for IC_{50} calculations of test inhibitors. Acquisition utilized the Tecan plate reader using 535nm excitation and 580 nm emission filters.

SCH-202676 inhibition and inactivation

Methods for evaluating SCH via gel-based methods utilized the following buffer conditions to emulate the FP assay: 50 mM Sodium-HEPES, 10 mM $MgCl_2$, 1 mg/mL BSA, 10% DMSO, 0.01% Tween-20. Sfp and hPPTase were used at top final concentrations of 50 nM, and top final SCH-202676 at 100 μM. PPTase samples were prepared in 1.43X reaction buffer with or without 1 mM DTT, and 14 uL of PPTase mixture was added to 2 μL SCH in DMSO or a DMSO blank. Samples were incubated 10 minutes at room temperature, followed by addition of 4 μL substrate mix (25 μM rhodamine-CoA & 50 μM carrier protein) to initiate the reaction. PPTases were also evaluated following desalting to removal residual DTT from protein purification by desalting into respective lysis buffers without DTT/DNAse/RNase/lysozyme using a PD-10 desalting column (GE Healthcare BioSciences, Pittsburgh, PA). Reactions were incubated 30 minute at room temperature, then prepared immediately for electrophoresis with Urea-PAGE (20% polyacrylamide) by the addition of 5 μL of 5X loading dye and loading 12.5 μL of the mixture and running the gel for 2 hours at 160V. Gels were imaged directly after electrophoresis without fixing for all BSA-containing VibB (**Supplementary Figure 10**) and ActACP (**Supplementary Figure 11**), and after fixing for reactions without BSA containing both VibB and ActACP (**Supplementary Figure 12**).

Possible thiol-reactivity was also evaluated for SCH-202676 by HPLC coupled with ESI-MS analysis. SCH-202676 was prepared at a volume of 20 μL at 200 μM in DMSO discretely, as well as with either 200 μM L-cysteine or 200 μM DTT. Samples were diluted with milliQ water to give the desired compound concentrations, as well as a final DMSO concentration of 30%. Samples were incubated at room temperature for 3 hours, subjected to HPLC/ESI-MS analysis

(**Supplementary Figure 13**), and compared to DTT and L-cys controls (**Supplementary Figure 14**).

Results & Discussion

Production and qualification of PPTases

Following the expression and purification of the proteins used in these studies, we initially sought to confirm the function of the hPPTase with a qualitative gel-based phosphopantetheinylation assay.[34] In this experiment, we tested the ability of PPTase enzymes to catalyze the transfer of a fluorescent phosphopantetheinyl appendage to a diverse set of carrier protein (CP) domains from a rhodamine-modified coenzyme A substrate. The results of these experiments clearly demonstrated function of the recombinant protein, and revealed relaxed substrate specificity with respect to the identity of the CP substrate as well as the modified CoA (**Figure 1**). Both hPPTase and Sfp modified the ACP domains of *S. coelicolor* polyketide synthase (PKS) ActACP, human fatty acid synthase (FAS) ACP, and *V. cholera* vibriobactin peptidyl carrier protein (PCP) VibB.

Next, we sought to implement the FRET screen that we previously described for both Sfp and AcpS PPTase,[24] with the idea that the assay may be implemented for hPPTase by simple substitution of the enzyme. Unfortunately, we observed very low significant change in the assay signal after an hour at room temperature, even with 100 nM hPPTase compared to 25 nM Sfp relative to a buffer control (**Figure 2**).We can speculate that the inability of hPPTase to transfer easily into the FRET screen protocol may arise from required sequence specificity not matching the Sfp peptide substrate, a result we have observed for other PPTase enzymes (data not shown). Thus, we sought another method to monitor enzymatic activity.

Design of the activity-based fluorescence polarization assay

We reviewed the literature for methods to monitor PPTase activity; as the enzyme class has seen been a target of interest recently in the infectious disease research community due to

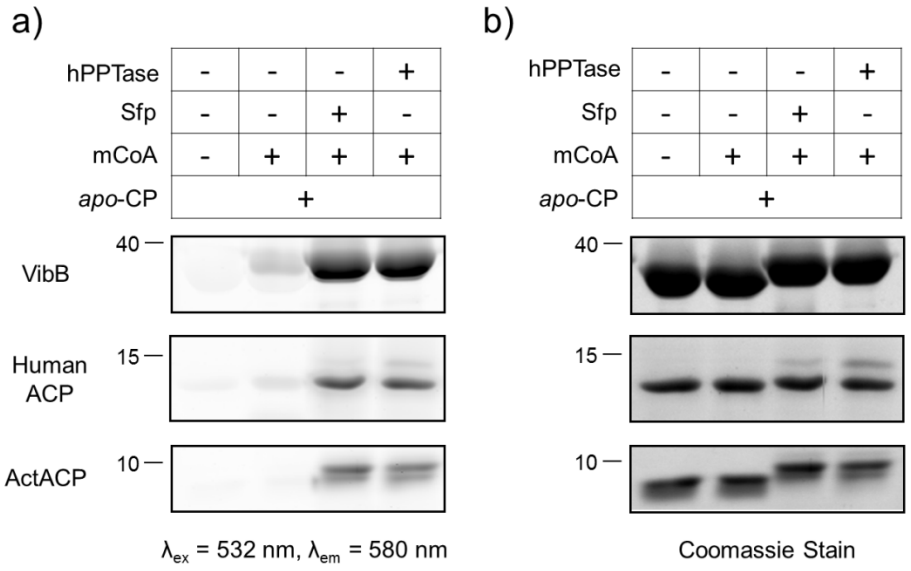

Figure 1. *Gel-based fluorescent carrier protein labeling*. We used SDS-PAGE gel analysis prior to implementing fluorescence polarization techniques to verify that both Sfp and human PPTase (hPPTase) can append rhodamine-CoA (mCoA) to three types of *apo* carrier proteins indicated by fluorescent (**a**) and coomassie (**b**) visualization. VibB represents the peptidyl carrier protein (PCP) from NRPS biosynthesis, human ACP represents fatty acid synthesis (FAS) pathways, and ActACP represents polyketide synthase (PKS) pathways

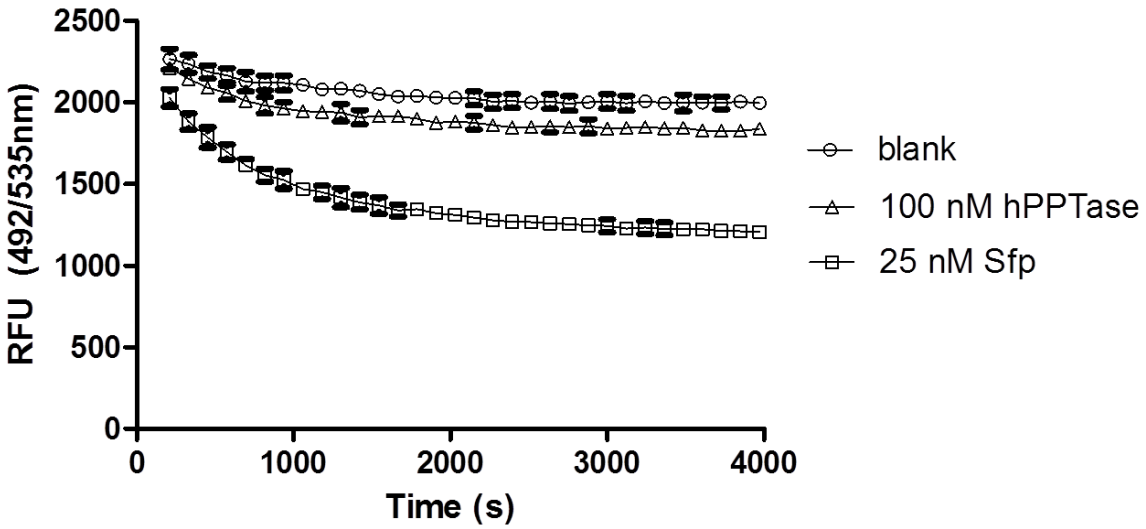

Figure 2. *Human PPTase tested in FRET assay format*. Fluorescein (FITC) conjugated to the minimal peptide Ybbr was subjected to PPTase activity evaluation using standard PPTase reaction conditions, including rhodamine-CoA. Reduction in fluorescent signal for fluorescein indicates rhodamine-pantetheine conjugation, and thus PPTase activity. Human PPTase (hPPTase) possesses poor labeling activity compared to Sfp under these conditions.

implication in virulence.[8-10] While we found numerous methods, we desired a homogenous format free of wash steps that directly monitors the complete landscape of the phosphopantetheinylation reaction without relying on readouts from coupled enzyme systems. These features would simplify the implementation of the method in an automated setting, focus on the bisubstrate phosphopantetheinylation reaction instead of individual substrate binding, and minimize the potential for false positive hits arising through inhibition of coupling partners; characteristics that we required from a finalized protocol. As such, we found the existing methods unsuitable, and envisioned the application of fluorescence polarization (FP) as a technique that could exploit the size difference between the species that phosphopantetheine is attached to in the CoA substrate and *holo*-CP product (**Figure 3**); a feature we have utilized routinely in gel-based PPTase activity detection.[20]

Throughout the development process, we found it important to work with Sfp PPTase since biochemical constants and parameters, as well as orthogonal detection methods already exist for this enzyme. To evaluate the ability of FP to distinguish between the substrate and product species, rhodamine-modified *crypto*- VibB and ActACP, were prepared by reaction with the corresponding rhodamine CoA in the presence of catalytic quantities of Sfp. These two proteins differ by more than 20 kDa in molecular weight, and allowed a comparison in the signal window between the two samples to inform future applications, since the small size of stand-alone CP-domains represents only a 10-fold increase in molecular weight vs. the corresponding CoA substrate. Following purification, these *crypto*-CP samples were used to assemble a series of solutions that contained a constant rhodamine fluorophore concentration, but varied by the degree to which the fluorescent species was attached to the protein; thus mimicking the enzymatic reaction at various states of conversion (**Figure 4**). We also compared the fluorescence polarization signal data for a linear dilution of *crypto*-VibB to its corresponding fluorescent gel densitometry data (**Figure 5**). In evaluating the data, a clear relationship was observed between the fluorescent polarization and densitometry data confirmed the feasibility of FP to detect the attachment of fluorescent phosphopantetheine arms to CP domains.

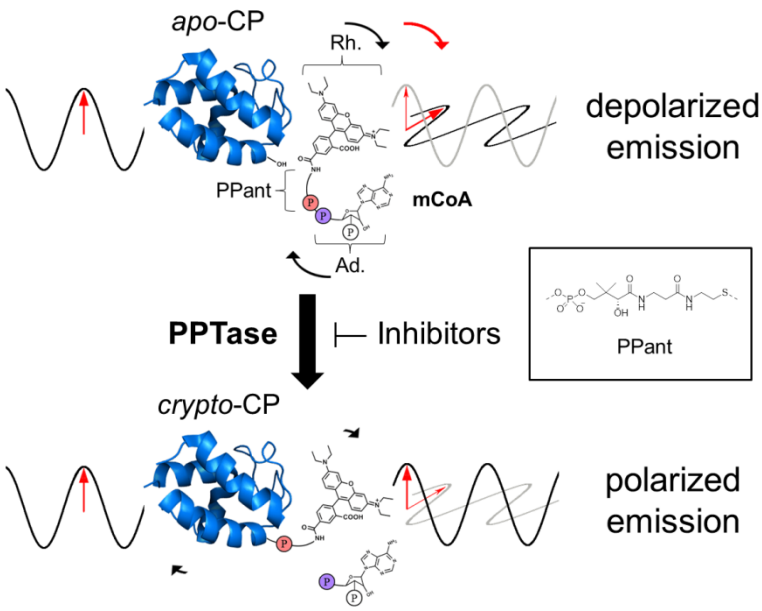

Figure 3. *Measuring PPTase Activity with Fluorescence Polarization*. Free rhodamine-CoA (mCoA) containing rhodamine (Rh.), phophopantetheine (PPant) and adenosine (Ad.) components has its rhodamine-phosphopantetheine moiety transferred from mCoA to the *apo* carrier protein by the PPTase, generating the modified *crypto* carrier protein. The difference in tumbling rates of the unreacted rhodamine-CoA, 1.3 kDa versus bound *crypto*-CP (34 kDa in the case of VibB) due to total complex size creates a stronger polarized signal for bound reaction fluorophore.

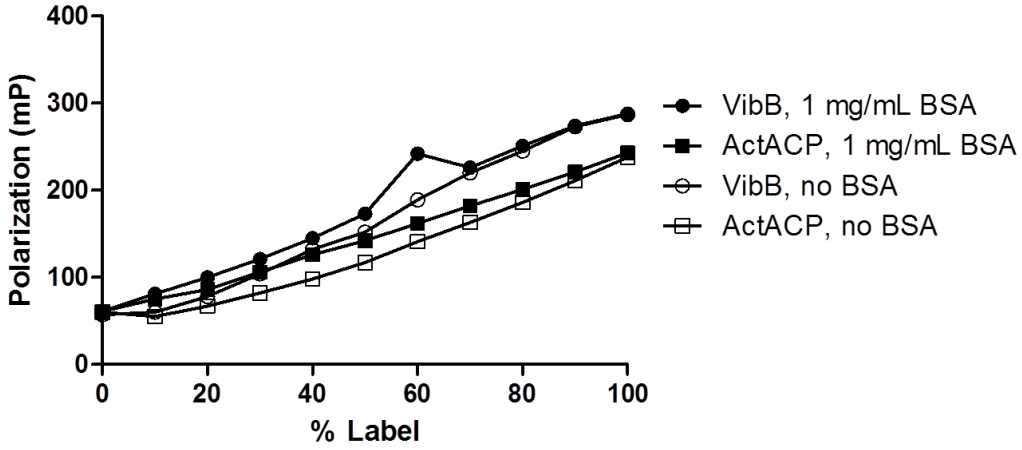

Figure 4. Crypto-VibB & ActACP linear dilution and fluorescence. Complete fluorescently labeled *crypto*- carrier proteins were linearly diluted against unlabeled carrier protein (total carrier protein and probe concentrations constant) to demonstrate that higher amounts of carrier protein labeling corresponds to higher total fluorescent polarization signal. The common enzyme-stabilizing agent bovine serum albumin (BSA) was also determined to not interfere significantly with polarization signal.

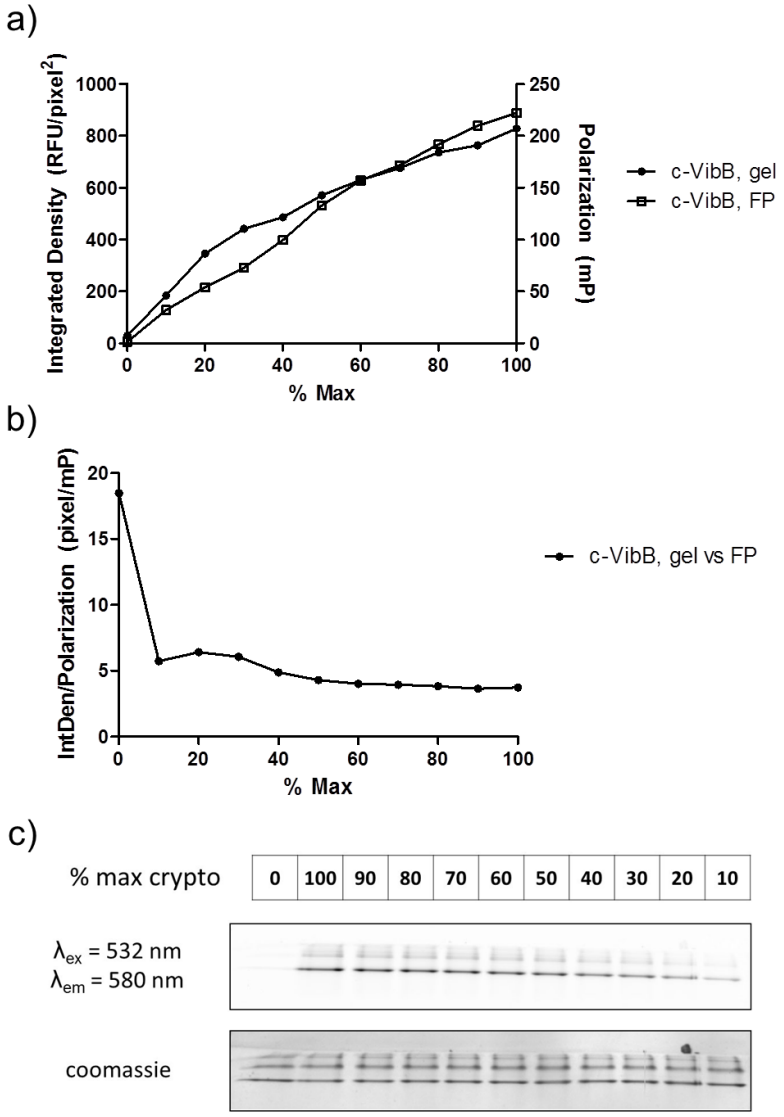

Figure 5. *Crypto-VibB monitoring by polarization vs. gel densitometry*. One particular strength of the fluorescence polarization assay lies in the ability to evaluate fluorescence polarization samples by gel electrophoresis if an EDTA quench is used to halt the reaction prior to analysis. Signal obtained from the same *crypto*-VibB (c-VibB) linear dilution scales with the percentage of labeling (**a**), as well as providing an almost static correlation above 10% labeling (**b**). Reference fluorescent gel imaging depicts the fluorescent intensity change with percent labeling (**c**).

We also evaluated PPTase and rhodamine-CoA association independently of carrier protein, using fluorescence polarization binding methodology instituted previously.[31] Both Sfp and hPPTase demonstrated complete binding curves (**Supplementary Figure 15**), which were used to calculate dissociation constants with **Equations 1 & 2**. Additionally, due to previous reports that Sfp co-purifies with coenzyme A when expressed in *E. coli*,[35] we performed a calf-intestinal phosphatase treatment that resulted in a shift downward in the inflection point of the Sfp binding curve. This result suggests that competing endogenous CoA removal increases binding response to rhodamine-CoA.

Development of the FP-based assay for PPTase

Evaluation of suitability for high-throughput screening applications is an important precursor to large scale implementation of assay formats.[36] HTS suitability is determined via the Z' value calculated using Equation **3**. We analyzed Sfp and hPPTase from 1 to 1000 nM with VibB (**Supplementary Figure 5**) and human ACP (**Supplementary Figure 6**) in order to determine optimal concentrations for assay implementation. The Z' score was calculated throughout the reaction time course to depict Z' data for VibB (**Supplementary Figure 16**) and hACP (**Supplementary Figure 17**) reactions. The lowest satisfactory Z' value for a high-throughput assay is 0.5, whereas values above 0.8 are considered robust.[36] Both Sfp and hPPTase displayed Z' values above 0.6 with concentrations as low as 10 nM at 30 minute time points with VibB. However, Z' values were much lower for both enzymes using hACP, such that Sfp only displayed Z' values near 0.6 with 125 nM and hPPTase only approached Z' = 0.6 at the highest 1000 nM concentration. We present sample Z' data for Sfp and hPPTase at 30 and 60 minute timepoints for VibB (**Supplementary Figure 1**) and hACP (**Supplementary Table 2**). We reason that the lower Z' hACP values result from the significantly smaller molecular weight of hACP at ~ 10 kDa giving lower signal when fluorescently labeled by the rhodamine fluorophore, whereas the larger VibB at ~34 kDa gives higher signal. As such, we decided that the human ACP was not suitable for high-throughput inhibitor evaluation and VibB would be the primary

screening substrate. As a compromise for further evaluation of both carrier proteins, we chose a working enzyme concentration of 100 nM for all other experiments unless otherwise noted.

We evaluated the effect of 0.01% v/v detergents Tween-20, Triton-X 100, NP-40 and 10% DMSO with respect to impact on Z' scoring for PPTases and carrier proteins. PPTases evaluated with VibB (**Supplementary Figure 7**) displayed similar performance at or above Z' scores of 0.6 at 30 minutes for all detergents, with marginally higher Z' scores (**Supplementary Figure 18**) for 0.01% Tween-20. DMSO noticeably lowered Z' scores for both Sfp and hPPTase with VibB, but maintained an acceptable Z' score. However, analysis of hACP with these additives (**Supplementary Figure 8**) once again displayed the lowest Z' scores over time (**Supplementary Figure 19**), only passing an acceptable Z' score of 0.6 without DMSO at approximately 45 minutes. Z' data at fixed timepoints of 30 and 60 minutes are supplied for VibB (**Supplementary Table 3**) and hACP (**Supplementary Table 4**). Since performance in the presence of DMSO is required for convenient inhibitor screening, this result disqualifies hACP for high-throughput screening without further optimization for increased Z' score.

We evaluated pH-sensitivity of Sfp and hPPTase labeling in our experimental format (**Figure 6**) to analyze the flexibility of the assay format with variable enzyme reactions. Both PPTases demonstrated a preference for lower pH using VibB, which corresponds to previous results with Sfp.[37] Upon testing human ACP at varied pH, we noticed the same low-pH preference for Sfp, but hPPTase lost its high activity at lower pH with this carrier protein. We may speculate that this could be due to truncation of the larger multi-domain synthase to a small carrier protein could impact substrate specificity. To maintain consistency with our previous screening work, we chose to conduct our inhibition studies at a pH of 7.6 that provides more biologically-relevant conditions.[33]

Applying known PPTase inhibitors to Sfp and hPPTase in FP assay

We evaluated a panel of inhibitors against the Sfp and human PPTases (**Table 1**). Typically, phosphoadenosine phosphate (PAP) is used as a product inhibitor for PPTase activity

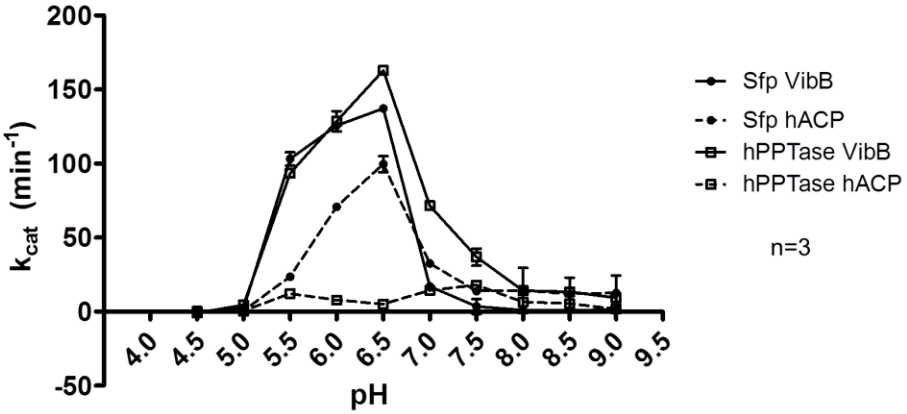

Figure 6. *pH-dependent PPTase activity*. Sfp and hPPTase activities were determined over a broad pH range with both VibB and hACP carrier proteins using rhodamine-CoA. Both PPTases appear to prefer slightly acidic labeling conditions, with the exception of the hPPTase/hACP combination.

Table 1. *Analysis of Sfp-type PPTase standard inhibitors*. We subjected Sfp and human PPTase to inhibitors hits from previous assay formats. The two PPTases both demonstrate inhibition with product inhibition analog 2'-deoxy-phosphoadenosinephosphate (2'-deoxy-PAP) as well as product inhibitor PAP and the competitive inhibitor coenzyme A. The compounds with previously identified Sfp inhibitory activity did not demonstrate any significant inhibition of human PPTase. However, some compounds slightly depressed human PPTase labeling, albeit not enough to calculate IC50 values. "NC" = not calculated.

IC_{50} (μM) - VibB

Compound	Sfp	hPPTase
2'-deoxy-3,5-phosphoadenosine	11 ± 1	51 ± 1
3,5-phosphoadenosine	7 ± 1	6 ± 1
coenzyme A	8 ± 1	14 ± 1
Mitoxantrone 2HCl	Inactive	Inactive
benserazide HCl	Inactive	NC
Bay 11-7085	Activator	Inactive
SCH-202676 HBr	0.2 ± 1	NC
6-nitroso-1,2-benzopyrone	3 ± 1	Inactive
PD 404,182	1 ± 1	Inactive
guanidinyl-naltrindole ditrifluoroacetate	Activator	NC
sanguinarine Cl	10 ± 1	NC
calmidazolium Cl	10 ± 1	Inactive
(-)-ephedrine hemisulfate	Inactive	Inactive

assays. In our case, we began our analysis with the analog 2'-deoxyadenosine-3,5-bisphosphate (2'-deoxy-PAP) (**Supplementary Figure 20a**) due to the ease of synthesis, production cost, and its relatively close IC_{50} to PAP in other adenosine-binding systems such as P2Y receptors.[32] In these experiments, hPPTase proved to be less sensitive to 2'-deoxy-PAP inhibition (IC_{50} = 50 μM) than Sfp (IC_{50} =11 μM). We next compared the effectiveness of the 2'-deoxy-PAP to the natural PAP (**Supplementary Figure 20b**), finding the IC50 values to be similar for Sfp at 7 μM and approximately an order of magnitude lower for hPPTase at 6 μM. This implies that the 2' hydroxyl group is more important in the binding of CoA for hPPTase. Additionally we utilized unlabeled CoA as an inhibitor of the assay because it will directly compete with rhodamine-CoA and the generation of the *holo*-CP will not increase polarization signal like the *crypto*-CP. The observed IC_{50} values for unlabeled CoA displayed for hPPTase and Sfp were close to the active rhodamine-CoA concentrations in the assay **(**14 & 7 μM, respectively), and indicated that both enzymes displayed little preference for natural CoA over the rhodamine-CoA analog.

Finally, we evaluated the ability of this assay to report on a panel of small molecule PPTase inhibitors that were identified from the library of pharmacologically active compounds 1280 (LOPAC^{1280}) when it was screened against Sfp in a FRET assay format.[33] Serial dilutions of these ten compounds were tested against both enzymes at 11 concentration points and the results summarized in **Table 1** (full dose-response curves are presented in **Supplementary Figure 20c-g**). In general, the activity profiles that these compounds displayed against Sfp in the FP assay were consistent with those observed previously in the FRET-based and gel methods, with SCH-202676 and PD 404,182 presenting the most potent inhibition. Interestingly, two compounds, BAY-11-7085 and guanidinyl-naltrindole, were apparent activators of Sfp but not hPPTase in the test. These findings were evaluated further by SDS-PAGE (**Supplementary Figure 22**) and confirmed to increase fluorescent labeling of the carrier protein substrate, but the source of this inhibition discrepancy between assay conditions is unknown.

Given the unusual SCH-202676 inhibition profile of Sfp and hPPTase (**Supplementary Figure 20c**), we further investigated the inhibition effect imparted by SCH-202676. Our initial

investigation of fluorescent labeling in gel format focused on the suspected thiol-reactive mechanism for SCH-202676 proposed previously,[38] and evaluated the presence or absence of additional 1 mM DTT above that which was present in protein preparations during VibB labeling. Gel results match those seen in fluorescent polarization as well as confirming significant inhibition in the case of free Ybbr (**Supplementary Figure 10**). Given the good apparent inhibition of Ybbr labeling in gel format, we also investigated the effect of SCH-202676 inhibiting labeling of ActACP (**Supplementary Figure 11**), with no apparent difference from the VibB results. We also investigated the effect BSA might have in blocking SCH-202676 activity due to its relatively higher concentration compared to PPTase in the reaction mixture, but no significant differences were seen (**Supplementary Figure 12**) compared to the former experiments with BSA. Lastly, we wanted to confirm the mode of potential SCH-202676 modifications with L-cysteine (L-cys) as a model for protein inhibition, and DTT as a model for degradation. We observed the correct 269 m/z for SCH-202676 when incubated at room temperature alone (**Supplementary Figure 13a**). However, incubation of SCH-202676 with one equivalent DTT provided both a clear new HPLC peak at 6.4 min and MS peak with a clear m/z of 271 (**Supplementary Figure 13b**) not present in controls (**Supplementary Figure 14a**), with the mass increase of 2 suggesting an opening of the SCH-202676 thiazole ring proposed previously.[38] We observed a new small HPLC peak at 6 minutes upon incubating with one equivalent of L-cys (**Supplementary Figure 13c**) not present in control with only L-cys (**Supplementary Figure 14b**). These results indicate that SCH-202676 is a fragile inhibitor with regard to standard biochemical reagents, and identifies reducing agents and other free thiols as potential sources of inhibitor interference.

Additionally, we noted that some members of the panel displayed absorbance under the assay conditions, as evaluated the data for signs of perturbation via auto-fluorescence or inner filter effect; two common modes of nonspecific inhibition in FP assays.[39] Evaluation of total intensity[40] (**Supplementary Figure 21**) revealed sanguinarine Cl and mitoxantrone impacted the raw signal at high concentrations; however, only sanguinarine Cl appeared to show inhibitory

activity. We followed up on this with the SDS-PAGE analysis, where sanguinarine Cl displayed inhibitory behavior with Sfp (**Supplementary Figure 22**).

In screening the Sfp inhibitors against hPPTase, we found that hPPTase was generally less susceptible to inhibition, as none of the Sfp LOPAC hit compounds presented IC_{50} values less than 100 μM against hPPTase. These results suggest we can expect a significant difference in inhibitory profiles of PPTase targets evaluated in the future, but presently allows facile detection of potential human side effects while pursuing these pathogenic PPTase drug targets using similar assay conditions.

Conclusion:

We have developed and validated a novel fluorescence polarization PPTase activity assay for high throughput screening of PPTases utilizing fluorescently modified CoA to covalently label intact target *apo*-carrier protein. This assay format improves upon existing PPTase inhibitor screens because it measures actual labeling activity, thereby allowing identification of non-competitive and uncompetitive inhibitors while accommodating variation in the identity of the intact carrier protein and PPTase of interest. Our fluorescence polarization observations of Sfp inhibition activity indicate comparable IC_{50} values to existing FRET and gel-based techniques. Extension of this technique with the inhibitor panel to hPPTase generated notable differences in response compared to Sfp, underlying the necessity of an assay format capable of implementing the appropriate target PPTase and carrier protein directly into the assay for activity comparison. We seek to further extend this assay to various suitable drug target PPTases and scale up screening throughput in collaboration with the NIH Chemical Genomics Center. This new screening methodology furthers development and optimization of new inhibitor drug leads targeting PPTases conferring virulence to human pathogens.

Acknowledgements:

Funding has been provided by NIH R21AI090213, NIH R01GM094924 and NIH R01 GM095970. We thank NIH Chemical Genomics Center (NCGC) for supplying LOPAC Sfp chemical inhibitors and human ACP plasmid, Udo Oppermann (Structural Genomics Consortorium, Oxford University) for gifting the human PPTase-containing plasmid, Susan Taylor Laboratory (UCSD) and Joe Noel (Salk Institute) for access to Tecan instruments for polarization measurements, Haydn Er Jun Cheng (UCSD) for synthesis of rhodamine-maleimide intermediate, Joris Beld (USCD) for performing LC/ESI-MS, and Mass Spectrometry Facility (UCSD) for performing ESI-MS & HR-MS analysis.

Supplementary Information

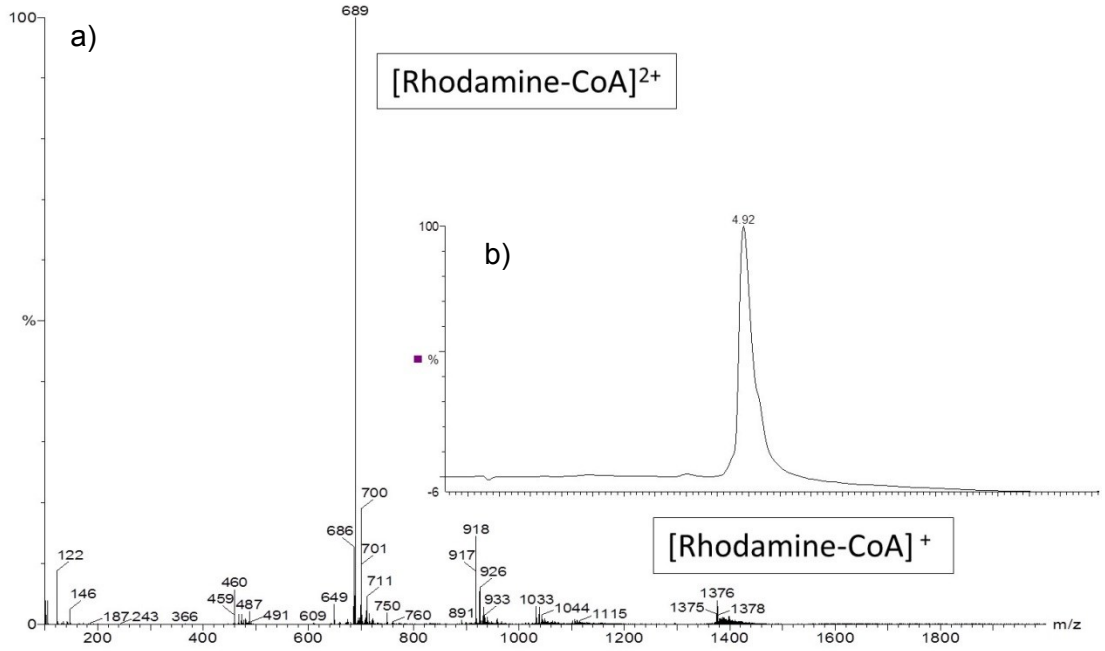

Supplementary Figure 1. *Rhodamine-CoA LC/ESI-MS evaluation*. Rhodamine-CoA substrate was evaluated for purity and correct mass prior to validation in the fluorescence polarization activity assay. Mass spectrometer analysis (**a**) indicates both single and double charged rhodamine-CoA of the appropriate mass, while the HPLC chromatograph (**b**) indicates a predominant single product peak.

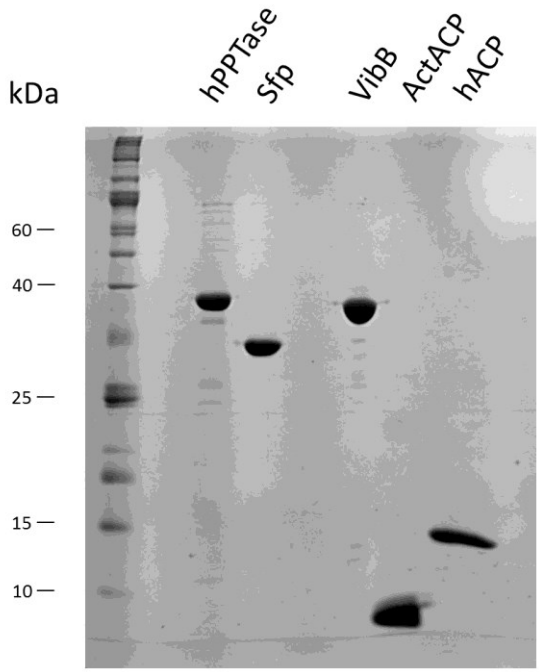

Supplementary Figure 2. *PPTase and carrier protein purity evaluation*. Proteins used in fluorescence polarization activity assay were purified using Ni-NTA resin. Human ACP was additionally subjected to size exclusion chromatography. Final protein stocks were sufficiently pure for assay purposes, as indicated by SDS-PAGE analysis.

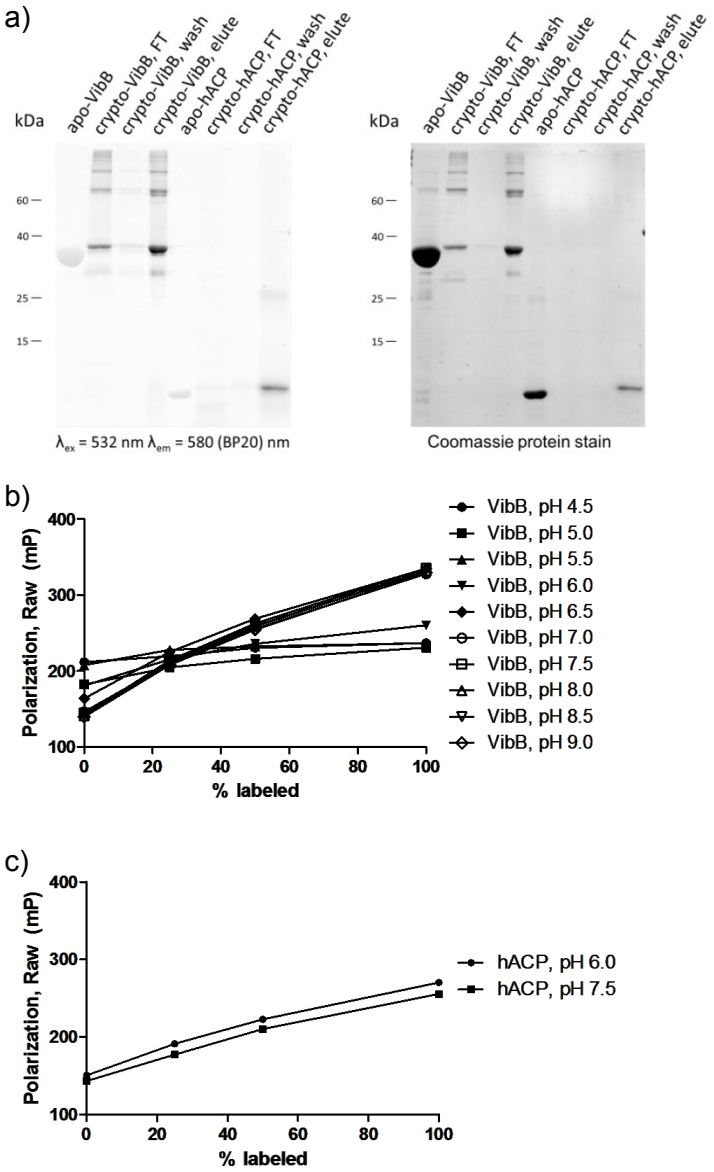

Supplementary Figure 3. *PPTase pH activity crypto- carrier protein standards***.** Fluorescent image and coomassie stain were conducted on *crypto*- carrier protein standards (**a**), following Ni-NTA resin purification (FT = flow through, wash = 10 mM imidazole in lysis buffer, elute = 300 mM imidazole in lysis buffer). *Crypto*-VibB standards were implemented over all pH conditions evaluated (**b**), due to an observed shift in polarization at more acidic pH conditions (pH 4.5-6.0). *Crypto*-hACP standard was found to behave similarly at pH 6.0 and 7.5, and these two standard curves were used for the purposes of calculating activity (**c**).

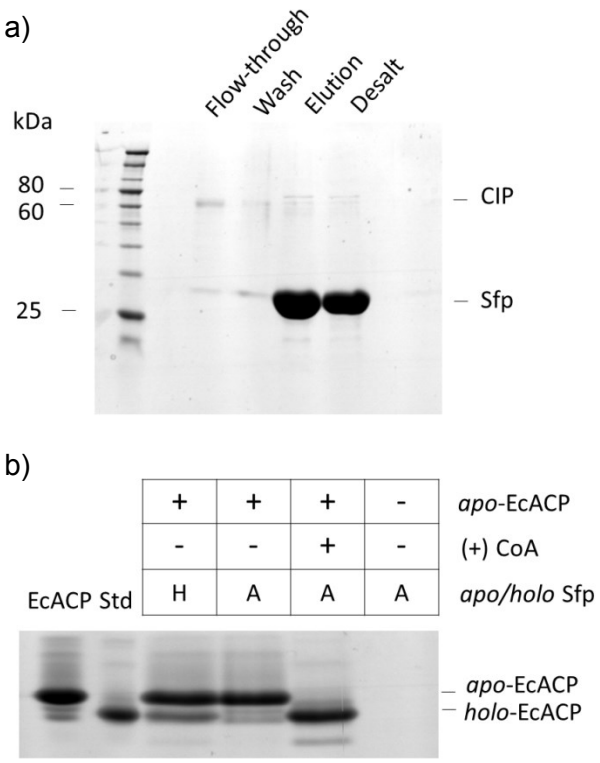

Supplementary Figure 4. *Sfp coenzyme A removal by calf intestinal phosphatase*. Sfp was treated with calf intestinal phosphatase (CIP) to generate *apo*-Sfp, re-purified with Ni-NTA chromatography and analyzed with SDS-PAGE to evaluate purity (**a**). In order to evaluate removal of coenzyme A from the stock Sfp preparation (*holo*-Sfp), both *holo*- and *apo*-Sfp were incubated in reaction conditions with *apo*-ACP from *E. coli* in the absence or presence of additional coenzyme A. Urea-PAGE analysis (**b**) reveals that the CIP treated *apo*-Sfp produces much less *holo*-ACP than the untreated *holo*-Sfp.

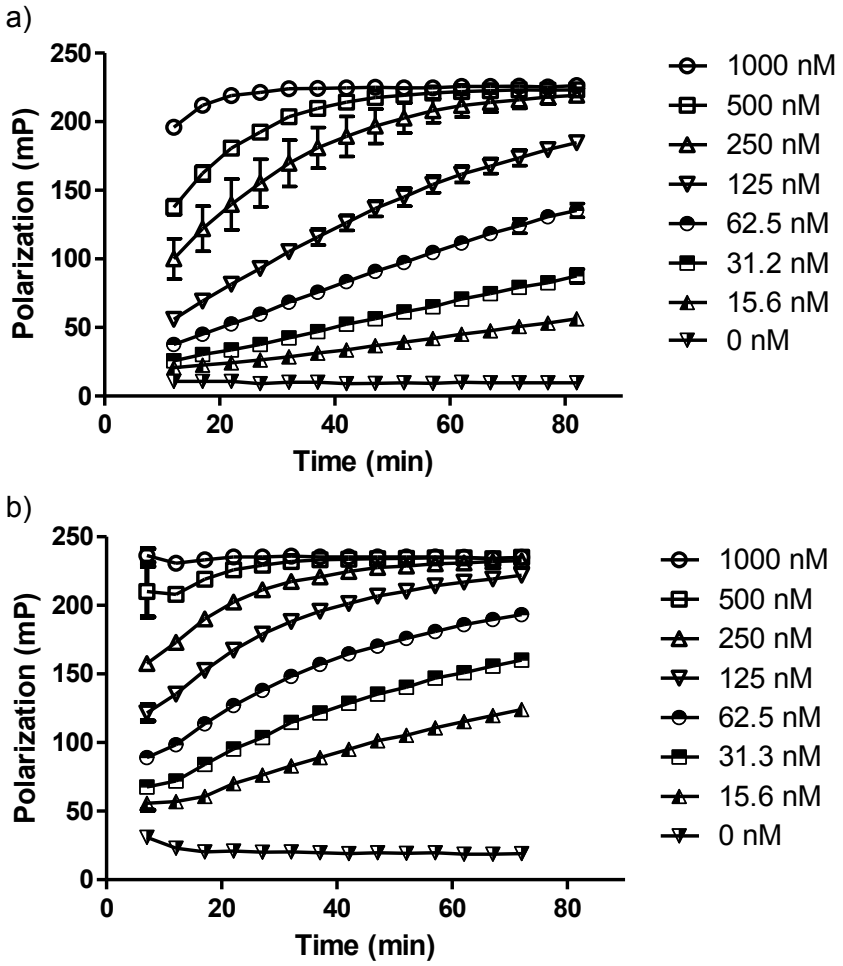

Supplementary Figure 5. *PPTase serial dilution activity assay with VibB carrier protein for Z' calculations*. Serial dilutions of PPTases Sfp (**a**) and human PPTase (**b**) with VibB subjected to fluorescence polarization kinetic analysis provide insight into optimal time and concentration parameters for high-throughput inhibitor evaluations.

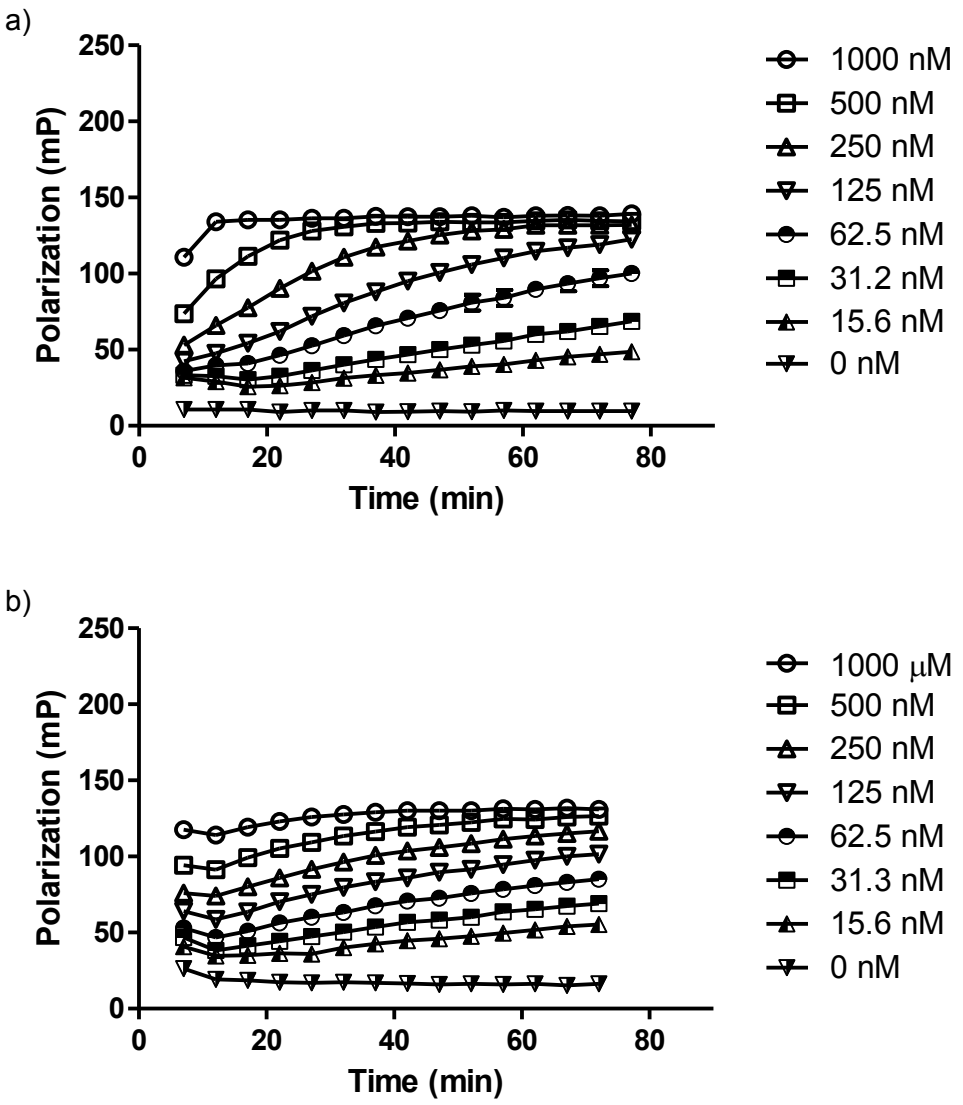

Supplementary Figure 6. *PPTase serial dilution activity assay with human acyl carrier protein for Z' calculations*. Serial dilutions of PPTases Sfp (a) and human PPTase (b) with human ACP subjected to fluorescence polarization kinetic analysis provide insight into optimal time and concentration parameters for high-throughput inhibitor evaluations.

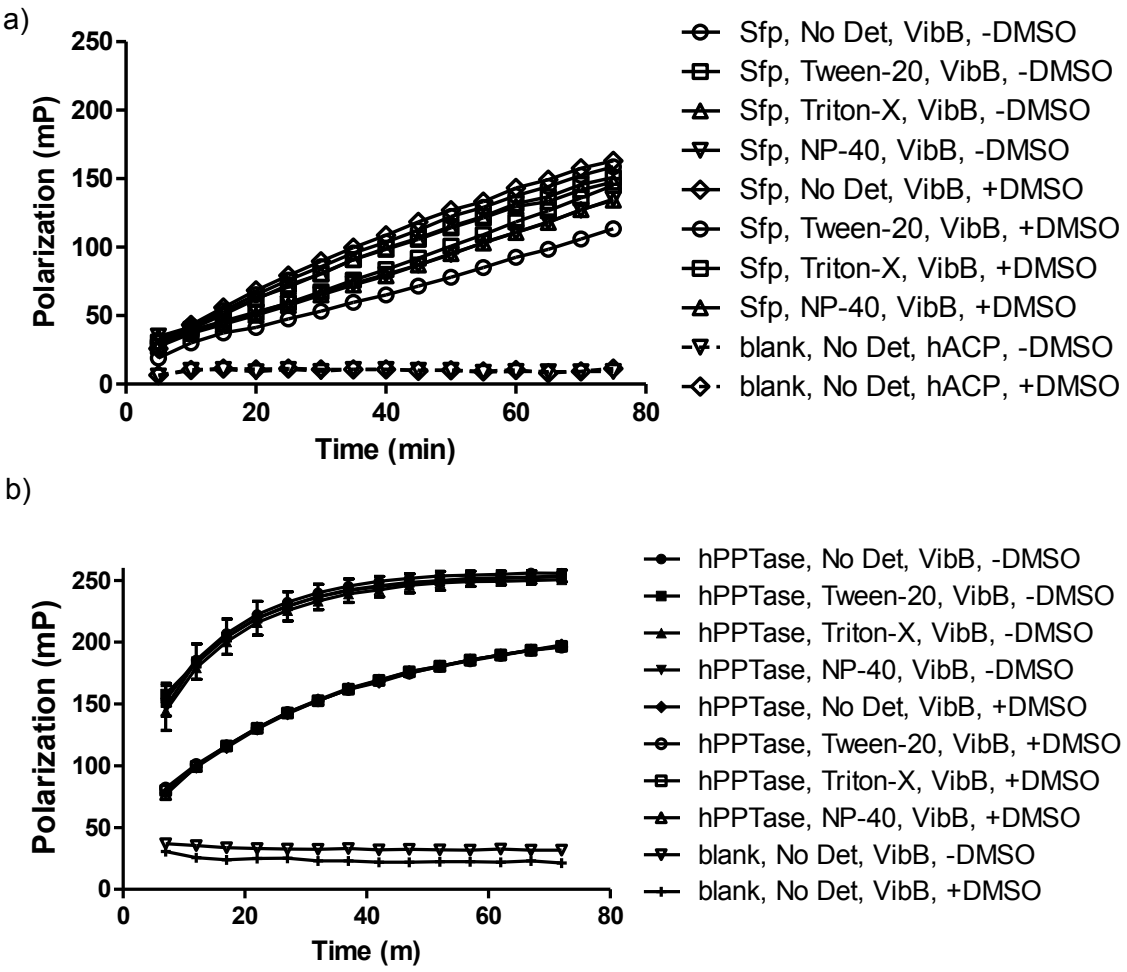

Supplementary Figure 7. *PPTase activity assays with VibB carrier protein and additives for Z' calculations*. Treatments of PPTases Sfp (**a**) and human PPTase (**b**) with VibB and common HTS additives (detergent and DMSO) subjected to fluorescence polarization kinetic analysis provide insight into optimal assay conditions.

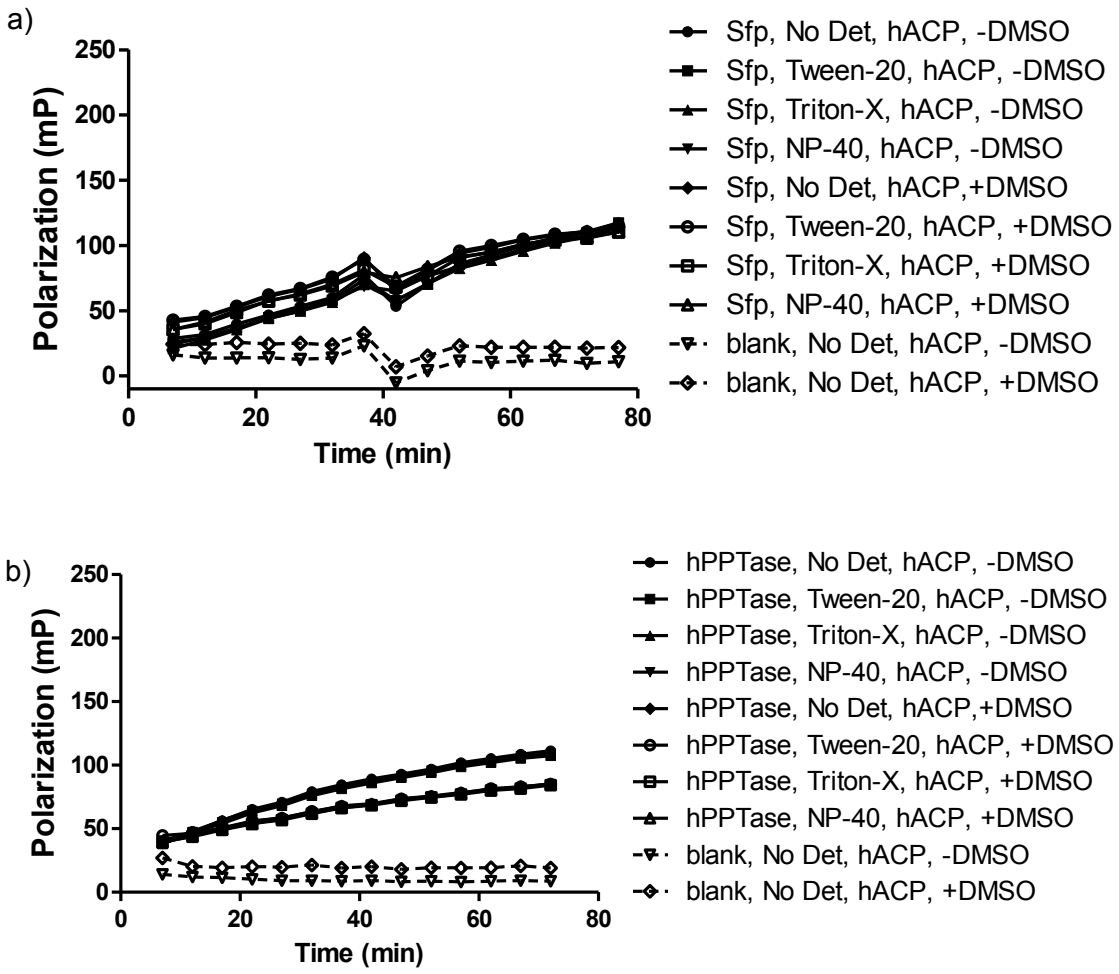

Supplementary Figure 8. *PPTase activity assays with human acyl carrier protein and additives for Z' calculations*. Treatments of PPTases Sfp (**a**) and human PPTase (**b**) with human ACP and common HTS additives (detergent and DMSO) subjected to fluorescence polarization kinetic analysis provide insight into optimal assay conditions.

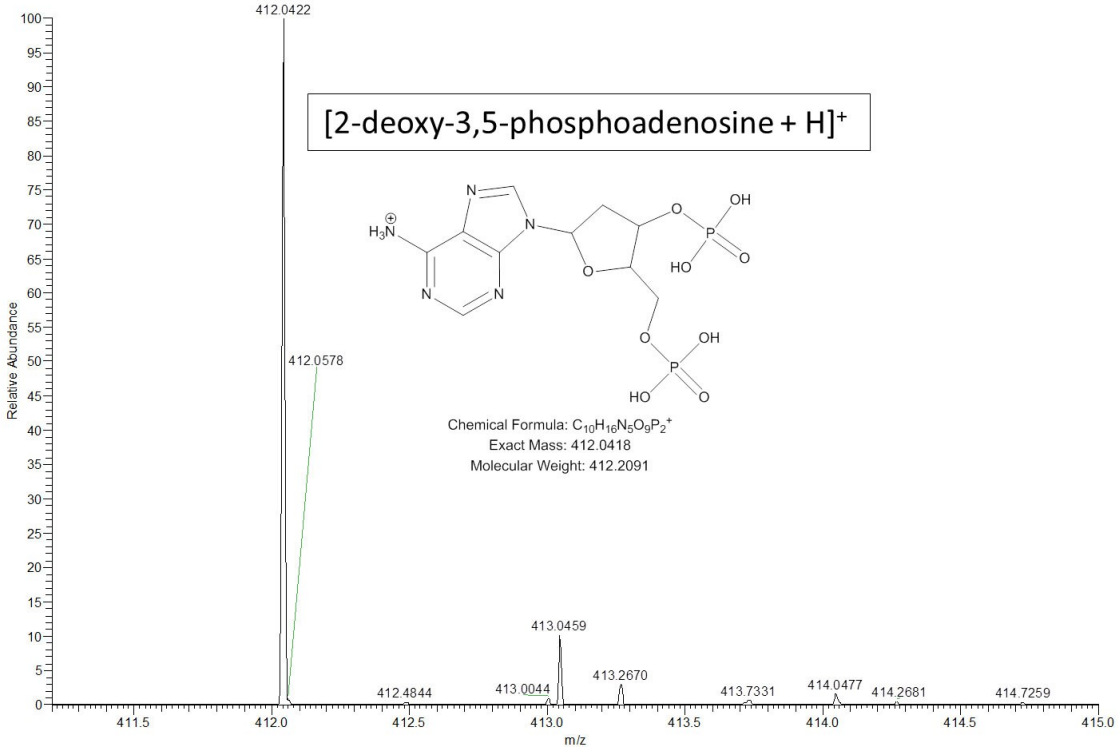

Supplementary Figure 9. *2'-deoxy-3,5-phosphoadenosine MS evaluation*. PPTase inhibitor standard was synthesized, purified, and subjected to mass spectrometric analysis to confirm desired product mass prior to implementation in the fluorescence polarization assay.

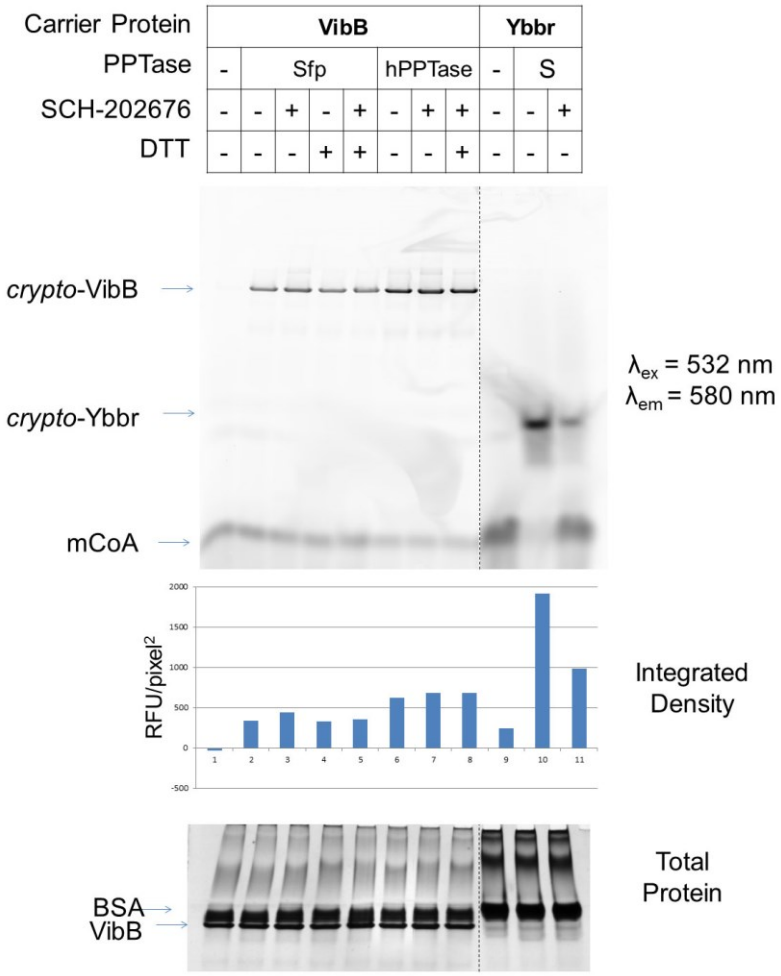

Supplementary Figure 10. *SCH-202676 gel evaluation with VibB vs. DTT (+) BSA*. SCH-202676 compound was evaluated for PPTase inhibition in gel format with Urea-PAGE to confirm fluorescence polarization findings. SCH-202676 did not appear to efficiently inhibit either Sfp or hPPTase when labeling VibB, regardless of 1 mM DTT addition. SCH-202676 did appear to inhibit Sfp activity with Ybbr substrate, judging by the relative drop in fluorescent band intensity evaluated with gel densitometry.

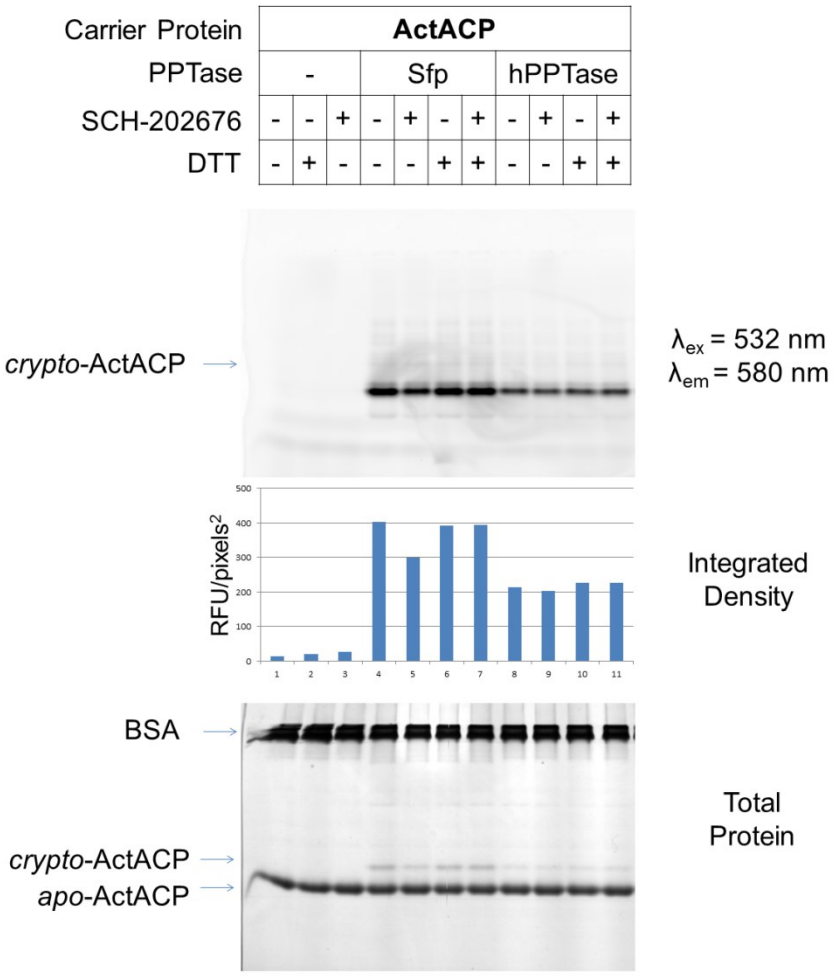

Supplementary Figure 11. *SCH-202676 gel evaluation with ActACP vs. DTT (+) BSA*. SCH-202676 compound was evaluated for PPTase inhibition in gel format with Urea-PAGE to confirm fluorescence polarization findings. SCH-202676 only marginally inhibited Sfp when labeling ActACP, with recovered activity in the presence of 1 mM DTT. SCH-202676 did not appear to inhibit hPPTase.

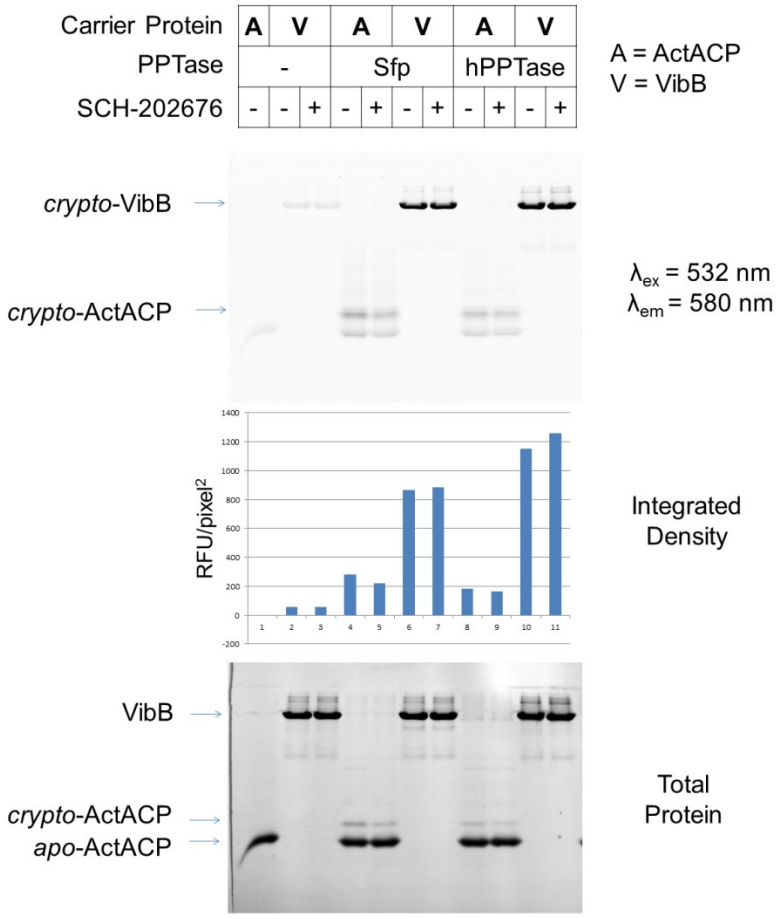

Supplementary Figure 12. *SCH-202676 gel evaluation with VibB/ActACP vs. DTT (-) BSA*. SCH-202676 compound was evaluated for PPTase inhibition with desalted protein to ensure removal of trace DTT from protein stocks. Enzyme reactions were run on Urea-PAGE. SCH-202676 only marginally inhibited Sfp when labeling ActACP, and did not appear to affect VibB labeling. SCH-202676 did not appear to inhibit hPPTase.

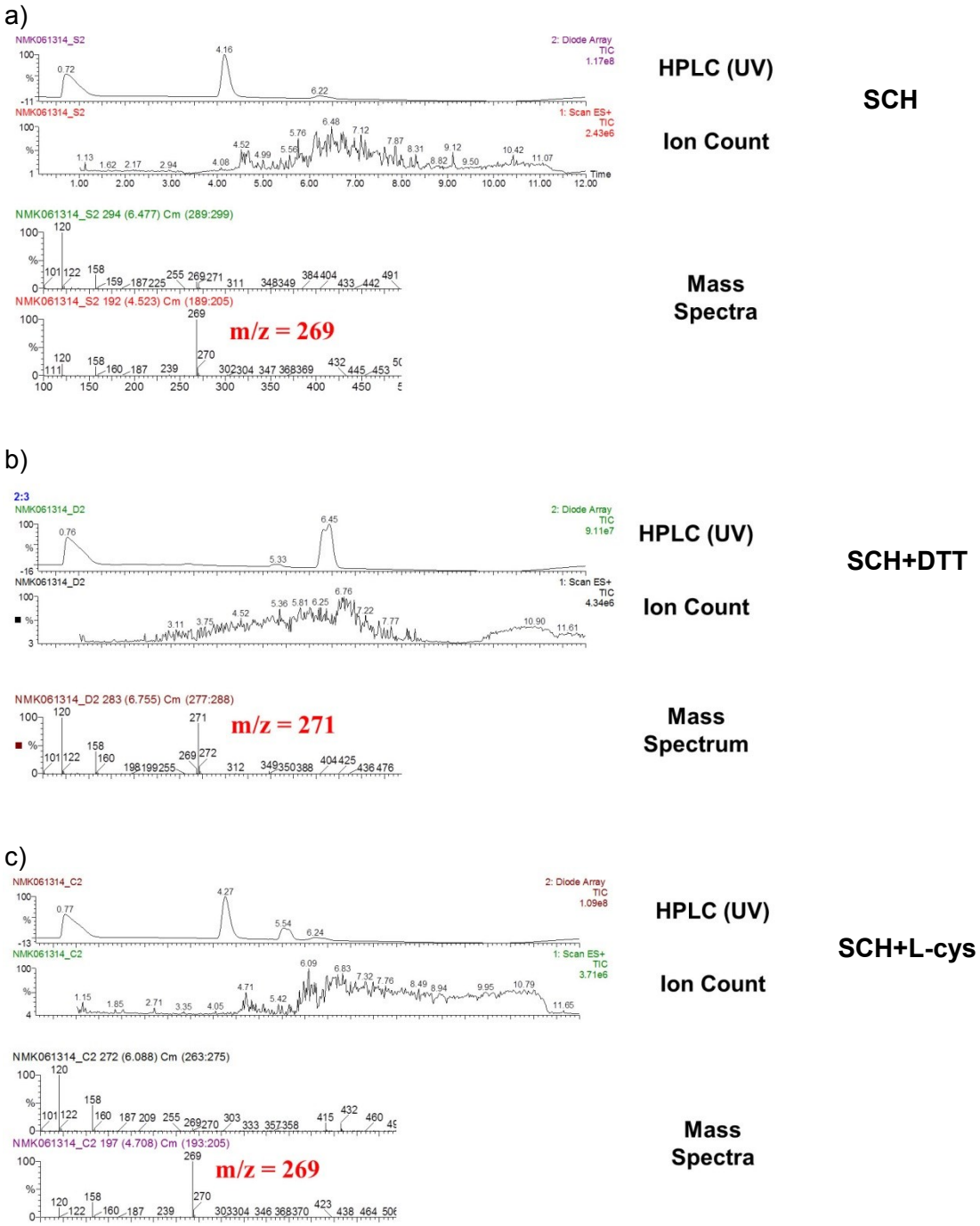

Supplementary Figure 13. *SCH-202676 DTT/L-cys incubation & LC/ESI-MS*. SCH-202676 (SCH) was incubated for 3 hours alone (**a**) or in the presence of DTT (**b**), or L-cysteine (**c**) to gauge the propensity towards modification by thiols. Incubation with DTT introduces a dramatic change in HPLC retention time, as well as a mass increase of 2. Incubation with L-cysteine or alone introduces no change in mass.

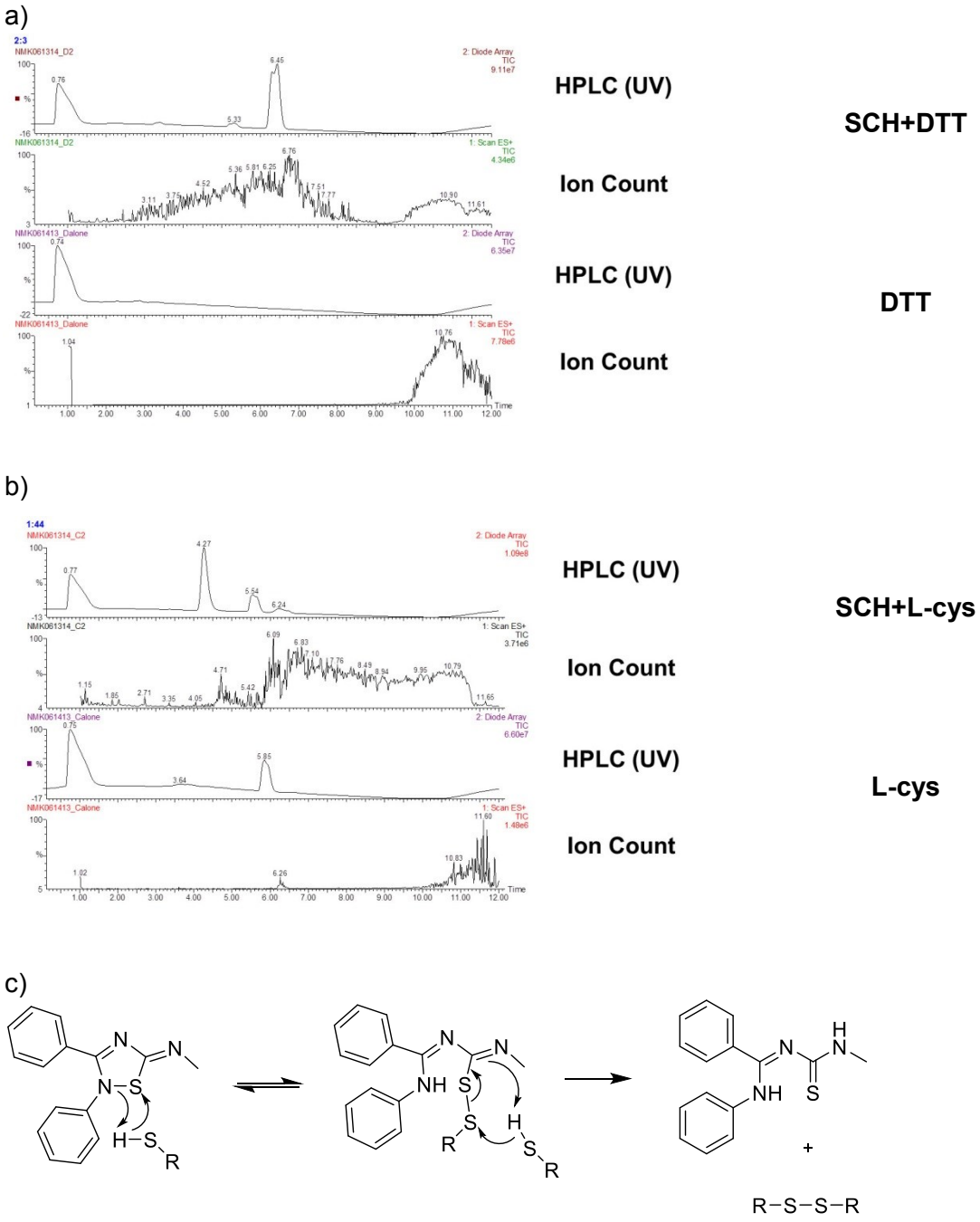

Supplementary Figure 14. *DTT/L-cys controls LC/ESI-MS*. The new peak resulting from SCH-202676 (SCH) incubation with DTT for 3 hours is not present in just DTT (**a**). However, the new HPLC peak observed with L-cysteine incubation is likely due to L-cysteine absorbance seen in the control (**b**). The probable cause for SCH-202676 modification is a previously proposed[38] thiol-mediated ring-opening (**c**), likely accelerated by the DTT possessing two free thiols to facilitate an intramolecular reaction in the terminal ring-opening.

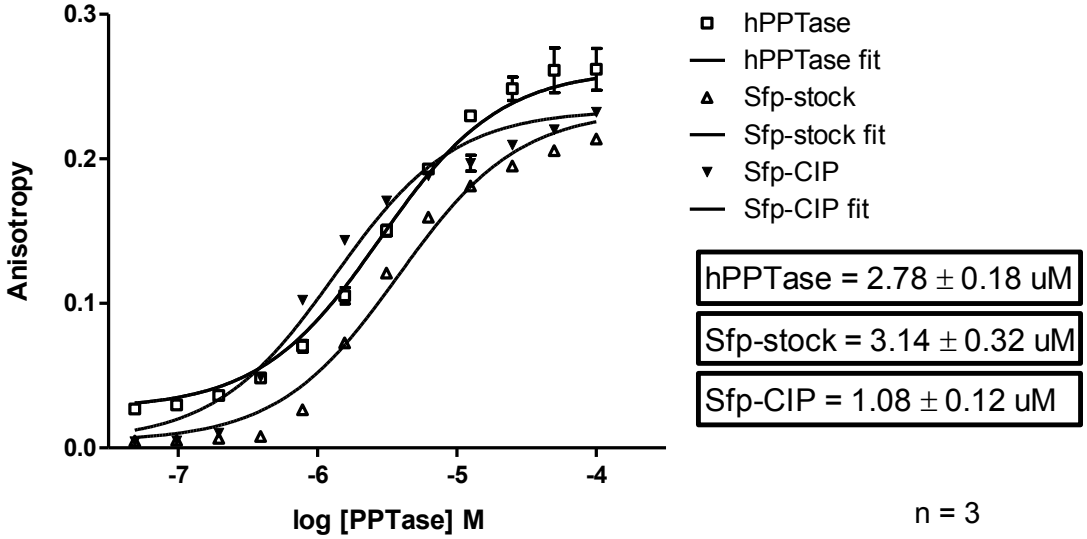

Supplementary Figure 15. *Measuring rhodamine-CoA substrate binding with fluorescence polarization*. Fluorescent polarization was used to analyze binding of rhodamine-CoA to Sfp and human PPTase (hPPTase) in the absence of carrier protein substrate. An additional sample of Sfp was treated with calf-intestinal phosphatase (CIP) and re-purified to remove pre-bound coenzyme A from the protein preparation. The stoichiometric point shift qualitatively indicates the presence of coenzyme A in the initial Sfp preparation.

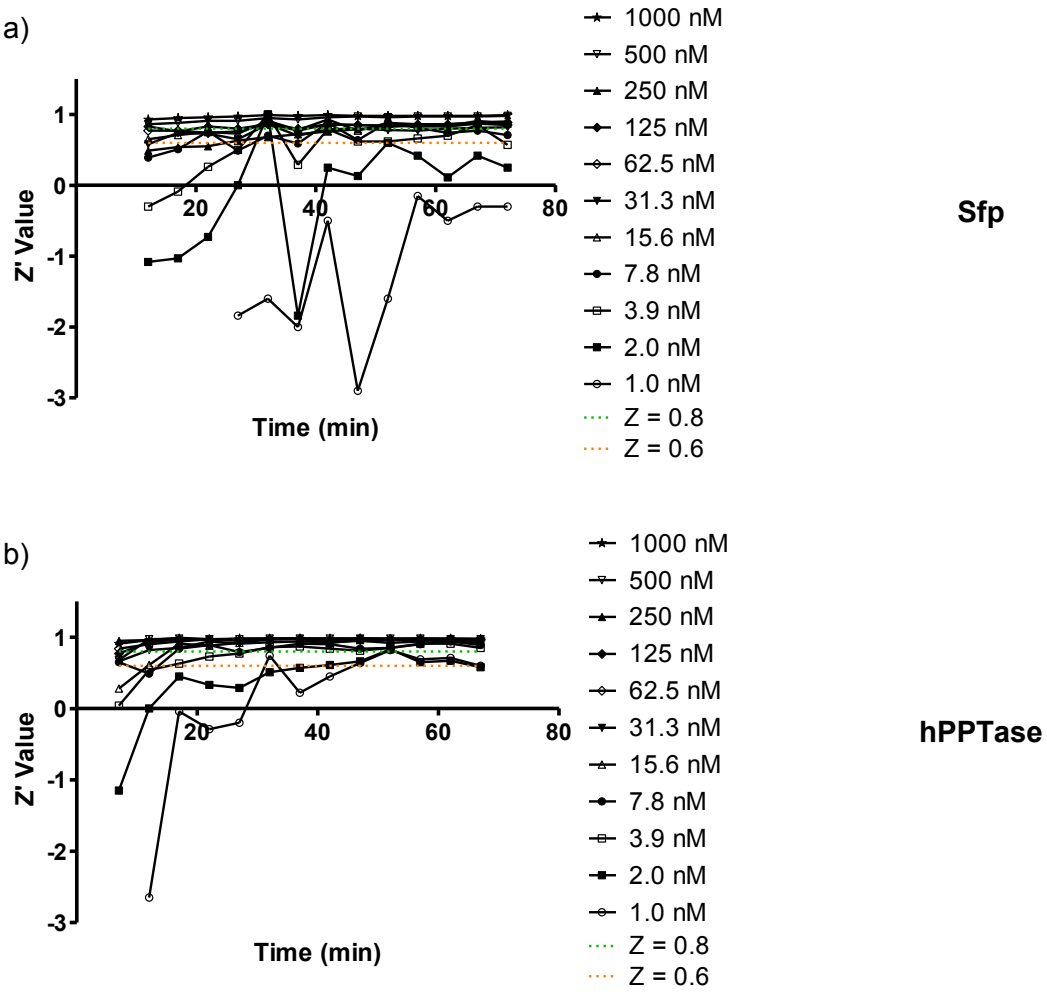

Supplementary Figure 16. *FP: PPTase serial dilution vs. VibB, Z' scores over time***.** Sfp and hPPTase serial dilutions were monitored for VibB labeling over time in fluorescence polarization format, and analyzed for assay suitability via Z' calculations. Lower concentrations of both Sfp and hPPTase at earlier timepoints did not give suitable Z' values at early time points, but with increased time or concentration provided optimal Z' values.

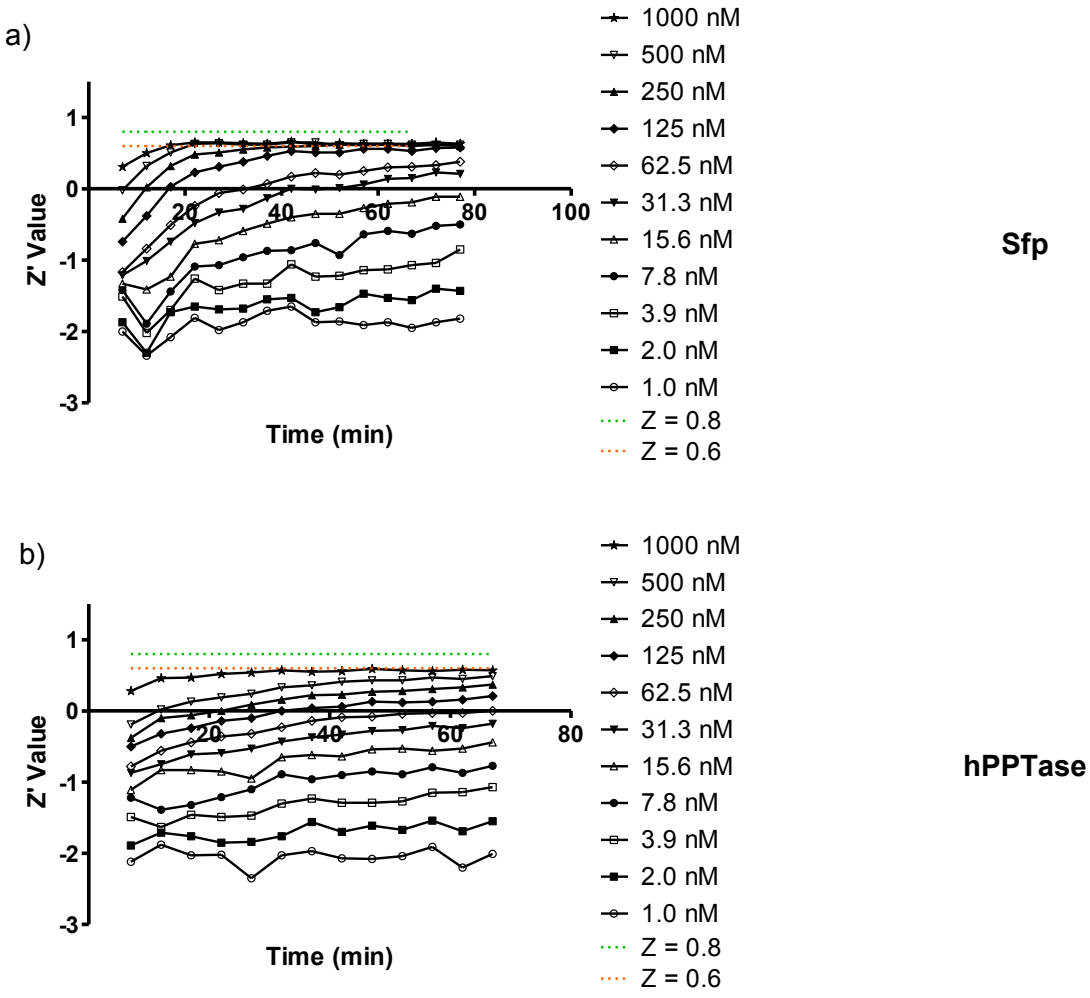

Supplementary Figure 17. *FP: PPTase serial dilution vs. hACP, Z' scores over time***.** Sfp and hPPTase serial dilutions were monitored for hACP labeling over time in fluorescence polarization format, and analyzed for assay suitability via Z' calculations. Only the highest concentrations at later timepoints gave suitable Z' values, but overall we determined that hACP was not a suitable substrate for high-throughput screening.

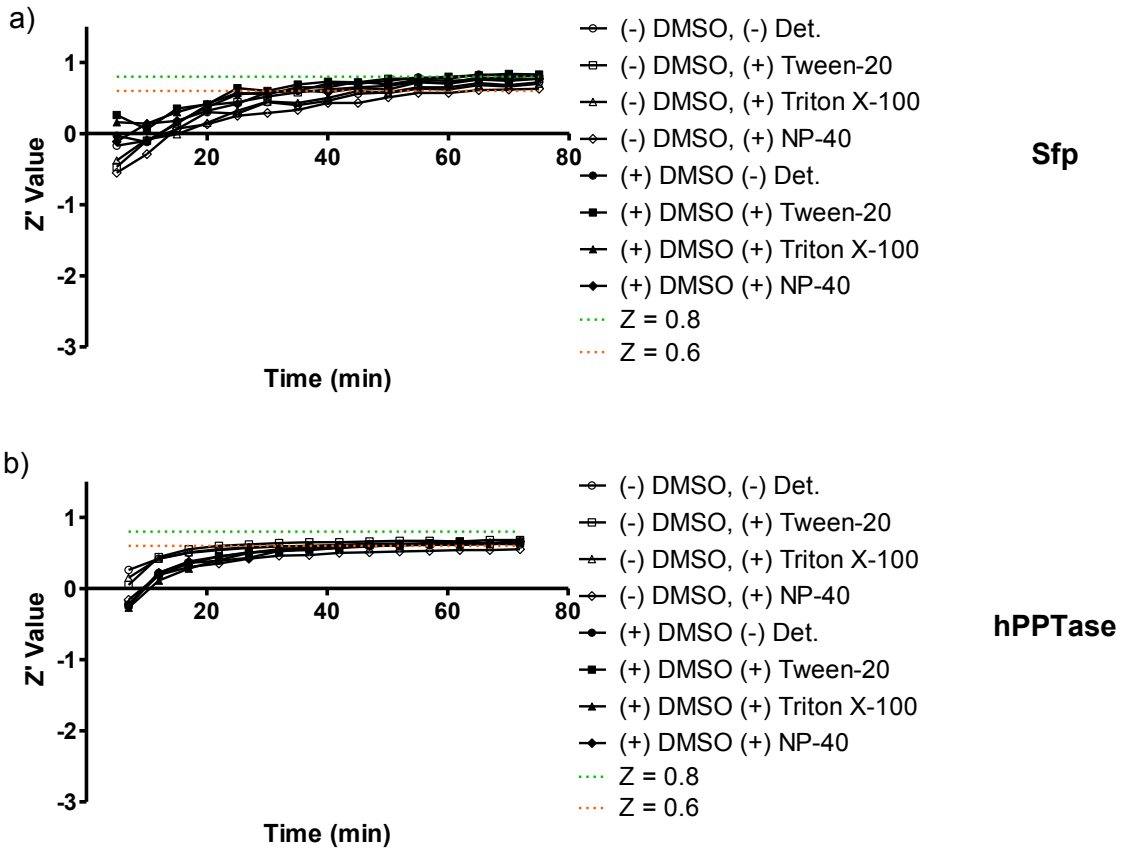

Supplementary Figure 18. *FP: PPTase + additives vs. VibB, Z' scores over time*. Sfp and hPPTase with additives were monitored for VibB labeling over time in fluorescence polarization format, and analyzed for assay suitability via Z' calculations. Detergents contributed slightly to higher Z' values, while DMSO lowered Z' values. Increased reaction time raised calculated Z' values to acceptable levels for both enzymes.

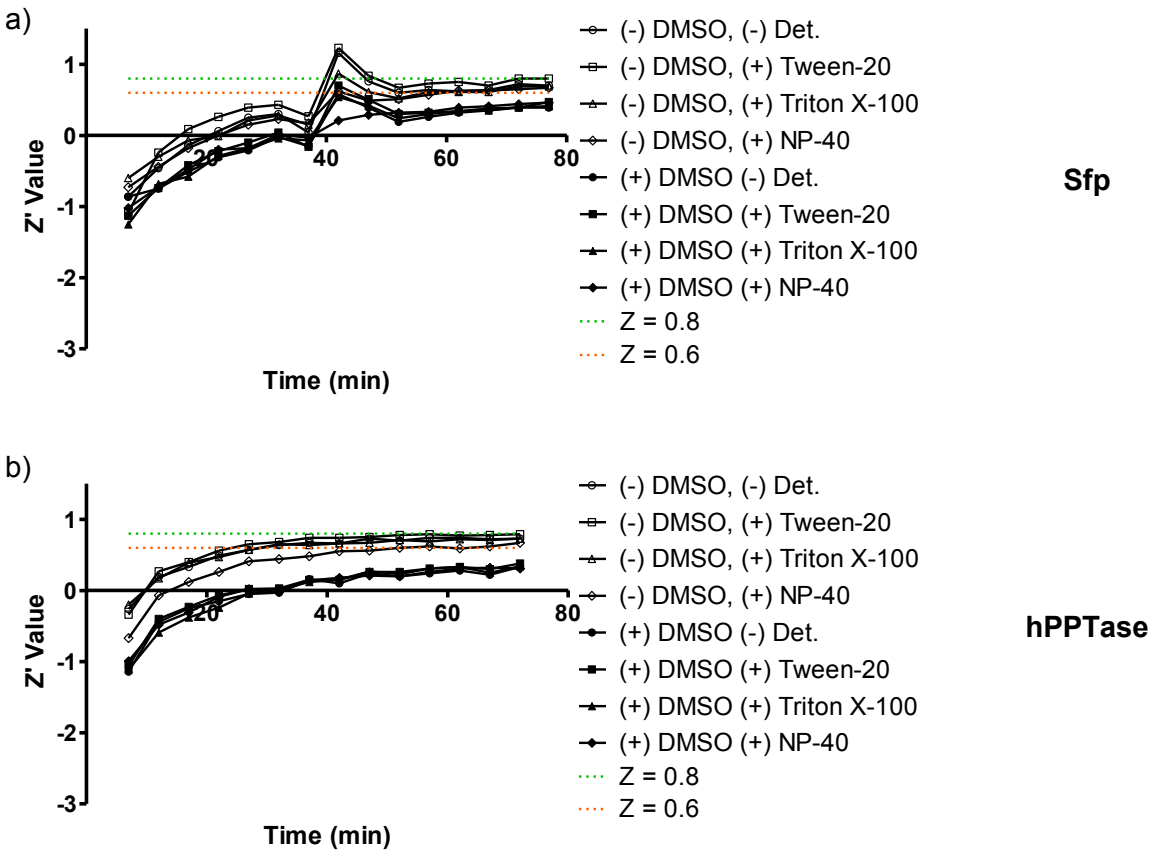

Supplementary Figure 19. *FP: PPTase + additives vs. hACP, Z' scores over time*. Sfp and hPPTase with additives were monitored for hACP labeling over time in fluorescence polarization format, and analyzed for assay suitability via Z' calculations. Detergents contributed slightly to higher Z' values, while DMSO lowered Z' values. Acceptable Z' values were only achieved in the absence of DMSO, which precludes high throughput inhibitor screening with DMSO as a chemical shuttle.

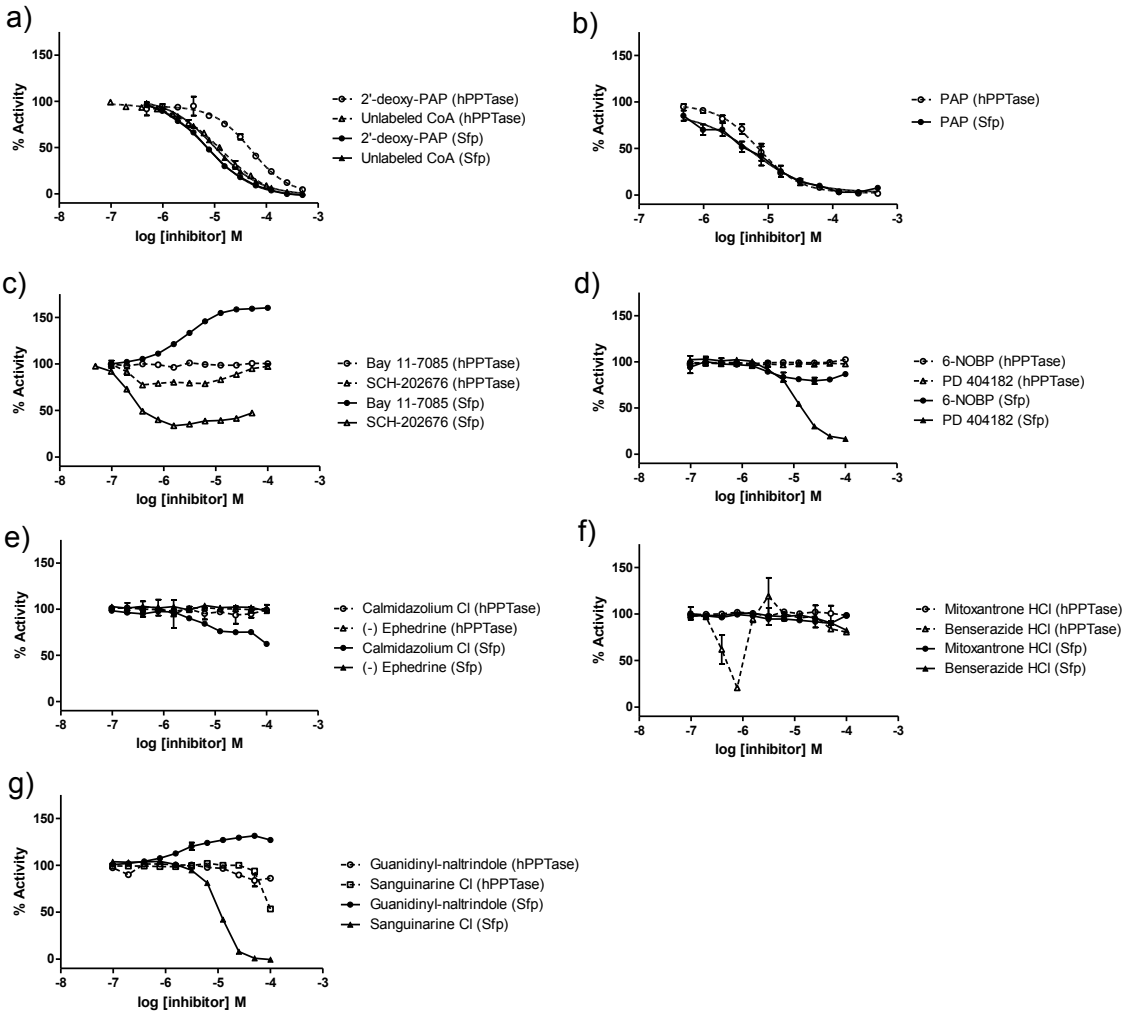

Supplementary Figure 20. *FP: PPTase inhibitors vs. VibB*. In evaluating Sfp and human PPTase, we evaluated standard inhibitors (**a** & **b**), as well as previously identified Sfp-type inhibitor hits (**c**-**g**). Human PPTase demonstrates very low susceptibility to inhibitors of Sfp.

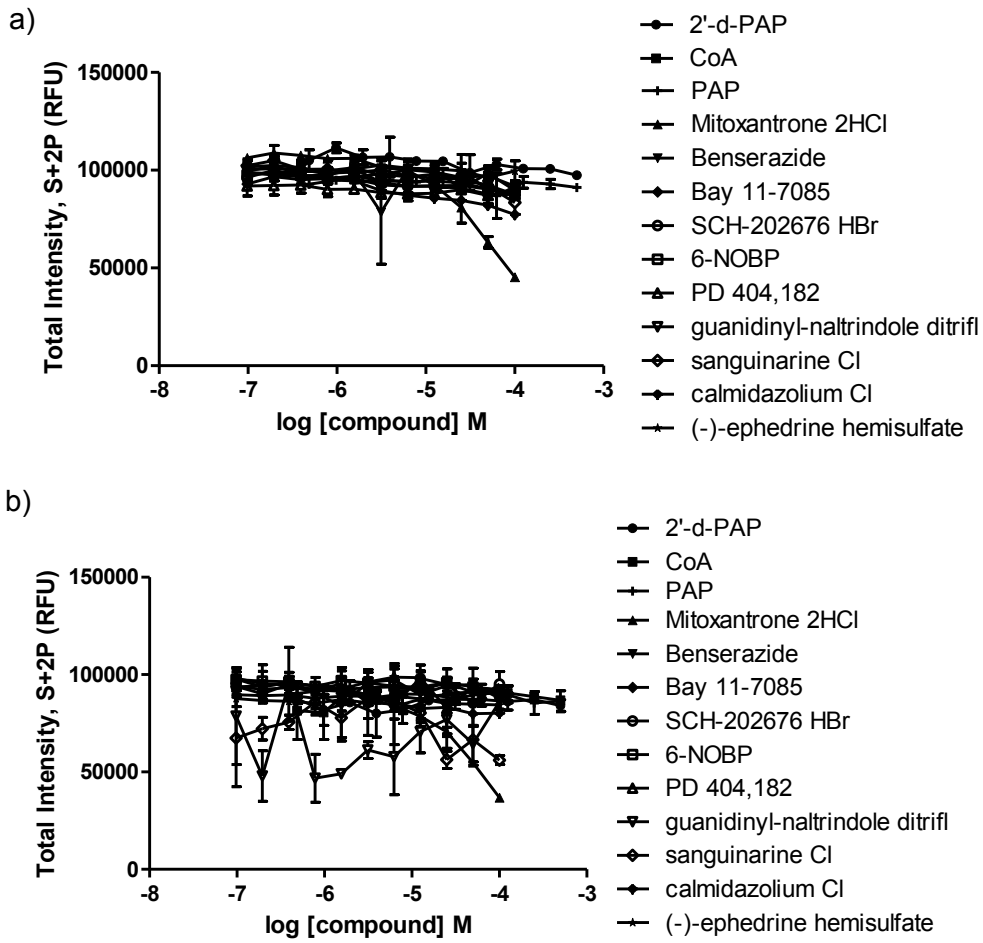

Supplementary Figure 21. *FP: Intensity analysis of PPTase inhibitor screening***.** Sfp inhibitor screening resulted in fairly consistent total intensities (**a**), with the exception of mitoxantrone exhibiting absorbance. hPPTase inhibitor screening evaluation (**b**) showed matching trends with Sfp intensities.

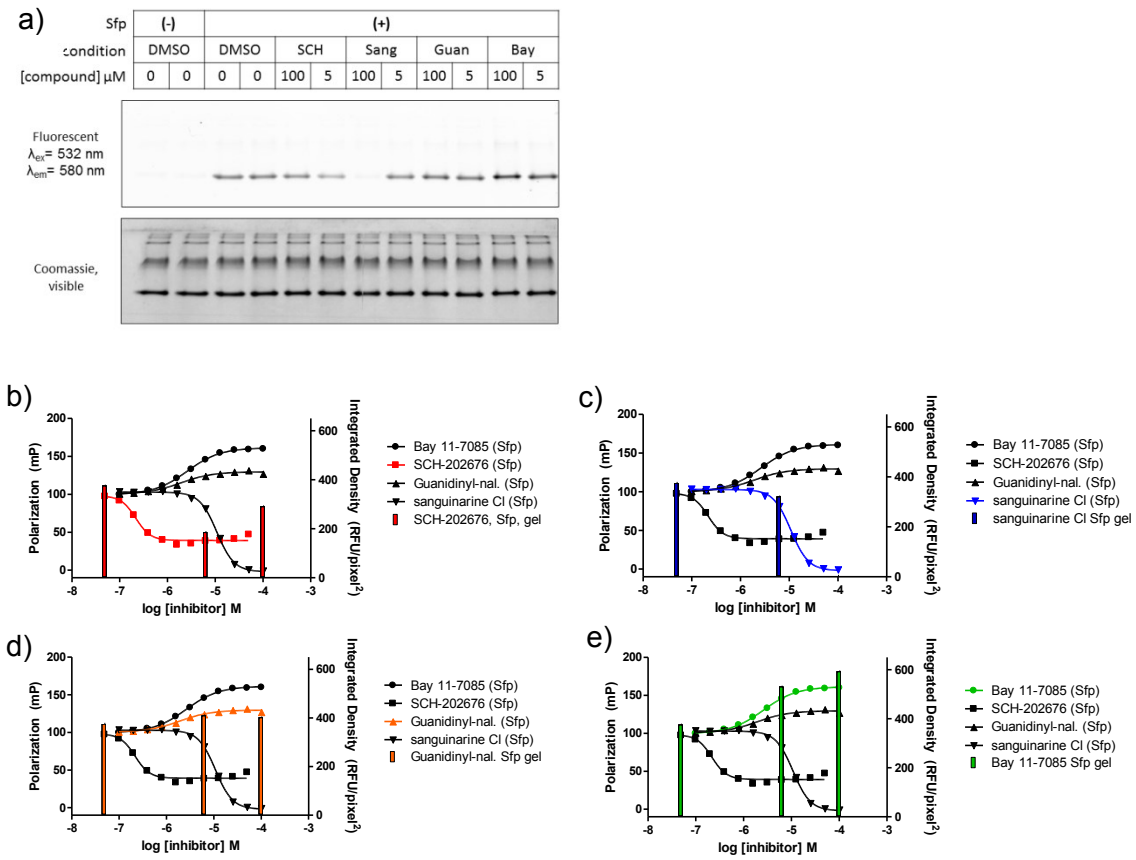

Supplementary Figure 22. *SDS-PAGE analysis of select Sfp-LOPAC compounds*. Select Sfp inhibitors were evaluated in gel format (**a**) to confirm inhibition and activation. Compounds were selected due to: incomplete inhibition of SCH-202676 (**b**), colored compound sanguinarine Cl (**c**), and apparent activation of Guanidinyl-naltrindole (**d**) and Bay 11-7085 (**e**). All gel results qualitatively matched fluorescence polarization results, as gauged by comparison of integrated density compared to polarization.

Supplementary Table 1. *PPTase serial dilution Z' calculations with VibB carrier protein*. Sfp (**a**) and hPPTase (**b**) serial dilution signals measured in millipolarization units (mP) were monitored for VibB labeling over time (30 and 60 minute time points portrayed) in fluorescence polarization format, and analyzed for assay suitability via Z' calculations. Lower concentrations of both Sfp and hPPTase at earlier time points did not give suitable Z' values at early time points, but with increased time or enzyme concentration provided optimal Z' values.

a)

[Sfp] nM:	1000	500	250	125	62.5	31.25	15.63
Avg mP (30 m)	224 ± 1	204 ± 4	170 ± 17	105 ± 5	68 ± 3	42 ± 2	29 ± 1
Z' (30 m)	**0.99**	**0.95**	**0.68**	**0.86**	**0.87**	**0.86**	**0.91**
Avg mP (60 m)	226 ± 1	222 ± 1	212 ± 8	162 ± 6	112 ± 5	71 ± 3	45 ± 1
Z' (60 m)	**0.98**	**0.97**	**0.86**	**0.86**	**0.83**	**0.80**	**0.83**

b)

[hPPTase] nM:	1000	500	250	125	62.5	31.25	15.63
Avg mP (30 m)	236 ± 1	232 ± 1	217± 1	188 ± 1	148 ± 1	115 ± 2	83 ± 0
Z' (30 m)	**0.98**	**0.98**	**0.98**	**0.97**	**0.97**	**0.93**	**0.97**
Avg mP (60 m)	235 ± 1	235 ± 2	231 ± 1	217 ± 2	186 ± 1	151 ± 2	115 ± 1
Z' (60 m)	**0.98**	**0.97**	**0.98**	**0.97**	**0.97**	**0.94**	**0.96**

Supplementary Table 2. *PPTase serial dilution Z' calculations with human acyl carrier protein*. Sfp (**a**) and hPPTase (**b**) serial dilution signals measured in millipolarization units (mP) were monitored for hACP labeling over time (30 and 60 minute time points portrayed) in fluorescence polarization format, and analyzed for assay suitability via Z' calculations. Only the highest concentrations at later time points gave suitable Z' values, but overall we determined that hACP was not a suitable substrate for high-throughput screening.

a)

[Sfp] nM:	1000	500	250	125	62.5	31.25	15.63
Avg mP (30 m)	136 ± 1	131 ± 4	111 ± 1	81 ± 1	59 ± 4	40 ± 1	31 ± 1
Z' (30 m)	**0.64**	**0.62**	**0.55**	**0.38**	**-0.01**	**-0.28**	**-0.59**
Avg mP (60 m)	138 ± 1	135 ± 1	132 ± 1	115 ± 1	90 ± 5	60 ± 1	43 ± 1
Z' (60 m)	**0.63**	**0.63**	**0.62**	**0.56**	**0.30**	**0.14**	**-0.21**

b)

[hPPTase] nM:	1000	500	250	125	62.5	31.25	15.63
Avg mP (30 m)	128 ± 0	118 ± 8	102 ± 10	85 ± 10	69 ± 10	55 ± 8	44 ± 6
Z' (30 m)	**0.57**	**0.33**	**0.16**	**0.00**	**-0.23**	**-0.43**	**-0.65**
Avg mP (60 m)	131 ± 0	126 ± 5	117 ± 8	103 ± 10	87 ± 11	71 ± 10	56 ± 9
Z' (60 m)	**0.58**	**0.45**	**0.33**	**0.16**	**-0.03**	**-0.24**	**-0.53**

Supplementary Table 3. *PPTase Z' calculation for additives with VibB carrier protein*. Sfp (**a**) and hPPTase (**b**) signal from additive samples measured in millipolarization units (mP) were monitored for VibB labeling over time (30 and 60 minute time points portrayed) in fluorescence polarization format, and analyzed for assay suitability via Z' calculations. Detergents contributed slightly to higher Z' values, while DMSO lowered Z' values. Increased reaction times raised calculated Z' values to acceptable levels for both enzymes.

a)

[Sfp] nM:	100							
DMSO:	0%	10%	0%	10%	0%	10%	0%	10%
detergent:	none		0.01% Tween-20		0.01% Triton X-100		0.01% NP-40	
Avg mP (30 m)	53 ± 1	56 ± 1	67 ± 1	71 ± 2	65 ± 0	68 ± 2	66 ± 1	70 ± 1
Z' (30 min)	**0.44**	**0.58**	**0.52**	**0.60**	**0.45**	**0.55**	**0.29**	**0.58**
Avg mP (60 m)	93 ± 2	98 ± 1	118 ± 1	120 ± 2	111 ± 1	116 ± 3	111 ± 1	116 ± 2
Z' (60 m)	**0.65**	**0.77**	**0.71**	**0.80**	**0.62**	**0.74**	**0.57**	**0.70**

b)

[hPPTase] nM:	100							
DMSO:	0%	10%	0%	10%	0%	10%	0%	10%
detergent:	none		0.01% Tween-20		0.01% Triton X-100		0.01% NP-40	
Avg mP (30 m)	240 ± 0	153 ± 1	233 ± 1	153 ± 2	233 ± 1	153 ± 1	237 ± 10	153 ± 1
Z' (30 m)	**0.59**	**0.53**	**0.59**	**0.52**	**0.59**	**0.55**	**0.46**	**0.54**
Avg mP (60 m)	255 ± 0	190 ± 1	252 ± 1	189 ± 1	249 ± 1	190 ± 1	252 ± 6	190 ± 1
Z' (60 m)	**0.61**	**0.63**	**0.66**	**0.66**	**0.63**	**0.64**	**0.54**	**0.65**

Supplementary Table 4. *PPTase Z' calculation for additives with human acyl carrier protein*. Sfp (**a**) and hPPTase (**b**) signal from additive samples measured in millipolarization units (mP) were monitored for hACP labeling over time (30 and 60 minute time points portrayed) in fluorescence polarization format, and analyzed for assay suitability via Z' calculations. Detergents contributed slightly to higher Z' values, while DMSO lowered Z' values. Acceptable Z' values were only achieved in the absence of DMSO, which precludes high throughput inhibitor screening with DMSO as a chemical shuttle.

a)

[Sfp] nM:	100							
DMSO:	0%	10%	0%	10%	0%	10%	0%	10%
detergent:	none		0.01% Tween-20		0.01% Triton X-100		0.01% NP-40	
Avg mP (30 m)	60 ± 0	74 ± 2	58± 1	76 ± 1	56 ± 2	70 ± 2	58 ± 2	69 ± 1
Z' (30 m)	**0.30**	**-0.02**	**0.43**	**0.04**	**0.28**	**-0.04**	**0.23**	**0.01**
Avg mP (60 m)	100 ± 1	104 ± 2	100 ± 1	105 ± 1	96 ± 2	101 ± 2	97 ± 2	101 ± 1
Z' (60 m)	**0.62**	**0.32**	**0.75**	**0.34**	**0.61**	**0.34**	**0.63**	**0.39**

b)

[hPPTase] nM:	100							
DMSO:	0%	10%	0%	10%	0%	10%	0%	10%
detergent:	none		0.01% Tween-20		0.01% Triton X-100		0.01% NP-40	
Avg mP (30 m)	79 ± 1	63 ± 0	76± 2	64 ± 1	78 ± 0	62 ± 1	77 ± 3	62 ± 1
Z' (30 m)	**0.64**	**-0.03**	**0.68**	**-0.03**	**0.68**	**0.01**	**0.44**	**0.01**
Avg mP (60 m)	105 ± 1	81 ± 0	102 ± 2	82 ± 1	103 ± 1	80 ± 0	103 ± 2	80 ± 1
Z' (60 m)	**0.74**	**0.28**	**0.77**	**0.33**	**0.72**	**0.33**	**0.59**	**0.31**

References:

1. World Health Organization, 2012. *Global Tuberculosis Report*

2. Klein, E., Smith, D.L. and Laxminarayan, R. Hospitalizations and deaths caused by methicillin-resistant Staphylococcus aureus, United States, 1999-2005. *Emerg. Infect. Dis.* 13, 1840-1846 (2007).

3. Kallen, A.J. et al. Health care-associated invasive MRSA infections, 2005-2008. *J. Am. Med. Assoc.* 304, 641-648 (2010).

4. Marin, M.A. et al. Cholera outbreaks in Nigeria are associated with multidrug resistant atypical El Tor and non-O1/non-O139 Vibrio cholerae. *PLoS Negl. Trop. Dis.* 7, e2049 (2013).

5. Fazeli, H. et al. Pseudomonas aeruginosa infections in patients, hospital means, and personnel's specimens. *J. Res. Med. Sci.*17, 332-337 (2012).

6. Moran, G.J., Rothman, R.E. and Volturo, G.A. Emergency management of community-acquired bacterial pneumonia: what is new since the 2007 Infectious Diseases Society of America/American Thoracic Society guidelines. *J. Am. Emerg. Med*. 31, 602-612 (2013).

7. Dass Hazarika, R. et al. Invasive Meningococcal Infection: Analysis of 110 cases from a tertiary care centre in north east India. *Indian J. Pediatr*. 80, 359-364 (2013).

8. Chalut, C., Botella, L., de Sousa-D'Auria, C., Houssin, C. and Guilhot, C. The nonredundant roles of two 4'-phosphopantetheinyl transferases in vital processes of Mycobacteria. *Proc. Natl. Acad. Sci. USA* 103, 8511-8516 (2006).

9. Leblanc, C. et al. 4'-Phosphopantetheinyl transferase PptT, a new drug target required for Mycobacterium tuberculosis growth and persistence in vivo. *PLoS Pathog*. 8, e1003097 (2012).

10. Barekzi, N. et al. Genetic characterization of pcpS, encoding the multifunctional phosphopantetheinyl transferase of Pseudomonas aeruginosa. *Microbiology* 150, 795-803 (2004).

11. Asghar, A.H. et al. The pobA gene of Burkholderia cenocepacia encodes a group I Sfp-type phosphopantetheinyltransferase required for biosynthesis of the siderophores ornibactin and pyochelin. *Microbiology* 157, 349-361 (2011).

12. Allen, G. et al. Functional analysis of a mitochondrial phosphopantetheinyl transferase (PPTase) gene pptB in Aspergillus fumigatus. *Fungal Genet. Biol*. 48, 456-464 (2011).

13. Horbach, R. et al. Sfp-type 4'-phosphopantetheinyl transferase is indispensable for fungal pathogenicity. *Plant Cell* 21, 3379-3396 (2009).

14. Quadri, L.E.N., Sello, J., Keating, T.A., Weinreb, P.H. and Walsh, C.T. Identification of a Mycobacterium tuberculosis gene cluster encoding the biosynthetic enzymes for assembly of the virulence-conferring siderophore mycobactin. *Chem. Biol*. 5, 631-645 (1998).

15. McMahon, M.D., Rush, J.S. and Thomas, M.G. Analyses of MbtB, MbtE, and MbtF suggest revisions to the mycobactin biosynthesis pathway in Mycobacterium tuberculosis. *J. Bact*. 194, 2809-2818 (2012).

16. Peek, M.E., Bhatnagar, A., McCarty, N.A. and Zughaier, S.M. Pyoverdine, the major siderophore in Pseudomonas aeruginosa, evades NGAL recognition. *Interdiscip. Perspect. Infect. Dis*. 2012, 843509 (2012).

17. Scherr, N. et al. Structure-activity relationship studies on the macrolide exotoxin mycolactone of Mycobacterium ulcerans. *PLoS Negl. Trop. Dis*. 7, e2143 (2013).

18. Li, N. et al. Unique iron coordination in iron-chelating molecule vibriobactin helps Vibrio cholerae evade mammalian siderocalin-mediated immune response. *J. Biol. Chem*. 287, 8912-8919 (2012).

19. Rakin, A., Schneider, L. and Podladchikova, O. Hunger for iron: the alternative siderophore iron scavenging systems in highly virulent Yersinia. *Front. Cell. Infect. Microbiol*. 2, 151 (2012).

20. Foley, T.L., Young, B.S. and Burkart, M.D. Phosphopantetheinyl transferase inhibition and secondary metabolism. *FEBS J.* 276, 7134-7145 (2009).

21. Mootz, H.D., Finking, R. and Marahiel, M.A. 4'-phosphopantetheine transfer in primary and secondary metabolism of Bacillus subtilis. *J. Biol. Chem*. 276, 37289-37298 (2001).

22. Finking, R. et al. Characterization of a new type of phosphopantetheinyl transferase for fatty acid and siderophore synthesis in Pseudomonas aeruginosa. *J. Biol. Chem*. 277, 50293-50302 (2002).

23. Joshi, A.K., Zhang, L., Rangan, V.S. and Smith, S. Cloning, expression, and characterization of a human 4'-phosphopantetheinyl transferase with broad substrate specificity. *J. Biol. Chem*. 278, 33142-33149 (2003).

24. Foley, T.L. and Burkart, M.D. A homogeneous resonance energy transfer assay for phosphopantetheinyl transferase. *Anal. Biochem*. 394, 39-47 (2009).

25. Foley, T.L. et al. Preparation of FRET reporters to support chemical probe development. *Org. Biomol. Chem*. 8, 4601-4606 (2010).

26. Yin, J., Lin, A.J., Golan, D.E. and Walsh, C.T. Site-specific protein labeling by Sfp phosphopantetheinyl transferase. *Nat. Prot*. 1, 280-285 (2006).

27. Marshall, C.G., Burkart, M.D., Meray, R.K., and Walsh, C.T. Carrier protein recognition in siderophore-producing nonribosomal peptide synthetases. *Biochemistry* 41, 8429-8437 (2002).

28. Haushalter, R.W. et al. Binding and "pKa" modulation of a polycyclic substrate analogue in a type II polyketide acyl carrier protein. *ACS Chem. Biol*. 6, 413-418 (2011).

29. Nakano, M.M., Corbell, N., Besson, J., and Zuber P. Isolation and characterization of sfp: a gene that functions in the production of the lipopeptide biosurfactant, surfactin, in Bacillus subtilis. *Mol. Gen. Genet*., 313-321 (1992).

30. ExPASy ProtParam Tool, http://web.expasy.org/protparam/

31. Duckworth, B.P. and Aldrich, C.C. Development of a high-throughput fluorescence polarization assay for the discovery of phosphopantetheinyl transferase inhibitors. *Anal. Biochem*. 403, 13-19 (2010).

32. Camaioni, E., Boyer, J.L., Mohanram, A., Harden, T.K. and Jacobson, K.A. Deoxyadenosine bisphosphate derivatives as potent antagonists at P2Y1 receptors. *J. Med. Chem*. 41, 183-190 (1998).

33. Yasgar, A. et al. A strategy to discover inhibitors of Bacillus subtilis surfactin-type phosphopantetheinyl transferase. *Mol. Biosyst*. 6, 365-375 (2010).

34. La Clair, J.J., Foley, T.L., Schegg, T.R., Regan, C.M. and Burkart, M.D. Manipulation of carrier proteins in antibiotic biosynthesis. *Chem. Biol*. 11, 195-201 (2004).

35. Mofid, M.R., Marahiel, M.A., Ficner, R. and Reuter, K. Crystallization and preliminary crystallographic studies of Sfp: a phosphopantetheinyl transferase of modular peptide synthetases. *Acta Crystallogr. D Biol. Crystallogr*. 55, 1098-1100 (1999).

36. Inglese, J. et al. High-throughput screening assays for the identification of chemical probes. *Nat. Chem. Biol*. 3, 466-479 (2007).

37. Quadri, L.E. et al. Characterization of Sfp, a Bacillus subtilis phosphopantetheinyl transferase for peptidyl carrier protein domains in peptide synthetases. *Biochemistry* 37, 1585-1595 (1998).

38. Göblyös A., de Vries, H., Brussee J., Ijzerman A.P. Synthesis and biological evaluation of a new series of 2,3,5-substituted [1,2,4]-thiadiazoles as modulators of adenosine A1 receptors and their molecular mechanism of action. *J. Med. Chem*. 48, 1145-1151 (2005).

39. Lea, W.A. & Simeonov, A. Fluorescence polarization assays in small molecule screening. *Expert Opin. Drug Discov*. 6, 17-32 (2011).

40. Turconi S., et al. Real experiences of uHTS: a prototypic 1536-well fluorescence anisotropy-based uHTS screen and application of well-level quality control procedures. *J. Biomol. Screen* 6, 275-290 (2001).

The chapter entitled “Fluorescent techniques for discovery and characterization of phosphopantetheinyl transferase inhibitors,” in full, is a reprint of the material as accepted by the Journal of Antibiotics. Kosa, Nicolas M.; Foley, Timothy L.; Burkart, Michael D. 2013. The dissertation author was the primary investigator and author of this paper.

Reversible labeling of native and fusion-protein motifs

Nicolas M Kosa, Robert W Haushalter, Andrew R Smith & Michael D Burkart

The reversible covalent attachment of chemical probes to proteins has long been sought as a means to visualize and manipulate proteins. Here we demonstrate the full reversibility of post-translational custom pantetheine modification of *Escherichia coli* acyl carrier protein for visualization and functional studies. We use this iterative enzymatic methodology *in vitro* to reversibly label acyl carrier protein variants and apply these tools to NMR structural studies of protein-substrate interactions.

Post-translational protein modification is important for adding functions to proteins that can be exploited for therapeutics[1], protein engineering[2], affinity design[3] and enzyme immobilization[4], among other applications[5]. Acyl carrier protein (ACP) labeling with 4′-phosphopantetheine (PPant), conjugated to a tag of choice by its transferase (PPTase), represents one of the most flexible covalent protein labeling methods, as illustrated by its application in tagging minimal-ACP peptides[6], bio-gel formation[7] and ACP-dependent protein immobilization[8]. The labeling of ACP and ACP fusion proteins with PPant analogs is also successfully leveraged for visualization[9], isolation[9,10] and functional[11] and structural[12] studies of carrier protein–dependent biosynthetic enzymes. Yet, further advancement of these tools is hampered by an inability to easily reverse PPant attachment. Naturally occurring ACPs, often isolated in holo form (which includes a native PPant modification), cannot be further modified directly with another PPant tag. To overcome these difficulties, we use ACP hydrolase (AcpH), a phosphodiesterase from *Pseudomonas aeruginosa*[13], and Sfp, a PPTase from *Bacillus subtilis*[14], to swap different PPant-conjugated small molecules on free ACP and ACP fusion proteins (**Fig. 1**). This reversible tagging system offers the ability to connect synthetic and biological chemistry with ease and provides uniformly labeled, high-quality ACP and ACP fusion proteins, as demonstrated here through fluorescence labeling and solution-phase protein NMR.

For evaluation of iterative labeling, we began with fluorescent ACP labeling directly in cellular lysate (**Supplementary Fig. 1a**) from *E. coli* strain DK554, which overexpresses native fatty acid ACP (AcpP) in predominantly apo form. Treatment of this lysate with coumarin-CoA and Sfp generated a blue fluorescent band upon excitation of SDS-PAGE samples at 254 nm that co-migrated with a coumarin-labeled ACP standard. Subsequent treatment of coumarin-labeled lysate with recombinant AcpH uniformly removed the coumarin-PPant from ACP, as demonstrated by the disappearance of the blue band (**Supplementary Fig. 1b**). Subsequent treatment of the sample with Sfp and rhodamine-CoA generated a new red fluorescent SDS-PAGE band upon excitation at 532 nm (**Supplementary Fig. 1c**); this label can also be removed (**Fig. 2a** and **Supplementary Fig. 2a**) with AcpH.

After demonstrating the compatibility of AcpH for removing various PPant analogs, we sought to demonstrate the flexibility of our technique by evaluating interaction with ACP fusion proteins. AcpH removed rhodamine-PPant from ACP attached to three different fusion partners: an N-terminal maltose-binding protein (MBP), a C-terminal GFP and an N-terminal bacterial luciferase fusion (Lux-ACP) (**Fig. 2b** and **Supplementary Figs. 2b**,**c**, **3** and **4**). The activity of the luciferase-ACP fusion did not change notably following label manipulation (**Supplementary Fig. 5**).

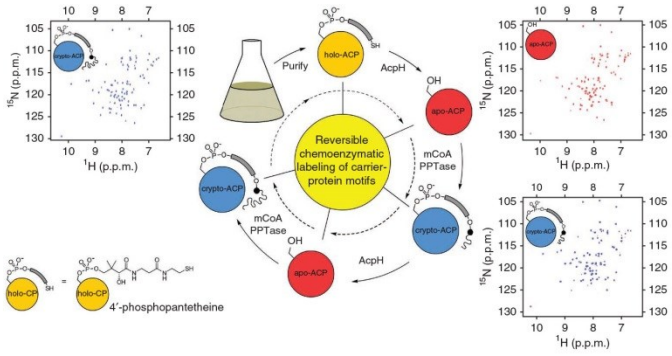

Figure 1 | Reversible labeling of *E. coli* ACP. Recombinant [^{15}N]ACP is isolated in the holo-state (top, yellow). [^{15}N]ACP is prepared for covalent labeling by treatment with AcpH to generate exclusively apo-[^{15}N]ACP (red). Protein purity and modification homogeneity is confirmed by two-dimensional NMR (top right). Labeling with acyl pantetheine analogs to the crypto-[^{15}N]ACP (blue), or 'labeled', form proceeds via PPTase and acyl-CoA (mCoA) modification that is analyzed by NMR (bottom right, top left). Modification is quantitatively reversed by AcpH, whereby labeled proteins are returned to the apo form.

Department of Chemistry and Biochemistry, University of California, San Diego (UCSD), La Jolla, California, USA. Correspondence should be addressed to M.D.B. (mburkart@ucsd.edu).

RECEIVED 24 APRIL; ACCEPTED 23 AUGUST; PUBLISHED ONLINE 16 SEPTEMBER 2012; DOI:10.1038/NMETH.2175

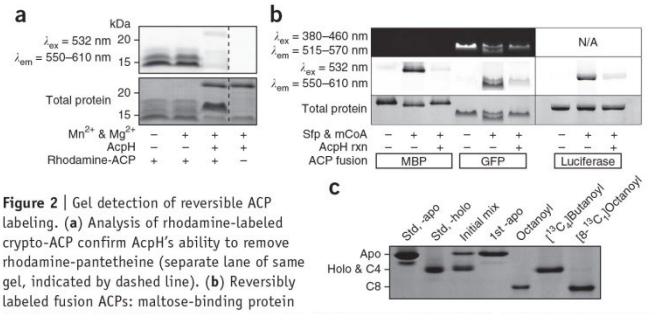

Figure 2 | Gel detection of reversible ACP labeling. (**a**) Analysis of rhodamine-labeled crypto-ACP confirm AcpH's ability to remove rhodamine-pantetheine (separate lane of same gel, indicated by dashed line). (**b**) Reversibly labeled fusion ACPs: maltose-binding protein (MBP)-PaACP, GFP-ACP and luciferase-ACP. Apo-ACP fusions are labeled with rhodamine-CoA (mCoA) and Sfp and are subsequently unlabeled with AcpH (separate gels indicated by demarcation). (**c**) Acyl-pantetheine analogs were installed on [^{15}N]ACP used for NMR analysis. ACP standards ('std') for apo and holo allow labeling evaluation. The initial mixture of apo- and holo-[^{15}N]ACP is readily converted to fully apo-[^{15}N]ACP with AcpH. 'One-pot' Sfp and AcpH methodology allows conversion of one protein sample to octanoyl-, [$^{13}C_4$]butanoyl- and [8-$^{13}C_1$]octanoyl-[^{15}N]ACP. Full-length gels are presented in **Supplementary Figure 2**.

We additionally found that labeling of the GFP-ACP fusion with rhodamine-CoA generates an observable Förster resonance energy transfer (FRET) signal (**Supplementary Fig. 6**), which enables observation of AcpH or PPTase activity in a simple and scalable assay format.

Recent studies of fatty acid and polyketide pathways focus on the extent and function of substrate sequestration by ACP, in which the growing acyl chain is covalently attached via a thioester linkage to the terminus of post-translationally added 4′-phosphopantetheine[15]. Biosynthetic intermediates with varied chemical structures participate in intramolecular interactions with ACP that modulate substrate dynamics and ACP structure[16]. The nature of these ACP-substrate interactions depends on the chemical structure of the biosynthetic intermediate and can vary with respect to chain length and oxidation state[17]. Furthermore, observations of this phenomenon appear to vary depending on the analytical method used. X-ray crystallography of hexanoyl-, heptanoyl- and decanoyl-ACPs from *E. coli* fatty acid biosynthesis all show the acyl chain clearly buried in ACP[18], whereas two different crystal forms of butanoyl-ACP show the acyl chain residing outside the protein with one form and inside the protein with the other[19]. NMR studies have shown that short-chain polyketide analogs protrude into solution when appended to *Streptomyces coelicolor* actinorhodin ACP, whereas saturated acyl chains of 4–8 carbons associate more closely with this polyketide ACP[16]. Variations in substrate dynamics must clearly play a role in the catalytic processivity of these synthases, and we hypothesize that the dynamics of substrate binding serves a critical function in substrate specificity.

To evaluate substrate dynamics with respect to substrate identity, it is necessary to perform multiple studies on the same protein with varying acyl substrates covalently attached. Given the labor and expense of preparing uniformly labeled, isotope-enriched proteins for NMR structural studies, we investigated the use of AcpH as a means to recycle ^{15}N-enriched ACP. We reversibly labeled a single sample of ^{15}N-enriched *E. coli* ACP with several acyl pantetheine analogs and characterized the dynamics of the acyl-[^{15}N]ACP species with NMR spectroscopy. By incorporating fatty acyl pantetheines with ^{13}C labels within the acyl chain, we directly observed intramolecular interactions of the [^{15}N]ACP with the pendant acyl chain using nuclear Overhauser effect (NOE) measurements.

We evaluated [^{15}N]ACP at each labeling conformation via gel (**Fig. 2c** and **Supplementary Figs. 7** and **8**) and NMR analysis (**Supplementary Figs. 9–14**). We obtained an initial apo and holo mixture following *E. coli* expression that required full conversion to the apo form using AcpH. Subsequent conversion to octanoyl-[^{15}N]ACP used the chemoenzymatic synthesis of an octanoyl-CoA analog with Sfp labeling[14] (**Fig. 2c**). After NMR evaluation, we converted the [^{15}N]ACP back to the apo form with AcpH for subsequent relabeling. We acquired ^{15}N-^{1}H heteronuclear single-quantum coherence (HSQC) spectra of all three [^{15}N]ACP species (apo, octanoyl- and regenerated apo). Comparing apo-[^{15}N]ACP to the octanoyl-[^{15}N]ACP (**Fig. 3a**), we observed chemical shift perturbations characteristic

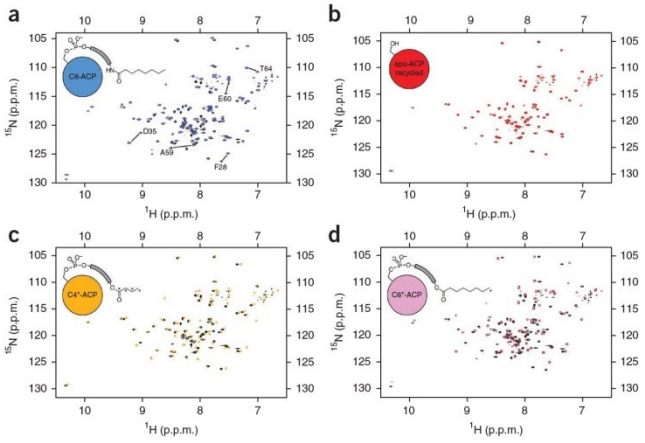

Figure 3 | HSQC spectra of recycled [^{15}N]ACP in various acyl states overlaid with apo-[^{15}N]ACP. All spectra were collected on the same protein sample. (**a–d**) ^{15}N-^{1}H HSQC of the originally prepared apo-[^{15}N]ACP (black) is overlaid with the HSQC of octanoyl-[^{15}N]ACP (blue; **a**), regenerated apo-[^{15}N]ACP (red; **b**), [$^{13}C_4$]butanoyl-[^{15}N]ACP (orange; **c**) and [8-$^{13}C_1$]octanoyl-[^{15}N]ACP (lavender; **d**). Full spectra are available in **Supplementary Figures 9–14**. Samples with asterisks denote ^{13}C-labeled acyl pantetheines.

Table 1 | Evaluating ACP Sfp/AcpH reaction efficiency

a

	E. coli ACP											
	Apo no. 1	Butanoyl	Apo no. 2	Apo no. 1	Octanoyl	Apo no. 2	Apo no. 1	Rhod	Apo no. 2	Apo no. 1	Coumarin	Apo no. 2
Mass (mg)	1.9	1.7	1.8[a]	1.6	1.2	1.0	1.6	–	1.0	1.6	–	1.4
Step yield	–	92%	99%	–	77%	83%	–	–	64%	–	–	85%
Cycle yield		98%			64%			64%			85%	

b

	MBP-PaACP			GFP-ACP			Luciferase-ACP		
	Apo no. 1	Rhod	Apo no. 2	Apo no. 1	Rhod	Apo no. 2	Apo no. 1	Rhod	Apo no. 2
Mass (mg)	1.7	1.3	0.9	2.5	2.2	1.6	1.7	1.5	1.0
Step yield	–	92%	74%	–	86%	75%	–	82%	68%
Cycle yield		57%			65%			56%	

All free (**a**) and fusion (**b**) ACPs were labeled and unlabeled to validate reaction yields. Rhod, rhodamine; MBP, maltose-binding protein. [a]Elevated yield calculation for obtaining apo-ACP from butanoyl-ACP is most likely due to minor protein or buffer contamination for this sample. Reaction completion was monitored by urea-PAGE (**Supplementary Fig. 16**) and SDS-PAGE (**Supplementary Fig. 17**) as appropriate.

of acyl chain sequestration in the hydrophobic binding pocket[20]. Conversion from this acylated form back to the apo form by AcpH provided uniformly unlabeled apo-[^{15}N]ACP, as confirmed by an HSQC spectrum of the regenerated protein that identically matched that of the original (**Fig. 3b**). This validated the feasibility of reversible ACP labeling, as it demonstrated that the regenerated apo-[^{15}N]ACP is properly folded and ready for subsequent modification.

We next labeled this regenerated apo-[^{15}N]ACP with a [$^{13}C_4$]butanoyl-CoA analog (**Fig. 2c**), which contained ^{13}C labels at carbons 1–4. [$^{13}C_4$]Butanoyl-[^{15}N]ACP demonstrated weaker HSQC chemical shift perturbations (**Fig. 3c**) than octanoyl-[^{15}N]ACP. Further sample treatment involved one last conversion to the apo form by AcpH followed by labeling with [8-$^{13}C_1$]octanoyl-CoA (containing a single ^{13}C label at carbon 8; **Figs. 2c** and **3d**). We performed ^{13}C-selective NOE experiments, in which we observe NMR signals for other protons within 5 Å from the ^{13}C label, on the [$^{13}C_4$]butanoyl-[^{15}N]ACP and [8-$^{13}C_1$]octanoyl-[^{15}N]ACP as a means to gain structural information about substrate-protein interactions. In collecting ^{13}C-edited NOE spectra of the ^{13}C-labeled acyl [^{15}N]ACP, we observed no NOE signal for [$^{13}C_4$]butanoyl-[^{15}N]ACP, whereas [8-$^{13}C_1$]octanoyl-[^{15}N]ACP produced a notable signal (**Supplementary Fig. 15**). This result was likely produced from spatial proximity of an aliphatic proton in a [^{15}N]ACP side chain and the $^{13}CH_3$ group in the [8-$^{13}C_1$]octanoyl acyl chain, indicating that the longer acyl chain resides in the protein binding pocket. This finding signifies a lack of dynamic mobility and sequestration of the acyl chain. Conversely, the negative result from [$^{13}C_4$]butanoyl-[^{15}N]ACP indicates that the shorter acyl chain is notably more dynamic in solution. The X-ray crystal structure indicates two states for a tethered butanoyl substrate: one outside (evidenced by a closed hydrophobic pocket) and one sequestered within the protein[19]. Our NMR-based finding highlights the differences of substrate-tethered ACP behavior between solution and crystalline structure and reveals that the solution-exposed acyl chain is the predominant form of [$^{13}C_4$]butanoyl-[^{15}N]ACP in solution. We conclude that analysis of ACP-substrate dynamics must necessarily be performed in the solution state.

In addition to observing the dynamics of tethered acyl substrates, these NMR studies provide a qualitative evaluation for protein quality after repeated labeling and unlabeling steps. This demonstration offered an ideal testing ground for the reversible labeling method, as we used only one isotope-enriched protein sample for the entire experiment. Any protein degradation or incomplete reactivity would severely compromise the quality of resulting NMR spectra. To provide quality control, we acquired HSQC spectra of purified [^{15}N]ACP at each discrete step throughout the process and compared them to the spectra of the original apo-[^{15}N]ACP sample (**Fig. 3**), which revealed retention of protein integrity throughout the experiment. By tracking the ultraviolet absorbance of [^{15}N]ACP throughout all conversions (**Supplementary Table 1**), we observed a final recovery of 27% protein after five discrete enzymatic reaction steps. We further evaluated reaction efficiency for all presented reactions (**Table 1** and **Supplementary Figs. 16** and **17**); the values demonstrate that two-step yields above 60% are feasible for most ACP constructs.

This work suggests that AcpH is capable of removing a broad variety of covalently tethered labels beyond those studied here, in addition to accommodating N- and C-terminal ACP fusion partners with ease. Given the multitude of existing opportunities for ACP labeling, particularly in work involving fusion-protein applications and natural-product biosynthetic studies, we believe that providing a reversible methodology will provide markedly improved flexibility for rapid modification of protein species. Additionally, the cost-saving measure of recovering valuable apo-ACP substrates cannot be overlooked. Because of the wide pantetheine substrate acceptance demonstrated by a combined Sfp and AcpH methodology, various fluorescent and functional tags can be exchanged on a single protein with robustness not offered by previous enzymatic methods.

METHODS

Methods and any associated references are available in the online version of the paper.

Note: Supplementary information is available in the online version of the paper.

ACKNOWLEDGMENTS

We wish to thank (all from UCSD) T.L. Foley for preparing rhodamine-CoA, coumarin-CoA and coumarin-ACP standard; S. Mayfield for providing the luciferase plasmid template; S. Duan for laboratory support; M. Rothmann for assisting with AcpH method development; R. Tsien for use of GFP-related gel-imaging equipment; the UCSD Chemistry & Biochemistry Mass Spectrometry Facility; and J. La Clair for manuscript design input.

This research was funded by US National Institutes of Health grants R21AI090213, R01GM094924 and R01GM095970.

AUTHOR CONTRIBUTIONS

N.M.K. performed all cloning, subcloning, enzymatic reactions, imaging and protein purifications (unless otherwise stated). R.W.H. conducted all protein NMR experiments and provided resulting NMR data. R.W.H. prepared the native Sfp, MBP-CoaA,D,E enzyme stocks used for 'one-pot' chemoenzymatic CoA analog synthesis. A.R.S. synthesized, purified and characterized all oxopantetheine probes in this work. N.M.K., R.W.H., A.R.S. and M.D.B. wrote the manuscript.

COMPETING FINANCIAL INTERESTS

The authors declare no competing financial interests.

Published online at http://www.nature.com/doifinder/10.1038/nmeth.2175. Reprints and permissions information is available online at http://www.nature.com/reprints/index.html.

1. Luchansky, S.J., Argade, S., Hayes, B.K. & Bertozzi, C.R. *Biochemistry* **43**, 12358–12366 (2004).
2. Stachler, M.D., Chen, I., Ting, A.Y. & Bartlett, J.S. *Mol. Ther.* **16**, 1467–1473 (2008).
3. Batra, G. *et al. Protein Expr. Purif.* **74**, 99–105 (2010).
4. Gauchet, C., Labadie, G.R. & Poulter, C.D. *J. Am. Chem. Soc.* **128**, 9274–9275 (2006).
5. Hinner, M.J. & Johnsson, K. *Curr. Opin. Biotechnol.* **21**, 766–776 (2010).
6. Yin, J. *et al. Proc. Natl. Acad. Sci. USA* **102**, 15815–15820 (2005).
7. Mosiewicz, K.A., Johnsson, K. & Lutolf, M.P. *J. Am. Chem. Soc.* **132**, 5972–5974 (2010).
8. Wong, L.S., Thirlway, J. & Micklefield, J. *J. Am. Chem. Soc.* **130**, 12456–12464 (2008).
9. Foley, T.L., Young, B.S. & Burkart, M.D. *FEBS J.* **276**, 7134–7145 (2009).
10. Meier, J.L. *et al. ACS Chem. Biol.* **4**, 948–957 (2009).
11. Meier, J.L., Haushalter, R.W. & Burkart, M.D. *Bioorg. Med. Chem. Lett.* **20**, 4936–4939 (2010).
12. Haushalter, R.W. *et al. ACS Chem. Biol.* **6**, 413–418 (2011).
13. Murugan, E., Kong, R., Sun, H., Rao, F. & Liang, Z.-X. *Protein Expr. Purif.* **71**, 132–138 (2010).
14. Quadri, L.E. *et al. Biochemistry* **37**, 1585–1595 (1998).
15. Chan, D.I. & Vogel, H.J. *Biochem. J.* **430**, 1–19 (2010).
16. Evans, S.E. *et al. J. Mol. Biol.* **389**, 511–528 (2009).
17. Płoskoń, E. *et al. Chem. Biol.* **17**, 776–785 (2010).
18. Roujeinikova, A. *et al. J. Mol. Biol.* **365**, 135–145 (2007).
19. Roujeinikova, A. *et al. Structure* **10**, 825–835 (2002).
20. Upadhyay, S.K. *et al. J. Biol. Chem.* **284**, 22390–22400 (2009).

ONLINE METHODS

Determination of protein concentration, protein gels, miscellaneous. ACP concentrations were determined by UV absorbance measurements at 280 nm unless otherwise noted. Extinction coefficients were calculated using the ExPASy (http://www.expasy.ch/) ProtParam tool: *E. coli* free ACP = 1,490 $M^{-1}cm^{-1}$, GFP-ACP = 69,000 $M^{-1}cm^{-1}$, MBP-PaACP = 66,000 $M^{-1}cm^{-1}$ and Lux-ACP = 85,720 $M^{-1}cm^{-1}$. Non-ACP protein concentrations and fusion ACPs used in the efficiency analysis (**Table 1b**) were determined using the Bradford method against a BSA standard. ACP was run on 20% 2 M urea-PAGE to resolve apo, holo and crypto conversions as well as 12% SDS-PAGE to evaluate overall purity during NMR workup. ACP fusions MBP-PaACP and GFP-ACP samples were run on 15% 2 M urea-PAGE and Lux-ACP was run on 10% SDS-PAGE for fluorescence imaging experiments. Electrophoresis of fluorescent coumarin and rhodamine nonfusion *E. coli* ACP modifications used 10% Tris-tricine SDS-PAGE.

Gel imaging. Coomassie-stained gels were imaged on a Fluor-S MultiImager (Bio-Rad) using visible light exposure. Coomassie-gel images were acquired as .tiff files, and excess white was discarded using the Auto Levels feature of Photoshop (Adobe). UV acquisition was also performed on the Fluor-S MultiImager, with short/long wave UV and a 520LP filter, and excess black was discarded using the Auto Levels feature of Photoshop (Adobe). GFP fluorescence imaging before gel fixing was performed on a UVP BioSpectrum (UVP LLC) system with a SYBR Green 515- to 570-nm–emission filter. Excitation was provided by transillumination from a UVP BioLite with a 420BP40 filter. GFP fluorescence images were collected as .tiff files and had gray input levels adjusted using Photoshop from '0,1.00,255' to '0,1.00,150' to discard excess black. Rhodamine-labeled protein gels were imaged on a Typhoon (GE Healthcare) gel scanner at 50-µm resolution with a photomultiplier tube (PMT) setting of 450 and using a 532-nm (green laser) excitation and 580BP30 emission filter. Typhoon gel images were collected as .gel files, converted to .tiff in ImageJ (NIH) and exported to Photoshop, with which gray input levels were adjusted from '0,1.00,255' to '80,1.00,255' to discard excess whites collected from the .gel file. All gels, with the exception of GFP-ACP containing gels, were fixed with 10% acetic acid, 40% methanol and 50% water for 1 h, then rinsed three times with water before UV fluorescence imaging and subsequent staining. GFP-ACP images were acquired before gel fixing, after which they were fixed and imaged as other gels.

Production of AcpH and recombinant ACP constructs. Cloning methods and primers are contained in the **Supplementary Methods** and **Supplementary Table 2**. For expression of *E. coli* [^{15}N]ACP, *E. coli* BL21 (DE3) cells containing plasmid pET22b encoding C-terminal 6×His-tagged *E. coli* ACP were cultured in 1 L M9 minimal medium supplemented with 1 g/L ^{15}N-enriched ammonium chloride and 100 µg/mL ampicillin. Culture was grown to OD_{600} = 0.6, induced with 1 mM IPTG and was shaken 4 h at 37 °C. *E. coli* BL-21(DE3) cells containing the MBP-AcpH plasmid were grown in 1 L LB, 0.2% D-glucose and 50 µg/mL kanamycin sulfate at 37 °C to OD = 0.6, induced with 1 mM isopropyl β-D-1-thiogalactopyranoside (IPTG), and shaken at 16 °C overnight. Medium was centrifuged 30 min at 2,000 r.p.m. to pellet cells. Cell pellets were stored at −20 °C overnight. AcpH-6×His construct was grown similarly without glucose. Cells were thawed on ice and suspended in lysis buffer (50 mM TrisCl, pH 8; 500 mM NaCl; and 10% glycerol) with additional ingredients 0.1 mg/mL lysozyme, 0.1 mM DTT, 5 µg/mL DNase I and 5 µg/mL RNase A and passed twice through a French pressure device at 1,000 p.s.i. Lysate was centrifuged 45 min at 10,000 r.p.m., and supernatant was incubated with amylose resin (New England Biolabs) for MBP-AcpH or with Ni-NTA (Novagen) for AcpH-6×His according to manufacturer protocols. Eluted MBP-AcpH was then concentrated to 10 mg/mL and subsequently FPLC-purified with 50 mM TrisCl and 250 mM TrisCl, pH 8.0, buffers to remove contaminating native *E. coli* MBP. MBP-AcpH was concentrated with a 10-kDa Amicon spin filter (Millipore) and stored in 40% glycerol at −80 °C after flash freezing aliquots in liquid nitrogen. 6×His-AcpH was lysed in a similar manner, but it was purified with Ni-NTA resin (Novagen). Ni-NTA resin with bound protein was washed with 10 mM imidazole and eluted with 300 mM imidazole in lysis buffer. 6×His-AcpH was desalted to remove imidazole and flash frozen at −80 °C at 1 mg/mL without further modification. MBP-PaACP and Lux-ACP were expressed in *E. coli* BL-21 (DE3) in LB with 50 µg/mL kanamycin. GFP-ACP (6×His-tagged in pCA24N vector)[21] was expressed in *E. coli* K-12 strain AG1 (ASKA library) cells in LB with 20 µg/mL chloramphenicol. Cells containing fusion ACPs were grown, induced and purified in an otherwise identical manner to 6×His-tagged AcpH. MBP and GFP fusion ACPs eluted with 300 mM imidazole were dialyzed into AcpH reaction buffer without Mg^{2+} or Mn^{2+} cofactors overnight. Lux-ACP was buffer exchanged using a PD-10 desalting column (GE Healthcare) into AcpH reaction buffer, flash frozen and stored overnight at −80 °C. Lux-ACP was thawed on ice, AcpH was added to 5 µM and the reaction was incubated at 37 °C for 4 h. Dialyzed ACP fusions next had appropriate amounts of 1 M $MgCl_2$ and $MnCl_2$ added to achieve 15 mM and 1 mM final concentrations, respectively. Free AcpH was added to free ACP and to MBP and GFP fusion ACPs at 5 µM final concentration, and the mixture was incubated overnight at 37 °C in a rotary wheel. Lux-ACP was reacted for 4 h at 37 °C. ACP reactions were centrifuged to remove any precipitate and purified by anion-exchange chromatography. Purity evaluation was conducted on MBP-PaACP and GFP-ACP (**Supplementary Fig. 3**) as well as on Lux-ACP (**Supplementary Fig. 4**) with SDS-PAGE.

Preparation of coumarin-ACP standard. *E. coli* DK554 cells were grown, induced and prepared to generate predominantly apo-ACP. Isopropanol supernatant containing ACP was applied to DEAE resin and eluted with a sodium chloride gradient. ACP was then labeled using 6×His-Sfp and coumarin-CoA. Sfp was removed with Ni-NTA resin, and excess coumarin-CoA was removed with size-exclusion chromatography on G25 Sephadex resin.

Preparation of *E. coli* DK554 lysate. 50 mL LB medium supplemented with 25 µM calcium D-pantothenate, 50 mM D-glucose and 50 µg/mL kanamycin used previously[22]. Medium was inoculated with 1 mL of overnight DK554 starter culture and grown to OD = 0.4. IPTG was added at a concentration of 1 mM to the medium and was shaken for 5 h at 37 °C. Medium was centrifuged at 4,000 r.p.m. at 4 °C for 30 min to pellet cells. Cell pellets were resuspended in 25 mM TrisCl, pH 7.5; 250 mM NaCl;

0.1 mg/mL lysozyme; 10 µM pepstatin; and 10 µM leupeptin and passed twice through a French pressure device at 1,000 p.s.i. Lysate was centrifuged 45 min at 10,000 r.p.m. and 4 °C to remove insoluble debris.

Removal of coumarin-pantetheine from ACP in 5 mL lysate was achieved using 10 µM MBP-AcpH fusion in 600 mL AcpH reaction buffer (50 mM TrisCl, pH 8.0; 100 mM NaCl; 10% glycerol; 15 mM $MgCl_2$; and 1 mM $MnCl_2$) within a 3-kDa-MWCO dialysis bag at 37 °C overnight.

Fluorescence labeling of *E. coli* DK554 lysate with modified coenzyme A. *E. coli* DK554 cell lysate with total protein concentration of approximately 2 mg/mL was added to the volume of premade 10× PPTase reaction buffer (500 mM Na-HEPES and 100 mM $MgCl_2$, pH 7.6) that brought the total reaction concentration to 50 mM Na-HEPES, pH 7.6; 10 mM $MgCl_2$; 5 µM coumarin-CoA[23]; and 2 µM Sfp. Samples were incubated at 37 °C for 1 h and then centrifuged to remove precipitate. Supernatant was passaged over an equilibrated G50 Sephadex (GE Healthcare) desalting column, and lysate was dialyzed using 3.5-kDa MWCO membrane into 50 mM TrisCl, pH 8.0; 100 mM NaCl; and 10% glycerol to further remove unreacted CoA analog.

AcpH treatment of coumarin-ACP in lysate. Coumarin-labeled DK554 cell-lysate supernatant was added to a freshly prepared 10× AcpH reaction buffer to generate the following reaction concentrations: 50 mM TrisCl, pH 8; 150 mM NaCl; 15 mM $MgCl_2$; and 1 mM $MnCl_2$. MBP-AcpH was added to 2 µM. Reaction contents were placed in a 3.5-kD MWCO dialysis membrane and dialyzed against 50-fold volume of reaction buffer stirred overnight at 37 °C. No remaining coumarin-ACP fluorescence was observed, and a substantial amount of MBP-AcpH appeared as precipitate afterward, as determined by SDS-PAGE analysis (not shown). Post-reaction contents were centrifuged 30 min at 4,000 r.p.m. at 6 °C. Supernatant was dialyzed back into 50 mM TrisCl, pH 7.5, and 250 mM NaCl in preparation for rhodamine labeling.

Sfp and AcpH treatment of purified rhodamine-ACP. The demonstrated activity of AcpH on rhodamine-ACP was performed with previously purified 6×His-tagged apo-ACP. First, 7 nmol of apo-ACP was treated with 5 µM native Sfp and 24 nmol of rhodamine-CoA[24] in 50 mM TrisCl, pH 8; 100 mM NaCl; and 10 mM $MgCl_2$ at 37 °C for 1 h. Rhodamine-ACP was repurified with Ni-NTA resin to remove excess rhodamine-CoA and Sfp and dialyzed to remove imidazole. Dialyzed rhodamine-ACP was then incubated with and without 7 µM AcpH at 37 °C for 2 h, and the resulting crude reactions were run on SDS-PAGE and imaged to illustrate fluorescent-label removal with AcpH.

AcpH treatment of [^{15}N]ACP for NMR study. An AcpH reaction was conducted to generate each apo-[^{15}N]ACP sample before labeling. Following NMR acquisition of each sample, ACP was dialyzed into AcpH reaction buffer without cofactors (50 mM TrisCl, pH 8.0 and 100 mM NaCl). Glycerol was found to be unnecessary for desired AcpH activity and was omitted. Following dialysis, $MgCl_2$ and $MnCl_2$ were added to achieve a final concentration of 15 mM and 1 mM, respectively. Free 6×His AcpH was added to a concentration of 5–10 µM, and the mixture was incubated at 37 °C for 8 h. Reaction completion was determined by urea-PAGE analysis. The completed reactions were centrifuged 30 min at 4,000 r.p.m. at 6 °C to remove precipitate.

Labeling of [^{15}N]ACP using 'one-pot' Sfp methodology. Apo-[^{15}N]ACP was mixed with MBP-CoaA, MBP-CoaD and MBP-CoaE, ATP disodium salt, native Sfp, and octanoyl-pantethenamide[12] in a one-pot chemoenzymatic reaction[25] to selectively generate octanoyl-[^{15}N]ACP *in vitro*. Additional generation of [$^{13}C_4$]butanoyl-[^{15}N]ACP and [8-$^{13}C_1$]octanoyl-[^{15}N]ACP analogs was conducted with the same methodology, except using regenerated apo-[^{15}N]ACP with [$^{13}C_4$]butanoyl-oxypantetheine and [8-$^{13}C_1$]octanoyl-oxypantetheine. Ni-NTA resin was used to repurify the [^{15}N]ACP after each labeling reaction. Monitoring of apo-, holo- and crypto-[^{15}N]ACP was conducted with separation on conformationally sensitive urea-PAGE.

ACP anion-exchange purification. All preparative ACP samples were dialyzed into low-salt buffer. *E. coli* ACP and MBP-PaACP ion-exchange running buffer was 25 mML-histidine, pH 6.0. GFP-ACP and Lux-ACP ion-exchange buffer was 25 mM bis-Tris, pH 6.0. Samples were then applied to a DEAE HiTrap (GE Healthcare) 1-mL or 5-mL column. Free ACP, MBP-ACP and GFP-ACP were loaded onto columns and washed with 10 mL of 25 mM buffer containing 25 mM NaCl and were eluted with 5 mL of 25 mM buffer and 500 mM NaCl. Lux-ACP was loaded onto a 5-mL DEAE HiTrap and washed with a step gradient of 0, 100, 200, 300 and 500 mM NaCl in 25 mM bis-Tris, pH 6.0. NMR *E. coli* [^{15}N]ACP samples were then dialyzed into 100 mM sodium phosphate and 1 mM DTT, pH 7.4, and then concentrated to 450 µL before NMR acquisition. *E. coli* [^{15}N]ACP NMR sample purity was evaluated by SDS-PAGE analysis (**Supplementary Fig. 8**). Following ion exchange, fusion ACPs were dialyzed or desalted, spin concentrated and stored at −80 °C before further use.

Fusion ACP rhodamine-CoA labeling and label removal. Purified apo-MBP-PaACP at 200 µM was labeled with 1 mM rhodamine-CoA and 13 µM native Sfp for 3 h at 37 °C. Purified apo-GFP-ACP at 150 µM was labeled with 1 mM rhodamine-CoA and 7 µM native Sfp for 3 h at 37 °C. Purified apo-Lux-ACP at 12 µM was labeled with 50 µM rhodamine-CoA and 3 µM native Sfp for 1 h at 37 °C. Fusion ACPs were then re-purified from excess rhodamine-CoA and native Sfp using Ni-NTA resin, buffer exchanged, and concentrated using 10-kDa MWCO 0.5 mL Amicon spin filters (Millipore). Label removal of MBP-ACP and GFP-ACP proceeded with 4 µL of the concentrated crypto-fusion ACPs with 10 µM AcpH in 10 µL AcpH reaction buffer for 3 h at 37 °C. For Lux-ACP, 6 µM crypto-Lux-ACP was reacted with 5 µM AcpH for 3 h at 37 °C. AcpH reaction samples were run immediately afterward on urea-PAGE (MBP-ACP and GFP-ACP) or SDS-PAGE (Lux-ACP) with no further purification.

Sfp and AcpH treatment of *E. coli* ACP and fusion ACPs for efficiency analysis. Labeling of butanoyl-, octanoyl- and coumarin-ACP proceeded via Sfp and CoA-A/D/E one-pot methodology. Labeling of free ACP and fusion ACPs with rhodamine proceeded via Sfp and rhodamine-CoA. Free *E. coli* ACP reactions were conducted overnight at 37 °C. MBP-PaACP labeling proceeded via native Sfp; GFP-ACP and luciferase-ACP reactions using Sfp conjugate proceeded for 6 h at 37 °C. MBP-PaACP was repurified

doi:10.1038/nmeth.2175

using Ni-NTA and desalted with PD-10 desalting column to remove imidazole. GFP-ACP and luciferase-ACP were separated from solids with a fritted spin column and desalted to remove excess CoA analog. Nonfluorescent *E. coli* ACPs were quantified using UV spectrometry. Label removal proceeded in AcpH reaction buffer with 10% glycerol via reaction with an AcpH conjugate for *E. coli* ACP at 37 °C overnight and at room temperature overnight for MBP-PaACP and GFP-ACP. Because of precipitation induced by extended incubation, luciferase ACP was reacted with AcpH at 37 °C for 2 h. Reaction completion was monitored by gel shifts and/or fluorescence depletion in 20% urea-PAGE for free ACPs and 10% SDS-PAGE for the fusion ACPs. Final apo-ACP samples were then desalted into AcpH reaction buffer lacking Mg^{2+}/Mn^{2+} and subsequently quantified (**Table 1**).

GFP-ACP: rhodamine-CoA and Sfp labeling monitoring by FRET. Apo-GFP-ACP and rhodamine-CoA were diluted to 100 µM and 200 µM, respectively, in 10 mM TrisCl, pH 7.5. Of this 10× substrate mix, 5 µL was added to 6 wells of a Costar 3694 96-well plate (Corning) in triplicate. To adjust final concentrations, 10 µL of milliQ water diluent was added. Next, 35 µL of 1.43 µM Sfp in 71.5 mM HEPES, pH 7.6; 14.3 mM $MgCl_2$; and 1.43 mg/mL BSA (stabilizer) was added to initiate the reaction, with reaction buffer lacking Sfp added to the control. Final 50-µL enzyme reactions contained 10 µM apo-GFP-ACP; 20 µM rhodamine-CoA; 1 µM Sfp; 50 mM HEPES, pH 7.6; and 10 mM $MgCl_2$. The 96-well plate was centrifuged 2 min at 1,000 r.p.m., and fluorescence was monitored at 405 nm excitation and 595 nm emission for 30 min in a PerkinElmer HTS 7000 Plus plate reader at room temperature.

Pantetheine probe synthesis. All CoA-related probes are depicted in **Supplementary Figure 18**. Pantetheine probe synthetic methods and chemical spectra are also contained within the **Supplementary Note** and **Supplementary Figures 19–42**.

21. Kitagawa, M. *et al. DNA Res.* **12**, 291–299 (2005).
22. Lambalot, R.H. & Walsh, C.T. *J. Biol. Chem.* **270**, 24658–24661 (1995).
23. Foley, T.L. & Burkart, M.D. *Anal. Biochem.* **394**, 39–47 (2009).
24. Foley, T.L. *et al. Org. Biomol. Chem.* **8**, 4601–4606 (2010).
25. Worthington, A.S. & Burkart, M.D. *Org. Biomol. Chem.* **4**, 44–46 (2006).

doi:10.1038/nmeth.2175

Supplementary Figure 1

Labeling of native *E. coli* ACP in DK554 cellular lysate

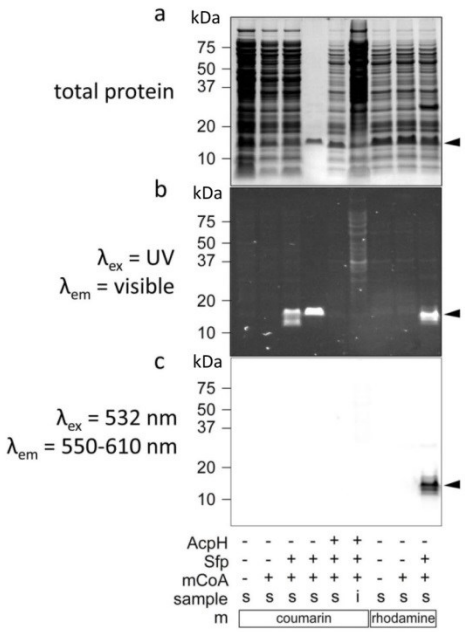

(**a-c**) *Apo*-ACP produced through over-expression with *E. coli* DK554 is present in cell lysate as monitored with (**a**) Coomassie stain, (**b**) 254 nm, and (**c**) 532 nm excitation 550-610 nm emission fluorescence. ACP is labeled using coumarin-CoA and Sfp but not without Sfp. Coumarin-labeled ACP co-migrates and fluoresces like purified coumarin-ACP standard. AcpH treatment results in the complete removal of the fluorescent coumarin from ACP in the soluble fraction "s", and non-ACP insoluble precipitate "i" is observed in the last coumarin sample. Further treatment of the lysate now removed of coumarin with rhodamine-CoA and Sfp results in rhodamine-labeling visible under both 532 and 254 nm excitation. Arrows indicate ACP.

Supplementary Figure 2

Full length gels for figure 2a-c ACP labeling

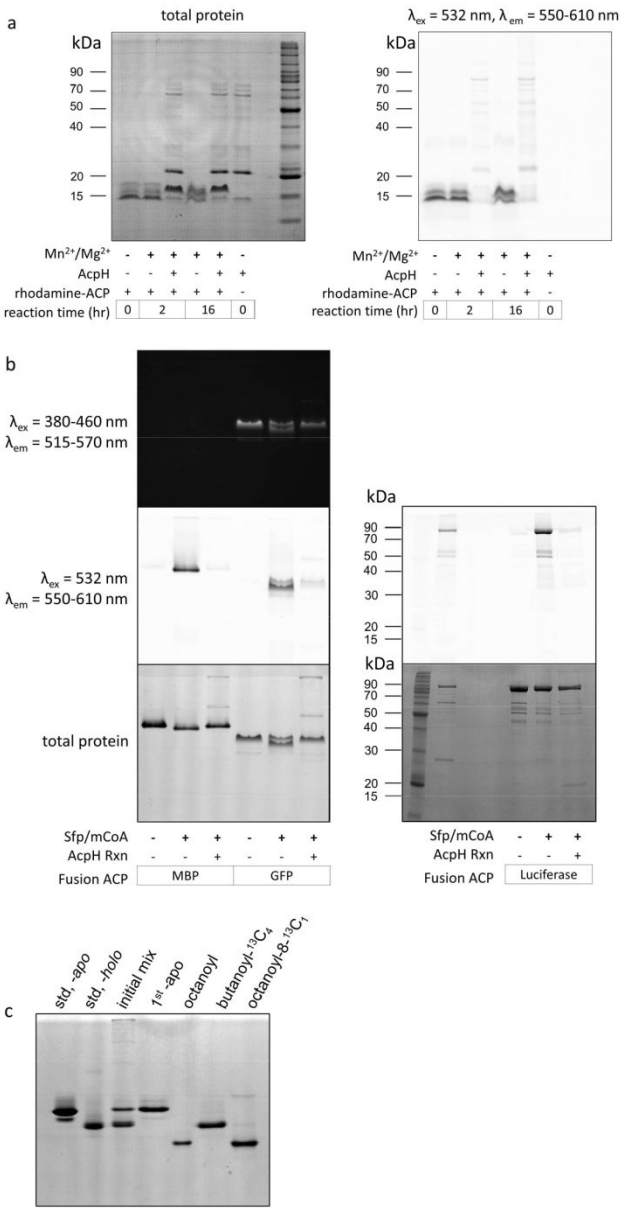

(**a**) Fig. 2a full SDS-PAGE gel, (**b**) Fig. 2b full Urea and SDS-PAGE gels, (**c**) Fig. 2c full Urea-PAGE gel

Supplementary Figure 3

MBP- & GFP- ACP Ni-NTA purification pel

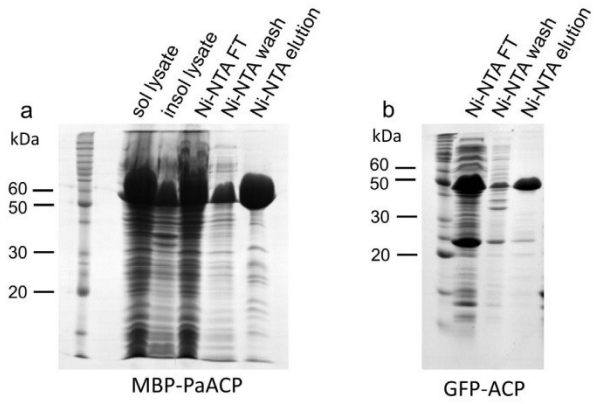

SDS-PAGE and coomassie staining was performed to estimate fusion ACP purity. MBP-PaACP (**a**) and GFP-ACP (**b**) were both purified separately by Ni-NTA resin and DEAE anion exchange resin (following initial AcpH treatment) prior to labeling experiments utilizing rhodamine-CoA.

Nature Methods: doi:10.1038/nmeth.2175

Supplementary Figure 4

Fusion luciferase-ACP purification gel

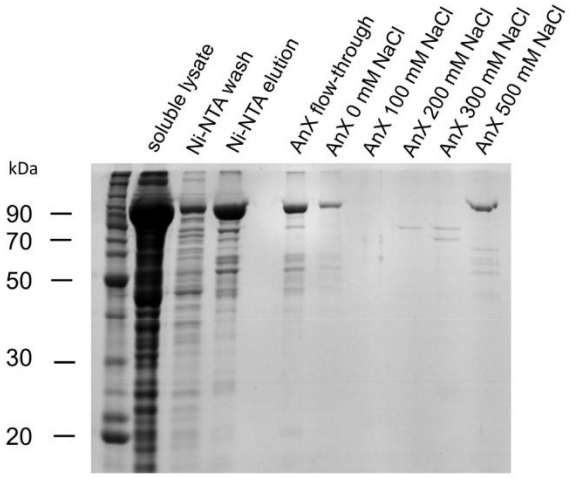

Purification of luciferase-ACP fusion was conducted with Ni-NTA resin affinity purification from the soluble lysate, followed with a 30 mM imidazole wash, and a 300 mM imidazole elution. Following preparative AcpH treatment and desalting into anion exchange ("AnX") buffer, the protein was applied to a DEAE column resulting in unbound protein in flow-through. Subsequent washes various NaCl concentrations further purified the sample. A final 500 mM NaCl elution resulted in protein used for labeling and activity analysis.

Supplementary Figure 5

Luciferase-ACP activity assay

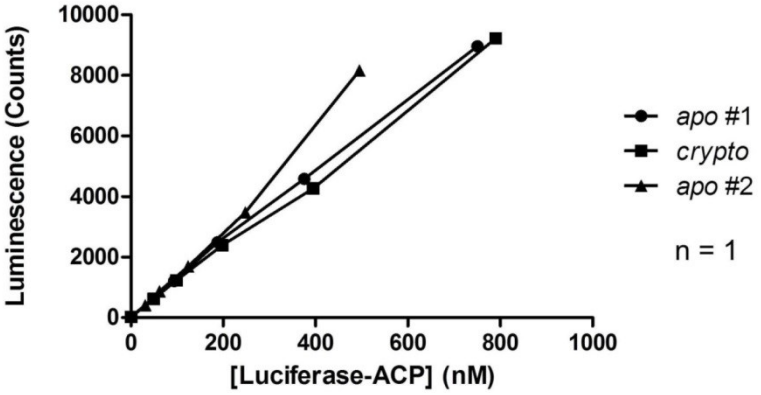

Bacterial luciferase was expressed as an ACP fusion (Lux-ACP), purified, and subjected to ACP labeling and unlabeling techniques. The original *apo*-Lux-ACP was generated and purified, followed by labeling with rhodamine-CoA and Sfp to generate *crypto*-Lux-ACP. The *crypto*-Lux-ACP was subsequently reacted with AcpH to remove the rhodamine-pantetheine and regenerate the *apo*-Lux-ACP. Activity assays with Lux-ACP were conducted with each discrete sample to ensure no significant loss of activity.

Supplementary Figure 6

GFP-ACP: rhodamine-CoA labeling & FRET evaluation

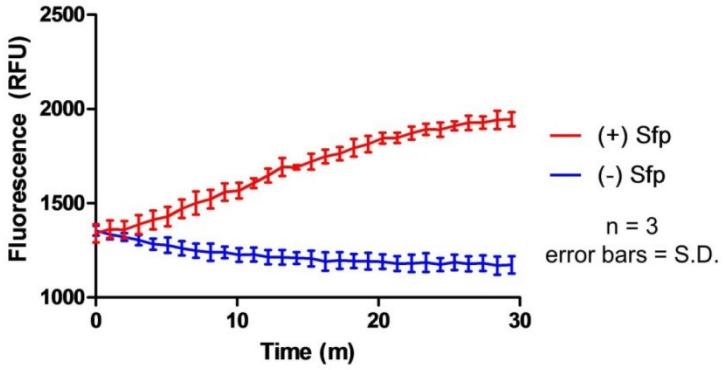

Labeling of 10 μM *apo*-GFP-ACP with 20 μM rhodamine-CoA & 1 μM Sfp generates a distinguished FRET effect when excited with 405nm light, and monitoring rhodamine emission at 595nm.

Nature Methods: doi:10.1038/nmeth.2175

Supplementary Figure 7

[^{15}N]ACP acyl-pantetheine analog Urea-PAGE

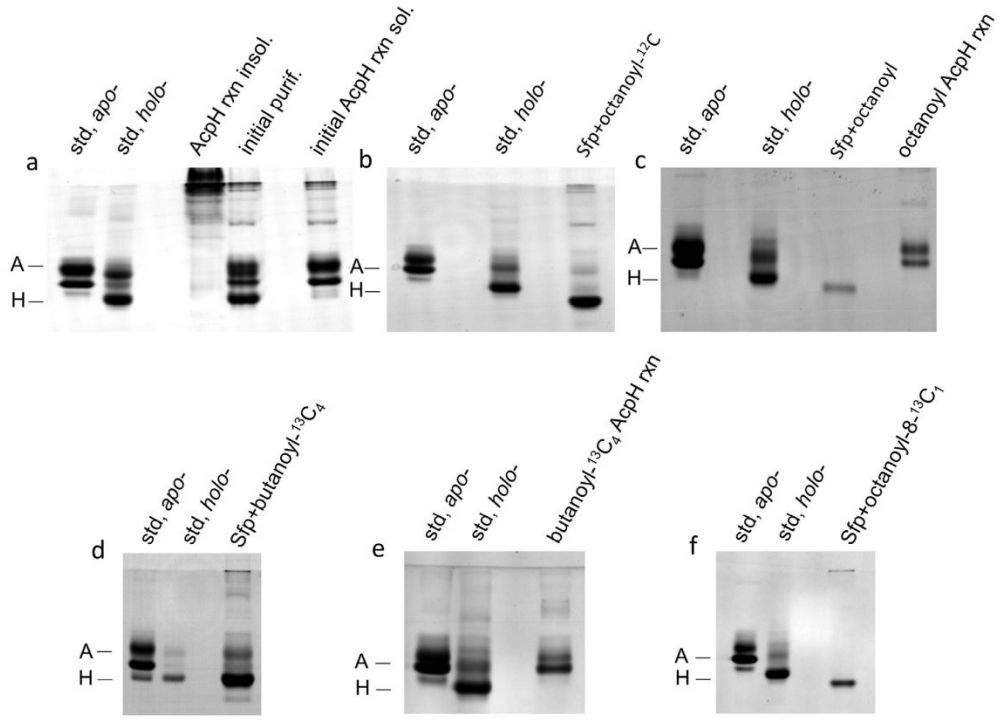

Labeling and regeneration of all AcpH and Sfp-mediated reactions were monitored via Urea-PAGE analysis and compared to pure *apo*- and *holo*-ACP standards (std). (**a**) Initially expressed/purified [^{15}N]ACP is a mixture of *apo*- and *holo*- carrier protein which is converted to *apo*-[^{15}N]ACP using AcpH. AcpH reaction insoluble fraction did not contain a significant amount of ACP-^{15}N. (**b**) Conversion of *apo*-[^{15}N]ACP to octanoyl-[^{15}N]ACP proceeded via "one-pot" Sfp methodology applying octanoyl-pantetheinamide. (**c**) AcpH is used to regenerate the *apo*- form of carrier protein from previous octanoyl-[^{15}N]ACP. (**d**) Regenerated *apo*-[^{15}N]ACP is converted to [$^{13}C_4$]butanoyl-[^{15}N]ACP using [$^{13}C_4$]butanoyl-pantetheine oxoester with "one-pot" Sfp methodology. (**e**) *apo*-[^{15}N]ACP is regenerated from [$^{13}C_4$]butanoyl-[^{15}N]ACP using an AcpH reaction. (**f**) Regenerated *apo*-[^{15}N]ACP is converted to [8-$^{13}C_1$]octanoyl-[^{15}N]ACP using [8-$^{13}C_1$]octanoyl-pantetheine oxoester with "one-pot" Sfp methodology.

Supplementary Figure 8

[^{15}N]ACP purification, SDS-PAGE

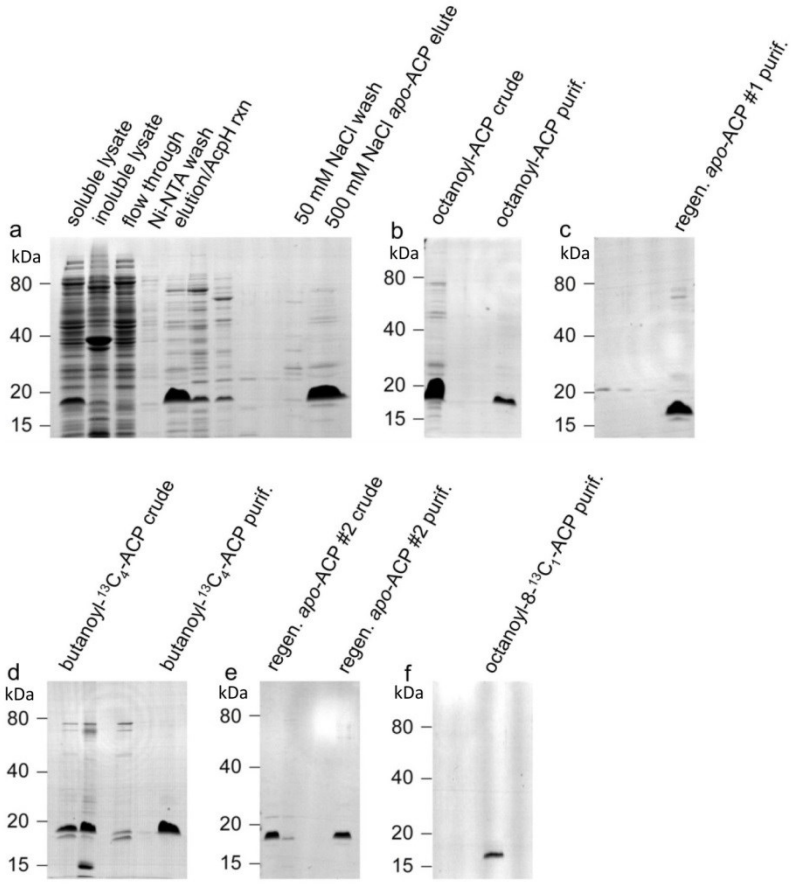

(**a**) SDS-PAGE analysis of [^{15}N]ACP purity following expression/purification/AcpH reaction of [^{15}N]ACP from *E. coli* to generate *apo*-[^{15}N]ACP and subsequent DEAE ion exchange prior to generate NMR-ready sample (NaCl elution). (**b**) Ni-NTA resin purification of octanoyl-[^{15}N]ACP from crude one-pot reaction results in NMR-ready sample**.** (**c**) DEAE purification of the regenerated/NMR-ready *apo*-[^{15}N]ACP**.** (**d**) Ni-NTA resin purification of [$^{13}C_4$]butanoyl-[^{15}N]ACP from "one-pot" crude reaction allows for NMR analysis. (**e**) DEAE purification of the second regenerated *apo*-[^{15}N]ACP from AcpH crude reaction precedes the next labeling step. (**f**) Ni-NTA resin purification of labeled [8-$^{13}C_1$]octanoyl-[^{15}N]ACP prior to NMR analysis.

Supplementary Figure 9

1st *apo*-[15N]ACP HSQC spectrum

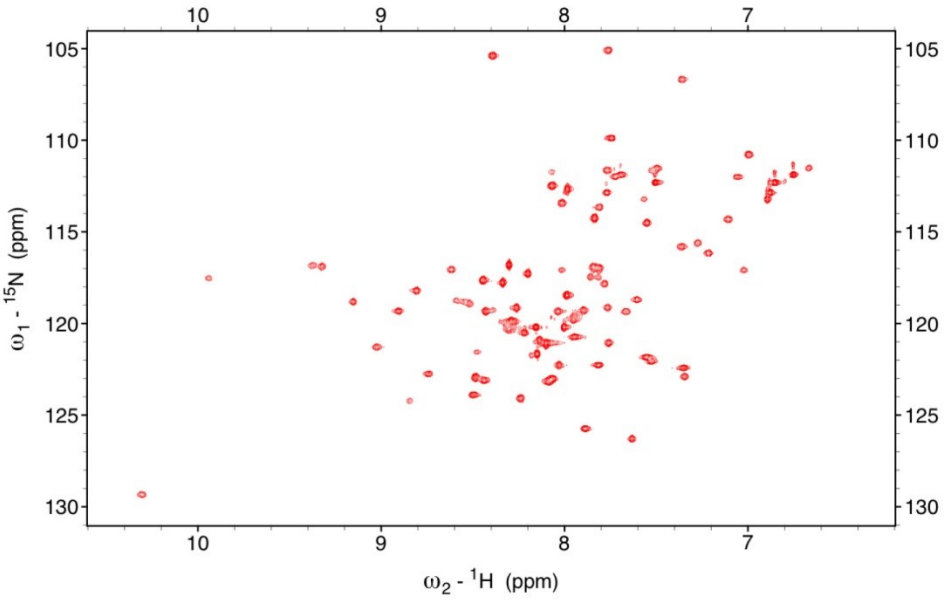

Nature Methods: doi:10.1038/nmeth.2175

Supplementary Figure 10

Octanoyl-[^{15}N]ACP HSQC spectrum

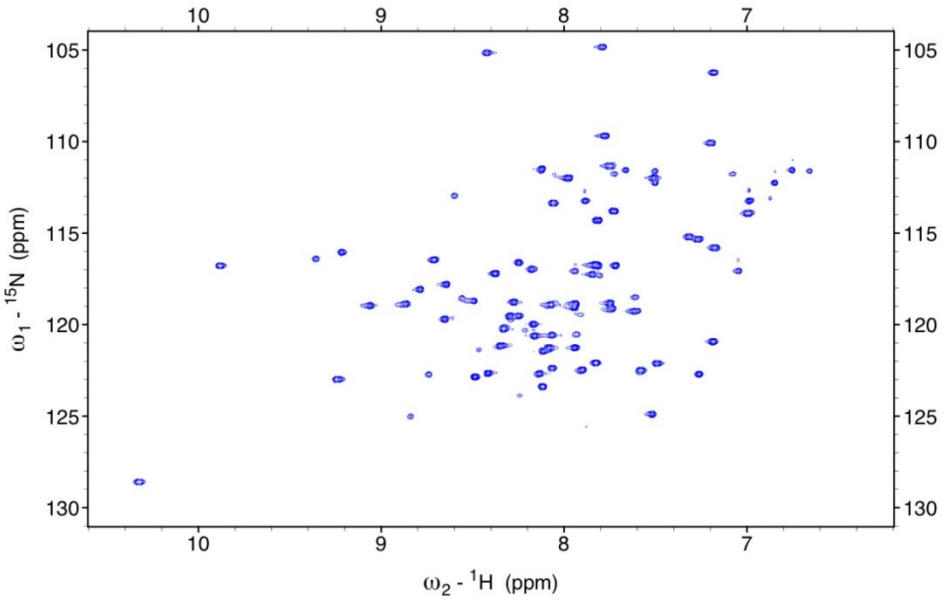

Nature Methods: doi:10.1038/nmeth.2175

Supplementary Figure 11

2nd *apo*-[15N]ACP HSQC spectrum

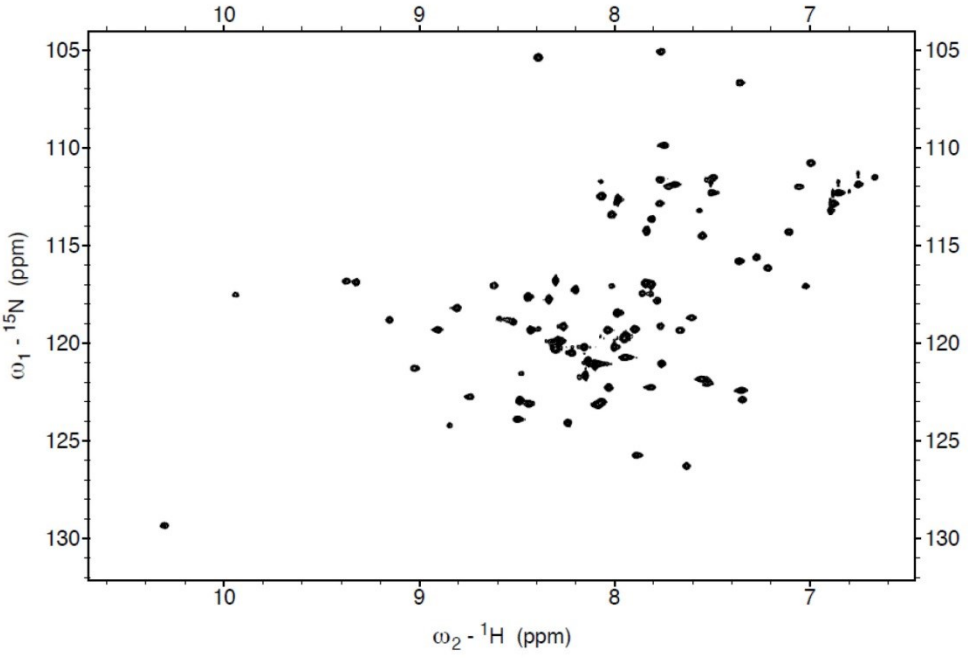

Nature Methods: doi:10.1038/nmeth.2175

Supplementary Figure 12

[$^{13}C_4$]Butanoyl-[^{15}N]ACP HSQC spectrum

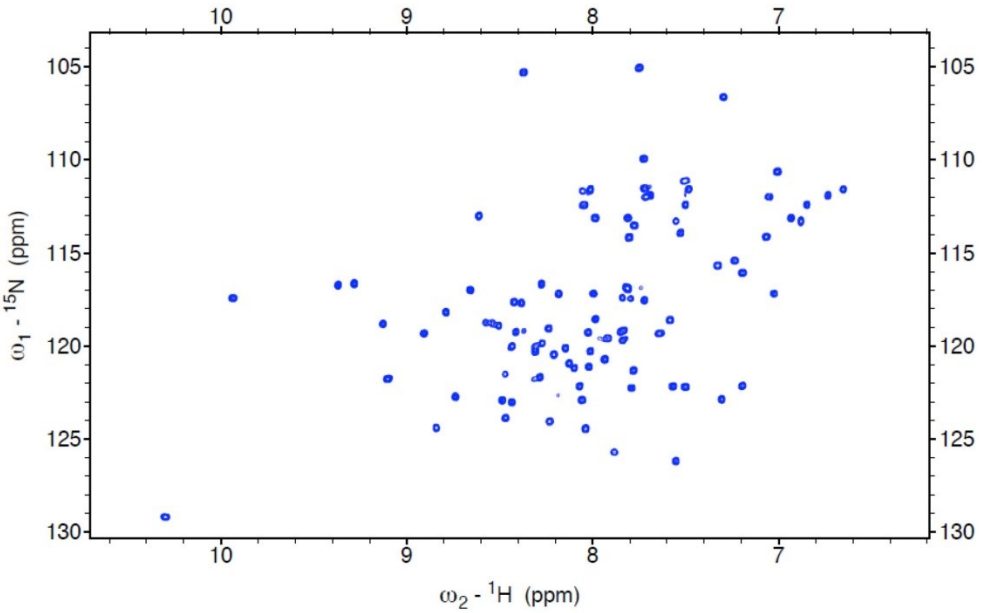

Nature Methods: doi:10.1038/nmeth.2175

Supplementary Figure 13

[8-$^{13}C_1$]Octanoyl-[^{15}N]ACP HSQC spectrum

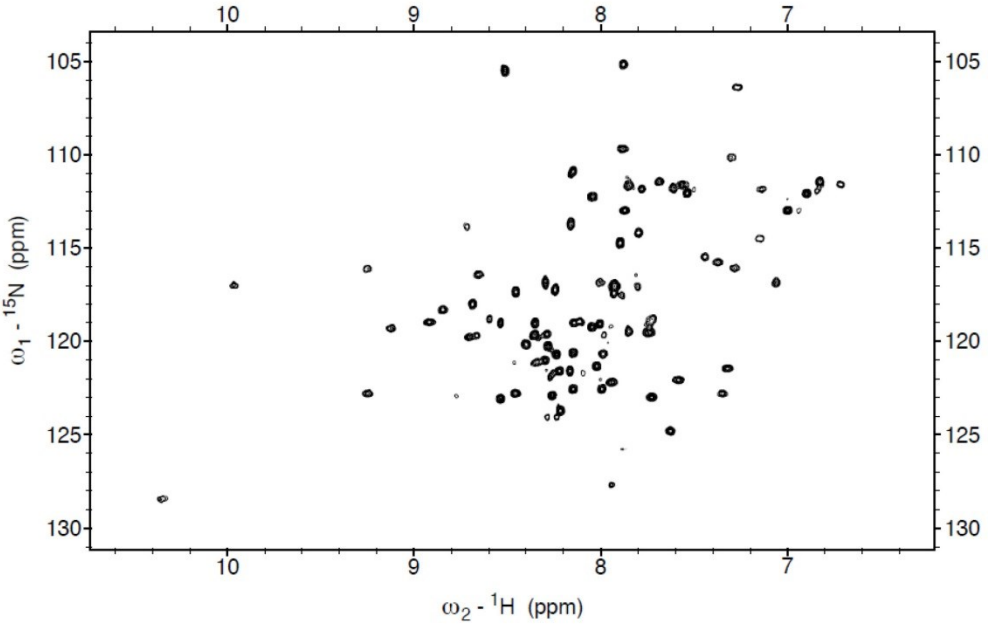

Nature Methods: doi:10.1038/nmeth.2175

Supplementary Figure 14

Octanoyl-[^{15}N]ACP / [8-$^{13}C_1$]octanoyl-[^{15}N]ACP HSQC spectrum overlay

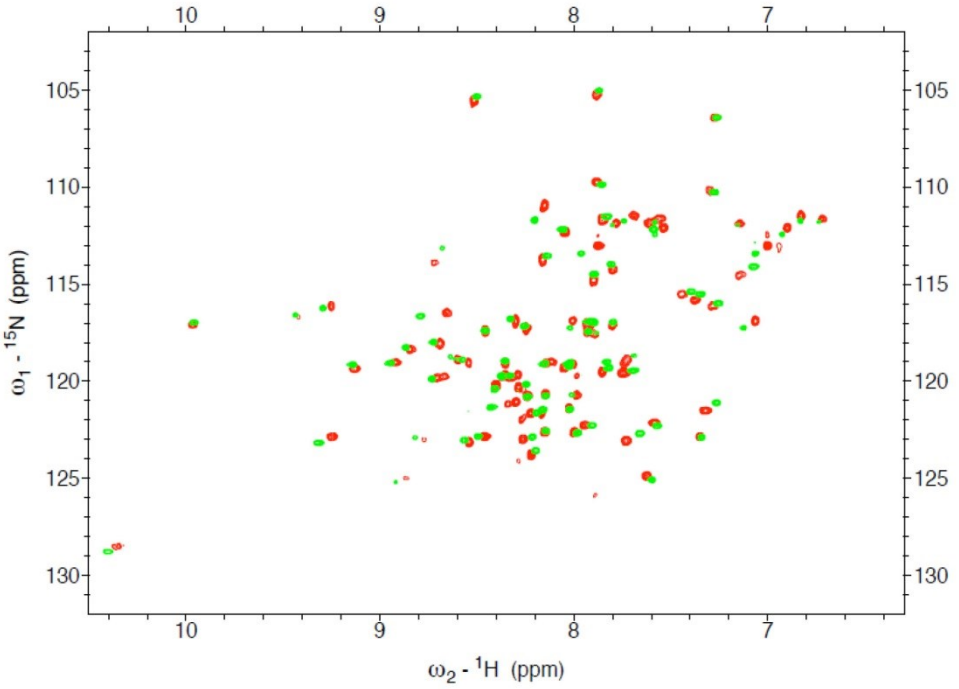

Supplementary Figure 15

[^{15}N]ACP NOE spectra: [$^{13}C_4$]butanoyl- vs. [8-$^{13}C_1$]octanoyl-[^{15}N]ACP

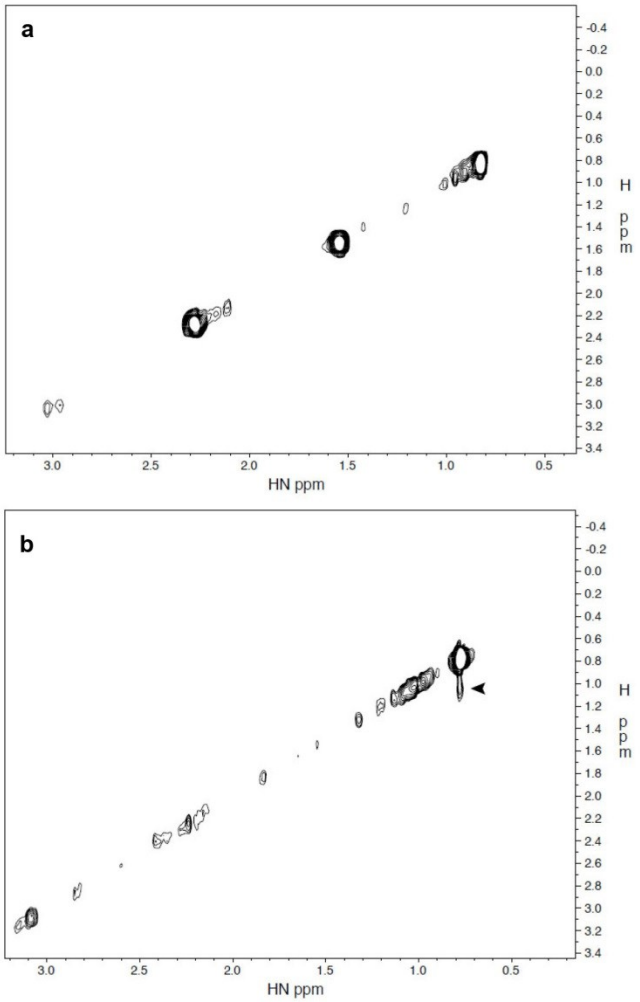

(**a**) NOE spectrum utilizing [$^{13}C_4$]butanoyl-oxypantetheine probe appended to [^{15}N]ACP. Lack of signal above background provides no evidence for sequestration into [^{15}N]ACP while the NOE spectrum for [8-$^{13}C_1$]octanoyl-oxypantetheine appended to [^{15}N]ACP (**b**) gives a noticeable signal (**arrow**) above baseline at approximately 1.0 H_{ppm} and 0.75 H-N_{ppm}.

Supplementary Figure 16

E. coli ACP reaction efficiency gels

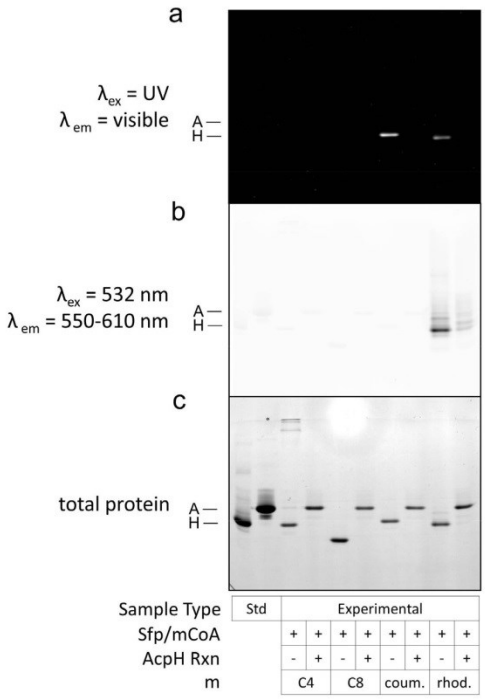

Labeling of *E. coli apo*-ACP proceeded using Sfp and a variety of pantetheine analogs. Butanoyl-pantetheine ("C4") was installed and removed with AcpH. Octanoyl-pantetheine ("C8") was installed and removed with AcpH. Coumarin-pantetheine ("coum.") was installed, giving a UV-fluorescent signal, and subsequently removed with AcpH. Lastly, rhodamine-CoA ("rhod.") was installed to give a UV and 532 nm excited fluorescent band, and was removed with AcpH. ACP products were evaluated on conformation-sensitive Urea-PAGE and compared to *apo*-/*holo*-ACP standards.

Supplementary Figure 17

Fusion-ACP reaction efficiency gels

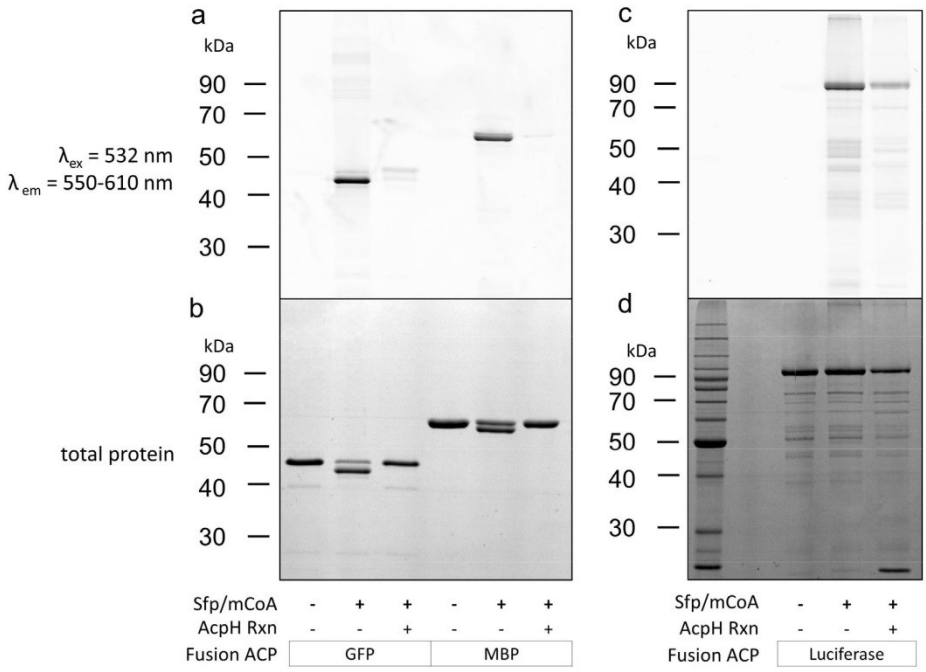

GFP-ACP, MBP-PaACP, and Luciferase-ACP proceed via Sfp/rhodamine-CoA reaction to convert the *apo*-ACPs into *crypto*-ACPs that fluoresce at 532 nm excitation and 550-610 nm emission. All *crypto*-fusion-ACPs are returned to the *apo*- form in good yield with AcpH treatment and evaluated by SDS-PAGE.

Nature Methods: doi:10.1038/nmeth.2175

Supplementary Figure 18

Utilized ACP probe structures

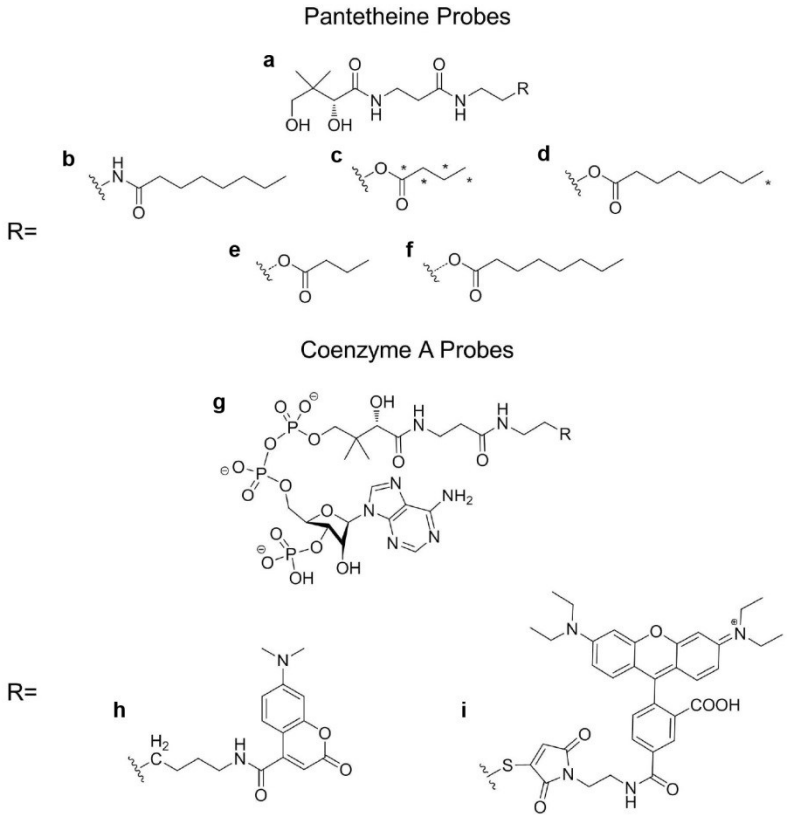

(a) The pantetheine moiety served as the basis for attachement of varied acyl groups to [^{15}N]ACP, including an octanoyl- group **(b)** via an amide linkage, as well as [$^{13}C_4$]butanoyl- **(c)** and [8-$^{13}C_1$]octanoyl- **(d)** via oxyester linkage for NMR studies, as well as regular butanoyl (**e**) and octanoyl (**f**) pantoxy analogs for ACP reaction efficiency studies. **(g)** Coenzyme A provided a scaffold for attachment of two different fluorophores for further reaction and linkage to ACP, including coumarin **(h)** and rhodamine **(i)**.

Supplementary Figure 19

PMP oxypantetheine [8-$^{13}C_1$]caprylic ester H-NMR

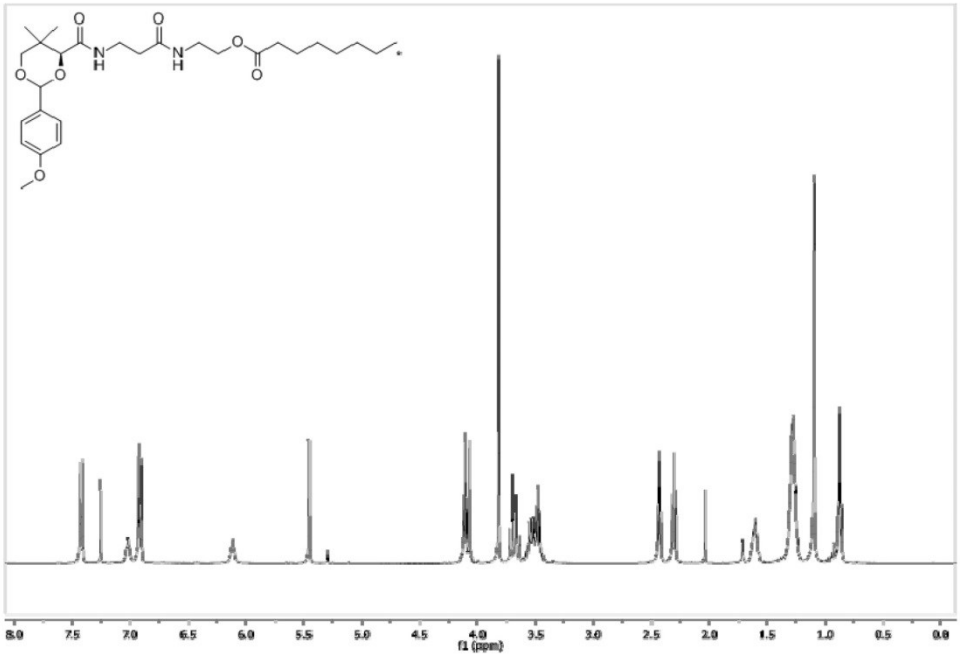

Nature Methods: doi:10.1038/nmeth.2175

Supplementary Figure 20

PMP oxypantetheine [8-$^{13}C_1$]caprylic ester C-NMR

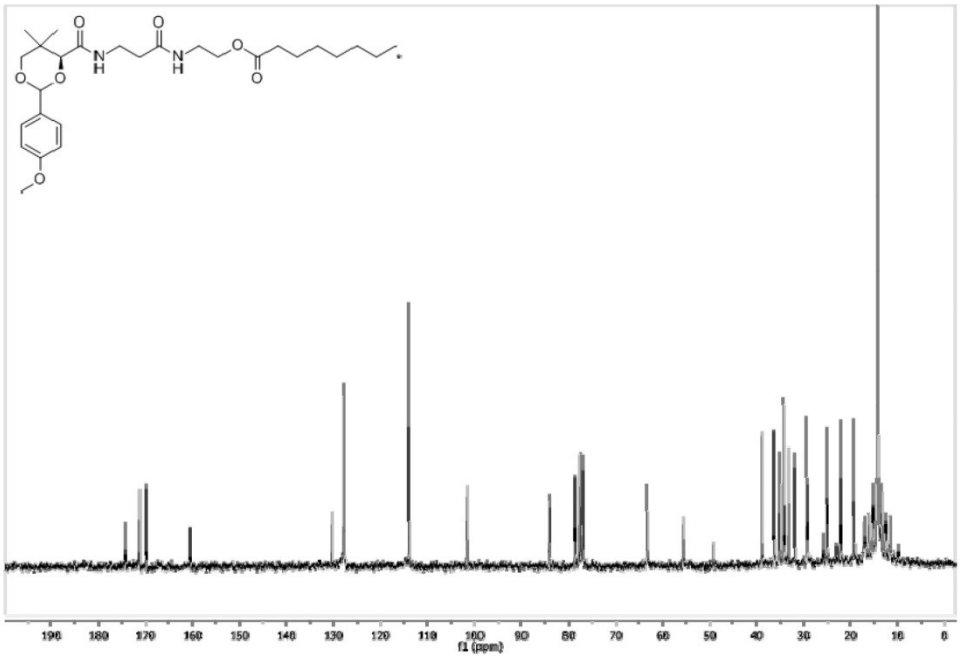

Supplementary Figure 21

PMP oxypantetheine [8-$^{13}C_1$]caprylic ester MS

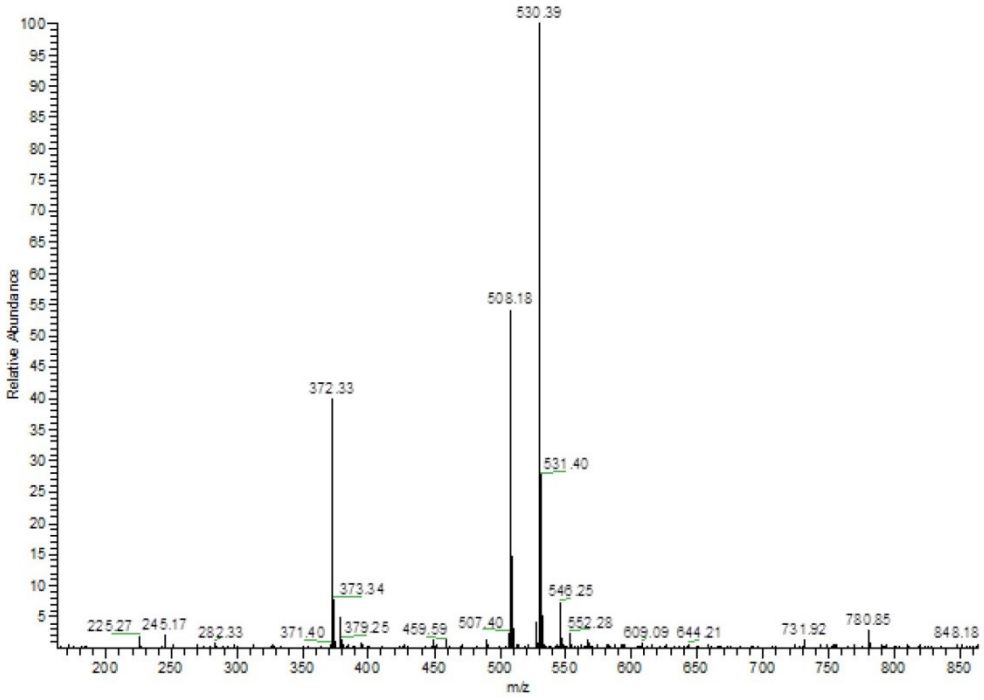

Nature Methods: doi:10.1038/nmeth.2175

Supplementary Figure 22

PMP Oxypantetheine caprylic ester H-NMR

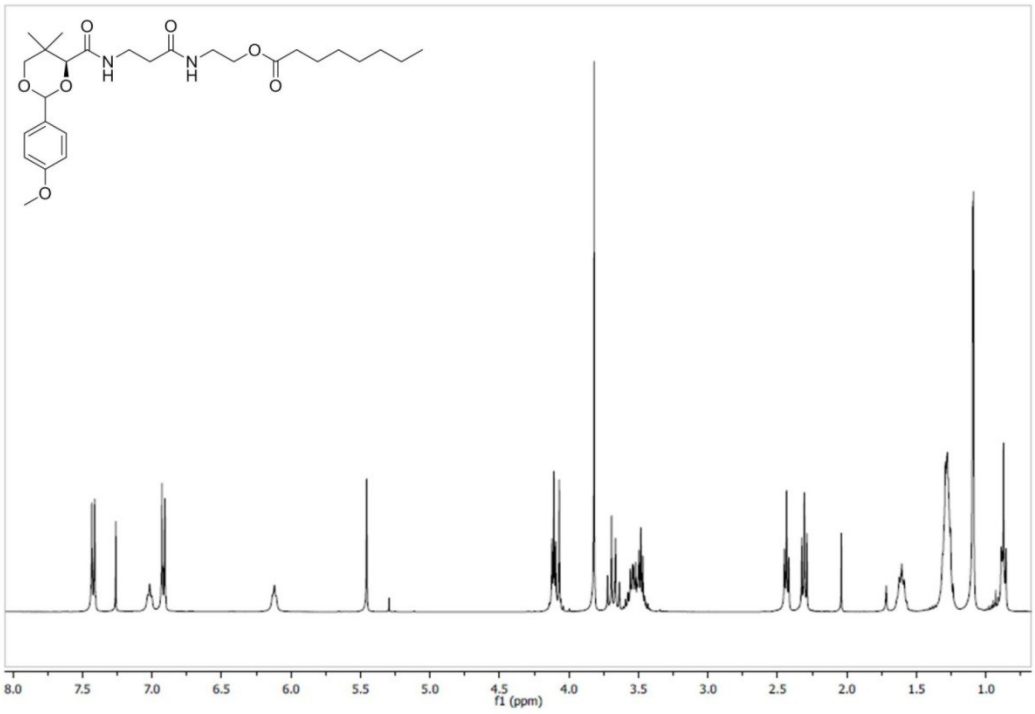

Supplementary Figure 23

PMP Oxypantetheine caprylic ester C-NMR

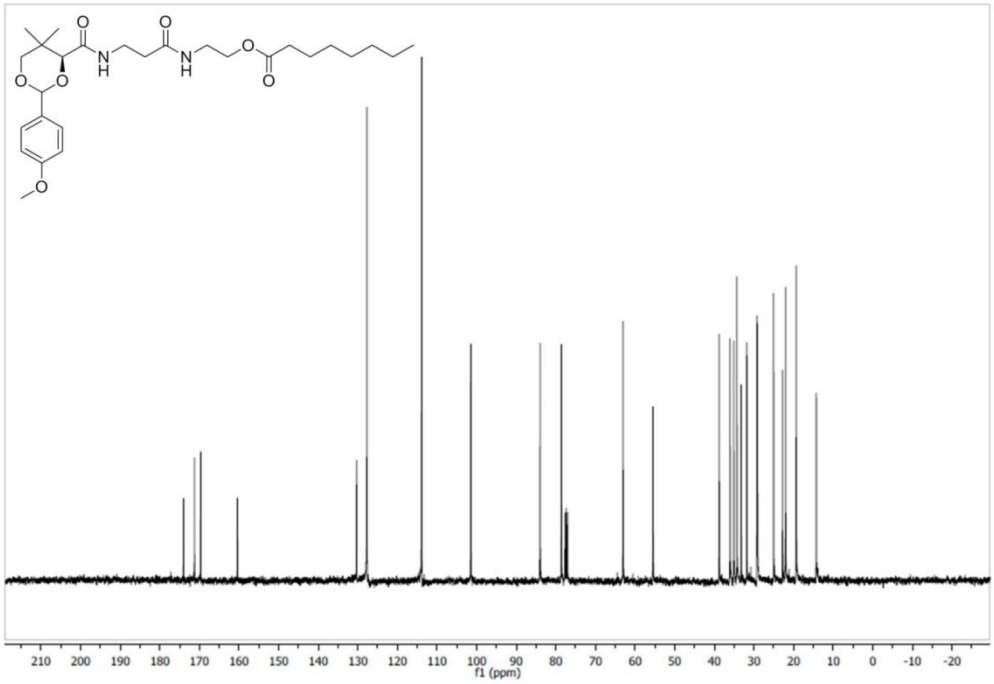

Supplementary Figure 24

PMP Oxypantetheine caprylic ester MS

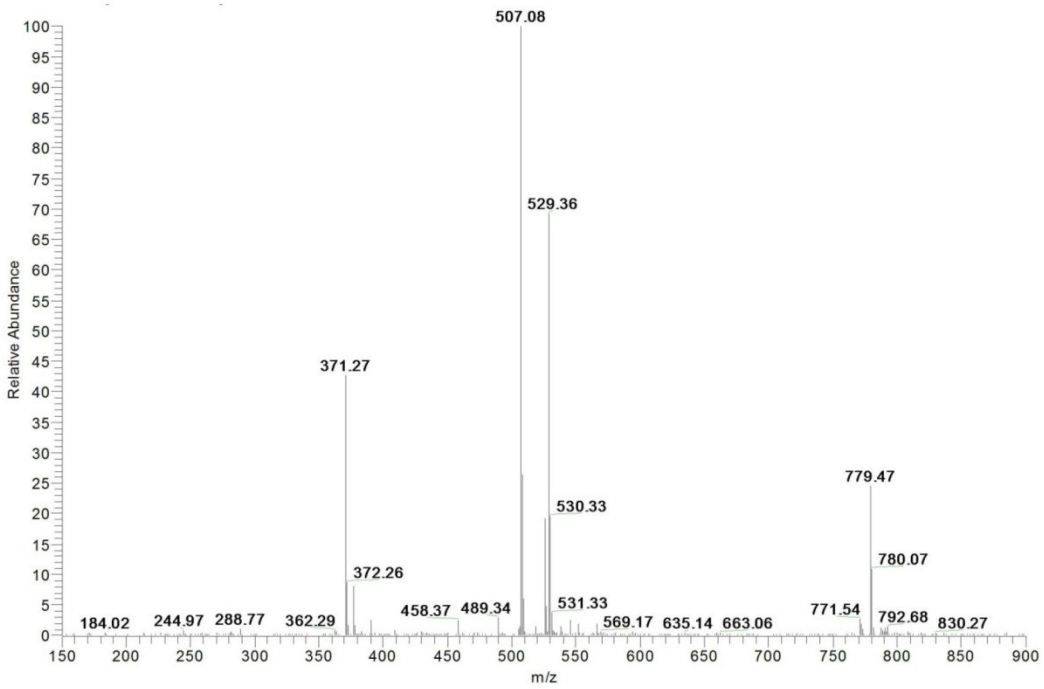

Supplementary Figure 25

Oxypantetheinediol [8-$^{13}C_1$]caprylic ester H-NMR

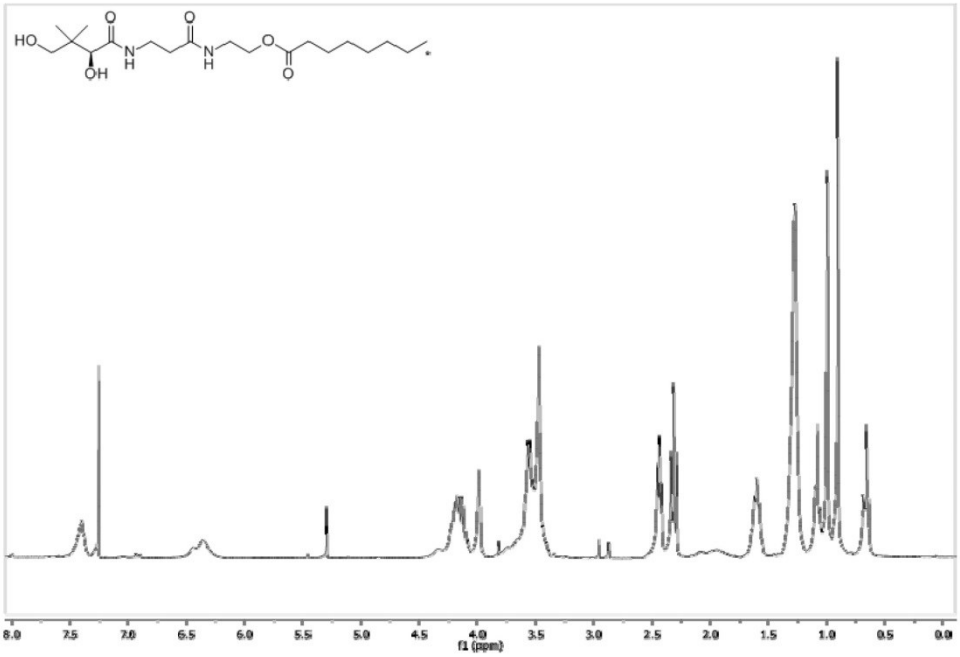

Supplementary Figure 26

Oxypantetheinediol [8-$^{13}C_1$]caprylic ester C-NMR

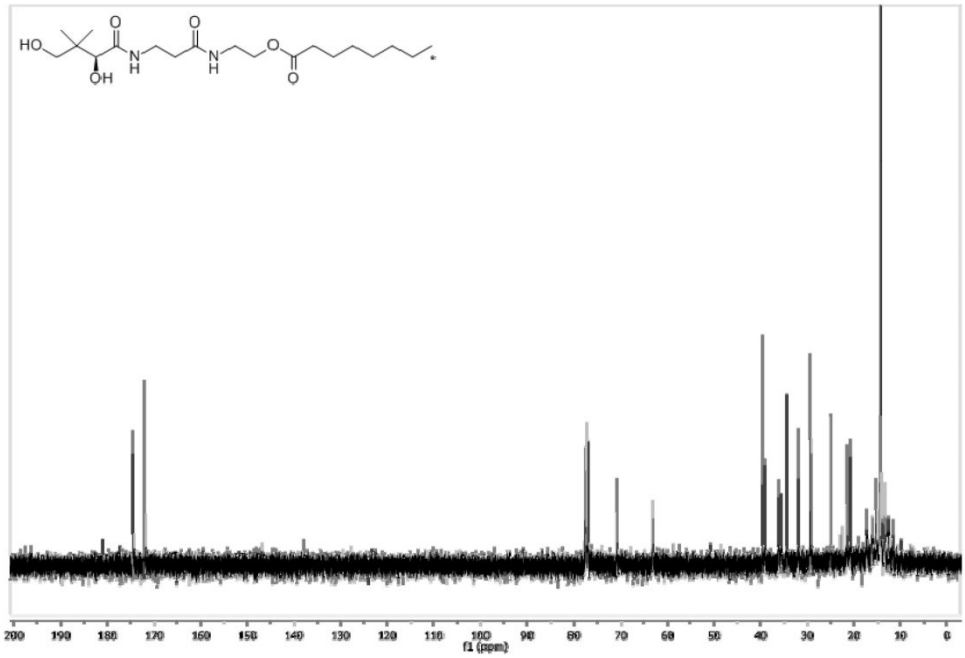

Supplementary Figure 27

Oxypantetheinediol [8-$^{13}C_1$]caprylic ester MS

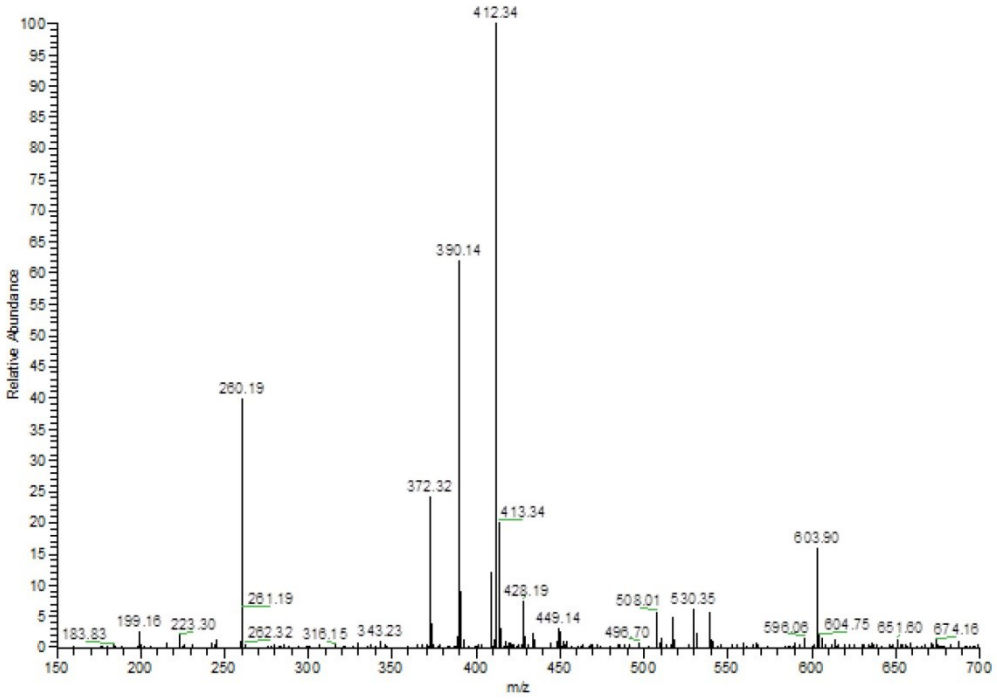

Supplementary Figure 28

Oxypantetheinediol caprylic ester H-NMR

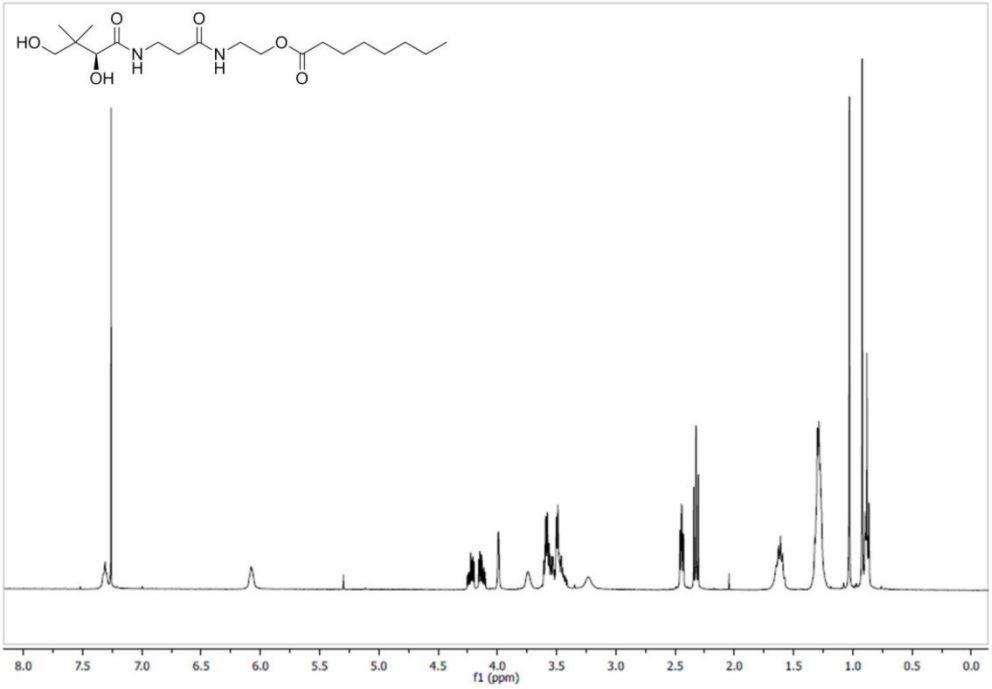

Supplementary Figure 29

Oxypantetheinediol caprylic ester C-NMR

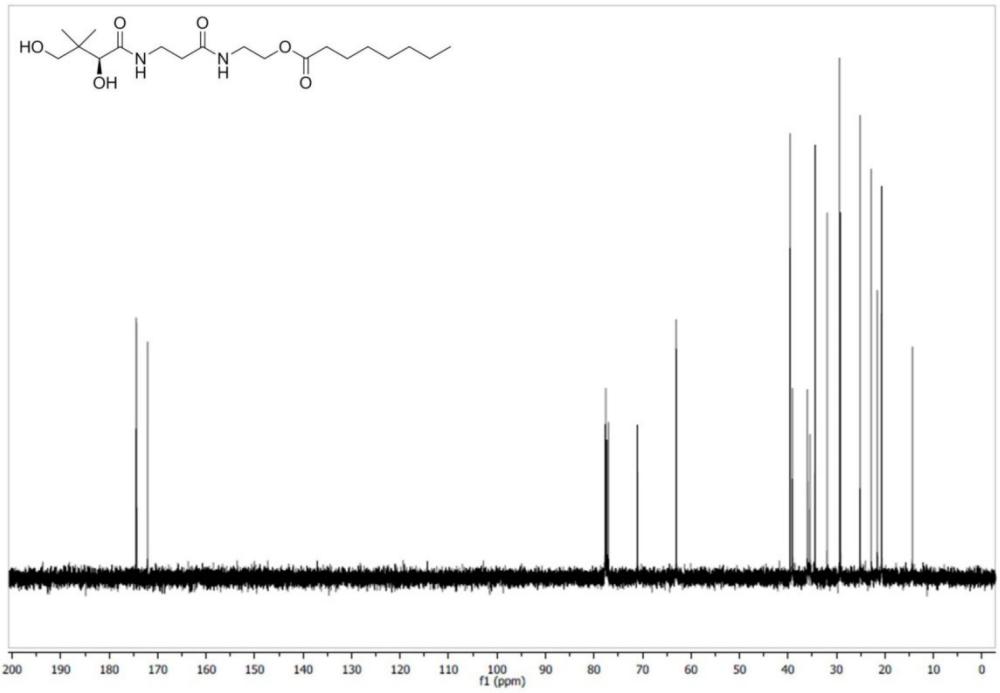

Nature Methods: doi:10.1038/nmeth.2175

Supplementary Figure 30

Oxypantetheinediol caprylic ester MS

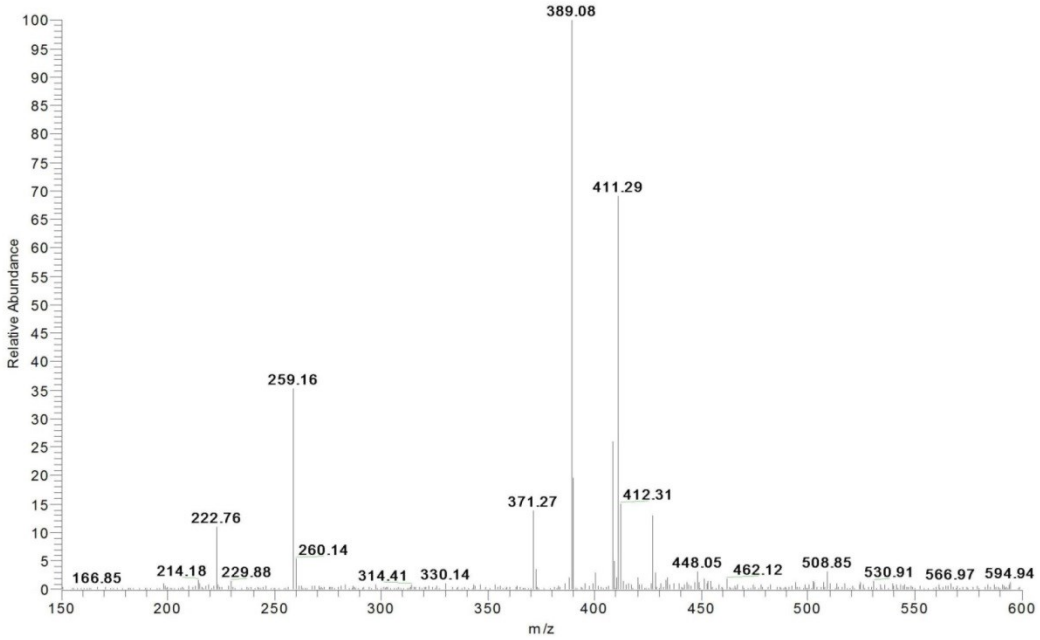

Supplementary Figure 31

PMP oxypantetheine [$^{13}C_4$]butyl ester H-NMR

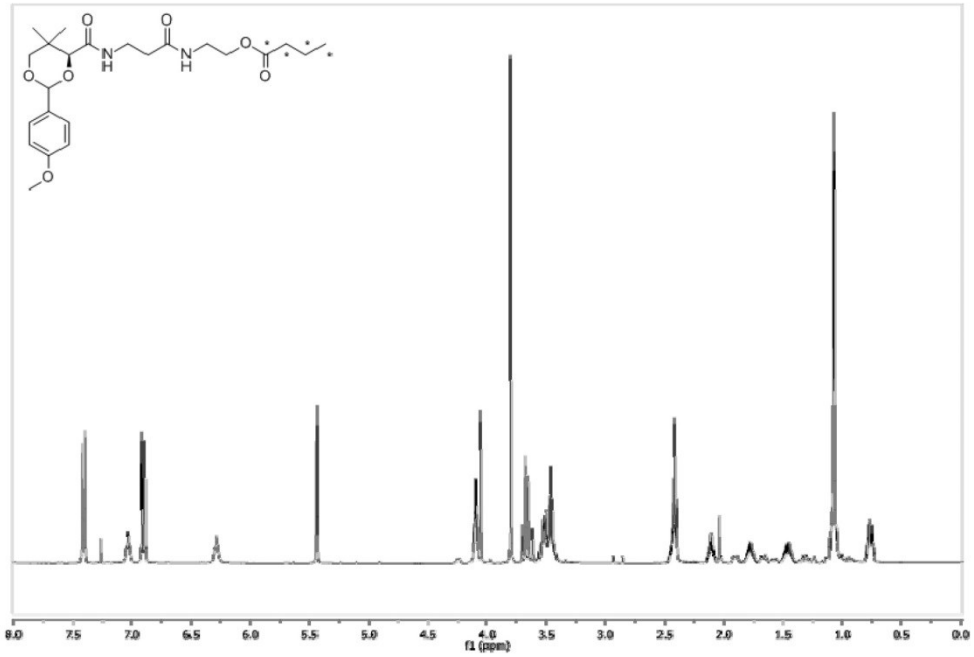

Supplementary Figure 32

PMP oxypantetheine [$^{13}C_4$]butyl ester C-NMR

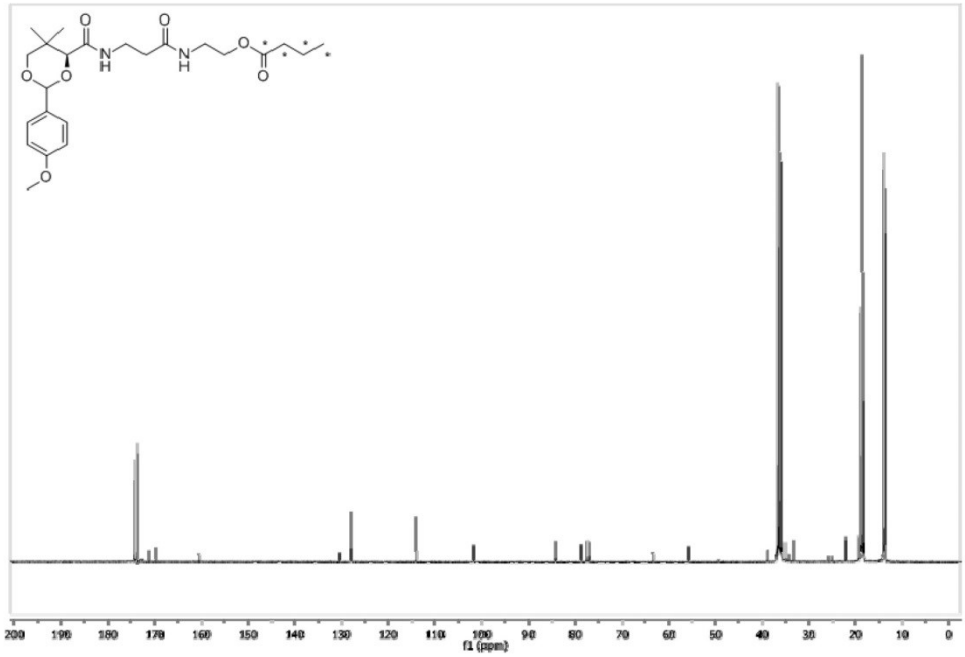

Nature Methods: doi:10.1038/nmeth.2175

Supplementary Figure 33

PMP oxypantetheine [$^{13}C_4$]butyl ester MS

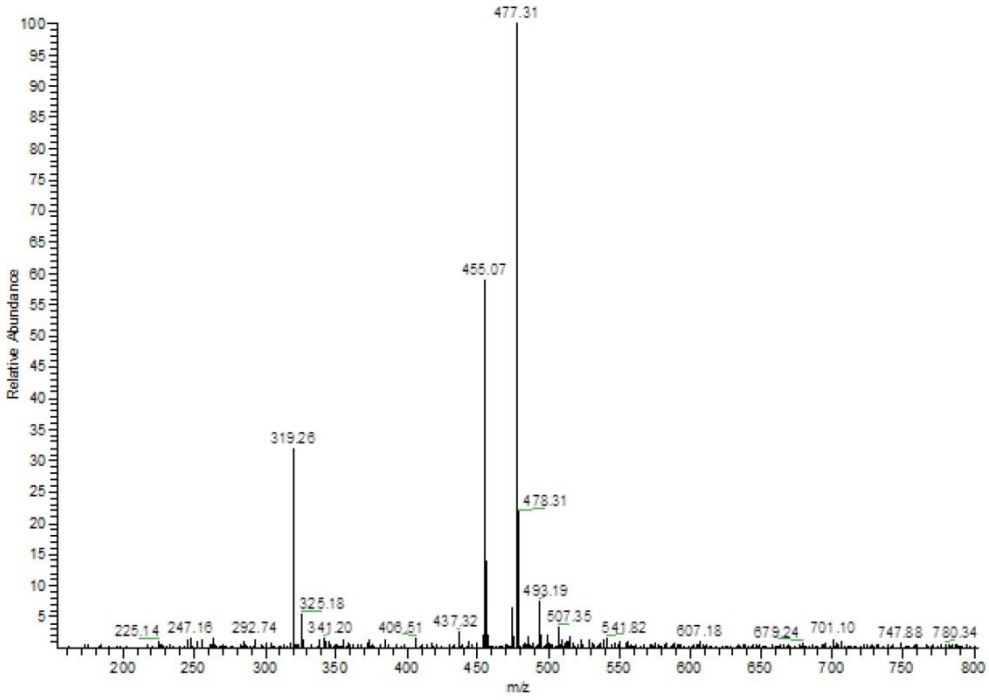

Nature Methods: doi:10.1038/nmeth.2175

Supplementary Figure 34

PMP Oxypantetheine butyl ester H-NMR

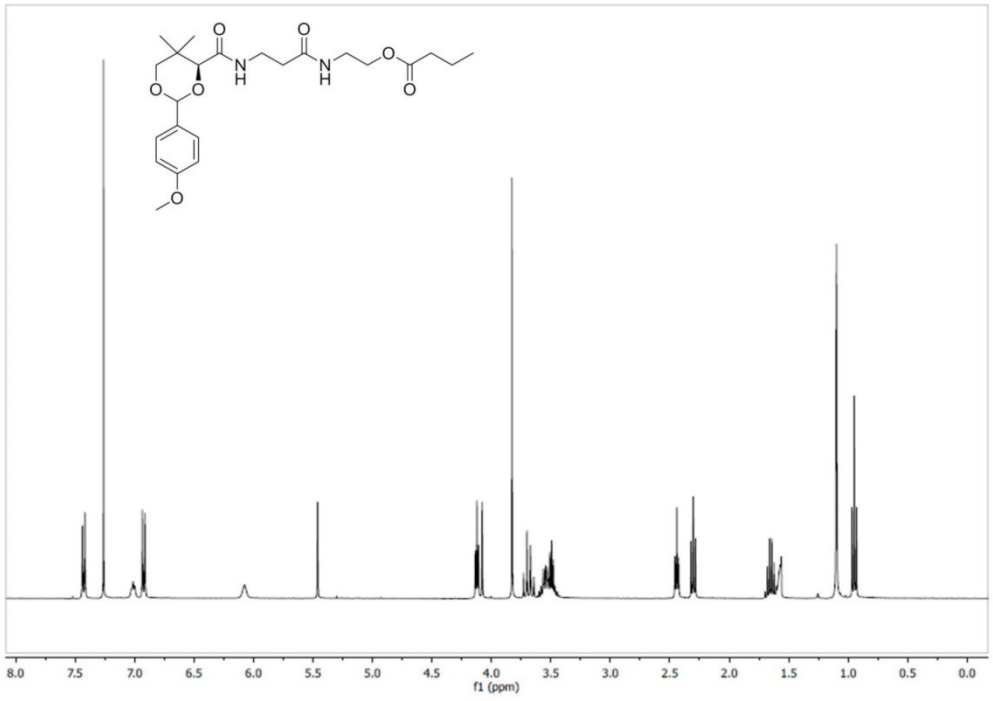

Supplementary Figure 35

PMP Oxypantetheine butyl ester C-NMR

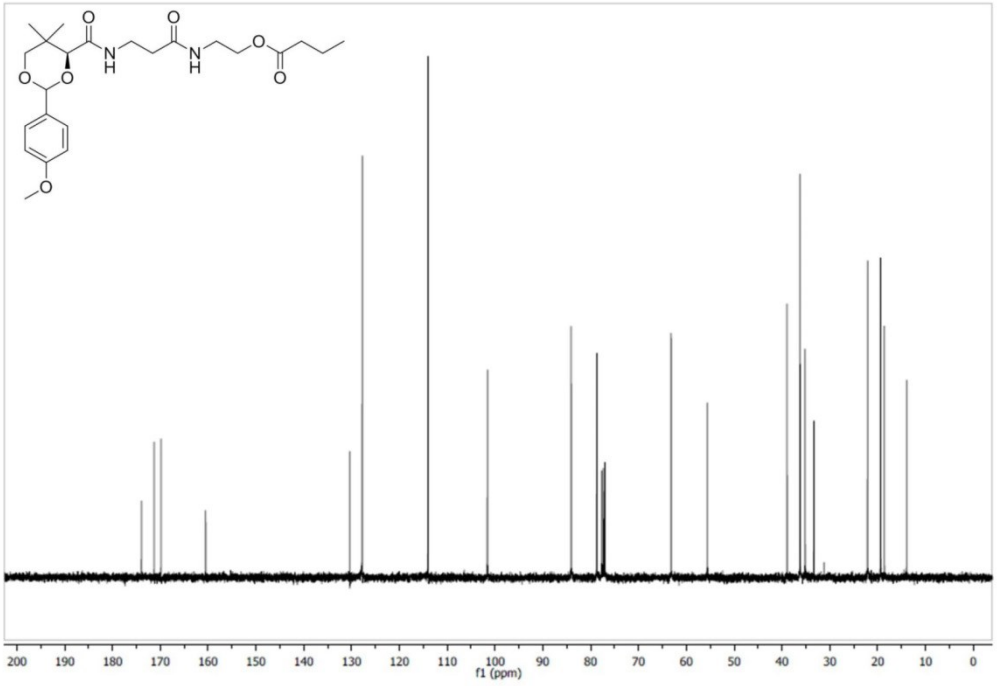

Nature Methods: doi:10.1038/nmeth.2175

Supplementary Figure 36

PMP Oxypantetheine butyl ester MS

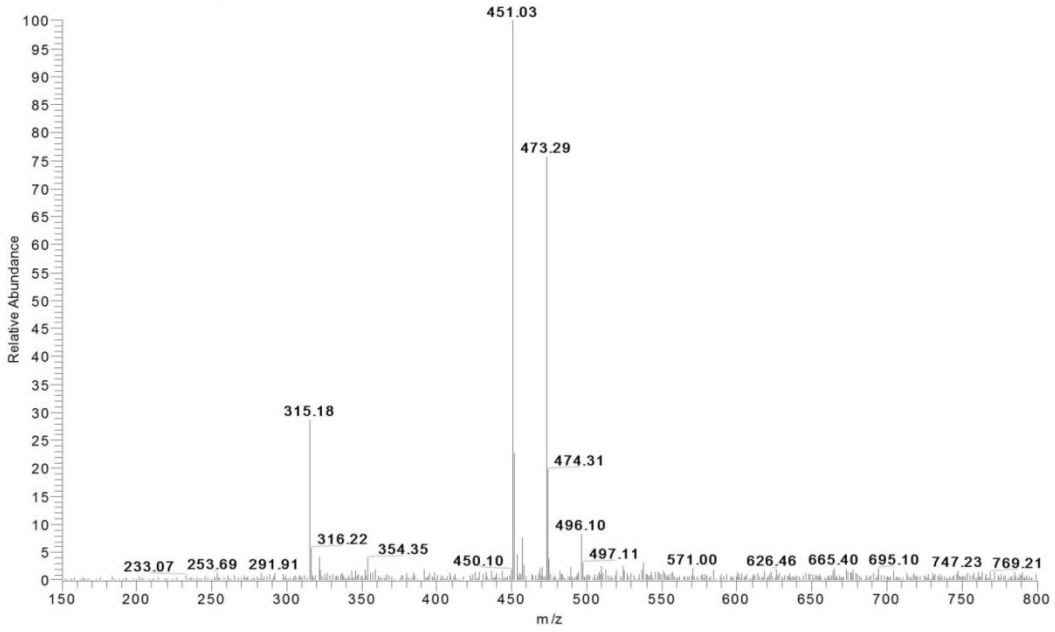

Supplementary Figure 37

Oxypantetheinediol [$^{13}C_4$]butyl ester H-NMR

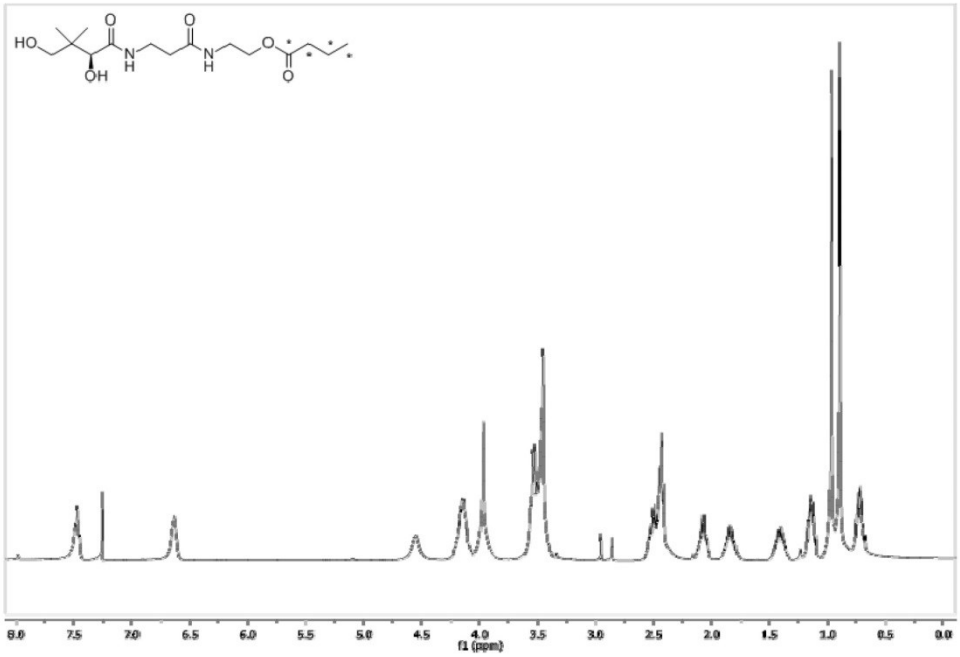

Nature Methods: doi:10.1038/nmeth.2175

Supplementary Figure 38

Oxypantetheinediol [$^{13}C_4$]butyl ester C-NMR

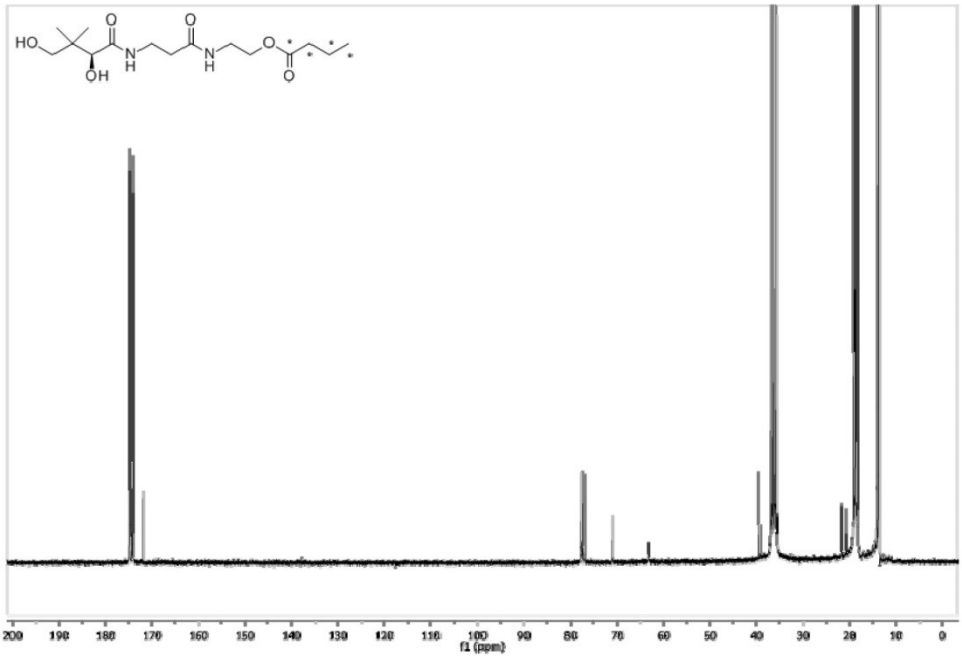

Supplementary Figure 39

Oxypantetheinediol [$^{13}C_4$]butyl ester MS

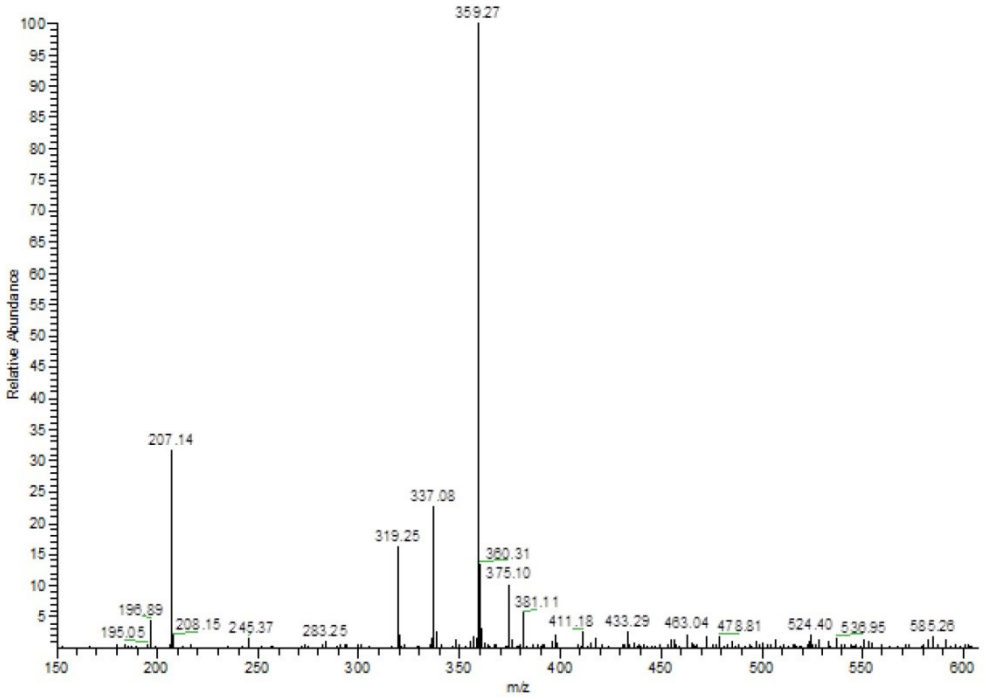

Supplementary Figure 40

Oxypantetheinediol butyl ester H-NMR

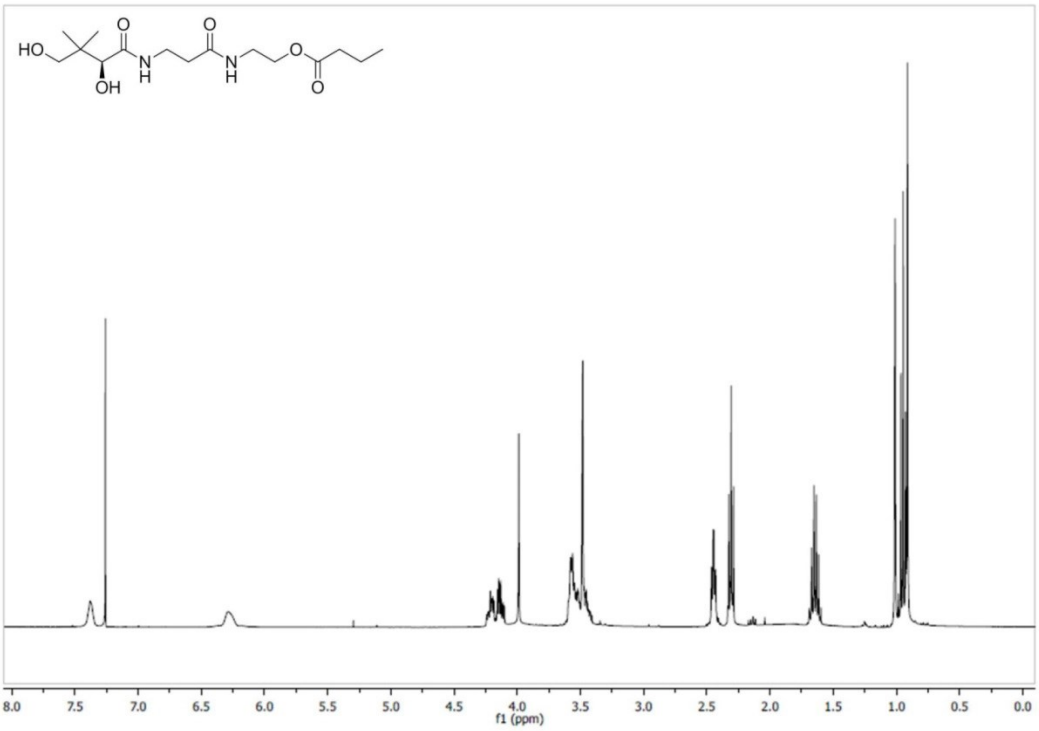

Supplementary Figure 41

Oxypantetheinediol butyl ester C-NMR

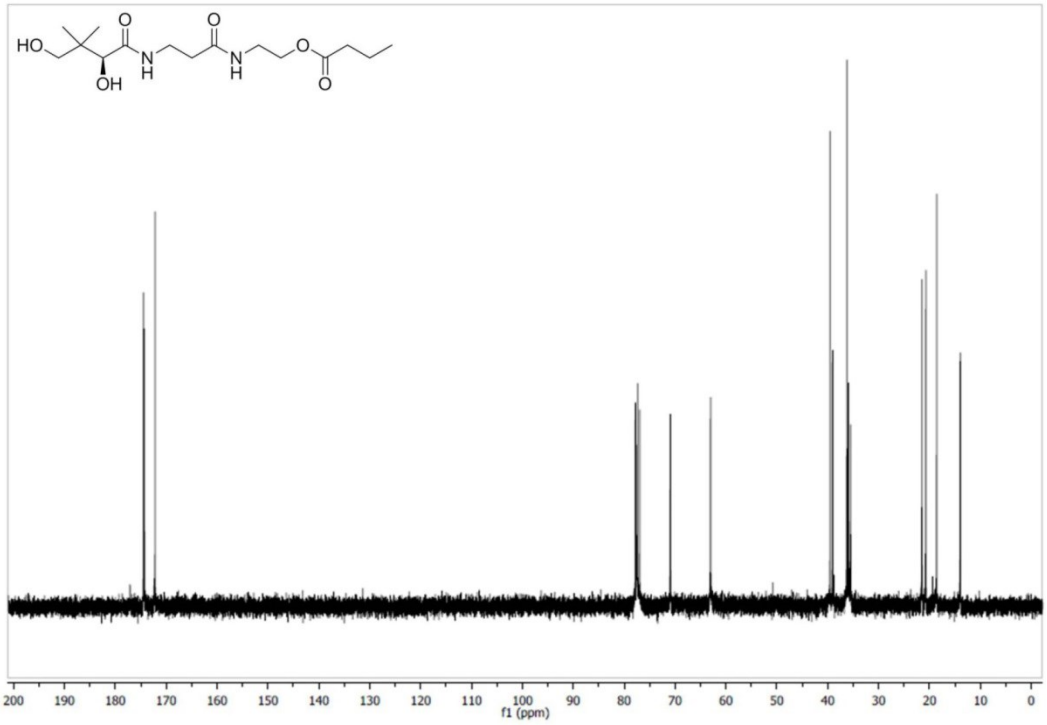

Supplementary Figure 42

Oxypantetheinediol butyl ester MS

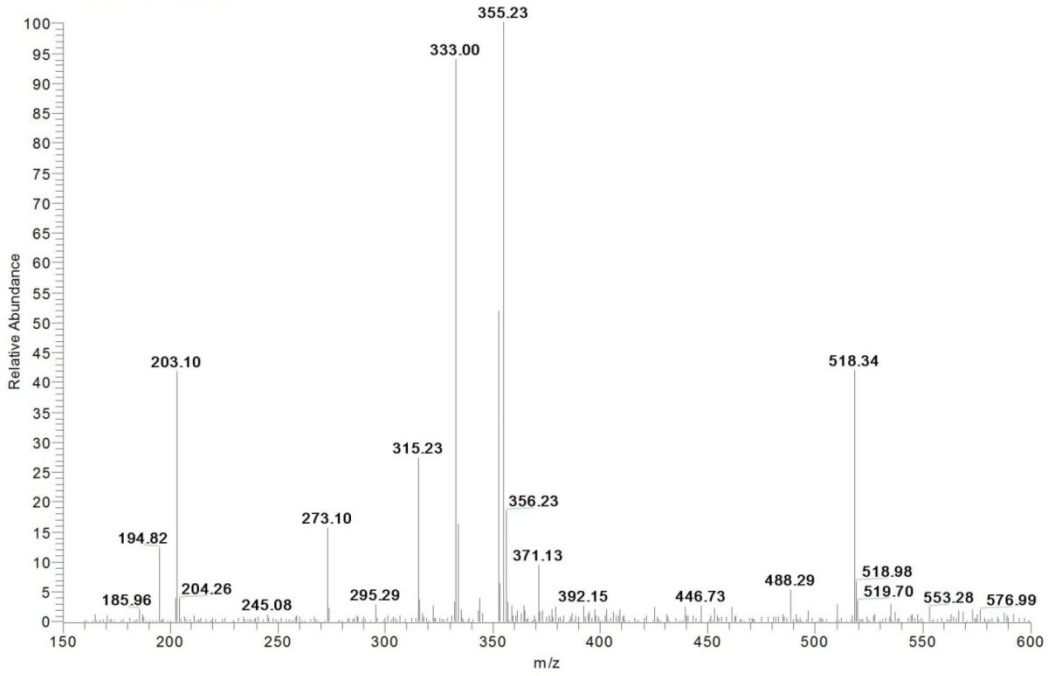

Supplementary Table 1

Recovery of [^{15}N]ACP from NMR experiments

Purified [^{15}N]ACP Sample Recovery

	***apo* #1**	**octanoyl**	***apo* #2**	**[$^{13}C_4$] butanoyl**	**[8-$^{13}C_1$] octanoyl**
Calculated Mass, A280 (mg)	4.6	2.7	2.0	1.6	1.2
Step Yield (%)	-	59%	74%	80%	75%†

UV absorbance measurements were conducted on the [^{15}N]ACP sample conducted at several discrete steps to track protein quantity. While sample recovery is not complete at each step, this method is well suited to *apo*-[^{15}N]ACP regeneration with slight modifications enhancing protein retention. †Note: Two-step yield is calculated for [8-$^{13}C_1$]octanoyl-[^{15}N]ACP, as the concentration was not determined for the intermediate *apo*-[^{15}N]ACP.

Supplementary Table 2

Primers used for ACP/AcpH cloning

Primer Name	Primer Sequence (5' → 3')
AcpH F1	AAAAAACATATGAACTACCTCGC
AcpH R1	AAAAAACTCGAGTCAGCGCTGGCTCAG
AcpH F2	AAAAAACATATGAACTATCTGGCACACC
AcpH R2	AAAAAACTCGAGTTAGCGCTGAGACAG
AcpH F3	GTCTCAGCGCGGACTCGAGCACCACCACCACC
AcpH R3	GTGCTCGAGTCCGCGCTGAGACAGGGCAAATGC
PaACP F1	AAAAAACATATGAGCACCATCG
PaACP R1	AAAAAACTCGAGTTGCTGGTGAG
EcACP F1	AAAAGGATCCAGCACTATCGAAGAACGCGTTAAG
EcACP R1	AAAACTCGAGCGCCTGGTGGCCGTTGATGTAATC
LuxCt F1	AAAACATATGAAATTTGGTAACTTCCTTTTAACTTATC
LuxCt R1	AAAAGGATCCTGAATGATATTTAACAATGTTAGCATTTACTAC
LuxCt 695bp	CAGTTGATCACGATTCAAACAAAGC
LuxCt 1390bp	CTTGATCAAATGAGTGAAGGTCG

Primers used in cloning/subcloning for gene products used in this manuscript. Intentionally placed restriction sites are underlined.

Supplementary Methods

Cloning of MBP-AcpH, AcpH-6xHis, MBP-PaACP, and Lux-ACP Constructs. The AcpH gene [PA4353] identified previously[1] was PCR-amplified from *P. aeruginosa* PAO1 genomic DNA using forward primer "AcpH F1" and reverse primer "AcpH R1" (**Supplementary Table 2**). NdeI/XhoI restriction-digested AcpH insert was then ligated into a pET24b vector modified with an N-terminal MBP fusion tag originally from pMALc2 according to procedure described elsewhere[2] for increased solubility and orthogonal purification purposes. A 'free' 6xHis-tagged version was also constructed using an *E. coli*-optimized sequence of PA4353 purchased in a pUC57 vector (GeneWiz Inc, South Plainfield, NJ). All attempts to sub-clone the gene into vectors providing N-terminal 6xHis tags produced insoluble protein (pET28b, pCDF-2, pBAD-HisC). The gene was subcloned into pET29b using NdeI/XhoI primers "AcpH F2" and "AcpH R2", restriction digested, and ligated to generate a native construct (not used in this experiment). The native construct was then subjected to site directed mutagenesis with forward primer "AcpH F3" and reverse primer "AcpH R3" to remove the stop codon to allow translation of the C-terminal 6xHis tag. This final construct was transformed into *E. coli* BL-21(DE3) for soluble expression of a free C-terminal 6xHis-tagged construct. The ACP gene [PA2966] used to generate MBP-PaACP was PCR-amplified from *P. aeruginosa* PAO1 genomic DNA using forward primer "PaACP F1" and reverse primer "PaACP R1". NdeI/XhoI restriction-digested PaACP was ligated into the same MBP pET24b-based vector as described for AcpH, except the ACP stop codon was omitted to generate a C-terminal 6xHis affinity tag. For construction of the luciferase-ACP fusion, *E. coli* ACP was cloned from stock plasmid encoding wild-type ACP using forward primer "EcACP F1" and reverse primer "EcACP R1". *E. coli* ACP PCR product was then restriction digested with BamHI/XhoI and inserted into pET29a. This *E. coli* ACP plasmid was sequenced for verification and subjected to NdeI/BamHI restriction digestion in preparation for luciferase gene insertion. Bacterial luciferase (*V. harveyi* luxAB fusion) was cloned from a synthetic construct termed luxCt[3] using forward primer "LuxCt F1" and reverse primer "LuxCt R1". The luxCt PCR product was restriction digested with NdeI/BamHI and ligated into the pET29 containing *E. coli* ACP. Sequence verification was performed using T7 promoter/terminator primers, as well as internal luxCt primers "LuxCt 695bp" and "LuxCt 1390bp".

Luciferase-ACP Activity Assay. The luciferase assay was conducted under the same parameters as reported previously[3], however with reduced well volume of 200 µL in 96-well plate Costar 3694 (Corning Inc, Lowell, MA) from 357.5 µL and substitution of 1 mM dithiothreitol (DTT) for 50 mM β-mercaptoethanol. All luciferase-ACP, including original/regenerated *apo* and *crypto*, were buffer exchanged into 50 mM NaH_2PO_4 pH 7.0, 400 mM sucrose, 1 mM DTT prior to analysis in the assay.

Generation and purification of *apo*/*crypto* luciferase-ACP were conducted with the same methods as for other ACPs. The 96-well plate was centrifuged 2 minutes and evaluated on a Perkin-Elmer HTS 7000 Plus plate reader at room temperature with 1 second integration time per well using a gain of 150.

Nature Methods: doi:10.1038/nmeth.2175

Supplementary Note

General Coupling Scheme of PMP Oxypantethiene to ^{13}C-labeled Fatty Acids (PMP Oxypantethiene [$^{13}C_4$]Butyl Ester, PMP Oxypantethiene Butyl Ester, [8-$^{13}C_1$]Caprylic-acid, Caprylic acid). In a 50ml round bottom reaction flask DCM was added as to generate a solution which was 0.1M with respect to the Fatty Acids. The solution was cooled to 0°C and the reagents added in the following order. 1.6 molar equivalents of Dicyclohexylcarbodimide were added followed by 1.0 molar equivalent of 4-Dimethylaminopyridine and 0.5 molar equivalence of Camphorsulfonic acid. The solution was allowed to stir momentarily before the addition of 1.1 molar equivalent of the PMP Oxypantethiene prepared previously[10]. The reaction was allowed to proceed over night and was quenched with a sufficient amount of water as to remove any existing carbodimide. The solution was filtered to remove the precipitated dicyclohexyl urea. Solvents were removed via vacuum followed by flash chromatography (elution conditions, 2:1, Hexanes:EtoAC to EtoAC neat) to give the analogues as a yellow oil (90-98% yield).

General Deprotection Scheme of PMP Oxypantethiene Esters. Deprotection was performed in a 25ml round bottom flask which contained sufficient THF to generate a 0.05M solution with respect to the Oxypantethiene Ester. A catalytic amount of 1M HCl was added to the solution and the reaction was allowed to proceed overnight. Solvent was reduced under vacuum followed by flash chromatography (elution conditions, Column charged with DCM increase MeOH gradient 10% until product elutes) to afford the analogues as a yellow oil. (80-85% yield)

Protein NMR Parameters. HSQC spectra were acquired on a Varian 500 MHz or a Varian 800 MHz spectrometer. The spectra of both apo-[15N]ACP preparations were acquired with identical parameters. The spectra were processed with NMRpipe and analyzed with Sparky.

Mass Spectrometry. Samples evaluated by mass spectrometry utilized electron spray ionization (ESI) in positive ion mode.

PMP-Oxypantethiene [8-$^{13}C_1$]caprylic ester (Supplementary Figures 19, 20, 21) & PMP-Oxypantethiene caprylic ester (Supplementary Figures 22, 23, 24). ^{1}H NMR (300MHz, $CDCl_3$) δ 7.48 – 7.38 (m, 2H, **H**Ar), 7.02 (t, *J* = 5.9 Hz, 1H, N**H**), 6.97 – 6.86 (m, 2H, **H**Ar), 6.12 (s, 1H, N**H**), 5.45 (s, 1H, $(CH_2O)_2C\mathbf{H}Ar$), 4.18 – 4.08 (m, 2H, (CO)O$\mathbf{CH_2}$CH2), 4.06 (s, 1H, CC**H**OH(CO)), 3.82 (s, 3H, O$\mathbf{CH_3}$), 3.68 (dd, *J* = 22.6, 11.4 Hz, 2H, NHC$\mathbf{H_2}CH_2$), 3.61 – 3.41 (m, 4H,(CO)NHC$\mathbf{H_2}CH_2$, O$\mathbf{CH_2}$C), 2.43 (t, *J* 6.3 Hz, 2H, $CH_2C\mathbf{H_2}$CO), 2.36 – 2.26 (m, 2H, CO$\mathbf{CH_2}CH_2$), 1.68 – 1.52 (m, 2H,

$COCH_2C\mathbf{H}_2CH_2$), 1.29 (tq, *J* = 14.4, 7.3 Hz, 8H, $CH_2C\mathbf{H}_2CH_2$), 1.09 (d, *J* = 1.9 Hz, 6H, $C(C\mathbf{H}_3)_2$), 0.94 – 0.82 (m, 3H, CH_2CH_3) ^{13}C NMR (300MHz, $CDCl_3$) δ 174.15, 171.27, 169.89, 160.49, 130.36, 127.77, 113.99, 101.61, 84.03, 78.71, 63.21, 55.57, 38.93, 36.22, 35.17, 34.39, 33.33, 31.92, 29.36, 29.17, 25.13, 22.63, 22.12, 19.39, 14.36; **PMP-Oxypantethiene [8-^{13}C$_1$]caprylic ester** LRMS exact mass calculated for $[M+Na]^+$ ($C_{27}H_{42}N_2O_7$) requires *m/z* 530.29, found *m/z* 530.39; **Oxypantethienecaprylic ester** LRMS exact mass calculated for $[M+Na]^+$ ($C_{27}H_{42}N_2O_7$) requires *m/z* 529.29, found *m/z* 529.36

Oxypantethienediol [8-^{13}C$_1$]caprylic ester (Supplementary Figures 25, 26, 27) & Oxypantethienediol caprylic ester (Supplementary Figures 28, 29, 30). ^{1}H NMR (400MHz, $CDCl_3$) δ 7.40 (s, 1H, $CON\mathbf{H}CH_2$), 6.36 (s, 1H, $CON\mathbf{H}CH_2$), 4.15 (m, 2H, $CH_2C\mathbf{H}_2$(CO)), 3.99 (s, 1H, $CC\mathbf{H}OH$(CO)), 3.57-3.38 (m, 6H, $HOC\mathbf{H}_2C$, (CO)$NC\mathbf{H}_2CH_2$), (CO)$NC\mathbf{H}_2CH_2$), 2.51 – 2.38 (m, 2H, $CH_2C\mathbf{H}_2$(CO)), 2.32 (t, *J* = 7.6 Hz, 2H, (COO)$C\mathbf{H}_2CH_2$), 1.69 – 1.52 (m, 2H, (CO)$CH_2C\mathbf{H}_2CH_2$), 1.28 (s, 6H, CH_2 $C\mathbf{H}_2C\mathbf{H}_2C\mathbf{H}_2CH_2$), 1.07 (d, *J* = 6.6 Hz, 2H, $CH_2C\mathbf{H}_2CH_3$), 1.00 (s, 3H, $CC\mathbf{H}_3$), 0.91 (s, 3H, $CC\mathbf{H}_3$), 0.66 (t, *J* = 6.5 Hz, 3H, $CH_2C\mathbf{H}_3$); ^{13}C NMR (300MHz, $CDCl_3$) δ 174.48, 174.40, 172.09, 77.63, 70.94, 63.08, 39.57, 39.08, 36.01, 35.51, 34.42, 31.94, 29.38, 29.19, 25.14, 22.65, 21.54, 20.75, 14.37; **Oxypantethienediol [8-^{13}C$_1$]caprylic ester** LRMS exact mass calculated for $[M+Na]^+$*m/z* ($C_{19}H_{36}N_2O_6$) requires 412.26, found *m/z* 412.34; **Oxypantethienediol caprylic ester** LRMS exact mass calculated for $[M+Na]^+$*m/z* ($C_{19}H_{36}N_2O_6$) requires 411.25, found *m/z* 411.33

PMP-Oxypantethiene [^{13}C$_4$]butyl ester (Supplementary Figures 31, 32, 33) & PMP-Oxypantethiene butyl ester (Supplementary Figures 34, 35, 36). ^{1}H NMR (400MHz, $CDCl_3$) δ 7.44 – 7.37 (m,2H, Ar**H**), 7.03 (t, *J* = 6.0 Hz, 1H, $CON\mathbf{H}CH_2$), 6.93 – 6.86 (m, 2H, Ar**H**), 6.28 (d, *J* = 4.9 Hz, 1H, $CON\mathbf{H}CH_2$), 5.44 (s, 1H, $(CH_2O)_2C\mathbf{H}$Ar), 4.10 (td, *J* = 5.4, 3.2 Hz, 2H, (CO)$OC\mathbf{H}_2$CH2), 4.05 (s, 1H, $CC\mathbf{H}OH$(CO)), 3.80 (s, 3H, $OC\mathbf{H}_3$), 3.66 (q, *J* = 11.5 Hz, 2H, $CONHC\mathbf{H}_2CH_2$), 3.59 – 3.39 (m, 4H, $CONHC\mathbf{H}_2CH_2$, $OC\mathbf{H}_2C$), 2.49 – 2.36 (m, 3H, $CH_2C\mathbf{H}_2CONH$, (CO)$OC\mathbf{H}_2CH_2$), 2.10 (m, 2H, $CH_2C\mathbf{H}_2CONH$), 1.75 (m, 2H, $COOC\mathbf{H}_2CH_2$), 1.46 (m, 2H, $CH_2C\mathbf{H}_2CH_3$), 0.78 (m, 3H, $CH_2CH_2C\mathbf{H}_3$); **PMP-Oxypantethiene [^{13}C$_4$]butyl ester** ^{13}C NMR (300MHz, $CDCl_3$) δ 174.24, 174.22, 174.21, 173.69, 173.67, 173.65, 173.64, 171.27, 169.84, 160.51, 130.40, 127.78, 114.02, 101.61, 84.09, 78.74, 63.18, 55.61, 38.95, 36.69, 36.35, 36.12, 35.78, 35.18, 34.29, 33.34, 25.91, 25.24, 22.12, 19.40,18.96, 18.94 ,18.62, 18.60, 18.28,18.26, 14.12, 14.08, 13.78, 13.74; **Oxypantethiene butyl ester** ^{13}C NMR (300MHz, $CDCl_3$) δ 173.94, 171.27, 169.83, 160.50, 130.39, 127.78, 114.00, 101.60, 84.08, 78.72, 61.18, 55.60, 38.94, 36.24, 35.17, 33.33, 22.11, 19.39, 18.61, 13.94; **PMP-Oxypantethiene [^{13}C$_4$]butyl ester** LRMS exact mass calculated for $[M+Na]^+$*m/z* ($C_{23}H_{34}N_2O_7$) requires 477.23, found *m/z* 477.31; **PMP-Oxypantethiene butyl ester** LRMS exact mass calculated for $[M+Na]^+$*m/z* ($C_{23}H_{34}N_2O_7$) requires 473.23, found *m/z* 473.29

Oxypantethienediol [$^{13}C_4$]butyl ester (Supplementary Figures 37, 38, 39) & Oxypantethienediol butyl ester (Supplementary Figures 40, 41, 42). ^{1}H NMR (400MHz, $CDCl_3$) δ 7.47 (t, *J* = 5.9 Hz, 1H, CON**H**CH_2), 6.63 (s, 1H, CON**H**CH_2), 4.55 (s, 1H, O**H**), 4.24 – 4.06 (m, 2H, CH_2C**H**$_2$(CO)O), 3.97 (s, 1H,CC**H**OH(CO)), 3.62 – 3.39 (m, 6H, HOC**H**$_2$C, (CO)NC**H**$_2CH_2$), 2.57 – 2.40 (m, 3H, (CO)NC**H**$_2CH_2$)), 2.16 – 2.00 (m, 2H, NHC**H**$_2CH_2$), 1.92 – 1.77 (m, 2H, (CO)C**H**$_2CH_2$), 1.48 – 1.32 (m, 2H, COO)C**H**$_2CH_2$), 0.97 (s, 3H, CC**H**$_3$), 0.89 (s, 3H, CC**H**$_3$), 0.72 (ddd, *J* = 12.5, 7.0, 4.0 Hz, 3H, CH_2C**H**$_3$); **Oxypantethienediol [$^{13}C_4$]butyl ester** ^{13}C NMR (300MHz, $CDCl_3$) δ 174.75, 174.73, 174.70, 174.68, 174.27, 173.99, 173.97, 173.94, 173.92, 172.04, 77.67, 71.14, 63.10, 39.61, 39.17, 36.88, 36.43, 36.12, 35.67, 21.67, 20.70, 19.09, 18.63, 18.18, 14.20,13.73; **Oxypantethienediol butyl ester** ^{13}C NMR (300MHz, $CDCl_3$) δ 174.46, 174.27, 172.18, 77.45, 70.91, 61.01, 39.53, 39.03, 36.24, 35.94, 35.52, 21.45, 20.71, 18.57, 13.92; **Oxypantethienediol [$^{13}C_4$]butyl ester** LRMS exact mass calculated for $[M+Na]^+$*m/z* ($C_{15}H_{28}N_2O_6$) requires 359.19, found *m/z* 359.27; **Oxypantethienediol butyl ester** LRMS exact mass calculated for $[M+Na]^+$*m/z* ($C_{15}H_{28}N_2O_6$) requires 355.18, found *m/z* 355.23

Supplementary References:

1. Murugan, E., Kong, R., Sun, H., Rao, F. & Liang, Z.-X. *Protein Expres. Purif.* **71**, 132–138 (2010).
2. McCafferty, D. G., Lessard, I. A. . & Walsh, C. T. *Biochemistry-US* **36**, 10498–10505 (1997).
3. Mayfield, S. P. & Schultz, J. *Plant J.* **37**, 449–458 (2004).
4. Meier, J. L., Haushalter, R. W. & Burkart, M. D. *Bioorgan. Med. Chem. Lett.* **20**, 4936–4939 (2010).

Nature Methods: doi:10.1038/nmeth.2175

The chapter entitled “Reversible labeling of native and fusion-protein motifs,” in full, is a reprint of the material as it appears in Nature Methods Vol. 9, 981-984, 2012. Kosa, Nicolas M.; Haushalter, Robert W.; Smith, Andrew R.; Burkart, Michael D. The dissertation author was the primary investigator and author of this paper.

Chemoenzymatic exchange of phosphopantetheine on protein and peptide

Evaluation of new acyl carrier protein hydrolase (AcpH) homologs from proteobacteria and cyanobacteria reveals significant variation in substrate selectivity and kinetic parameters for phosphopantetheine hydrolysis from carrier proteins. Evaluation with carrier proteins from both primary and secondary metabolic pathways reveals an overall preference for acyl carrier protein (ACP) substrates from type II fatty acid synthases, as well as variable activity for polyketide ACPs and carrier proteins from non-ribosomal peptide synthases. We also demonstrate the kinetic parameters of these homologs for the 11-mer peptide substrate YbbR. These findings enable the fully reversible labeling of all three classes of natural product synthase carrier proteins as well as full and minimal fusion protein constructs.

Introduction:

Post-translational protein modification allows engineering of extra utility into biochemical systems for a variety of medically and scientifically useful purposes.[1-4] A particularly useful post-translational modification of the carrier proteins (CP) from fatty acid synthase (FAS), polyketide synthase (PKS) and non-ribosomal peptide synthase (NRPS) pathways entails the addition of 4'-phosphopantetheine (PPant) analogs, turning unmodified *apo*-CP into modified *crypto*-CP.[5-10] The Walsh laboratory identified a minimal peptide (YbbR) that can be modified alone or as a fusion protein.[11,12] We have recently shown the ability to selectively remove functional labels from the *E. coli* FAS ACP, AcpP, using the recombinant *Pseudomonas aeruginosa* acyl carrier protein hydrolase (AcpH) EC 3.1.4.14, which offers the ability to iteratively label and un-label ACPs and ACP fusions with a wide variety of functionalities.[13] Here we expand these tools in the evaluation of AcpH homologs from proteobacteria and cyanobacteria that not only display superior kinetics for PPant removal from *E. coli* ACP, but also depict the first known specific hydrolase activity against the 11- amino acid YbbR peptide substrate.

Since the first identification of *E. coli* AcpH activity and characterization,[14,15] we have searched for ways to broadly incorporate a specific biocompatible hydrolase activity into the tool

set of phosphopantetheine labeling first introduced with the phosphopantetheinyl-transferase (PPTase) Sfp.[5,11,12,16] Despite an otherwise unknown natural role for the AcpH, an enzyme not consistently present in all bacteria, the identification of a more stable AcpH homolog from *P. aeruginosa*[17] and its subsequent characterization using free and fusion-ACPs with phosphopantetheine analogs[13] offered the potential of a promiscuous AcpH with which to establish a robust reversible labeling strategy. However, while this PaAcpH has primarily demonstrated promiscuity for a broad range of modified phosphopantetheines appended to the *E. coli* type II FAS ACP, we were unable to constitute activity on many carrier proteins in our library. These results highlighted the need for a broader AcpH homolog activity analysis.

Here we present a thorough substrate evaluation and kinetic analysis of four AcpH homologs identified in proteobacteria and cyanobacteria: *P. aeruginosa* PAO1 (PaAcpH, NP_253043.1), *Cyanothece* sp. PCC 7822 (CyAcpH, YP_003888700.1), *Shewanella oneidensis* MR-1 (SoAcpH, NP_718678.1), and *Pseudomoans fluorescens* NCIMB 10586. We chose these organismic sources to represent a snapshot of currently annotated AcpH homologs (Figure 1), comparing proximal phylogenetic relations (*P. fluorescens*), and more distal relationships (*Cyanothece*, *S. oneidensis*). In addition, we selected AcpH homologs with broad sequence variation to provide additional confirmation of active site residue predictions.[18] Finally, to truly cement Sfp/AcpH methodology as a site-specific reversible labeling tool, we evaluated function of these homologs with YbbR and S6 peptides discovered for PPant labeling, containing 11 and 12 amino acids respectively.[11,12]

Results & Discussion:

Cloning and expression produced soluble protein for all constructs (**Figure 2a** & **Supplementary Figure 1**). The nucleotide sequence for the obtained *P. fluorescens* NCIMB 10586 AcpH gene is uploaded to NCBI with accession number KF667507, as the source strain's genome is not sequenced.

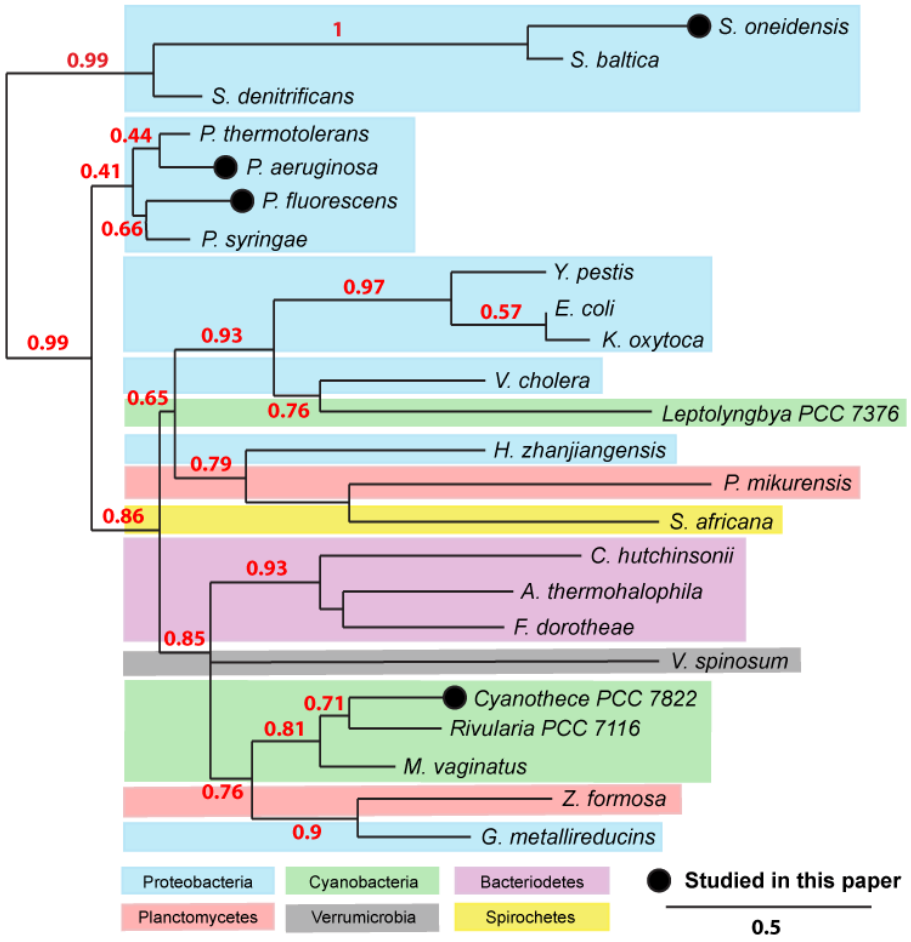

Figure 1. *Phylogenetic analysis of AcpH sources*. AcpH homologs are currently predicted for a diverse set of bacterial phyla, including proteobacteria, cyanobacteria, bacteriodetes, planctomycetes, spirochetes, and verrumicrobia. We analyze the activity for two closely-related AcpH homologs (*P. aeruginosa* & *P. fluorescens*) as well as two distantly-related AcpH homologs (*Cyanothece PCC 7822* & *S. oneidensis*). Phylogenetic map calculations are derived from protein sequences using Phylogeny.fr web utility.[20]

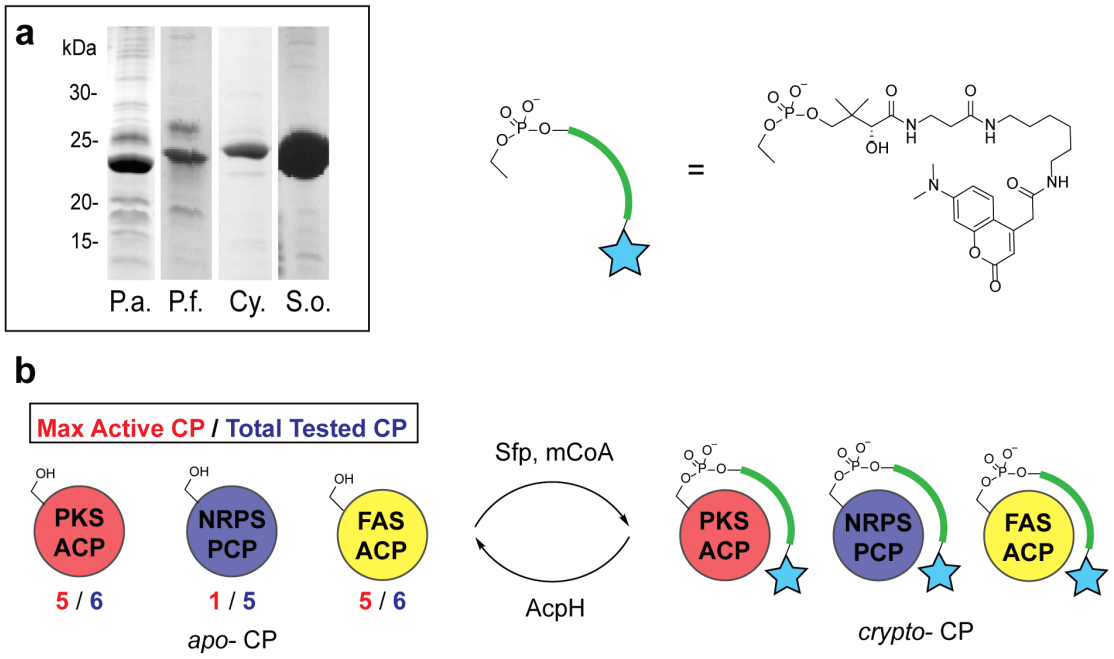

Figure 2. *AcpH homolog activity against crypto-CP*. AcpH homologs were cloned and expressed as soluble proteins (a). *Crypto*- carrier proteins (CP) were generated by labeling *apo*-CP with Sfp and modified coenzyme A (mCoA) generated *in situ* with CoaA, CoaD, CoaE, ATP and coumarin-pantetheine (b). The most active substrates were from FAS and PKS-type CP.

Our initial goal was to establish the AcpH substrate preference with regards to carrier proteins from FAS, PKS, and NRPS pathways (**Supplementary Table 1**). We labeled all carrier proteins with a coumarin-pantetheine analog using the published one-pot methodology (**Figure 2b**)[16,19] and quantified AcpH activity as a significant reduction in protein band fluorescence on SDS-PAGE. FAS ACPs were all derived from bacterial protein targets with the exception of the apicoplast ACP from *P. falciparum*. Carrier proteins included *E. coli* AcpP (EcAcpP, type II), *P. aeruginosa* AcpP (PaAcpP, type II), *S. oneidensis* AcpP (SoAcpP, type II), *P. falciparum* apicoplast ACP (PfACP, Type II),[21] *M. tuberculosis* AcpM (Type II) and MAS (FAS/PKS hybrid). PaAcpH, PfAcpH, and CyAcpH were active against all type II FAS ACPs. No activity was found with the type I *M. tuberculosis* MAS (**Table 1**, **Supplementary Figures 2-9**), which resembles the vertebrate FAS in size and domain organization. SoAcpH showed inactivity with all *crypto*-ACPs tested, so we implemented *holo*-SoAcpP as a suitable model of its anticipated natural substrate. This was performed in order to confirm inactivity was not a result of incompatibility with a non-native coumarin-PPant appendage on *crypto*-ACP. Interestingly, both *crypto*-SoAcpP and *holo*-SoAcpP demonstrated spontaneous, non-enzymatic PPant hydrolysis overnight (**Supplementary Figures 6 & 10a**), requiring the subsequent *holo*-SoAcpP analysis be conducted on a shorter timescale (**Supplementary Figure 10b**).

PKS-type ACPs were derived from a mixture of bacterial and fungal targets. Carrier proteins included *S. coelicolor* ActACP,[7] *A. parasiticus* PksA,[22] *G. fujikuroi* Pks4, [23] *L. majuscula* JamC[24] and JamF,[25] and *P. agglomerans* AdmA.[26] Activity in this category was less consistent (**Table 1**, **Supplementary Figures 2-3, 8-9, 11-12**), with PfAcpH demonstrating the only activity with *crypto*- ActACP and Pks4, while all other AcpH except SoAcpH were capable of activity with *crypto*- PksA and JamC.

NRPS-type peptidyl carrier proteins (PCP) FAS ACPs were derived from bacterial protein targets. Carrier proteins included *P. agglomerans* AdmI,[26] *V. cholerae* VibB,[27] *A. orientalis* CepK, *P. protogens* PltL, *P. syringae* SyrB1.[28] The only detected activities resulted from PfAcpH

Table 1. *Qualitative AcpH substrate selectivity for carrier proteins*. AcpH homolog activity was determined through overnight reaction with *crypto*-CP except in the case of *holo*-SoAcpP. A significant reduction in fluorescence of AcpH-treated CP from controls (**Supplementary Figures 2-9, 11-14**) or Urea-PAGE gel-shift (**Supplementary Figures 10**) are labeled as active "+".

	Carrier Protein Organism	Enzyme Name	PaAcpH	PfAcpH	CyAcpH	SoAcpH
FAS	*E. coli*	AcpP	+	+	+	-
	P. aeruginosa	AcpP	+	+	+	-
	S. oneidensis	AcpP	+	+	+	-
	P. falciparum	ACP‡	+	+	+	-
	M. tuberculosis	AcpM	+	+	+	-
	M. tuberculosis	MAS	-	-	-	-
PKS	*S. coelicolor*	ActACP	-	+	-	-
	A. parasiticus	PksA	+	+	+	-
	G. fujikuroi	Pks4	-	+	-	-
	L. majuscula	JamC	+	+	+	-
	L. majuscula	JamF	-	-	-	-
	P. agglomerans	AdmI	-	+	-	-
NRPS	*P. agglomerans*	AdmA	-	-	-	-
	V. cholerae	VibB	-	-	-	-
	A. orientalis	CepK	-	-	-	-
	P. fluorescens	PltL	+	-	-	-
	P. syringae	SyrB1	-	-	-	-

with AdmI and PaAcpH with PltL (**Table 1**, **Supplementary Figures 4, 8-9, 12-14**). It is particularly interesting that an AcpH from *P. aeruginosa* worked with a PCP another *Pseudomonas* species while the *P. fluorescens* AcpH did not. Without knowing the true overall role of AcpH within each organism, it is difficult to predict how AcpH activity is dictated. However, in analyzing the sequence variation between *P. fluorescens* from which our PfAcpH was derived, and *P. protogens* from which PltL was derived, we find that the amino acid sequence identity of PaAcpH to the *P. protogens* Pf-5 annotated AcpH (not studied) is 70%, while the PfAcpH to *P. protogens* identity is closer at 82%.

The first intriguing finding is that even moderately small difference in sequence between PaAcpH and PfAcpH enzymes (62% identity) results in significant difference in substrate specificity. This indicates that sequence alone may not be used to predict substrate specificity. Despite the promising results demonstrating improved substrate promiscuity of the PfAcpH and CyAcpH homologs compared to the established PaAcpH, the inactivity of SoAcpH raised more questions. We suspected some possibilities for this were that the protein is not purified in its active form (despite high yields and purity), is misannotated as an AcpH while possessing alternate function, or underwent a loss of function mutation in its genetic past that was not detrimental to the survival of *S. oneidensis*. To further investigate its inactivity, we evaluated the secondary structure of SoAcpH compared to the known active CyAcpH. Circular dichroism revealed strong alpha helical character (**Supplementary Figure 15**), indicating a consistent protein fold. Additionally, we aligned the SoAcpH protein sequence to those of PaAcpH, PfAcpH, CyAcpH, and EcAcpH for comparison to the existing EcAcpH analysis based off SPoT.[18] This analysis reveals all predicted aspartate active site Mn^{2+} binding residues in the case of all AcpH except SoAcpH (**Supplementary Figure 16**), lending additional support to our results demonstrating the *S. oneidensis* protein is inactive as an AcpH. SoAcpH lacks two out of three AcpH Mn^{2+}-binding aspartates predicted by the Cronan laboratory, whose mutation of a single one of these residues in EcAcpH reduces measurable activity to nearly undetectable levels.[18]

Due to the observations of improved activity of PfAcpH and CyAcpH from the original PaAcpH, our next goal was characterization of activity against phosphopantetheine-labeled YbbR13 and S6.[11,12] Considering that the reversible phosphopantetheine labeling is compared to existing techniques involving labeling of short peptides, including sortase (5AA),[29,30] farnesyl-transferase (4AA),[31] and transglutaminase (5AA),[32,33] we chose to evaluate S6 and variations of YbbR. YbbR variations include free peptide (11AA) (**Figure 3a** & **Supplementary Figure 17a**), fluoresceinisothiocyanate (FITC)-YbbR conjugate (**Supplementary Figure 17b**),[34] and eGFP-YbbR fusions.[11] Coumarin-PPant was conjugated to S6 and YbbR variations with one-pot methodology and analyzed with Urea-PAGE using all AcpH homologs, demonstrating qualitative activity for all YbbR constructs with PfAcpH and CyAcpH and no activity for SoAcpH (**Table 2**, **Supplementary Figures 18 & 20**). PfAcpH, PaAcpH, and CyAcpH also showed activity with *crypto*-S6 peptide, while SoAcpH did not (**Supplementary Figure 21**).These observations point to a wide variety of bioconjugation applications using minimal peptides and phosphopantetheine analogs and provides potential advantages for increased substrate variety and experimental flexibility.

Given the demonstrated variation in AcpH substrate compatibility for both full carrier proteins, S6 peptide, and variations of the 11-mer YbbR substrate, we sought to further distinguish the new AcpH homologs with kinetic evaluation using the representative *E. coli* AcpP and YbbR substrates. Kinetic analysis of the AcpH homologs with *holo*- *E. coli* AcpP at 37°C resulted in superior kinetic values for CyAcpH compared to PaAcpH and PfAcpH (**Table 3**, **Supplementary Figure 22**). K_{cat} values obtained were 211 min^{-1} for CyAcpH, 3.7 min^{-1} for PfAcpH, and 0.6 min^{-1} for PaAcpH, with k_{cat}/K_m values of 3.6 $min^{-1}*\mu M^{-1}$ for CyAcpH, 0.06 $min^{-1}*\mu M^{-1}$ for PfAcpH, and 0.05 $min^{-1}*\mu M^{-1}$ for PaAcpH. Cronan previously determined a k_{cat} of 13.1 min^{-1} for EcAcpH, and k_{cat}/K_m of 2.4 $min^{-1}/\mu M$,[18] which compares favorably to the more soluble PaAcpH and PfAcpH, but is still significantly lower than CyAcpH. We were at first suspicious of the high apparent turnover for CyAcpH, but these results were further confirmed using EDTA

Table 2. *AcpH activity with modified YbbR*. Various YbbR peptide substrate variations were evaluated for AcpH activity qualitatively (**Supplementary Figure 12-14**). AcpH from both *P. fluorescens* and *Cyanothece* PCC7822 demonstrated detectable activity with qualitative analysis.

	Fusion Location		Enzyme			
	N-term	C-term	PaAcpH	PfAcpH	CyAcpH	SoAcpH
YbbR13	N/A	N/A	no	**YES**	**YES**	no
	FITC	N/A	no	**YES**	**YES**	N/A
	GFP	6xHis	no	**YES**	**YES**	no
	6xHis	GFP	no	**YES**	**YES**	no

Table 3. *AcpH homolog AcpP and YbbR kinetics*. AcpH homolog activity was determined at 37°C with *holo- E. coli* AcpP using HPLC detection (**Supplementary Figure 21**), as well as *crypto*-FITC-YbbR in a FRET-quench microwell plate assay (**Supplementary Figure 23**). Best in-class kinetics for evaluated substrates are CyAcpH for *holo*-AcpP, and PfAcpH for *crypto*- FITC-YbbR. A lower CyAcpH concentration of 5 nM was required for obtaining *holo*-ACP kinetics due to high turnover.

Enzyme	Substrate	[AcpH], μM	V_{max} (min^{-1})	K_m (μM)	**k_{cat} (min^{-1})**	k_{cat}/K_M (min^{-1} *μM^{-1})
PaAcpH	*holo*-ACP (*E. coli*)	1	0.59 ± 0.02	12 ± 2	**0.59 ± 0.02**	0.049
PfAcpH		1	3.7 ± 0.1	61 ± 7	**3.7 ± 0.1**	0.060
CyAcpH		0.005	1.1 ± 0.1	58 ± 9	**211 ± 11**	3.6
PaAcpH	*crypto*-FITC-YbbR (**3**)	1	0.008 ± 0.016	177 ± 744	**0.008 ± 0.016**	4.7E-05
PfAcpH		1	0.17 ± 0.01	48 ± 5	**0.17 ± 0.01**	0.003
CyAcpH		1	0.004 ± 0.004	21 ± 68	**0.004 ± 0.004**	2.0E-04

quench to terminate hydrolysis, resulting in enzyme arrest prior to HPLC analysis (**Supplementary Figure 23**). These results indicate the significant finding that turnover of *E. coli holo*- AcpP by CyAcpH surpasses the kinetic parameters of Sfp for *E. coli apo*- AcpP (k_{cat} = 5.8 min^{-1} and k_{cat}/K_m = 1 $min^{-1}\mu M^{-1}$).[35] While the CyAcpH kinetic results are derived from free *E. coli* AcpP, this result implies an remarkable advantage for this newly characterized enzyme in designing reversible labeling scenarios with AcpP as a protein handle.

Kinetics of AcpH homologs with the YbbR substrate were determined using a FRET-reporter system with rhodamine WT PPant-labeled FITC-YbbR, as previously utilized to monitor Sfp activity (**Figure 3b**).[34,36] Here FITC-YbbR was conjugated with Rhodamine-CoA[36] to generate the *crypto*- FITC-YbbR substrate (**Supplementary Figure 17c**). HPLC purification and lyophilization of the *crypto*- FITC-YbbR supplied the substrate necessary for AcpH kinetic analysis. SoAcpH was not analyzed for kinetics, as it did not display activity in the qualitative YbbR activity analysis. Real-time analysis of AcpH homologs at 37°C in 96-well format provided kinetic data clearly favoring the activity of PfAcpH for *crypto*- FITC-YbbR. K_{cat} values obtained were 0.17 min^{-1} for PfAcpH with k_{cat}/K_m of 0.003 $min^{-1}\mu M^{-1}$ (**Supplementary Figure 24** and **Table 3**). Compared to the Sfp for YbbR (k_{cat} = 11 min^{-1}, k_{cat}/K_m of 0.091 $min^{-1}\mu M^{-1}$),[11] the PfAcpH demonstrated two orders of magnitude slower reaction rates.

This method provides significant advantages when compared to other reversible protein labeling systems. First, the labeling step utilizing Sfp and a coenzyme A analog possesses very good kinetics. Additionally, both the Sfp and AcpH reactions favor product formation due to energy released upon phosphodiester bond breakage in both cases, unlike the equilibrium kinetics experienced by the sortase reaction and the consequently high substrate concentrations required to achieve efficient labeling. Compared to farnesyl-transferase, the Sfp labeling step possesses a similar k_{cat}, but allows flexible YbbR placement at the amino/carboxy-terminus or internal to the target protein[11] In comparison, the farnesyl prosthetic attachment site must be at the protein C-terminus, and removal of the farnesyl group requires an irreversible

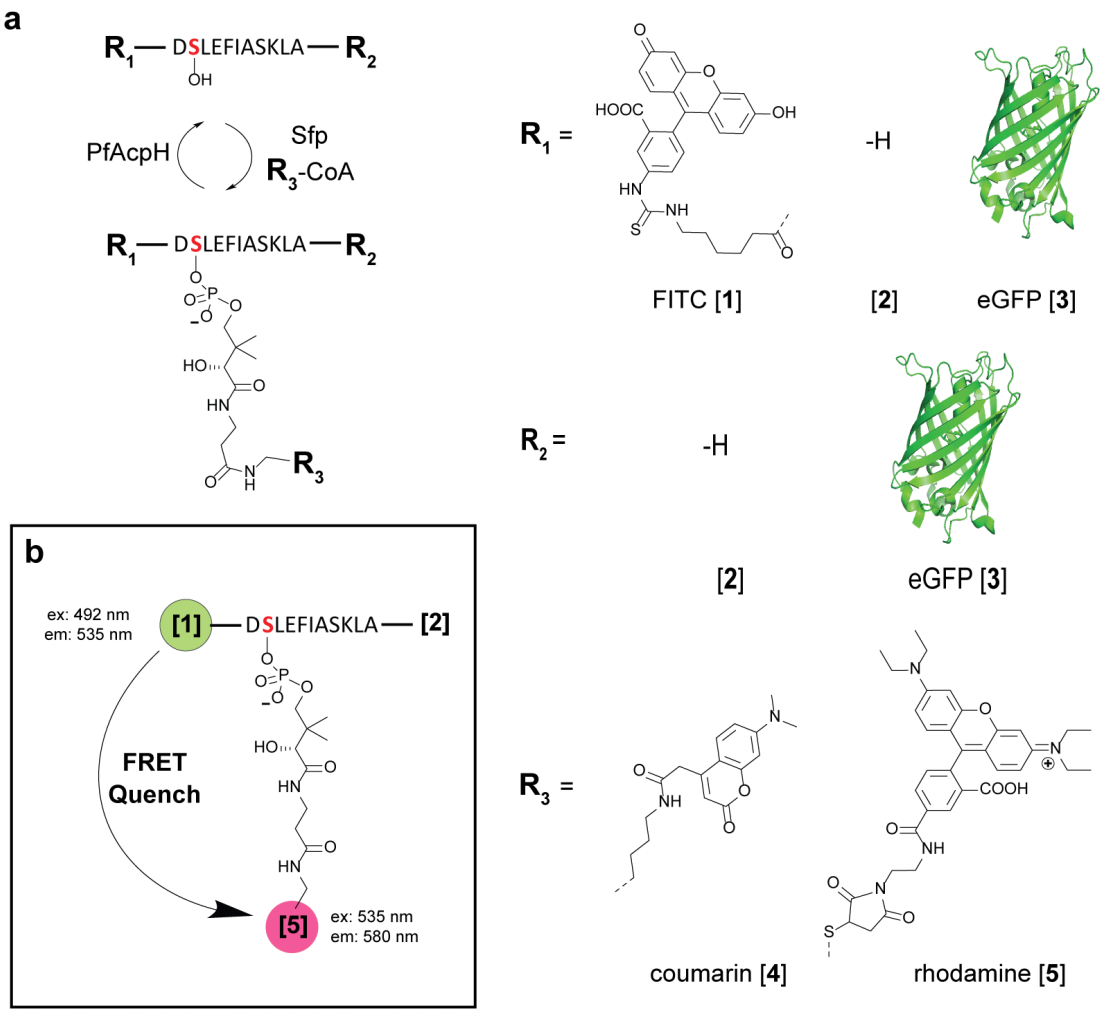

Figure 3. *AcpH accommodates YbbR modifications*. Various YbbR peptide substrate variations were evaluated for AcpH activity (a) qualitatively by SDS-PAGE (**Supplementary Figures 8-9, 18-20**), and (b) quantitatively using a FRET quench assay (**Supplementary Figure 23**). PfAcpH was found to accommodate all YbbR appendages, and generate useful kinetic data. (**Table 3**).

carboxypetidase protease cleavage of the transfer site sequence. Thus, for bioconjugation applications requiring short fusion sequences, truly reversible and site-specific labeling can be implemented with the 11 amino acid YbbR using combined Sfp/PfAcpH methodology. The incidental activity of PfAcpH with a peptide discovered originally for Sfp[11] implies that there is significant room for AcpH activity improvement, either by modification of the YbbR sequence, or pursuit of a new dual-purpose peptide that possesses desirable kinetics for both Sfp and AcpH activity.

Following the completion of our substrate panels and the identification of our most promiscuous AcpH from *P. fluorescens*, we lastly wished to identify any particularly important consensus residues from active protein sequences to guide future substrate prediction. The sequences from 10 amino acids flanking the modified serine were aligned and used to generate a consensus sequence from all carrier proteins active with PfAcpH (**Supplementary Figure 25**). This procedure generated a core consensus of "DLGXD**S**LDXVEL" with "X" being an unconserved amino acid, which displays a strong homology with amino acids residing in type II FAS ACP. This absolute sequence is not required for activity, but our results indicate that most carrier proteins with 5 or fewer matching amino acids are inactive, the exceptions being AdmI and YbbR/S6 peptide substrates. The "D**S**L" portion appears to be especially important, as only one PKS ACP, JamC, and one NRPS PCP, AdmI, is active with the variation "D**S**S" and "DSV" respectively. In comparison, none of the inactive NRPS PCPs contain the "DSL" active site sequences or possess more than 6 matching identical amino acids surrounding the active site.

In conclusion, our analysis of three new AcpH gene products and comparison to existing *P. aeruginosa* AcpH reveals a remarkable array of information regarding substrate compatibility. Despite the apparent inactivity of the hypothetical *S. oneidensis* AcpH, the AcpH homologs from *P. fluorescens* and *Cyanothece sp*. PCC 7822 present superior alternative to the existing methods for phosphopantetheine removal, with CyAcpH demonstrating remarkable kinetic values for *holo*-AcpP hydrolysis, while PfAcpH possesses the best available kinetics for *crypto*-YbbR hydrolysis, as well as the broadest apparent substrate promiscuity with the evaluated carrier

protein panel. These new enzymes demonstrate substantial potential for further substrate truncation and peptide sequence modification, as well as ready implementation with established reversible ACP labeling methods.

Methods:

General. Protein concentrations were determined using UV absorbance at 280 nm, with extinction coefficients calculated using ExPASy online tool for each protein.[37]

Cloning. The *P. aeruginosa* PAO1 AcpH gene [genID: 881435] identified previously[17] was cloned as described previously.[13] All primers used for cloning are located in supplemental information (Supplementary Table 2) *Cyanothece* PCC 7822 AcpH gene [genID: 9739974], and *Shewanella oneidensis* AcpH gene [genID: 1170805] were cloned from genomic DNA using standard techniques. *P. fluorescens* NCIMB 10586 AcpH [KF667507] was cloned using homology primers designed from *P. fluorescens* SBW25 AcpH gene [genID: 7817947]. Sequencing of intermediate PCR product allowed design of more specific primers and production of final PCR gene product. CepK was codon-optimized for *E. coli* and synthesized encoding a C-terminally his-tagged construct. All AcpH gene PCR products were treated with restriction endonuclease and ligated into pET29b plasmids containing a C-terminal 6xHis tag.

Protein expression. All AcpH growth, and purification procedures are previously described.[13] *E. coli* thioesterase TesA[38] was expressed and purified in the same manner as AcpH. Lysis buffer for CyAcpH and PfAcpH are excepted in that they utilized higher glycerol content. CyAcpH and PfAcpH were purified and desalted in the presence of 50 mM TrisCl pH 8.0, 250 mM NaCl, and 25% glycerol. The additional glycerol contributed significantly to higher perceived protein recovery and prolonged stability. *E. coli AcpP*, and *P. aeruginosa* MBP-AcpP were prepared as previously described.[13] *S. oneidensis* AcpP was prepared in the same manner as *E. coli* AcpP. MtbAcpM, ActACP, JamC, JamF, AdmA, AdmI, SyrB1-AT, PltL, CepK, VibB, and MAS containing cells were grown in LB with appropriate antibiotic at 37°C until they reached an optical density of 0.6. IPTG was added to 1 mM, and the cells were incubated with shaking at 16°C

overnight. *Plasmodium* ACP was grown as previously described.[21] All ACP constructs were grown in antibiotics appropriate for the contained plasmid. All cells were centrifuged to obtain a pellet, which was re-dissolved in lysis buffer. MtbAcpM expressed as an *apo*/*holo*/acyl mixture, and required overnight treatment with Affigel-25 conjugates of TesA and PfAcpH prior to labeling. *Plasmodium* ACP expressed as *holo*- and was treated with PaAcpH conjugated to Affigel-25 prior to labeling. Spin concentration of all carrier proteins with 3 kDa MWCO centrifugal filters (EMD Millipore, Billerica, Massachusetts) resulted in concentrated protein stocks.

One-pot carrier protein coumarin-labeling strategy. Unless otherwise noted, all coumarin-PPant labeling proceeded as follows: *apo*- carrier protein or peptide at 50-200 μM were labeled in 50 mM Na-HEPES pH 7.5, 10 mM $MgCl_2$, 8 mM ATP, 0.1 μM MBP-CoaA/D/E, 0.1 μM native Sfp, and 1.1 equivalents of coumarin-pantetheine at 37°C overnight. *Crypto*- protein samples were re-purified using standard IMAC techniques in pH 8.0 lysis buffer with Ni-NTA resin, and spin-concentrated/buffer exchanged to remove imidazole and concentrate with 0.5 mL 3 kDa MWCO cellulose filters. *Crypto*- peptide samples were purified via HPLC, lyophilized, and re-dissolved in 50 mM TrisCl pH 8.0 prior to analysis.

General AcpH gel-based activity. Specific procedures for AcpH activity are described previously.[13] Briefly, qualitative analysis of *crypto*- carrier protein or peptide samples proceeded at 37°C overnight reaction with 1 μM AcpH homolog. Following AcpH treatment, an equal volume of 2X SDS-PAGE loading dye was added to *crypto*-carrier proteins samples and heated 5 min at 90°C, and run on 12% or 15% SDS-PAGE. Gels were fixed in 50/40/10% water/methanol/acetic acid for 30 minutes, and washed with water three times before UV imaging. *Holo*- carrier protein reactions were analyzed with Urea-PAGE as previously described.[13] All protein gels were Coomassie stained for evaluating total protein. *Crypto*- peptides were evaluated on Urea-PAGE, and were imaged immediately after running with no gel fixing.

FITC-YbbR labeling & purification. Preparation of rhodamine-labeled FITC-YbbR proceeded via reaction of 200 μM FITC-YbbR with 200 μM rhodamine WT-CoA synthesized as described previously[36] with 1 μM Sfp in 50 mM HEPES pH 7.5 and 10 mM $MgCl_2$ for 2 hours at

37°C. *Crypto*- peptide samples were purified with HPLC, lyophilized, and re-dissolved in 50 mM TrisCl pH 8.0 at 4 mM prior to analysis.

HPLC AcpH kinetics. *Holo*- *E. coli* AcpP was prepared as a serial dilution in 50 mM TrisCl, 250 mM NaCl, 30 mM $MgCl_2$, and 2 mM $MnCl_2$. PaAcpH, and PfAcpH were prepared at 2 μM in similar buffer with 10% glycerol but lacking Mg/Mn. CyAcpH was prepared at 10 nM in the same AcpH buffer. Addition of AcpH into *holo*-AcpP samples provided final top concentrations of 400, 200, 100, 50, 25, 12.5 μM for PaAcpH/PfAcpH, and 450, 225, 112.5, 56.25, 28.1, 14 μM for CyAcpH. Reactions were transferred to pre-warmed shaker at 37°C and were quenched with 100 mM EDTA pH 7.0 after 10 minutes. Samples were centrifuged and evaluated at 210 nm with HPLC using an acetonitrile gradient to determine *apo*-AcpP product formation. Michaelis-Menten kinetics were calculated using GraphPad Prism.

FRET AcpH kinetics: Rhodamine-labeled FITC-Ybbr as well as standard 1:1 *apo*- FITC-YbbR:rhodamine-CoA was subjected to an 11-point serial dilution in 50 mM TrisCl pH 8.0 to achieve final concentrations of 400 – 0.4 μM. PfAcpH, CyAcpH, PaAcpH and buffer blank were prepared to give a final solution added concentration of 1 or 0 μM AcpH, 50 mM TrisCl pH 8.0, 15 mM $MgCl_2$, 1 mM $MnCl_2$, and 1 mg/mL BSA. Total reaction volumes were 50 μL and utilized a 96-well Costar 3694 plate (Corning, Lowell, MA). Following mixing, reactions were centrifuged for 2 minutes at 1500 rpm, and incubated at 37°C for 4 hours in a HTS 7000 plus Bioassay Reader (Perkin Elmer, Waltham, MA) in kinetic mode. Comparison of activity from 20-30 minutes to buffer blank and 1:1 *apo*-FITC-YbbR:rhodamine-CoA standard allowed calculation of product formation and determination of Michaelis-Menten kinetics using GraphPad Prism.

Supplementary Information

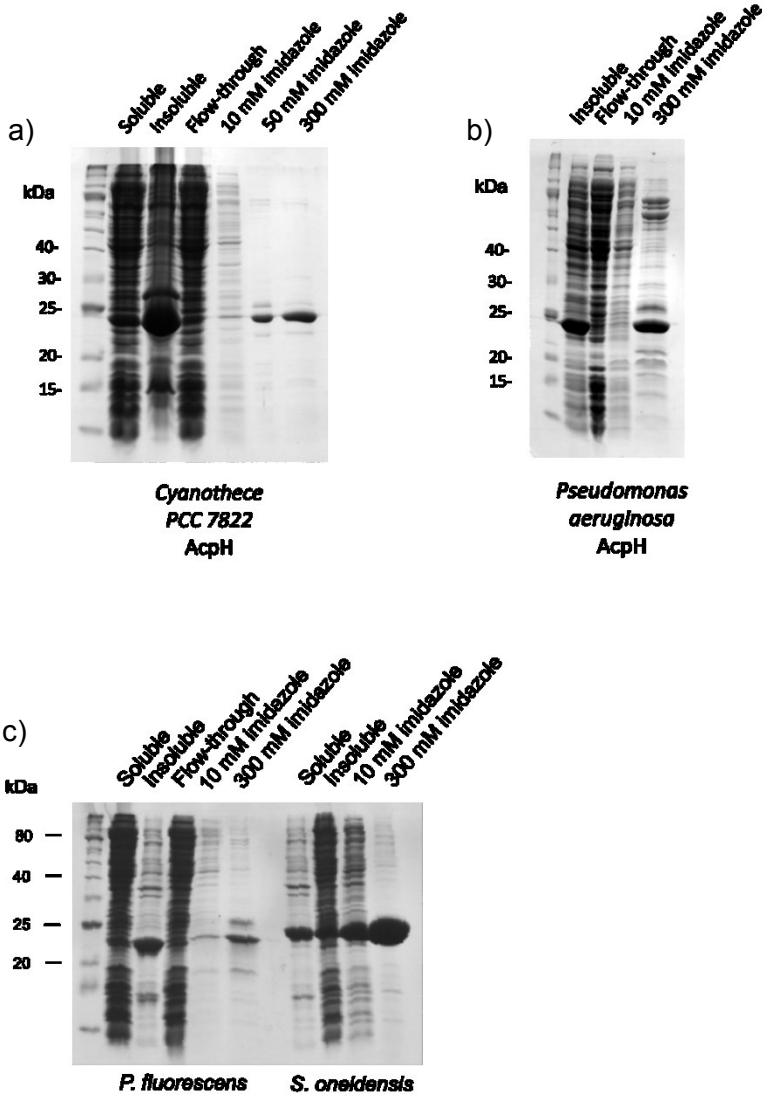

Supplementary Figure 1. Purification of AcpH protein homologs. AcpH homolog protein from *Cyanothece* PCC7822 (**a**), *P. aeruginosa (**b**)*, *P. fluorescens* (**c**), and *S. oneidensis* (**c**) was expressed recombinantly and purified using Ni-NTA chromatography.

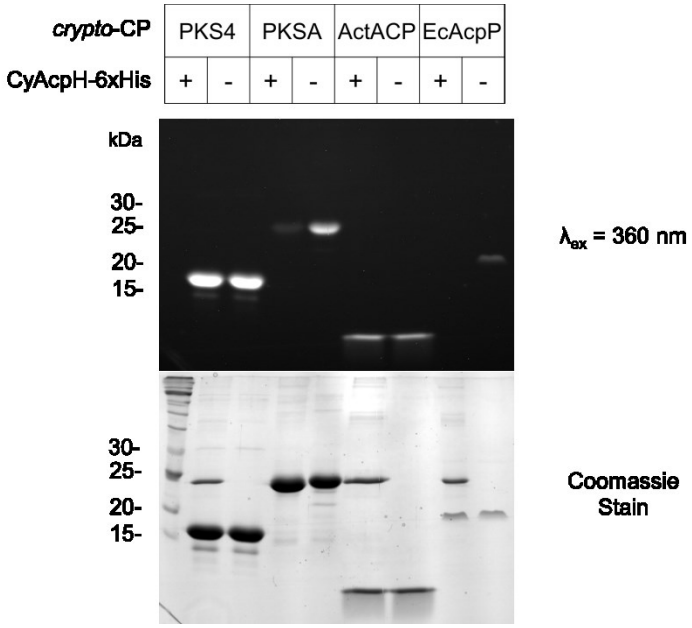

Supplementary Figure 2. *Analysis of CyAcpH activity with PKS-ACP and E. coli AcpP*. CyAcpH is evaluated by SDS-PAGE with various *crypto*-CP (+) compared to buffer blanks (-) after overnight incubation at 37°C.

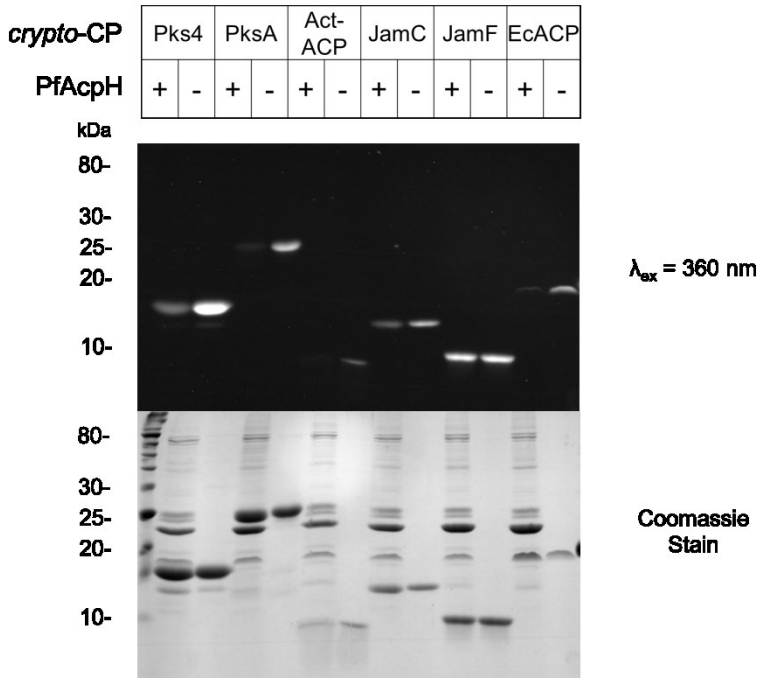

Supplementary Figure 3. *P. fluorescens AcpH activity vs. various CP*. PfAcpH is evaluated by SDS-PAGE with various *crypto*-CP (+) compared to buffer blanks (-) after overnight incubation at 37°C.

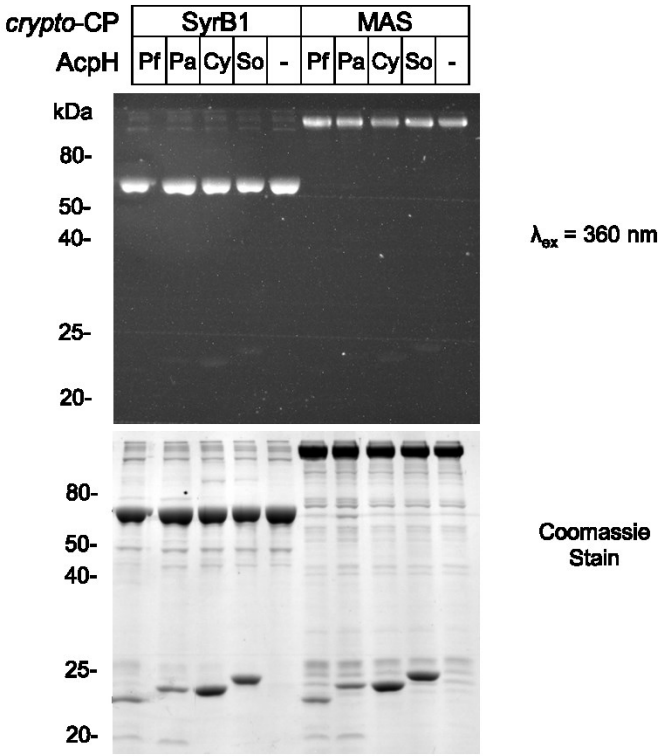

Supplementary Figure 4. *Analysis of AcpH homolog activity with SyrB1 and MAS*. AcpH homologs from *P. fluorescens* (Pf), *P. aeruginosa* (Pa), *Cyanothece* PCC 7822 (Cy) and *S. oneidensis* (So) are evaluated by SDS-PAGE with various *crypto*-CP (+) compared to buffer blanks (-) after overnight incubation at 37°C.

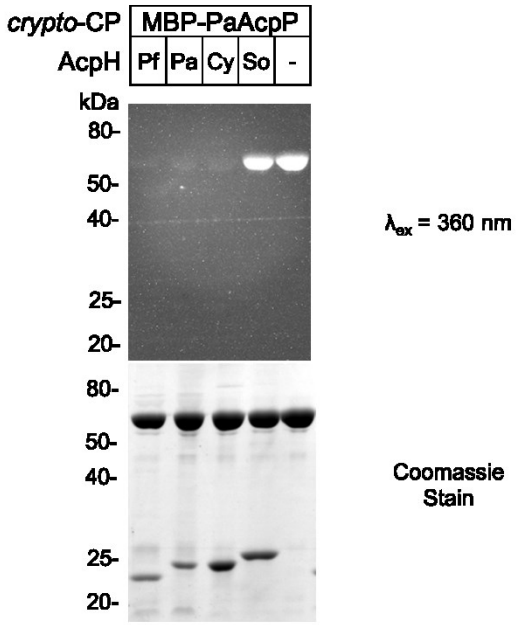

Supplementary Figure 5. *Analysis of AcpH homolog activity with MBP-PaAcpP*. AcpH homologs from *P. fluorescens* (Pf), *P. aeruginosa* (Pa), *Cyanothece* PCC 7822 (Cy) and *S. oneidensis* (So) are evaluated by SDS-PAGE with various *crypto*-CP (+) compared to buffer blanks (-) after overnight incubation at 37°C.

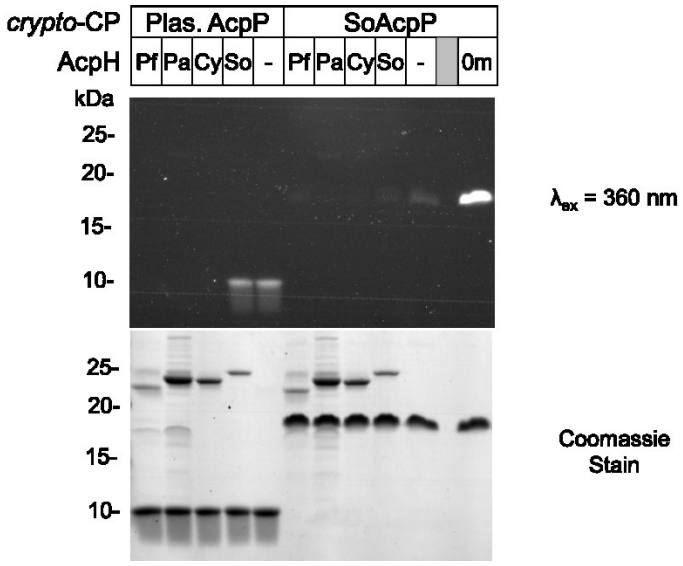

Supplementary Figure 6. *Analysis of AcpH homolog activity with Plasmodium AcpP and SoAcpP*. AcpH homologs from *P. fluorescens* (Pf), *P. aeruginosa* (Pa), *Cyanothece* PCC 7822 (Cy) and *S. oneidensis* (So) are evaluated by SDS-PAGE with various *crypto*-CP (+) compared to buffer blanks (-) after overnight incubation at 37°C. Coumarin-PPant from SoAcpP appeared to hydrolyze overnight in incubated samples compared to non-incubated sample “0m”.

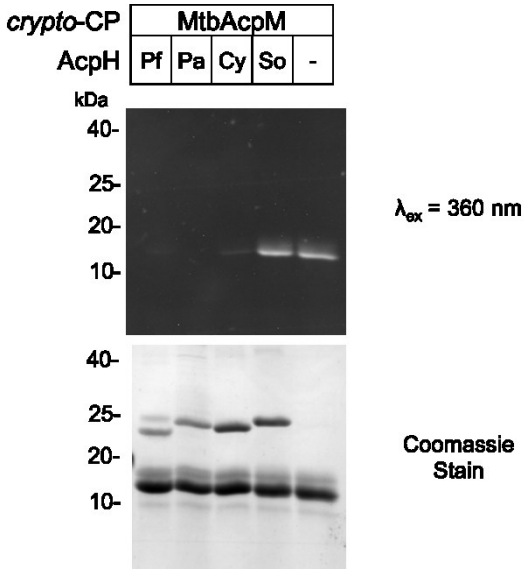

Supplementary Figure 7. *Analysis of AcpH homolog activity with MtbAcpM*. AcpH homologs from *P. fluorescens* (Pf), *P. aeruginosa* (Pa), *Cyanothece* PCC 7822 (Cy) and *S. oneidensis* (So) are evaluated by SDS-PAGE with various *crypto*-CP (+) compared to buffer blanks (-) after overnight incubation at 37°C.

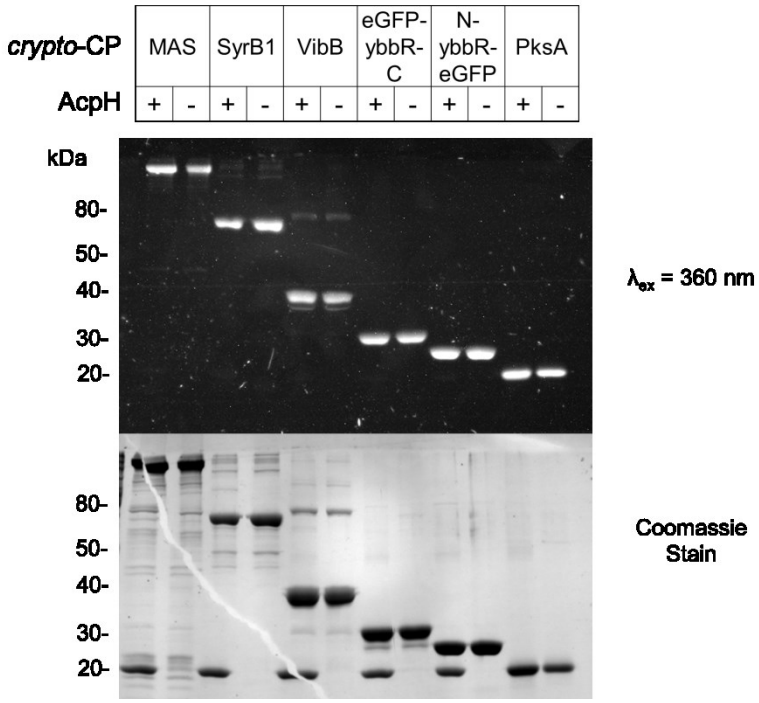

Supplementary Figure 8. *Analysis of SoAcpH activity with various CP #1*. AcpH homolog from *S. oneidensis* (So) is evaluated by SDS-PAGE with various *crypto*-CP (+) compared to buffer blanks (-) after overnight incubation at 37°C.

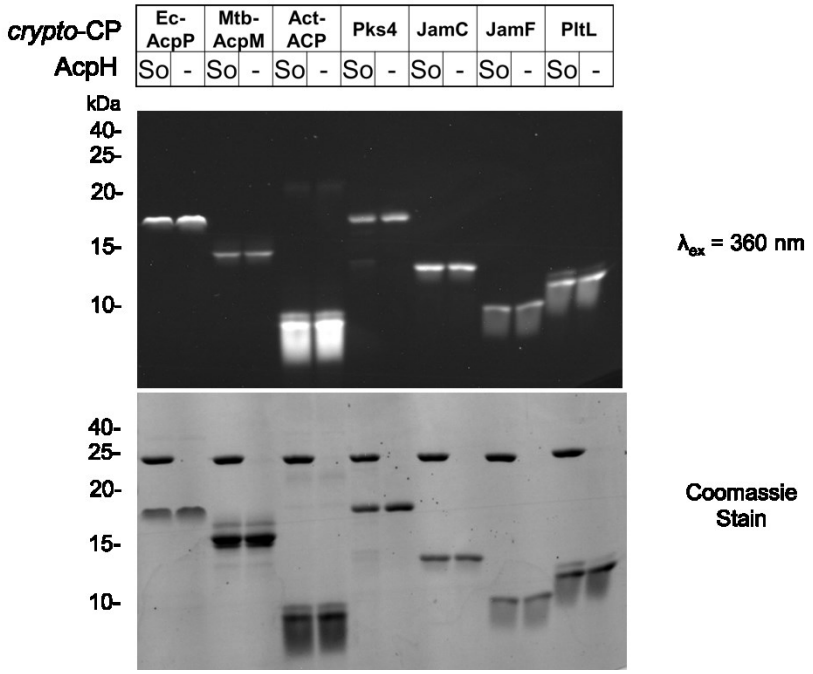

Supplementary Figure 9. *Analysis of SoAcpH activity with various CP #2*. AcpH homolog from *S. oneidensis* (So) are evaluated by SDS-PAGE with various *crypto*-CP (+) compared to buffer blanks (-) after overnight incubation at 37°C.

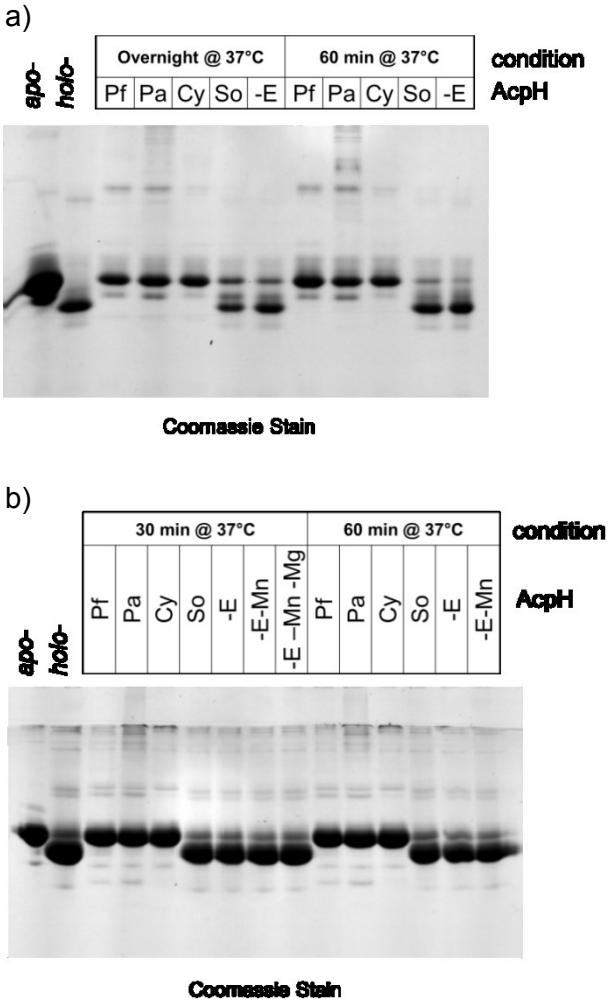

Supplementary Figure 10. *Analysis of AcpH activity with holo-SoAcpP at various time-points*. AcpH homologs from *P. fluorescens* (Pf), *P. aeruginosa* (Pa), *Cyanothece* PCC 7822 (Cy) and *S. oneidensis* (So) are evaluated by Urea-PAGE with *holo*-CP (+) compared to buffer blanks (-E) after various incubation times at 37°C. Samples were quenched with EDTA at listed times. Blank samples were also prepared without Mn^{2+} (-E-Mn) and without Mn^{2+}/Mg^{2+} in order to evaluate non-enzymatic PPant hydrolysis.

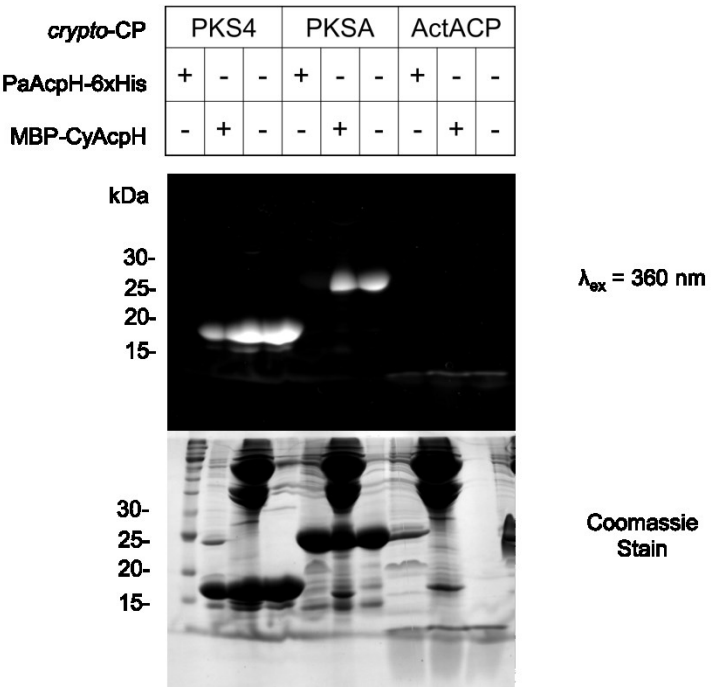

Supplementary Figure 11. *Analysis of PaAcpH and MBP-CyAcpH with PKS-ACP activity*. AcpH homologs from *P. aeruginosa* (Pa) and MBP- fusion AcpH homolog from *Cyanothece* PCC7822 (MBP-CyAcpH) are evaluated by SDS-PAGE with various *crypto*-CP (+) compared to buffer blanks (-) after overnight incubation at 37°C.

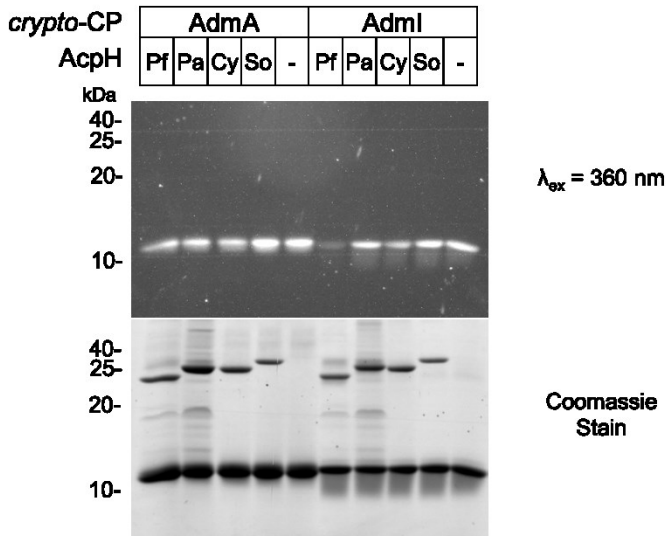

Supplementary Figure 12. *Analysis of AcpH homolog activity with AdmA and AdmI*. AcpH homologs from *P. fluorescens* (Pf), *P. aeruginosa* (Pa), *Cyanothece* PCC 7822 (Cy) and *S. oneidensis* (So) are evaluated by SDS-PAGE with various *crypto*-CP (+) compared to buffer blanks (-) after overnight incubation at 37°C.

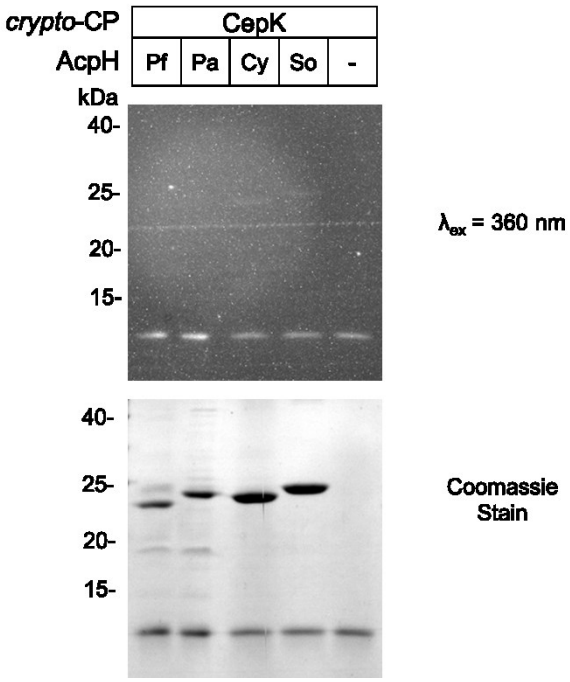

Supplementary Figure 13. Analysis of AcpH homolog activity with CepK. AcpH homologs from *P. fluorescens* (Pf), *P. aeruginosa* (Pa), *Cyanothece* PCC 7822 (Cy) and *S. oneidensis* (So) are evaluated by SDS-PAGE with various *crypto*-CP (+) compared to buffer blanks (-) after overnight incubation at 37°C.

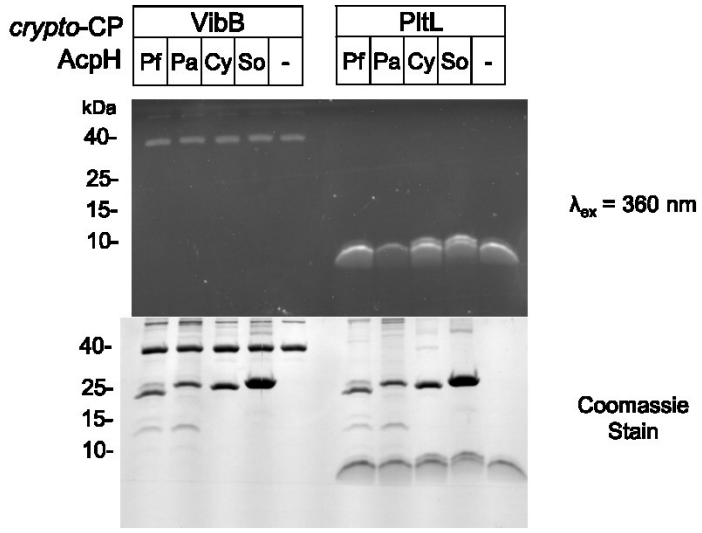

Supplementary Figure 14. *Analysis of AcpH homolog activity with VibB and PltL*. AcpH homologs from *P. fluorescens* (Pf), *P. aeruginosa* (Pa), *Cyanothece* PCC 7822 (Cy) and *S. oneidensis* (So) are evaluated by SDS-PAGE with various *crypto*-CP (+) compared to buffer blanks (-) after overnight incubation at 37°C.

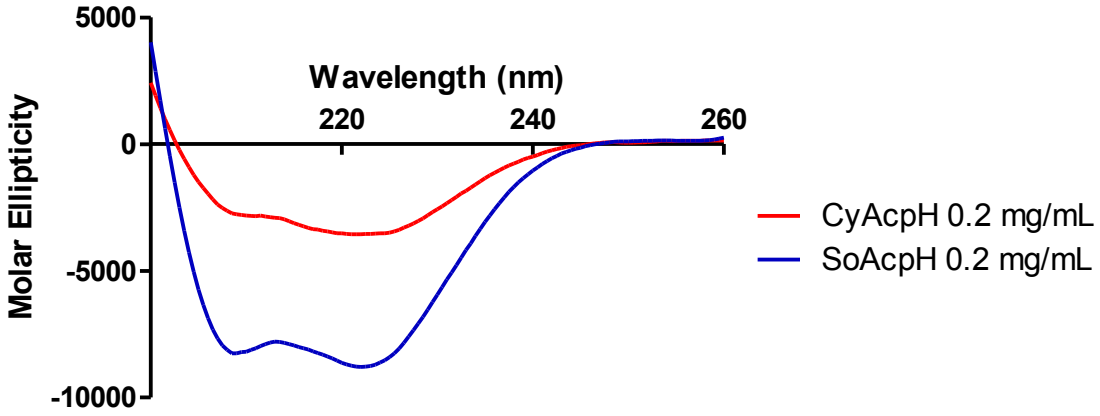

Supplementary Figure 15. *Circular dichroism analysis of CyAcpH and SoAcpH*. Circular dichroism analysis of suspected inactive *S. oneidensis* AcpH (SoAcpH) compared to known active *Cyanothece* PCC7822 (CyAcpH) reveals strong alpha-helical character in SoAcpH at similar protein concentrations. This suggests that SoAcpH maintains consistent secondary structure.

Supplementary Figure 16. *Sequence alignment of known active AcpH homologs to SoAcpH.* Known active AcpH homologs from *E. coli* (EcAcpH),[14,18] *Cyanothece* PCC7822 (CyAcpH), *P. aeruginosa* (PaAcpH),[13,17] and *P. fluorescens* (PfAcpH) are aligned to the annotated hypothetical AcpH homolog from *S. oneidensis* (SoAcpH). The alignment reveals that only the SoAcpH lacks the suspected active-site aspartate residues predicted for Mn^{2+} binding.[14]

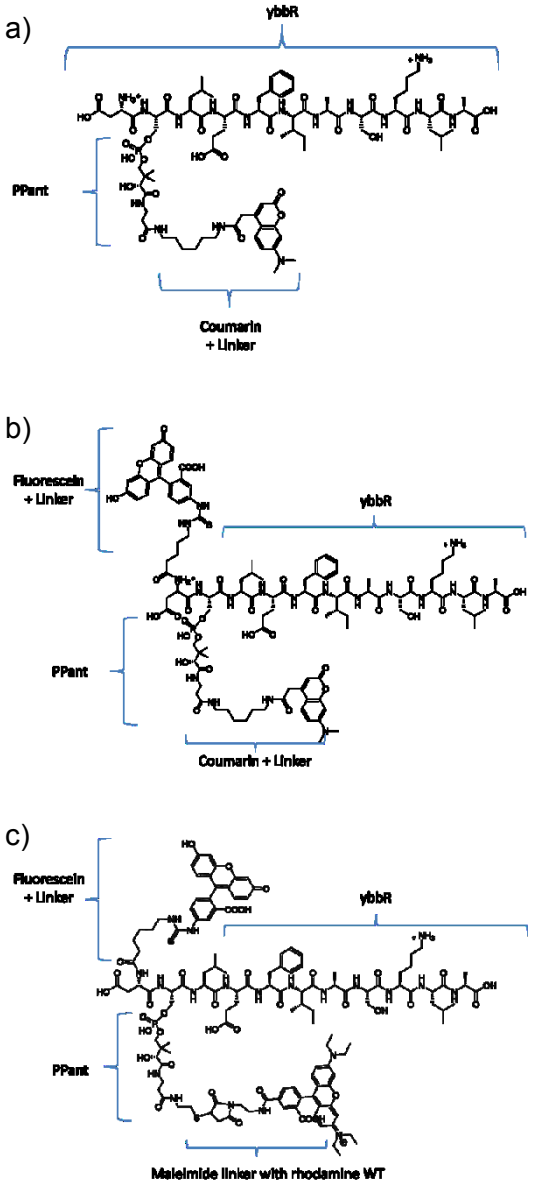

Supplementary Figure 17. *Chemical structures of non-fusion ybbR peptide substrates*. Variations of ybbR subjected to coumarin-PPant labeling AcpH activity Urea-PAGE analysis include free peptide (**a**), and FITC-conjugated peptide (**b**). A rhodamine-PPant conjugate was synthesized for FRET kinetics evaluation (**c**).

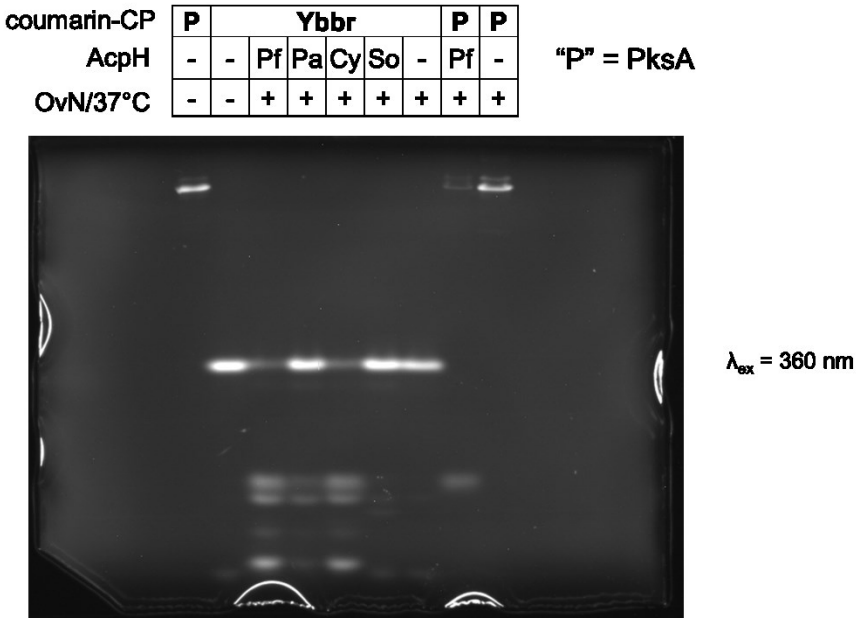

Supplementary Figure 18. *Analysis of AcpH activity with coumarin-ybbR*. AcpH homologs from *P. fluorescens* (Pf), *P. aeruginosa* (Pa), *Cyanothece* PCC 7822 (Cy) and *S. oneidensis* (So) are evaluated by Urea-PAGE with *crypto*-ybbR and *crypto*-PksA (P) compared to buffer blanks (-) after overnight incubation at 37°C (+) or non-incubation (-).

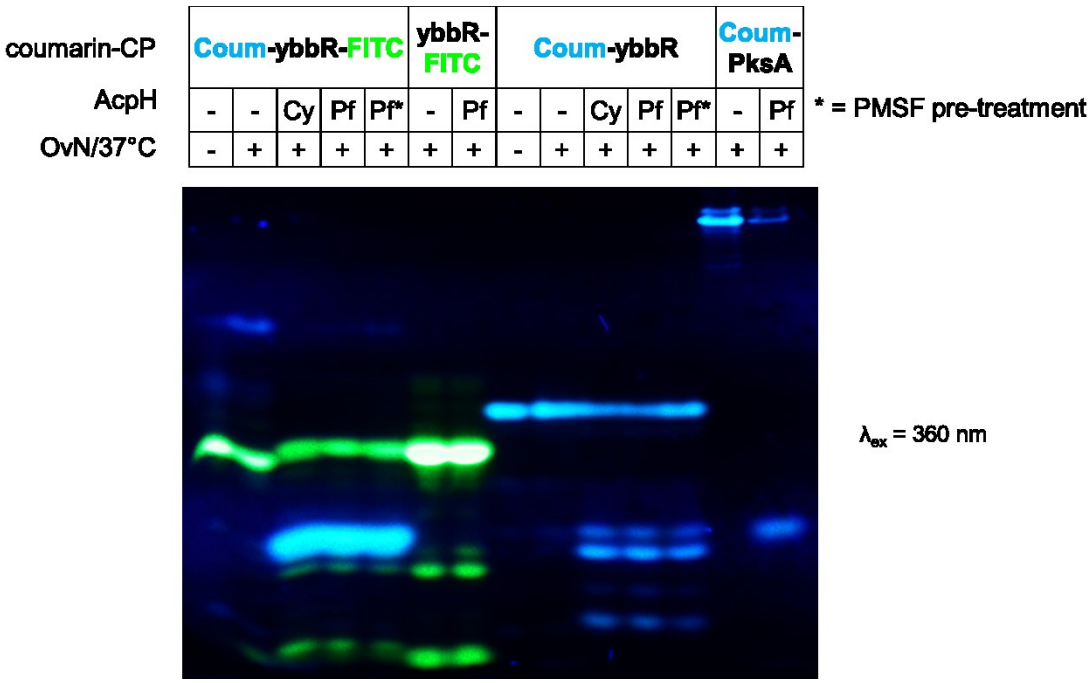

Supplementary Figure 19. *Analysis of AcpH activity with coumarin-labeled ybbR and FITC-ybbR*. AcpH homologs from *P. fluorescens* (Pf), and *Cyanothece* PCC 7822 (Cy) are evaluated by Urea-PAGE with *crypto*-ybbR and *crypto*-PksA compared to buffer blanks (-) after overnight incubation at 37°C (+) or non-incubation (-). PMSF is also used to pretreat a PfAcpH sample to ensure that probe hydrolysis is not due to serine-protease.

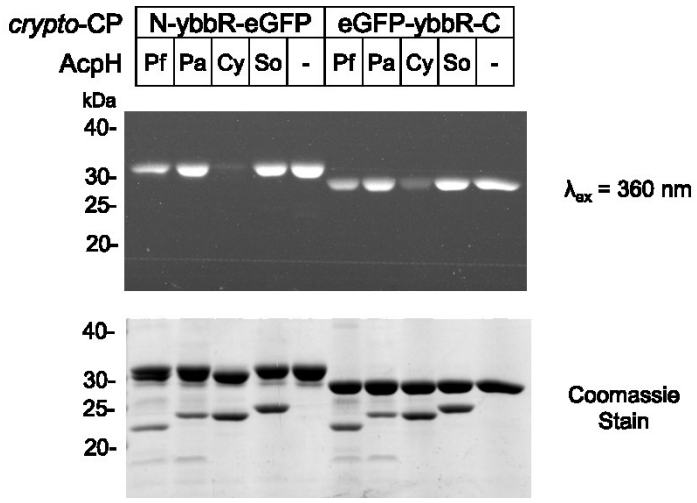

Supplementary Figure 20. *Analysis of AcpH homolog activity with ybbR-eGFP fusions*. AcpH homologs from *P. fluorescens* (Pf), *P. aeruginosa* (Pa), *Cyanothece* PCC 7822 (Cy) and *S. oneidensis* (So) are evaluated by SDS-PAGE with *crypto*- ybbR-eGFP N- and C-terminal fusions compared to buffer blanks (-) after overnight incubation at 37°C.

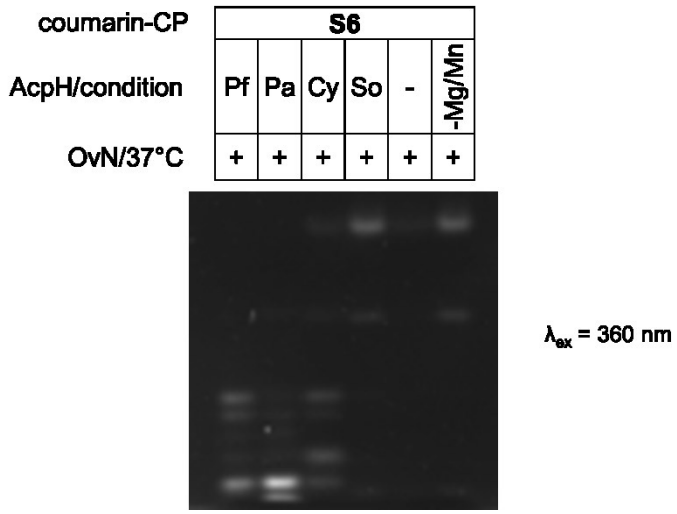

Supplementary Figure 21. *Analysis of AcpH homolog activity with S6 peptide*. AcpH homologs from *P. fluorescens* (Pf), *P. aeruginosa* (Pa), *Cyanothece* PCC 7822 (Cy) and *S. oneidensis* (So) are evaluated by Urea-PAGE with *crypto*-S6 compared to no enzyme blanks (-), and no enzyme/Mg/Mn blank (-Mg/Mn) after overnight incubation at 37°C (+).

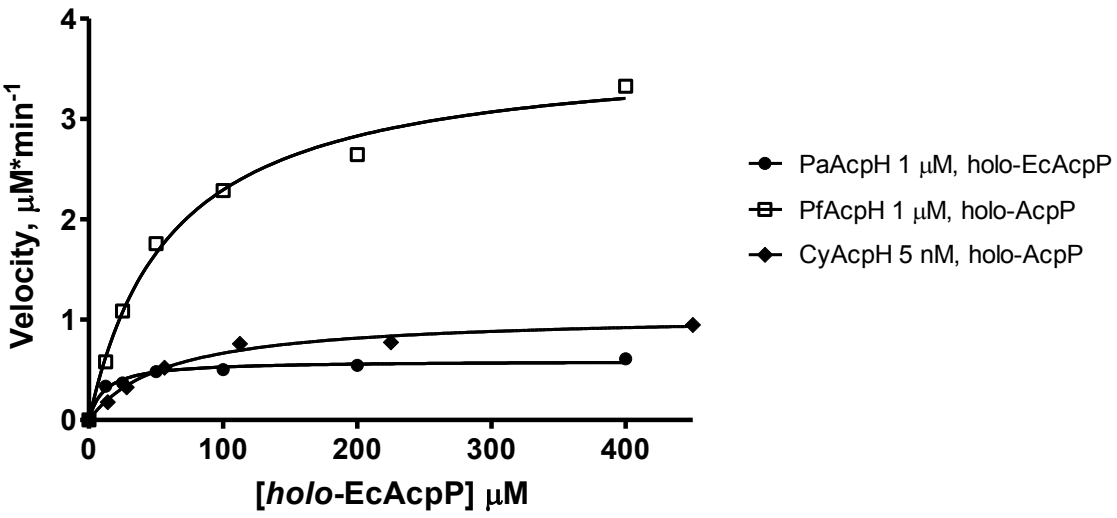

Supplementary Figure 22. Analysis of AcpH homolog kinetics with *holo*-EcAcpP. Reaction of AcpH homologs from *P. fluorescens* (Pf), *P. aeruginosa* (Pa), *Cyanothece* PCC 7822 (Cy) with *holo*-EcAcpP, and subsequent EDTA-quenching allow derivation of HPLC kinetic values. CyAcpH demonstrated significantly higher turnover, and required a lower enzyme concentration of 5 nM, compared to 1 μM utilized for other AcpH homologs. SoAcpH did not demonstrate activity in the qualitative assays, so was not evaluated for kinetics.

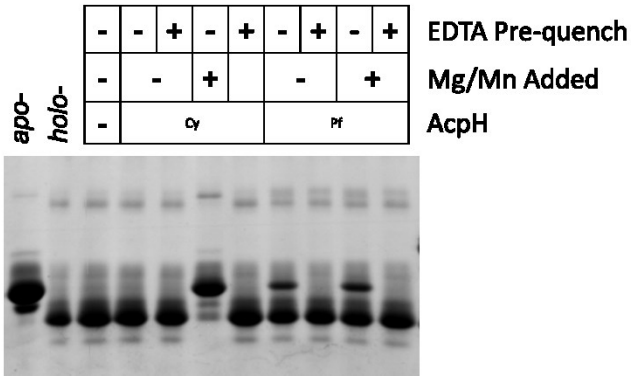

Supplementary Figure 23. *Verification of EDTA quench method*. AcpH homologs from *P. fluorescens* (Pf), and *Cyanothece* PCC 7822 (Cy) are evaluated to verify the *holo- E. coli* AcpP reaction termination expected by EDTA addition prior to evaluating HPLC kinetic samples. No conversion of *holo-* to *apo-* AcpP was observed following a10 minute incubation at 37°C, followed by overnight incubation at room temperature.

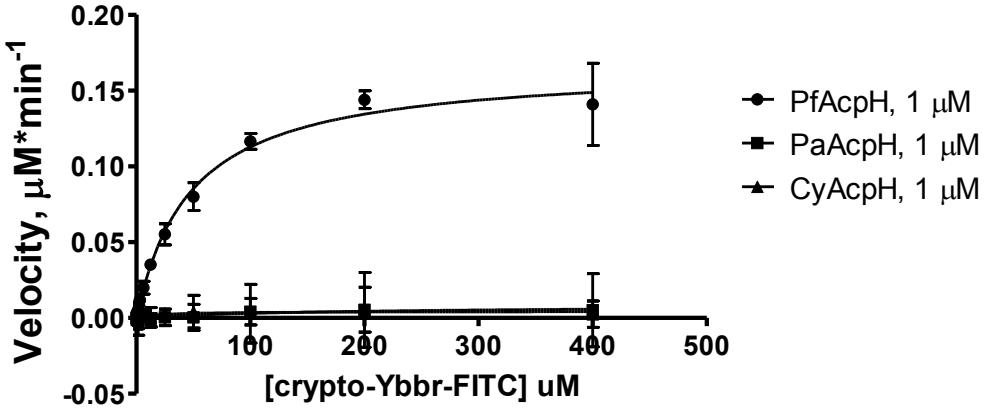

Supplementary Figure 24. *Analysis of AcpH homolog kinetics with crypto-ybbR-FITC*. Reaction of AcpH homologs from *P. fluorescens* (Pf), *P. aeruginosa* (Pa),and *Cyanothece* PCC 7822 (Cy) in microwell format with *crypto*-yBBR-FITC allows derivation of HPLC kinetic values. While PaAcpH and CyAcpH appeared to demonstrate signal above background, PfAcpH demonstrated clear signal indicating substrate turnover.

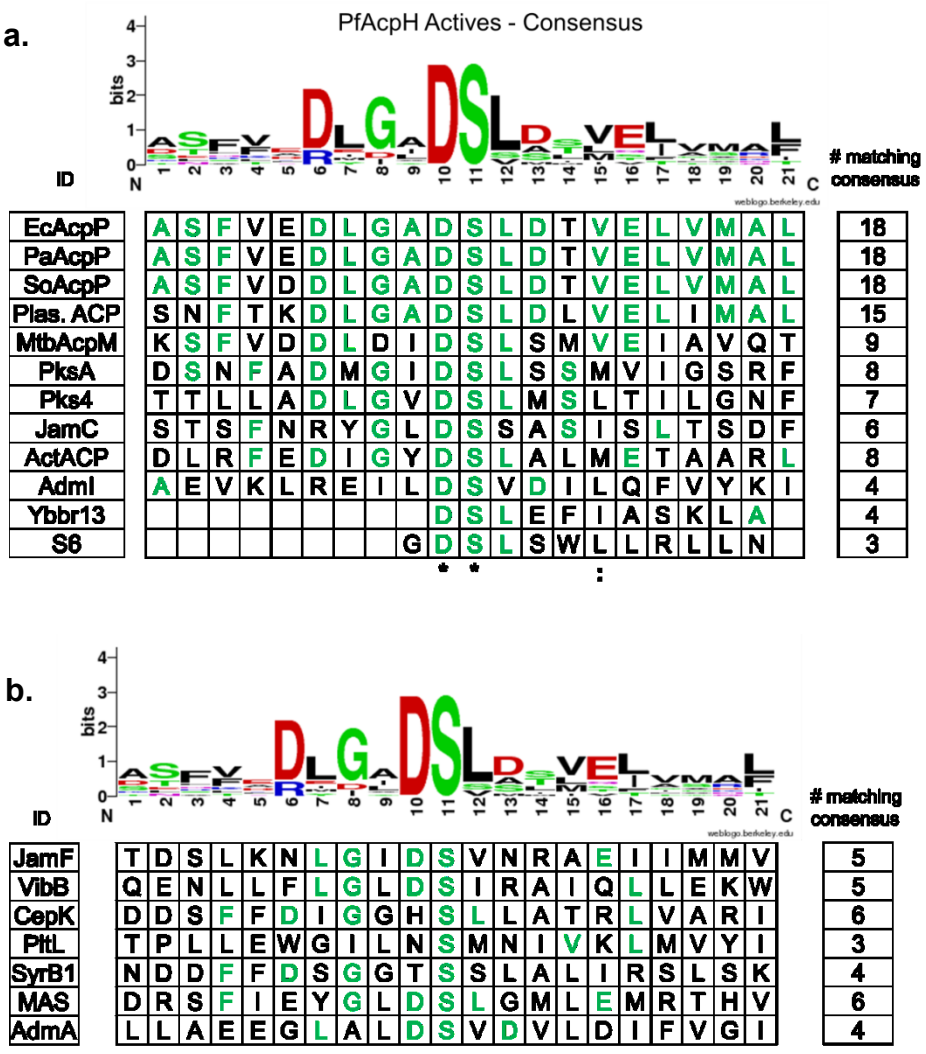

Supplementary Figure 25. *PfAcpH consensus substrate sequence and CP alignments*. The consensus sequence of all PfAcpH active carrier protein sequences was generated using WebLogo (http://weblogo.berkeley.edu). The consensus demonstrates several residues matching those of the type II FAS ACPs as being particularly pervasive across active substrates (**a**). Inactive substrates contain 6 or fewer residues matching the consensus (**b**), while only one active substrate, ybbR, contains fewer than 6 residues matching the consensus.

Supplementary Table 1. *Carrier proteins studied for AcpH activity*. Carrier proteins used in this study used for PPant labeling and subsequent analysis of AcpH homolog activity via PPant hydrolysis.

	Protein Name	Source Organism	Accession Number
FAS	AcpP	*E. coli*	NP_287228
	AcpP	*P. aeruginosa*	NP_251656
	AcpP	*S. oneidensis*	NP_718356
	PfACP	*P. falciparum*	3GZL_A
	AcpM	*M. tuberculosis*	NP_216760
	MAS	*M. tuberculosis*	YP_006516394
PKS	ActACP	*S. coelicolor*	NP_629239
	PksA	*A. parasiticus*	2KR5_A
	Pks4	*G. fujikuroi*	CAB92399
	JamC	*L. majuscula*	AAS98798
	JamF	*L. majuscula*	CAB46501
	AdmA	*P. agglomerans*	AAO39095
NRPS	AdmI	*P. agglomerans*	AAO39103
	VibB	*V. cholerae*	AAC45926
	CepK	*A. orientalis*	KF672793
	PltL	*P. protogens*	AAD24885
	SyrB1	*P. syringae*	AAZ99831

Supplementary Table 2. *Primers used for cloning*. Primers used in the cloning/sub-cloning for gene products used in this manuscript are depicted.

Primer Name	Primer Sequence (5' → 3')
PfAcpH F1	AAAACATATGAATTATCTCGCACATCTGCACC
PfAcpH R1	AAAACTCGAGTGCAAAGGCCTGCAACTCTGG
PfAcpH R2	AAAACTCGAGTTAAAATTGGAGTGCAAAGGCCTGC
PfAcpH R3	AAAACTCGAGAAATTGGAGTGCAAAGGCCTGCAAC
CyAcpH F1	AAAACATATGAATTATCTGGCTCATTTATTTTTAGC
CyAcpH R1	AAAACTCGAGAGCCAAGTTAACATAATCAATCAGTTG
SoAcpH F1	AAAACATATGAACATTCTTACACACTTACATCTGG
SoAcpH R1	AAAACTCGAGCTCGGGTAAGTAGTCAATTGGAG

Supplementary Methods

General methods. All protein concentrations were determined using UV spectroscopy at 280 nM with the extinction coefficient calculated from derived amino acid sequences with the ExPASy (http://www.expasy.org/) ProtParam tool.[37]

Cloning of AcpH constructs. The *Pseudomonas aeruginosa* PAO1 AcpH gene [PA4353] identified previously[17] was cloned as described previously.[13] *Cyanothece PCC7822* AcpH (CyAcpH) PCR product was generated from genomic DNA using forward primer “CyAcpH F1” and reverse primer “CyAcpH R1” with Phusion polymerase (New England Biolabs). Shewanella oneidensis MR-1 AcpH (SoAcpH) PCR product was generated from genomic DNA using forward primer “SoAcpH F1” and reverse primer “SoAcpH R1” with Phusion polymerase. *Pseudomonas fluorescens* NCIMB 10586 AcpH (PfAcpH) primers were designed using the AcpH homolog sequence from *Pseudomonas fluorescens* SBW25, as it is the closest strain phylogenetically. PCR product was first generated from genomic DNA using forward primer “PfAcpH F1” and reverse primer “PfAcpH R1” using Phusion polymerase, generating low amounts of ~600bp and ~1000bp products. Both ~600bp and ~1000bp products were submitted for sequencing using “PfAcpH F1” and “PfAcpH R1”and the 1000bp product contained a gene coding for a homologous AcpH. Reverse primer “PfAcpH R2” containing the stop codon and “PfAcpH R3” without the stop codon were designed from the derived PCR product sequence and used with forward primer “PfAcpH F1 to generate a new ~600bp band using nested PCR with Pfu polymerase, as Phusion did not generate product with the new primers. All final PCR products and template plasmid pET29b (Novagen) were treated with NdeI and XhoI restriction endonucleases (New England Biolabs), gel-purified, ligated, transformed into *E. coli* DH5a, and sequenced for confirmation.

AcpH *holo*-ACP kinetics sample preparation. *E. coli holo*-ACP was diluted into 50 mM TrisCl pH 8.0, 250 mM NaCl, 10% glycerol, 30 mM MgCl2 and 2 mM MnCl2 buffer to a concentration of 800 μM. Serial dilution of *holo*-ACP resulted in a final concentration range of 800-25 μM. AcpH was diluted from MOPS lysis buffer into 50 mM TrisCl pH 8.0, 250 mM NaCl, 10% glycerol and added to an equal volume of the *holo*-ACP serial dilution to initiate the reaction. Reaction tubes were transferred to a pre-warmed rack at 37°C and shaken for the duration of the experiment. Time points were collected at 10 minutes for Cy and PfAcpH and 60 minutes for SoAcpH by addition of reaction contents to 100 mM EDTA (pH 8.0). All samples were frozen at -80°C until evaluated by HPLC.

Verification of EDTA quench with PfAcpH and CyAcpH. PfAcpH and CyAcpH were prepared in the same buffer conditions as the HPLC assay format in a 20 μL reaction volume, with the following alterations. *Holo*- E. coli AcpP was utilized at a final concentration of 150 μM. Each AcpH was prepared in four different manners: with no Mg^{2+}/Mn^{2+}, no Mg^{2+}/Mn^{2+} + EDTA pre-quench, Mg^{2+}/Mn^{2+}, and Mg^{2+}/Mn^{2+} + EDTA pre-quench. EDTA quench involved an equal volume addition of 100 mM EDTA pH 7.5. Samples were incubated 10 minutes at 37°C and then quenched with EDTA if not already pre-quenched. Samples were then incubated overnight at room temperature to simulate the conditions experienced by HPLC samples while awaiting injection. One fourth volume of 5X Native-PAGE loading dye was added to samples, and 10 μL of that mixture was run on 20% Urea-PAGE for analysis.

HPLC detection method. Kinetics samples were mixed briefly with finger flicking, and centrifuged at 13000 rpm for 10 minutes at room temperature prior to transferring contents into HPLC vials. 20 μL of each reaction time point was injected on

an Agilent 1100 series HPLC with column (Burdick & Jackson OD5 # 9575, 25cm x 4.6 mm ID) using an acetonitrile/water gradient. Both water and acetonitrile contained 0.05% TFA. Method gradient for each injection: 0-5 min with 10% acetonitrile, 5-30 min with 10-100% acetonitrile, 30-35 min with 100% acetonitrile, 35-37 min with 100-10% acetonitrile, 37-40 min with 10% acetonitrile. HPLC-grade solvents (J.T. Baker, Phillipsburg, New Jersey) were used exclusively. *Apo*- & *holo*-ACP protein standards were used to validate the retention times identified using 210nm UV light at approximately 21 and 19 minutes, respectively. Peak integration was performed for all samples, and substrate turnover was calculated from the ratio of *apo*- to *holo*- ACP present in the HPLC trace and the known concentration of total ACP in reaction samples. Calculated rates for AcpH versus substrate concentration were obtained through Excel data analysis and graphed in Prism GraphPad using the "Michaelis-Menten" function for enzyme kinetics, with a zero data point added for substrate concentration of 0 μM*min-1 and 0 μM substrate for AcpH graphs.

Circular dichroism analysis of select AcpH homologs. CyAcpH and SoAcpH protein preparations in Tris lysis buffer were desalted with PD-10 desalting columns (GE Healthcare) into 0.2 μm filtered 50 mM K_2HPO_4 pH 8.0, and subsequently diluted to 0.2 mg/mL. Samples were kept on ice until transfer to 2 mm width quartz cuvette for analysis at 25°C. Scans were acquired in 0.5 nm increments averaged over 5 seconds from 260 nm to 200 nm. Sample data was subjected to smooth and raw ellipticity was used in conjunction with specific protein residue number and molecular weight to calculate molar ellipticity using established procedures.

References

1. Prescher, J. A. and Bertozzi, C. R. (2005) Chemistry in living systems, *Nat. Chem. Biol. 1*, 13-21.

2. Luchansky, S. J., Argade, S., Hayes, B. K., and Bertozzi, C. R. (2004) Metabolic functionalization of recombinant glycoproteins, *Biochemistry 43*, 12358-12366.

3. Batra, G., Talha, S. M., Nemani, S. K., Dhar, N., Swaminathan, S., and Khanna, N. (2010) Expression, purification and characterization of in vivo biotinylated dengue virus envelope domain III based tetravalent antigen, *Protein Expres. Purif. 74*, 99-105.

4. Stachler, M. D., Chen, I., Ting, A. Y., and Bartlett, J. S. (2008) Site-specific modification of AAV vector particles with biophysical probes and targeting ligands using biotin ligase, *Mol. Ther. 16*, 1467-1473.

5. Quadri, L. E., Weinreb, P. H., Lei, M., Nakano, M. M., Zuber, P., and Walsh, C. T. (1998) Characterization of Sfp, a Bacillus subtilis phosphopantetheinyl transferase for peptidyl carrier protein domains in peptide synthetases, *Biochemistry 37*, 1585-1595.

6. Foley, T. L., Young, B. S., and Burkart, M. D. (2009) Phosphopantetheinyl transferase inhibition and secondary metabolism, *FEBS J. 276*, 7134-7145.

7. Haushalter, R. W., Filipp, F. V., Ko, K. S., Yu, R., Opella, S. J., and Burkart, M. D. (2011) Binding and "pKa" modulation of a polycyclic substrate analogue in a type II polyketide acyl carrier protein, *ACS Chem. Biol. 6*, 413-418.

8. Ishikawa, F., Haushalter, R. W., and Burkart, M. D. (2012) Dehydratase-specific probes for fatty acid and polyketide synthases, J*. Am. Chem. Soc. 134*, 769-772.

9. La Clair, J. J., Foley, T. L., Schegg, T. R., Regan, C. M., and Burkart, M. D. (2004) Manipulation of carrier proteins in antibiotic biosynthesis, *Chem. Biol. 11*, 195-201.

10. Meier, J. L., Haushalter, R. W., and Burkart, M. D. (2010) A mechanism based protein crosslinker for acyl carrier protein dehydratases, *Bioorg. Med. Chem. Lett. 20*, 4936-4939.

11. Yin, J., Straight, P. D., McLoughlin, S. M., Zhou, Z., Lin, A. J., Golan, D. E., Kelleher, N. L., Kolter, R., and Walsh, C. T. (2005) Genetically encoded short peptide tag for versatile protein labeling by Sfp phosphopantetheinyl transferase, *P. Natl. Acad. Sci. USA 102*, 15815-15820.

12. Yin, J., Lin, A.J., Golan, D.E. & Walsh, C.T. . (2006) Site-specific protein labeling by Sfp phosphopantetheinyl transferase., *Nat. Protoc. 1*, 280-285.

13. Kosa, N. M., Haushalter, R. W., Smith, A. R., and Burkart, M. D. (2012) Reversible labeling of native and fusion-protein motifs, *Nat. Methods 9*, 981-984.

14. Thomas, J., and Cronan, J. E. (2005) The enigmatic acyl carrier protein phosphodiesterase of Escherichia coli: genetic and enzymological characterization, *J. Biol. Chem. 280*, 34675-34683.

15. Vagelos, P. R. and Larrabee, A. R (1967) Acyl carrier protein, *J. Biol. Chem. 242*, 1776-1781.

16. Worthington, A. S., and Burkart, M. D. (2006) One-pot chemo-enzymatic synthesis of reporter-modified proteins, *Org. Biomol. Chem. 4*, 44-46.

17. Murugan, E., Kong, R., Sun, H., Rao, F., and Liang, Z. X. (2010) Expression, purification and characterization of the acyl carrier protein phosphodiesterase from Pseudomonas Aeruginosa, *Protein Expres. Purif. 71*, 132-138.

18. Thomas, J., Rigden, D. J., and Cronan, J. E. (2007) Acyl carrier protein phosphodiesterase (AcpH) of Escherichia coli is a non-canonical member of the HD phosphatase/phosphodiesterase family, *Biochemistry 46*, 129-136.

19. Clarke, K. M., Mercer, A. C., La Clair, J. J., and Burkart, M. D. (2005) In vivo reporter labeling of proteins via metabolic delivery of coenzyme A analogues, *J. Am. Chem. Soc. 127*, 11234-11235.

20. Dereeper, A., Guignon, V., Blanc, G., Audic, S., Buffet, S., Chevenet, F., Dufayard, J. F., Guindon, S., Lefort, V., Lescot, M., Claverie, J. M., and Gascuel, O. (2008) Phylogeny.fr: robust phylogenetic analysis for the non-specialist, *Nucleic Acids Res. 36*, W465-469.

21. Prigge, S. T., He, X., Gerena, L., Waters, N. C., and Reynolds, K. A. (2003) The Initiating Steps of a Type II fatty acid synthase in Plasmodium falciparum are catalyzed by pfACP, pfMCAT, and pfKASIII, *Biochemistry 42*, 1160-1169.

22. Crawford, J. M., Korman, T. P., Labonte, J. W., Vagstad, A. L., Hill, E. A., Kamari-Bidkorpeh, O., Tsai, S. C., and Townsend, C. A. (2009) Structural basis for biosynthetic programming of fungal aromatic polyketide cyclization, *Nature 461*, 1139-1143.

23. Linnemannstons, P., Schulte, J., del Mar Prado, M., Proctor, R. H., Avalos, J., and Tudzynski, B. (2002) The polyketide synthase gene pks4 from Gibberella fujikuroi encodes a key enzyme in the biosynthesis of the red pigment bikaverin, *Fungal Genet. Biol. 37*, 134-148.

24. Dorrestein, P. C., Blackhall, J., Straight, P. D., Fischbach, M. A., Garneau-Tsodikova, S., Edwards, D. J., McLaughlin, S., Lin, M., Gerwick, W. H., Kolter, R., Walsh, C. T., and Kelleher, N. L. (2006) Activity screening of carrier domains within nonribosomal peptide synthetases using complex substrate mixtures and large molecule mass spectrometry, *Biochemistry 45*, 1537-1546.

25. Edwards, D. J., Marquez, B. L., Nogle, L. M., McPhail, K., Goeger, D. E., Roberts, M. A., and Gerwick, W. H. (2004) Structure and biosynthesis of the jamaicamides, new mixed polyketide-peptide neurotoxins from the marine cyanobacterium Lyngbya majuscula, *Chem. Biol. 11*, 817-833.

26. Fortin, P. D., Walsh, C. T., and Magarvey, N. A. (2007) A transglutaminase homologue as a condensation catalyst in antibiotic assembly lines, *Nature 448*, 824-827.

27. Marshall, C. G., Burkart, M. D., Meray, R. K., and Walsh, C. T. (2002) Carrier protein recognition in siderophore-producing nonribosomal peptide synthetases, *Biochemistry 41*, 8429-8437.

28. Matthews, M. L., Krest, C. M., Barr, E. W., Vaillancourt, F. H., Walsh, C. T., Green, M. T., Krebs, C., and Bollinger, J. M. (2009) Substrate-triggered formation and remarkable stability of the C-H bond-cleaving chloroferryl intermediate in the aliphatic halogenase, SyrB2, *Biochemistry 48*, 4331-4343.

29. Williamson, D. J., Fascione, M. A., Webb, M. E., and Turnbull, W. B. (2012) Efficient N-terminal labeling of proteins by use of sortase, *Angew. Chem. Int. Edit. 51*, 9377-9380.

30. Hirakawa, H., Ishikawa, S., and Nagamune, T. (2012) Design of Ca2R-independent Staphylococcus aureus sortase A mutants, *Biotechnol. Bioeng. 109*, 2955-2961.

31. Rashidian, M., Song, J. M., Pricer, R. E., and Distefano, M. D. (2012) Chemoenzymatic reversible immobilization and labeling of proteins without prior purification, *J. Am. Chem. Soc. 134*, 8455-8467.

32. Lee, J. H., Song, C., Kim, D. H., Park, I. H., Lee, S. G., Lee, Y. S., and Kim, B. G. (2012) Glutamine (Q)-peptide screening for transglutaminase reaction using mRNA display, *Biotechnol. Bioeng. 110*, 353-362.

33. Takahara, M., Hayashi, K., Goto, M., and Kamiya, N. (2013) Tailing DNA aptamers with a functional protein by two-step enzymatic reaction, *J. Biosci. Bioeng,* S1389-1723(13)00207-7.

34. Foley, T. L., and Burkart, M. D. (2009) A homogeneous resonance energy transfer assay for phosphopantetheinyl transferase, *Anal. Biochem. 394*, 39-47.

35. Quadri, L. E., Weinreb, P. H., Lei, M., Nakano, M. M., Zuber, P., and Walsh, C. T. (1998) Characterization of Sfp, a Bacillus subtilis phosphopantetheinyl transferase for peptidyl carrier protein domains in peptide synthetases, *Biochemistry 37*, 1585-1595.

36. Foley, T. L., Yasgar, A., Garcia, C. J., Jadhav, A., Simeonov, A., and Burkart, M. D. (2010) Preparation of FRET reporters to support chemical probe development, *Org. Biomol. Chem. 8*, 4601-4606.

37. ExPASy ProtParam Tool, (2013) http://web.expasy.org/protparam/.

38. Goh, E. B., Baidoo, E. E., Keasling, J. D., and Beller, H. R. (2012) Engineering of bacterial methyl ketone synthesis for biofuels, *Appl. Environ. Microb. 78*, 70-80.

The chapter entitled “Chemoenzymatic exchange of phosphopantetheine on protein and peptide,” in full, is currently being prepared for submission for publication of the material. Kosa, Nicolas M.; Pham, Kevin M.; Burkart, Michael D. The dissertation author was the primary investigator and author of this material.